1977

Excited Electronic States: A. Polar Aromatics. B. Inorganic Anions.

Thomas Preston Carsey
Louisiana State University and Agricultural & Mechanical College

INFORMATION TO USERS

This material was produced from a microfilm copy of the original document. While the most advanced technological means to photograph and reproduce this document have been used, the quality is heavily dependent upon the quality of the original submitted.

The following explanation of techniques is provided to help you understand markings or patterns which may appear on this reproduction.

1. The sign or "target" for pages apparently lacking from the document photographed is "Missing Page(s)". If it was possible to obtain the missing page(s) or section, they are spliced into the film along with adjacent pages. This may have necessitated cutting thru an image and duplicating adjacent pages to insure you complete continuity.

2. When an image on the film is obliterated with a large round black mark, it is an indication that the photographer suspected that the copy may have moved during exposure and thus cause a blurred image. You will find a good image of the page in the adjacent frame.

3. When a map, drawing or chart, etc., was part of the material being photographed the photographer followed a definite method in "sectioning" the material. It is customary to begin photoing at the upper left hand corner of a large sheet and to continue photoing from left to right in equal sections with a small overlap. If necessary, sectioning is continued again – beginning below the first row and continuing on until complete.

4. The majority of users indicate that the textual content is of greatest value, however, a somewhat higher quality reproduction could be made from "photographs" if essential to the understanding of the dissertation. Silver prints of "photographs" may be ordered at additional charge by writing the Order Department, giving the catalog number, title, author and specific pages you wish reproduced.

5. PLEASE NOTE: Some pages may have indistinct print. Filmed as received.

University Microfilms International
300 North Zeeb Road
Ann Arbor, Michigan 48106 USA
St. John's Road, Tyler's Green
High Wycombe, Bucks, England HP10 8HR

EXCITED ELECTRONIC STATES
A. POLAR AROMATICS
B. INORGANIC ANIONS

A Dissertation

Submitted to the Graduate Faculty of the
Louisiana State University and
Agriculture and Mechanical College
in partial fulfillment of the
requirements for the degree of
Doctor of Philosophy

in

the Department of Chemistry

by
Thomas Preston Carsey
B.S., New Mexico State University, 1969
May, 1977

EXAMINATION AND THESIS REPORT

Candidate: Thomas Preston Carsey

Major Field: Chemistry

Title of Thesis: Excited Electronic States
A. Polar Aromatics
B. Inorganic Anions

Approved:

Major Professor and Chairman

Dean of the Graduate School

EXAMINING COMMITTEE:

Date of Examination:

December 16, 1976

Dedication

To Pamela, Daniel, and Lorien Carsey

ACKNOWLEDGEMENT

I wish to express my sincere appreciation to Dr. Sean P. McGlynn under whose direction this work was performed. I would also like to thank present and past members of Dr. McGlynn's Research Group for their discussions and suggestions.

This work was supported by the United States Atomic Energy Commision-Division of Biomedical and Environmental Research--Physics and Technological Program and the Louisiana State University. Financial assistance in preparation of this dissertation was provided by the Charles E. Coates Memorial Fund of Louisiana State University Foundation donated by George H. Coates. This support and assistance is gratefully acknowledged.

Finally, I express my gratitude to my wife, Pam, and to our children, for their patience and inspiration during the years of my graduate work.

Foreword

This dissertation is divided into two sections:

Section A: This Section consists of Chapter 1 only. It is concerned with the absorption and emission spectroscopy of o-, m-, and p-isomers of various disubstituted benzenes, one substituent being an electron donor and the other an electron acceptor.

Section B: This section consists of Chapters 2 and 3. It is concerned with the absorption and emission spectroscopy of several small inorganic ions and with the development of a quantum-mechanical model of singlet-triplet transition intensities in the silver nitrite molecule.

TABLE OF CONTENTS

LIST OF TABLES

TABLE PAGE

LIST OF FIGURES

Abstract

The absorption and emission of a number of highly-polar molecules of the type D-ϕ-A, where D is an electron-donor substituent, ϕ is a benzene ring, and A is an electron-acceptor substituent, have been investigated. The electronic spectra of o-, m-, and p-fluorobenzonitriles, cyanoanisole, cyanoaniline, aminoacetophenone, and nitroaniline are presented in detail. For the weakly-polar fluorobenzonitriles, the lowest-energy absorption band consists of only one ^1L_b-related transition. For the more-polar cyanoanisoles and the highly-polar cyanoanilines, aminoacetophenones, and nitroanilines, the lowest-energy absorption band of the p-isomer is shown to be a composite of at least two transitions. The more intense ^1L_a-related band is of higher energy than the ^1L_b-related band, but undergoes an energy decrease as the polarity of the molecule increases.

The lowest-energy band of the o- and m-derivatives consists of only one ^1L_b-related transition. The second intense band of the o- and m-derivatives consists of one ^1L_a-related transition. Both of these transitions undergoes an energy decrement as the polarity of the molecule increases. In all o- and m-molecules, fluorescence is shown to be the inverse of the ^1L_b-related absorption.

The trends observed in these five D-ϕ-A sub-sets have been qualitatively investigated in a large selection of other disubstituted

benzenes. The ^1L_a- and ^1L_b-related bands display considerable regularity of energy and intensity trends. In a sufficiently polar p-derivative, the ^1L_a-related band may coincide with or even drop below the ^1L_b-related band, with significant effects on the emission characteristics. Because of symmetry, the ^1L_a-related band in the p-derivatives is very strongly affected by substituents whereas the ^1L_b-related band is not. With strong electron donors and acceptors, the ^1L_a-related band acquires more charge-transfer character. In the o- and m-derivatives, on the other hand, the charge-transfer effect of the substituents is shared somewhat equally by both the ^1L_b- and ^1L_a-related bands.

Quantum-chemical calculations on a representative sampling of o-, m-, and p-derivatives are presented and analyzed. The degree of charge-transfer, the energies and the intensities of the various electronic transitions are examined. Considerable attention is also devoted to singlet-triplet intervals and ground state dipole moments.

The excited states of simple metal ion - inorganic cation complexes have been investigated. Two mechanisms which rationalize the non-additivity of certain absorption bands in the spectra of these complexes are described: charge-transfer transitions and enhanced singlet-triplet transitions. The latter effect is more likely to be present if the cation is a heavy-metal ion.

The electronic spectra of the chlorite and sulfate ion have been investigated. In the spectrum of the chlorite ion, a transition is observed which is interpreted as a singlet-triplet transition. An examination of the electronic spectrum of the sulfate ion reveals a previously unreported transition which is identified as a singlet-triplet transition.

The tungstate and molybdate ions are known to emit in the solid phase. In the solution spectra of salts of these anions, a previously unreported transition is observed which resembles the emission excitation band. This transition is examined and interpreted as a singlet-triplet transition of the anion.

A model which describes the interaction between a metal cation and an inorganic anion is developed using first-order perturbation theory. The model does not invoke vibronic spin-orbit coupling. All one-electron excitations of the highest-occupied and lowest-occupied metal and anion orbitals are investigated. Expressions which describe all sources of $S_o \rightarrow T_1$ intensity are derived and given. These expressions are computed for the silver nitrite molecule and are compared with experiment. The results indicate the critical role of charge-transfer transitions in the mechanism of the enhancement of $T_1 \leftrightarrow S_o$ probabilities.

CHAPTER ONE.

THE EXCITED ELECTRONIC STATES OF POLAR AROMATICS

Abstract

The absorption and emission of a number of highly-polar molecules of the type D-Φ-A, where D is an electron-donor substituent, Φ is a benzene ring, and A is an electron-acceptor substituent, have been investigated. The electronic spectra of o-, m-, and p-fluorobenzonitriles, cyanoanisole, cyanoaniline, aminoacetophenone, and nitroaniline are presented in detail. For the weakly-polar fluorobenzonitriles, the lowest-energy absorption band consists of only one ^1L_b-related transition. For the more-polar cyanoanisoles and the highly-polar cyanoanilines, aminoacetophenones, and nitroanilines, the lowest-energy absorption band of the p-isomer is shown to be a composite of at least two transitions. The more intense ^1L_a-related band is of higher energy than the ^1L_b-related band, but undergoes an energy decrease as the polarity of the molecule increases.

The lowest-energy band of the o- and m-derivatives consists of only one ^1L_b-related transition. The second intense band of the o- and m-derivatives consists of one ^1L_a-related transition. Both of these transitions undergoes an energy decrement as the polarity of the molecule increases. In all o- and m-molecules, fluorescence is shown to be the inverse of the ^1L_b-related absorption.

The trends observed in these five D-ϕ-A sub-sets have been qualitatively investigated in a large selection of other disubstituted benzenes. The ^1L_a- and ^1L_b-related bands display considerable regularity of energy and intensity trends. In a sufficiently polar p-derivative, the ^1L_a-related band may coincide with or even drop below

the ^1L_b-related band, with significant effects on the emission characteristics. Because of symmetry, the ^1L_a-related band in the p-derivatives is very strongly affected by substituents whereas the ^1L_b-related band is not. With strong electron donors and acceptors, the ^1L_a-related band acquires more charge-transfer character. In the o- and m-derivatives, on the other hand, the charge-transfer effect of the substituents is shared somewhat equally by both the ^1L_b- and ^1L_a-related bands.

Quantum-chemical calculations on a representative sampling of o-, m-, and p-derivatives are presented and analyzed. The degree of charge-transfer, the energies and the intensities of the various electronic transitions are examined. Considerable attention is also devoted to singlet-triplet intervals and ground state dipole moments.

I. INTRODUCTION

Disubstituted benzenes of the type D-ϕ-A (where D represents a donor and A an acceptor substituent) constitute a sub-set of the broad class of organic compounds which exhibits large ground state dipole moments. The electronic spectroscopy of this subset has been discussed in terms of substituent effects on benzene[1-5], solvent[6,7] and steric[8-11] effects on electronic transitions, the relevance of intramolecular charge-transfer concepts[12-18], electrically-induced dichroism[19-27], etc. No general understanding of the electronic structure of these molecules seems to be available.

The D-ϕ-A sub-set is prototypical of the highly-polar aromatics. It also has the advantage that substituents may be varied systematically so that a series of molecules of increasing polarity may be generated. This last property is the major reason for our choice of this sub-set.

Our interest lies in the way in which the properties of the lower-energy singlet and triplet states depend on the molecular polarity. The approach we adopt is correlative. We begin with a discussion of experimental data for five representative ortho, meta and para (omp) triads which span the weakly-polar to highly-polar range of D-ϕ-A species. Our aim is to categorize those general absorptive and emissive characteristics which, within a given triad, appear to be a function of molecular polarity. Thereafter, we present an extensive set of data for a great variety of omp triads; The aim, in this instance, is to discern those characteristics of the ortho (or meta, or para) series which are distinctly dependent on the molecular

polarity. Finally, the same molecules are subjected to quantum chemical processing in order to gain insight into the nature of the regularities displayed by the empirical data.

This work, then, is an attempt to systematize the experimental and theoretical results. To this end, we ask the following questions:

---Do any electronic and spectroscopic regularities exist among the members of the D-ϕ-A sub-set?

---What are the effects of molecular polarity on the absorption and emission characteristics of these molecules?

---Can the empirical regularities be formulated in a theoretical way?

---Is molecular polarity the best and/or the most convenient independent variable for the observed correlations?

The results of this work may be of interest for a number of reasons. Firstly, the class of highly-polar aromatics contains a large number of biological molecules. Secondly, many of the extrinsic chromophores (or "fluorescent probes") which are used to gauge microenvironments within macromolecules[28-31] fall in this category. And, thirdly, the ability to vary the fluorescence energy and polarization by merely altering the solvent medium, and the possibility that many of the excited states possess very large static dipole moments (30D or larger), may well be of technological advantage.

II. EXPERIMENTAL METHODS

All compounds were recrystallized from ethanol and/or vacuum sublimed until no further change of the absorption spectrum was detectable. Solvents were purified as follows: Ethanol was refluxed over calcium oxide and distilled from magnesium turnings; methyl-

cyclohexane (MCH) and 3-methylpentane(3MP) were washed with fuming sulfuric acid and water, passed through a silica gel column and distilled over sodium wire; and ether, which was maintained in slow reflux over sodium wire, was drained off as needed.

Absorption measurements, whether at 300 or 77°K, were made with either a Cary-14 or Cary-15 spectrometer. Emission measurements, usually at 77°K, were recorded with a Jarrel-Ash Mark V 0.5m scanning monochromator, used in conjunction with a PAR phase-sensitive detection sytem, a 500W Xenon arc source, and a Cary 15 f18 excitation monochromator. Luminescence spectra were corrected for the response properties of the detection system. All luminescing samples were optically homogeneous and were thoroughly degassed by repeated freeze-thaw-evacuate cycles. Solute concentrations were less than 10^{-4}M in all instances, in order to minimize aggregation and inner-filter effects.

Polarization measurements were performed using the techniques of Azumi and McGlynn[32]. The EPA solvent, which forms an excellent glassy solution at 77°K, consists of ether, isopentane and alcohol in a 5/5/2 (by volume) mixture.

III. EXPERIMENTAL RESULTS

The series of D-ϕ-A molecules may be ranked according to molecular polarity by using the substituent activation of the benzene ring toward electrophilic substitution as a guage. This guage classifies substituents according to the direction and degree of induced electron migration in the following manner[33].

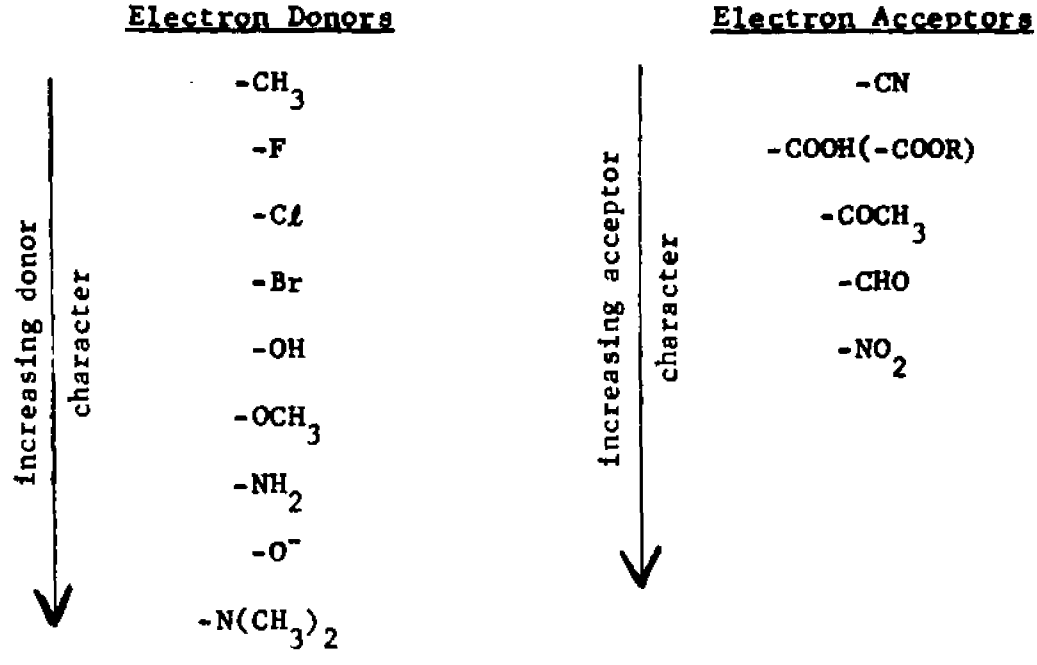

Three distinct types of series, all ranked according to increasing molecular polarity, may be defined:

---SERIES A: The electron donor and the electron acceptor are both held constant, while their relative positions (i.e., ortho, meta or para) are varied;

---SERIES B: The electron donor is held constant, while the electron acceptor is varied; and

---SERIES C: The electron acceptor is held constant, while the electron donor is varied.

We will discuss Series A first. We consider five OMP triads taken in order of increasing polarity: Fluorobenzonitriles, cyanoanisoles, cyanoanilines, aminoacetophenones and nitroanilines.

A. SERIES A.

1. FLUOROBENZONITRILES: The fluorobenzonitriles are weakly-polar. The spectra of the omp triad are given in Figures 1 and 2. The following observations may be made:

Figure 1.

Absorption spectra of o-, m-, and p-fluorobenzonitrile in ethanol at room temperature.

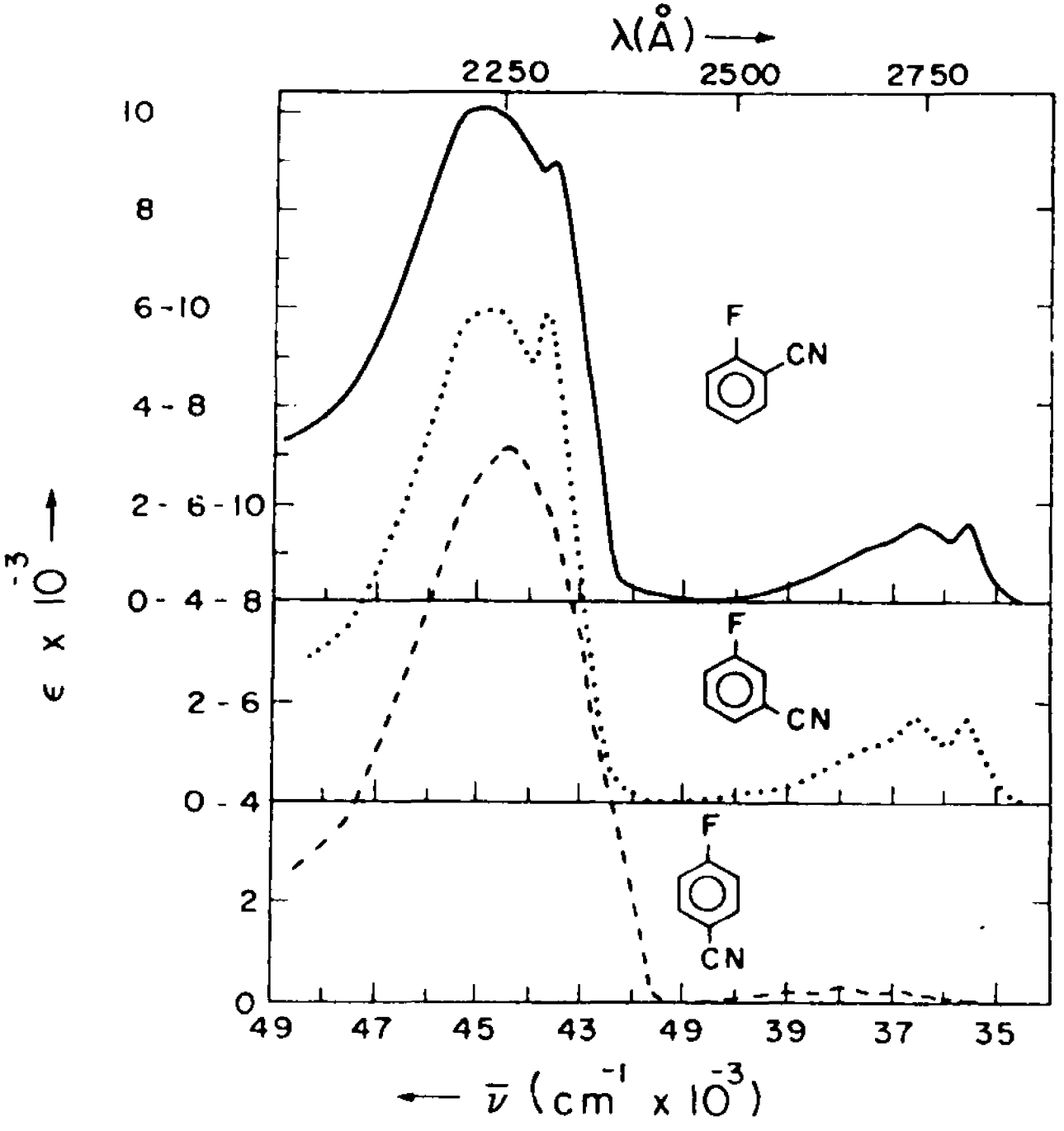
λ(Å) ⟶
2250
2500
2750
10
8
6-10
4-8
2-6-10
0-4-8
2-6
0-4
2
0
ε x 10^-3
F
CN
F
CN
F
CN
49
47
45
43
49
39
37
35
ν̄ (cm^-1 x 10^-3)

Figure 2.

Total emission spectra of o-, m-, and p-fluorobenzonitriles in ethanol glass at 77°K. The spectra are corrected for all instrument parameters.

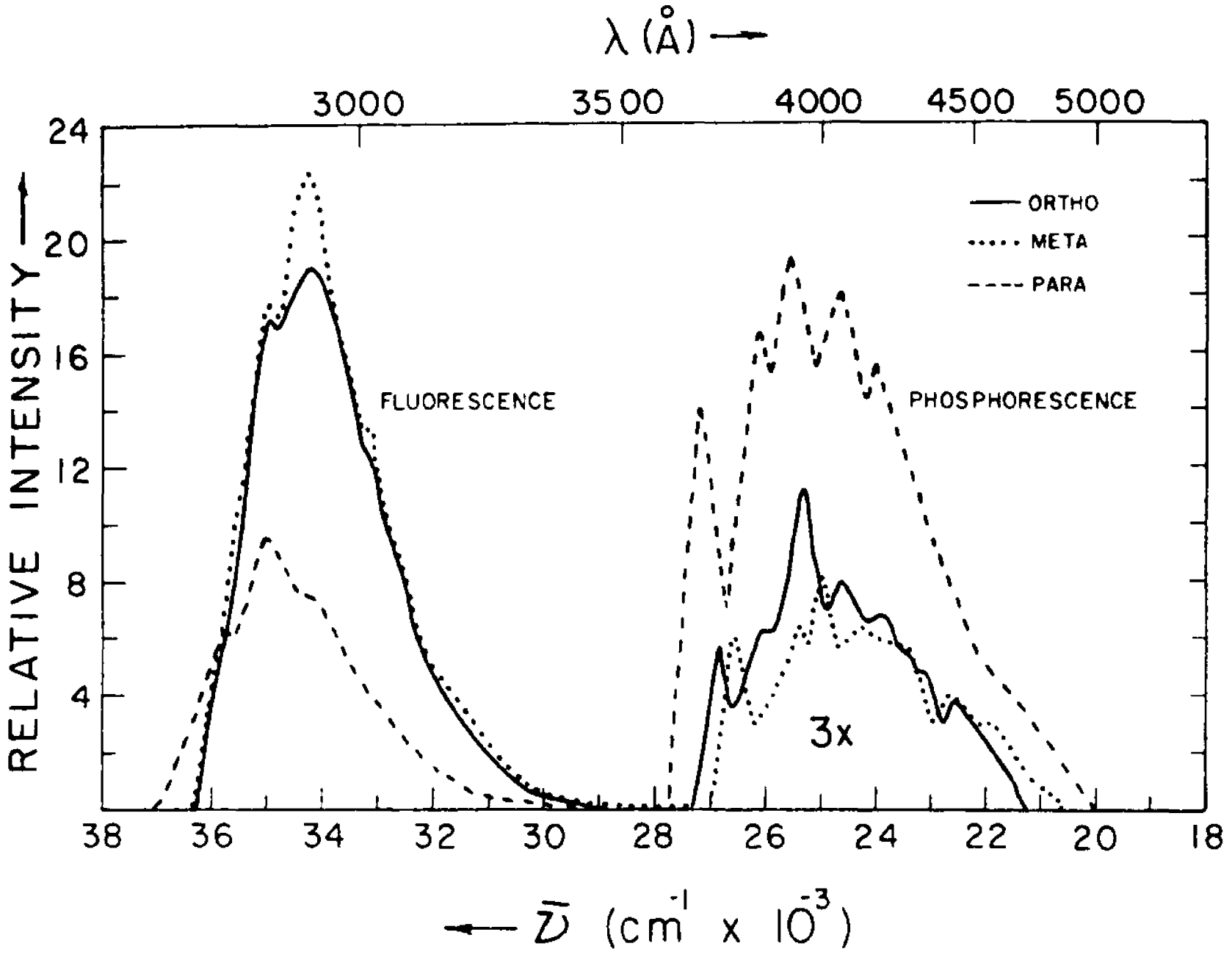
λ (Å) →
3000
3500
4000
4500
5000
24
20
16
12
8
4
RELATIVE INTENSITY →
ORTHO
META
PARA
FLUORESCENCE
PHOSPHORESCENCE
3x
38
36
34
32
30
28
26
24
22
20
18
← ν̄ (cm⁻¹ x 10⁻³)

---The absorption spectra of all three omp members are almost identical and very similar to that of benzene. An even closer similarity exists between the omp spectra and that of benzonitrile. This is as expected: Fluorine, according to our criterion, merely functions as a weak perturbation to the benzene ring.

---The 36,000cm^{-1} band ($^1L_b \leftarrow {}^1A$) is of lower intensity and slightly higher energy in the para-isomer. The 44,000cm^{-1} band ($^1L_a \leftarrow {}^1A$) is of slightly lower energy and slightly higher intensity in the para isomer. The details of these two transitions are collected in Table 1.

---The ^1L_a - ^1L_b band gap is quite large (7000cm^{-1}) for all three isomers but is smallest for the para-isomer.

---No evidence of new transitions to or from orbitals localized on the substituents (charge-transfer), or of $n \rightarrow \pi^*$ transitions is found at wavelengths greater than 200nm.

---Fluorescence is a "mirror image" of the 36,000cm^{-1} band ($^1L_b \leftarrow {}^1A$) in every case. The lifetimes and quantum yield data are also presented in Table 1. The intrinsic emissive lifetimes obtained from the fluorescence data are 50, 46 and 141ns for o, m and p, respectively. The same lifetimes obtained from absorption data[34] by assuming that fluorescence is the inverse of the lowest-energy absorption event, are 56, 57 and 180ns, respectively. It is concluded that the fluorescence is $^1L_b \rightarrow {}^1A$ in nature.

---The phosphorescence possesses more vibronic structure than the fluorescence. The triplet state, in all three isomers, may be assigned as ^3L_a because of its energetic similarity to the ^3L_a state of benzene (29,500cm^{-1}).

TABLE 1

FLUOROBENZONITRILE[a]

ABSORPTION AND EMISSION DATA

MOLECULE	$^1L_b \leftrightarrow {}^1A$ TRANSITION			$^1L_a \leftrightarrow {}^1A$	
	Absorption 0,0 energy (cm^{-1})	Emission 0,0 energy (cm^{-1})	Absorption ϵ (f)	0,0 energy (cm^{-1})	ϵ(f)
ϕCN	36,200	35,500	800(0.0093)	43,390	10160(.21)
o-FϕCN	35,590	35,000	1670(0.020)	43,570	8930(.18)
m-FϕCN	35,520	34,900	1700(0.020)	43,670	9860(.15)
p-FϕCN	36,540	35,750	310(0.005)	43,300	9000(.19)

LIFETIME (τ) AND QUANTUM YIELD (Φ) DATA

MOLECULE	τ_F(ns)	τ_P(s)	Φ_P	Φ_F	Φ_P/Φ_F
o-FϕCN	25.3	2.43	0.093	0.51	0.18
m-FϕCN	24.7	2.60	0.082	0.54	0.15
p-FϕCN	33.9	2.05	0.23	0.24	0.96

[a]Absorption measurements were made in ethanol at 298°K; emission studies were made in ethanol at 77°K. The experimental error is 50 cm^{-1}. The symbol ϵ refers to extinction coefficient (in ℓ $mole^{-1}cm^{-1}$) and the symbol f refers to oscillator strength. The subscripts P and F refer to phosphorescence and fluorescence, respectively.

---The larger Φ_P/Φ_F value for p-fluorobenzonitrile is the result of a greater rate constant for intersystem crossing (k_{ISC}) and a smaller rate constant for fluorescence (k_F), both of which act to produce a relative decrease of Φ_F in the p-isomer.

For further details on the fluorobenzonitriles, consult Lui and McGlynn[35].

2. CYANOANISOLES: The cyanoanisoles are moderately polar. The spectra of the omp triad are given in Figures 3 and 4. The following general observations may be made:

---The absorption spectra of o and m are similar but differ from that of P.

---The lowest-energy absorption band of p consists of at least two separate electronic transitions. These are partially resolved in a non-polar solvent. By comparison with p-fluorobenzonitrile, the low-energy "tail" of the lowest-energy absorption band may be assigned as $^1L_b \leftarrow {}^1A$, while the intense part of this band is assigned as $^1L_a \leftarrow {}^1A$. The details of these transitions are presented in Table 2.

---The primary difference between the spectra of o and m and that of p is an increase in energy and decrease in intensity of the $^1L_b \leftarrow {}^1A$ band in p, along with a decrease in energy and increase in intensity of the $^1L_a \leftarrow {}^1A$ band of p.

---In o and m, fluorescence is structured and is the mirror image of the lowest-energy absorption band. The intrinsic emissive lifetimes obtained from the fluorescence data are 19 and 23ns for o and m, respectively. The same lifetimes, calculated from absorption data on the assumption that fluorescence is the inverse of the

Figure 4.

The absorption spectra of o-, m-, and p-cyano-anisoles in methylcyclohexane at room temperature.

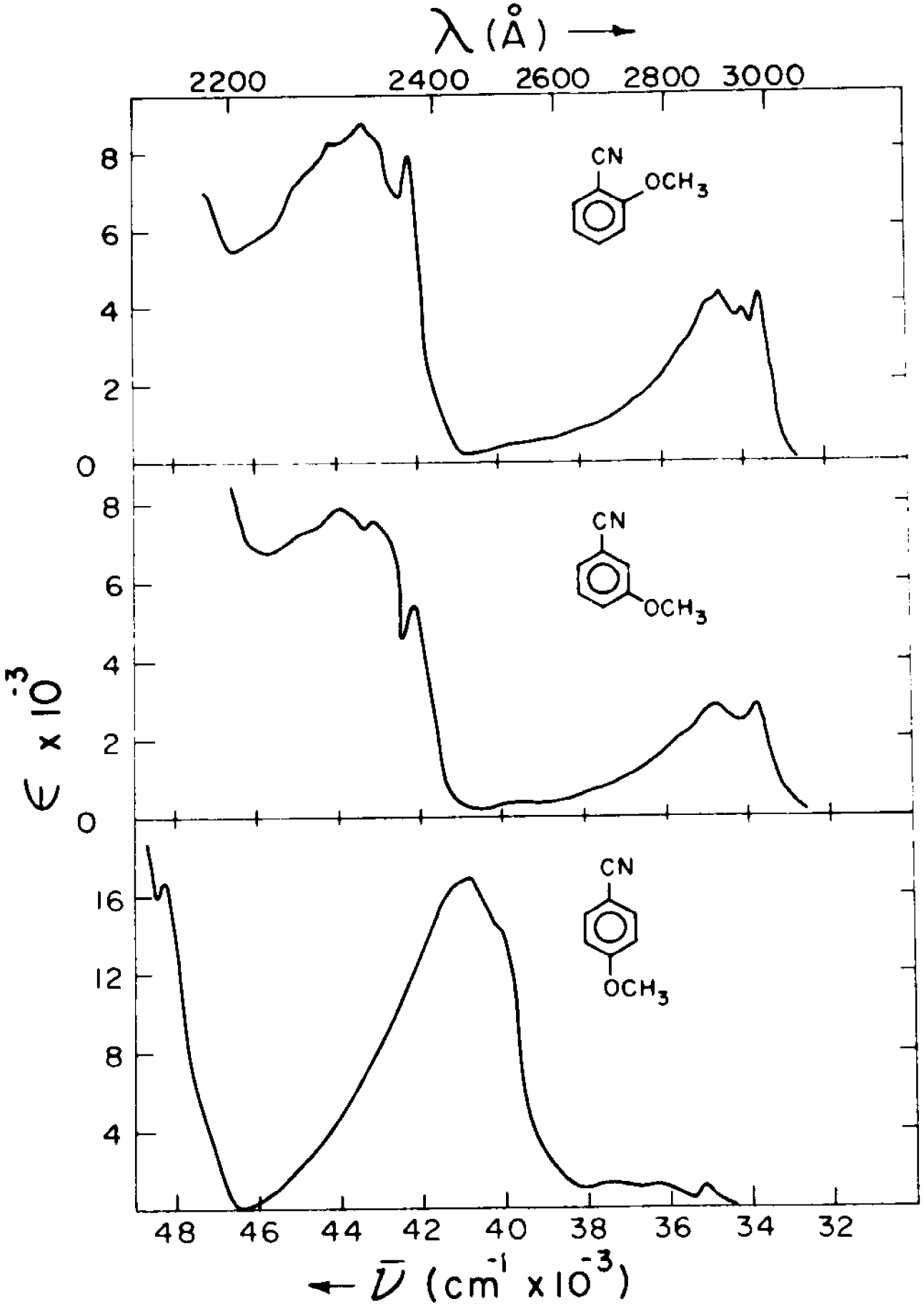
λ (Å) →
2200
2400
2600
2800
3000
CN
OCH3
CN
OCH3
CN
OCH3
ε x 10^-3
0
2
4
6
8
0
2
4
6
8
4
8
12
16
48
46
44
42
40
38
36
34
32
← ν̄ (cm^-1 x 10^-3)

Figure 4.

The total emission spectra of o-, m-, and p-cyanoanisoles in ethanol glass at 77°K. The spectra are corrected for all instrument parameters.

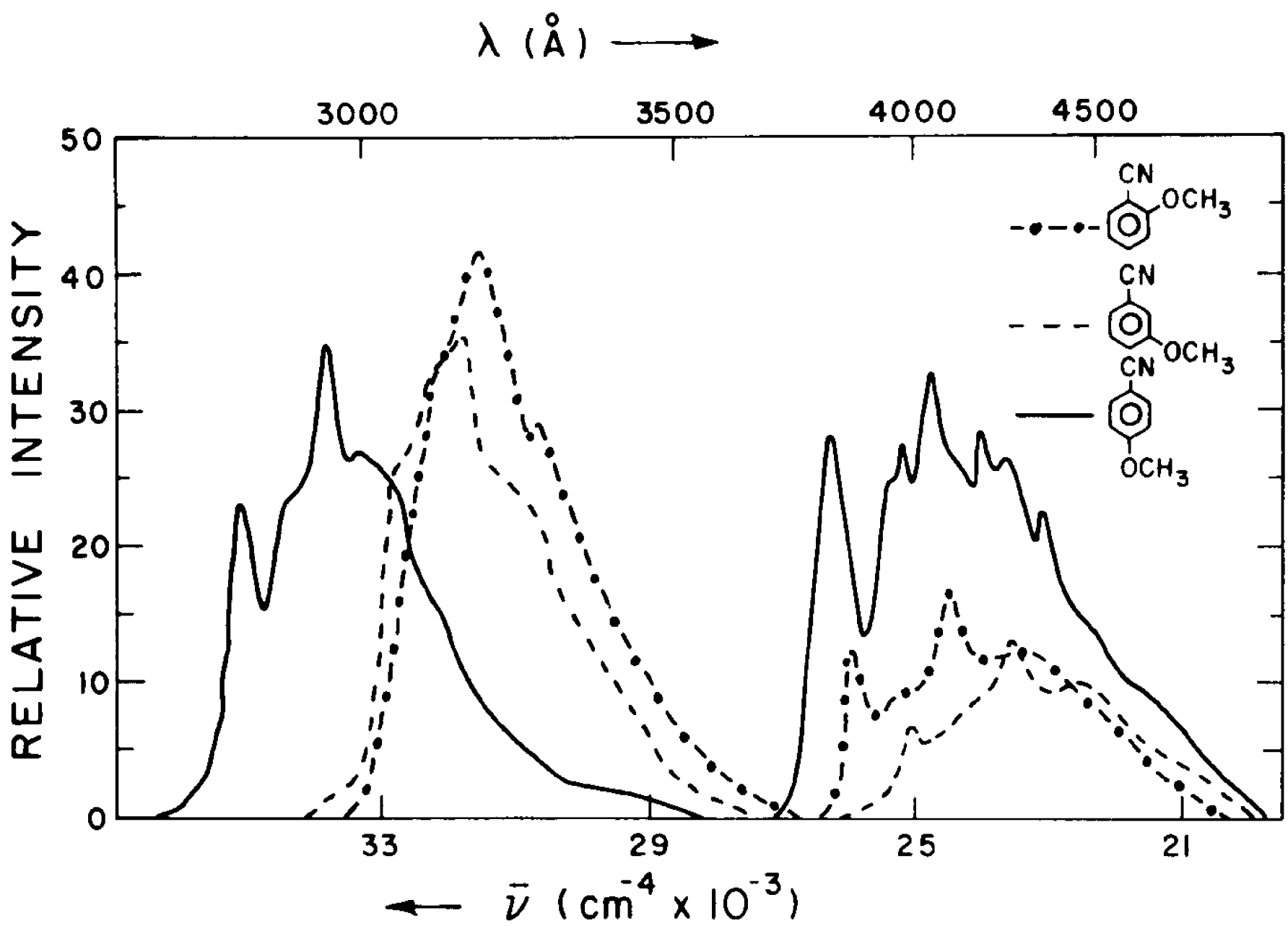
λ (Å) ⟶
3000
3500
4000
4500
50
40
30
20
10
0
RELATIVE INTENSITY
CN
OCH3
CN
OCH3
CN
OCH3
33
29
25
21
⟵ ν̄ (cm-4 x 10-3)

TABLE 2

CYANOANISOLE[a]

ABSORPTION AND EMISSION DATA

$^1L_b \leftrightarrow {}^1A$ TRANSITION

MOLECULE	Absorption 0,0 energy(cm^{-1})		Emission 0,0 energy(cm^{-1})		Absorption $\epsilon(f)$	
	MCH	Ethanol	MCH	Ethanol	MCH	Ethanol
o-CNΦOMe	33,560	33,900m	33,200	32,260	3,800(.047)	4,100(.054)m
m-CNΦOMe	33,700	33,600	33,000	32,600	2,680(.031)	2,600(.034)
p-CNΦOMe	35,200	35,340	~35,000 53,900m	35,200	1,030(.013)m	2,000(.024)

$^1L_a \leftrightarrow {}^1A$ TRANSITION

MOLECULE	Absorption		Absorption $\epsilon(f)$	
	MCH	Ethanol	MCH	Ethanol
o-CNΦOMe	42,200	42,020	6,500(.16)	7,220(.16)
m-CNΦOMe	42,020	43,480	4,820(.18)	7,220(.16)m
p-CNΦOMe	40,800m	40,150	16,700(.24)m	19,400(.31)m

LIFETIME (τ) AND QUANTUM YIELD (ϕ) DATA

MOLECULE	τ_F(ns)	τ_P(s)	Φ_P	Φ_F	Φ_P/Φ_F
o-CNΦOMe	5±2	1.4±0.2	0.11	0.26	0.42
m-CNΦOMe	5±2	1.8±0.2	0.094	0.21	0.45
p-CNΦOMe	7±2	1.6±0.2	0.24	0.22	1.0

[a]Absorption measurements were made at 25°C; emission studies were at 77° K. The experimental error is ±50 cm^{-1}. Energies marked by "m" refer to band maxima because of inability ro resolve the origin bands in these instances. The symbol "ε" refers to the extinction coefficient and the symbol "f" to the oscillator strength. Lifetime and quantum yield data

FOOTNOTE TO TABLE 2

refer to an ethanol solution. The subscripts P and F denote phosphorescence and fluorescence, respectively.

Figure 5.

The fluorescence, absorption, and fluorescence-excitation spectra for p-cyanoanisole in an ethanol glass at 77°K. The fluorescence spectrum is corrected; the fluorescence-excitation spectrum is not. Arrows refer the individual spectra to the appropriate scales.

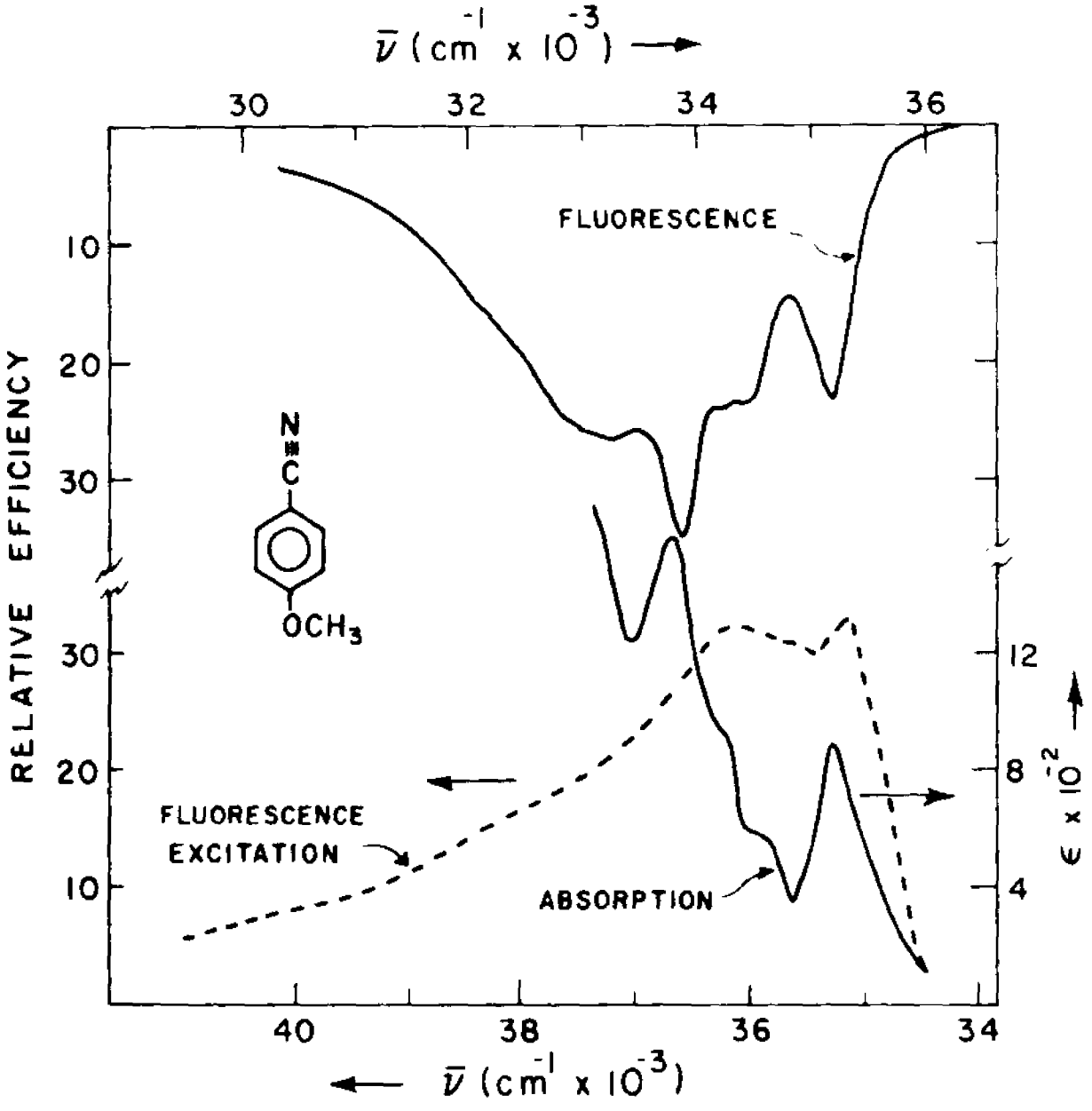
$\bar{\nu}$ (cm^{-1} x 10^{-3}) →
30
32
34
36
FLUORESCENCE
RELATIVE EFFICIENCY
10
20
30
N≡C
OCH3
30
20
10
FLUORESCENCE
EXCITATION
ABSORPTION
12
8
4
ε x 10^{-2}
40
38
36
34
← $\bar{\nu}$ (cm^{-1} x 10^{-3})

lowest-energy absorption band, are 24 and 34ns, respectively. It is concluded that the fluorescence of o and m is $^1L_b \rightarrow {}^1A$.

---For p, the situation is different (See Figure 5). The mirror image relationship now exists between the fluorescence and the low-energy "tail" of the lowest-energy absorption band. While the intrinsic emissive lifetime, obtained from fluorescence data is 32ns, that calculated from absorption data, assuming fluorescence to be the inverse of the whole lowest-energy absorption band, is ~2ns. This is clearly too low. The same lifetime, calculated by assuming that fluorescence is the inverse of the low-energy "tail" of the lowest-energy absorption band, is ~46ns. It is concluded that fluorescence is the inverse of the "tail" region of the lowest-energy absorption band and is $^1L_b \rightarrow {}^1A$. Lifetimes and quantum yields are presented in Table 2.

---Phosphorescence is vibronically structured, indicating that the T_1 state is less polar than either the ^1L_a or ^1L_b states.

---The Φ_P/Φ_F ratio is largest for the p-isomer because of the smaller value of k_F for this isomer.

For further details on the cyanoanisoles, consult Lui and McGlynn[36].

3. CYANOANILINES: The polarity of the cyanoanilines, while moderate, exceeds that of the cyanoanisoles. The spectra of the OMP triad are given in Figures 6 and 7. The following general observations may be noted:

---The absorption spectra of o and m are similar and not much affected by an increase of solvent polarity. The absorption spectrum of p is distinct from that of o and m and is more sensitive to solvent

Figure 6.

The absorption spectra of o-, m-, and p-cyanoanilines in ethanol (solid line) and in 3-methylpentane (dashed line) at room temperature.

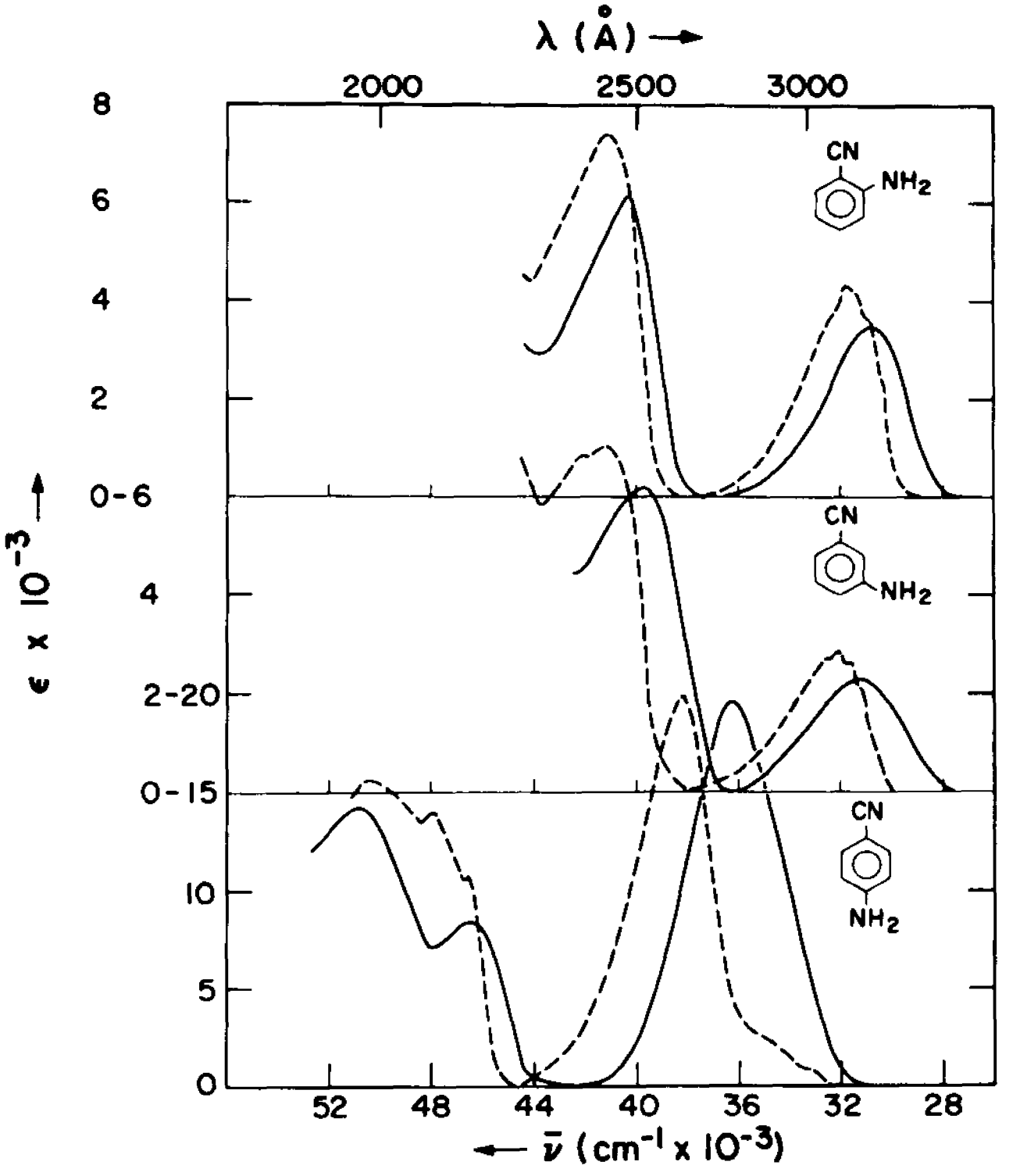
λ (Å) →
2000
2500
3000
8
6
4
2
0-6
4
2-20
0-15
10
5
0
ε x 10⁻³ →
CN
NH2
CN
NH2
CN
NH2
52
48
44
40
36
32
28
← ν̄ (cm⁻¹ x 10⁻³)

Figure 7.

The total luminescence spectra of o-, m-, and p-cyanoanilines in ethanol at 77°K. The spectra are corrected for all instrumental parameters.

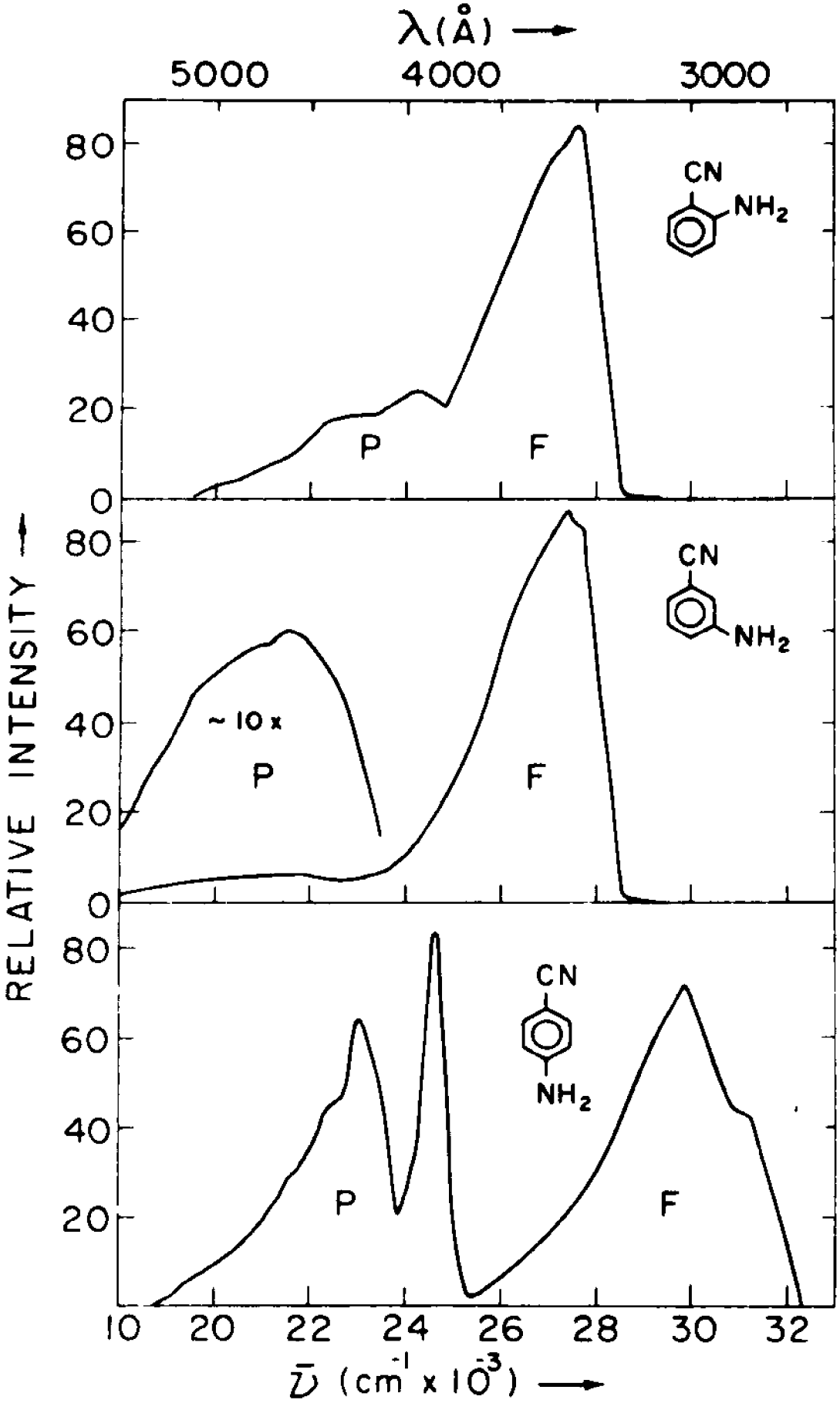
λ(Å) →
5000
4000
3000
RELATIVE INTENSITY →
80
60
40
20
0
CN
NH2
P
F
~ 10 x
10
20
22
24
26
28
30
32
ν̄ (cm⁻¹ x 10⁻³) →

polarity.

---The low-energy absorption band of p consists of at least two separate electronic transitions. These are partially resolved in non-polar solvents. In 3-methyl pentane (3MP), the lowest-energy band maximizes at ~34,500cm^{-1} and consists primarily of $^1L_b \leftarrow {}^1A$. The band that maximizes at 38,000cm^{-1} corresponds to $^1L_a \leftarrow {}^1A$ and has an increased charge-transfer character (vide infra). Details are collected in Table 3.

---The primary differences between the spectra of o and m and that of p is a decrease in energy and increase in intensity of $^1L_a \leftarrow {}^1A$ in p and an increase in energy and decrease in intensity of $^1L_b \leftarrow {}^1A$ in p. Thus, in comparison to the weakly-polar p-fluorobenzonitrile, in which the $^1L_b \leftarrow {}^1A$ transition is still distinct, the $^1L_b \leftarrow {}^1A$ transition of p-cyanoaniline in a polar solvent is completely occluded by the $^1L_a \leftarrow {}^1A$ transition.

---As a result of the large charge-transfer character (See Computational Results) of the $^1L_a \leftarrow {}^1A$ transition of p, this transition is very sensitive to solvent polarity. Thus, the $^1L_a \leftarrow {}^1A$ transition of p exhibits a larger energy decrement on going from non-polar to polar solvent than does the $^1L_b \leftarrow {}^1A$ transition.

---The fluorescence spectra of o, m and p exhibit little or no vibronic structure (when compared to the fluorescence spectra of the weakly-polar fluorobenzonitriles and the moderately-polar cyanoanisoles). In part, this may be attributable to the near degeneracy of the ^1L_a and ^1L_b states in the cyanoanilines but, more probably, it reflects the increased solvent-solute and solute-solute interactions in the more-polar cyanoanilines.

TABLE 3

CYANOANILINES[a]

ABSORPTION AND EMISSION DATA

$^1L_b \leftarrow {}^1A$ TRANSITION

	Absorption Energy (cm^{-1})		Emission Energy (cm^{-1})	Absorption Intensity	
	0.0	Maximum	Maximum	ϵ_{max}(f)	
	3MP	Ethanol	Ethanol	3MP	Ethanol
o-CNϕNH$_2$	~30,440	30,750	27,600	4,330(0.062)	3,450(0.055)
m-CNϕNH$_2$	30,900	31,200	27,500	2,860(0.042)	2,350(0.042)
p-CNϕNH$_2$	33,000	---	30,000	2,350(0.038)	---

$^1L_a \leftarrow {}^1A$ TRANSITION

	Absorption Energy (cm^{-1})		Absorption Intensity	
	Band Maximum		ϵ_{max}(f)	
	3MP	Ethanol	3MP	Ethanol
o-CNϕNH$_2$	41,200	40,300	7,460(0.17)	6,110(0.11)
m-CNϕNH$_2$	41,200	39,700	7,050(0.20)	6,220(0.16)
p-CNϕNH$_2$	38,200	36,200	19,900(0.30)	19,600(0.37)

LIFETIME (τ) AND QUANTUM YIELD (Φ) DATA

	τ_F(ns)	τ_F^o(ns)		τ_P(s)	Φ_F	Φ_P	Φ_P/Φ_F
		Abs.	Em.				
o-CNϕNH$_2$	6.9	22[b]	22	3.65	0.31	0.096	0.31
m-CNϕNH$_2$	12.9	22[b]	15	2.65	0.87	0.047	0.054
p-CNϕNH$_2$	3.3	27[b]	33	2.45	0.15	0.11	0.73

FOOTNOTE TO TABLE 3

[a]Absorption measurements were made at 298°K; emission studies were made in ethanol at 77°K. The experimental error is ±50 cm^{-1}. The symbol ε denotes the extinction coefficient (in $\ell\ mole^{-1}cm^{-1}$) and f denotes the oscillator strength. The subscripts F and P denote fluorescence and phosphorescence, respectively.

[b]The absorption data used here refer to glassy ethanol solutions at 77°K.

---The absorption and fluorescence spectra of p do not exhibit a mirror image relationship (See Figure 8). The vibronic intervals (800 and 1200cm^{-1}) which occur in the fluorescence spectrum, however, also appear in the low energy "tail" of the lowest-energy absorption band, and suggest that fluorescence is the inverse of the $^1L_b \leftarrow {}^1A$ absorption. This conclusion is substantiated by the large half-width of the lowest-energy absorption band (~4500cm^{-1}) relative to that of the fluorescence band (~3000cm^{-1}). Finally, the intrinsic fluorescence lifetime calculated from the absorption data, assuming fluorescence to be the inverse of the low energy "tail", is ~27ns, and is in good agreement with the observed value of 33ns. In contrast, the intrinsic radiative lifetime calculated by assuming that fluorescence is the inverse of the entire lowest-energy band is ~2ns. The luminescence lifetimes and quantum yield data are given in Table 3.

---The diffuseness of the fluorescence spectra prohibits any mirror image correlations for o and m. Nonetheless, the half-widths of the fluorescence and the lowest-energy absorption ($^1L_b \leftarrow {}^1A$) bands are almost identical (~3000cm^{-1}). In addition, the intrinsic emissive lifetimes (22 and 15ns, respectively) agree well with those calculated from absorption data (~22ns in both cases) by assuming the fluorescence to be the inverse of the whole lowest-energy absorption band.

---The increased vibronic structure of the phosphorescence spectrum of p as compared to the fluorescence spectrum, indicates that the T_1 state is less-polar than the ^1L_b state.

---As is the case for the fluorobenzonitriles and the cyanoanisoles, the Φ_P/Φ_F ratio is largest for p. Again, this is primarily attributed to a larger k_{ISC} and a smaller k_F for p than for either

Figure 8.

The fluorescence and absorption spectra of p-cyano aniline at 77°K. The fluorescence spectrum is for glassy ethanol solution and is corrected. The absorption spectrum was obtained in an EPA glass at 77°K. The mirror plane is supposed to lie at 31750 cm^{-1} and is denoted by a vertical line.

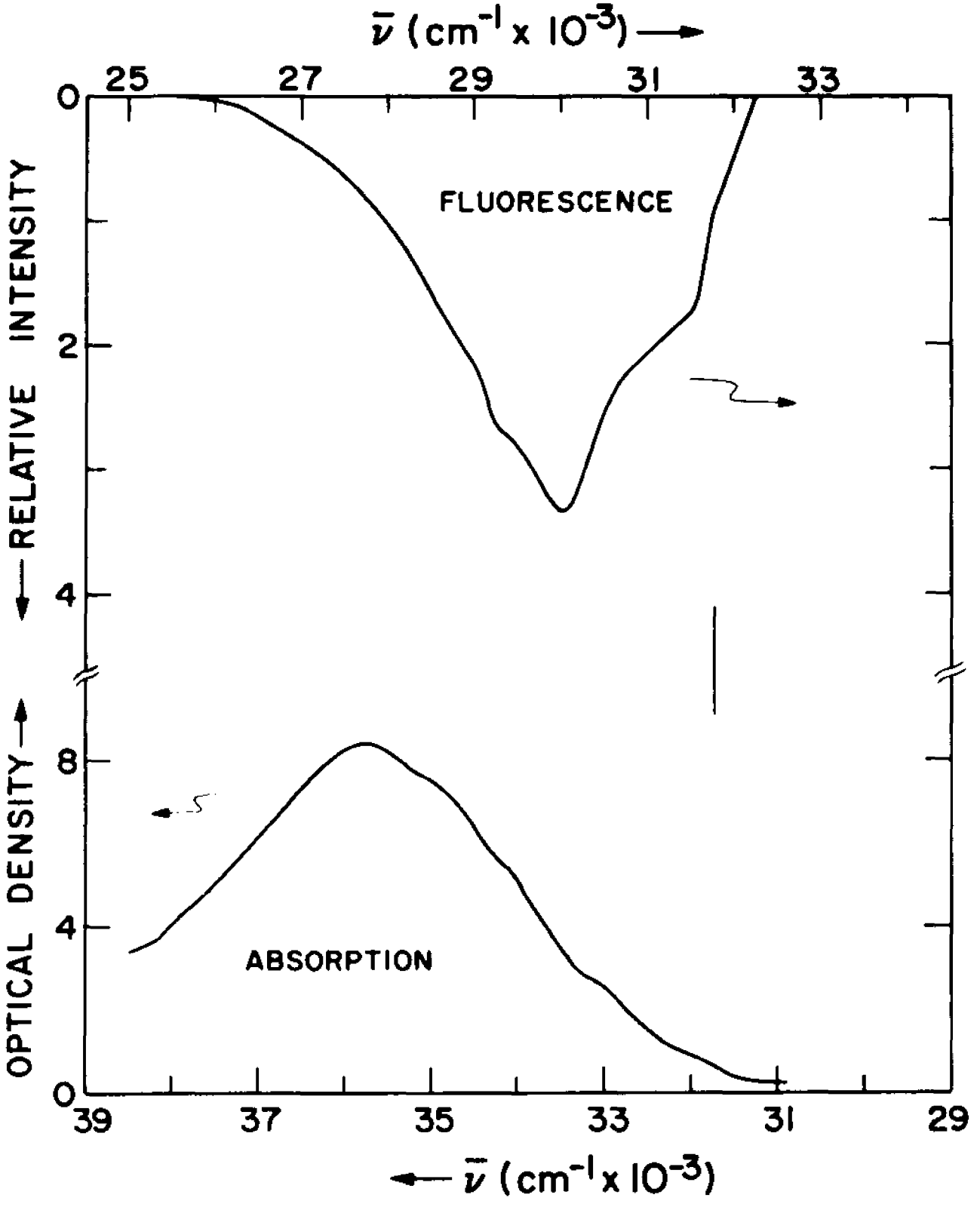
$\bar{\nu}$ (cm^{-1} x 10^{-3}) →
25
27
29
31
33
0
2
4
← RELATIVE INTENSITY
FLUORESCENCE
OPTICAL DENSITY →
8
4
0
39
37
35
33
31
29
← $\bar{\nu}$ (cm^{-1} x 10^{-3})
ABSORPTION

o or m. For further details, see Lui and McGlynn[37].

4. AMINOACETOPHENONES: The aminoacetophenones are relatively polar. Their spectra are given in Figures 9 and 10. The following results may be noted:

---The absorption spectra of o and m are quite similar but different from that of p.

---The lowest-energy absorption bands ($^1L_b \leftarrow {}^1A$) of o and m are quite similar but different from that of p.

---The lowest-energy absorption bands ($^1L_b \leftarrow {}^1A$) of o and m are structureless in ethanol and 3MP. The lowest-energy absorption band of p is much more intense than that of either o or m, and it is also structureless in ethanol solution. In 3MP solution, however, a weakly structured edge is observed on the low-energy "tail" of this band (Figure 9). This low-energy "tail" lies at ~29,400cm^{-1} and is assigned as the $^1L_b \leftarrow {}^1A$.

---Apart from the "tail" region, the lowest-energy absorption band in p maximizes at 35,090cm^{-1} in 3MP, and is assigned as the $^1L_a \leftarrow {}^1A$ transition. On the basis of correlative arguments (vide infra), the 40,000cm^{-1} band of o and m is assigned as $^1L_a \leftarrow {}^1A$.

---The 44,000cm^{-1} band in o and m and the 43,000cm^{-1} and 51,000cm^{-1} bands of p must be assigned to transitions other than ^1L_a, $^1L_b \leftarrow {}^1A$. These, presumably, involve π^* excited states of ^1B_a and ^1B_b symmetries. The details of the S_3, ^1L_a, $^1L_b \leftarrow {}^1A$ transitions are collected in Table 4.

---o and m exhibit broad structureless fluorescences with a half-band-width of ~4000cm^{-1}. The half-band-width of the lowest-energy absorption is also ~4000cm^{-1}, and an approximate mirror image rela-

Figure 9.

The absorption spectra of o-, m-, and p-aminoacetophenones in ethanol (solid line) and 3-methylpentane (dashed line) at room temperature.

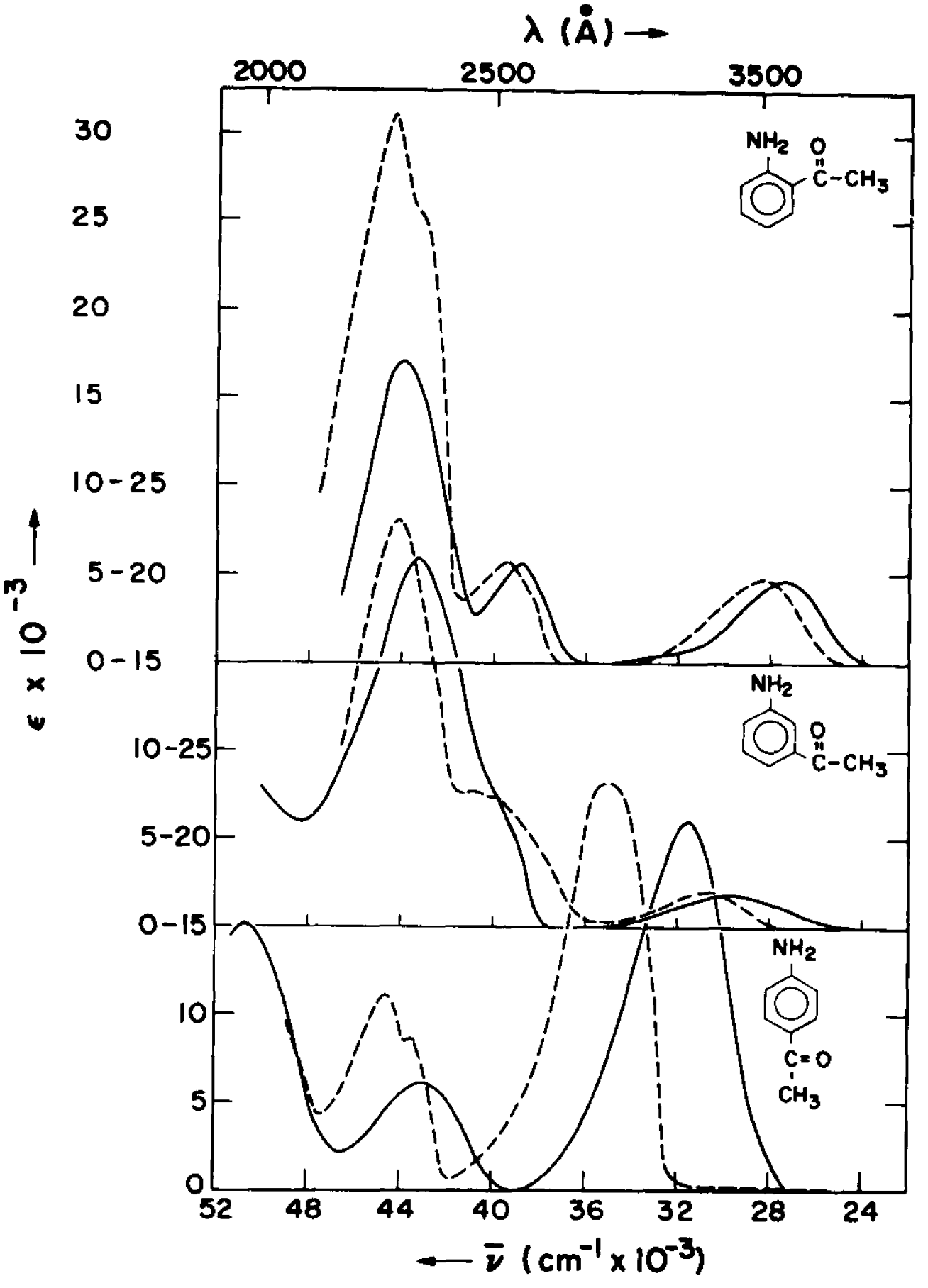
λ (Å) →
2000
2500
3500
30
25
20
15
10-25
5-20
0-15
ε x 10⁻³ →
NH2
O
C-CH3
10-25
5-20
0-15
10
5
0
C=O
CH3
52
48
44
40
36
32
28
24
← ν̄ (cm⁻¹ x 10⁻³)

Figure 10.

The total luminescence spectra of o-, m-, and p-amino-acetophenones in an ethanol glass at 77°K. The spectra are corrected for all instrumental parameters.

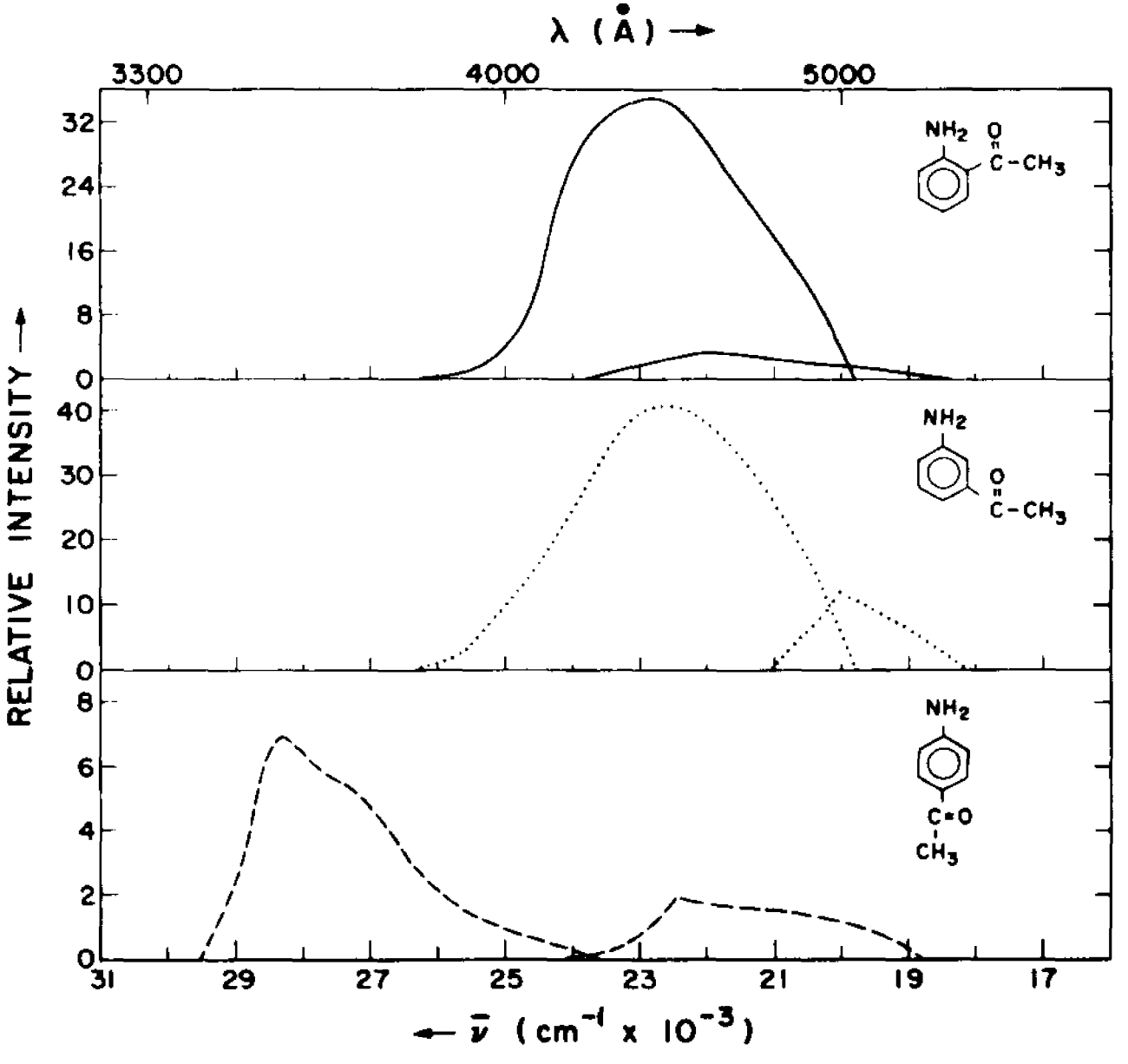
λ (Å) →
3300
4000
5000
RELATIVE INTENSITY →
32
24
16
8
0
40
30
20
10
0
8
6
4
2
0
NH2
O
C-CH3
NH2
O
C-CH3
NH2
C=O
CH3
31
29
27
25
23
21
19
17
← ν̄ (cm-1 x 10-3)

TABLE 4

AMINOACETOPHENONES[a]

ABSORPTION AND EMISSION DATA

$^1L_b \leftrightarrow {}^1A$ TRANSITION

	Absorption (Maximum) Energy(cm^{-1})		Emission (Maximum) Energy(cm^{-1})	Absorption $\epsilon_{max}(f)$
	3MP	Ethanol	Ethanol	3MP
o-$NH_2\phi COCH_3$	28,410	27,400	22,800	4,770(0.083)
m-$NH_2\phi COCH_3$	30,770	29,500	22,600	2,000(0.033)
p-$NH_2\phi COCH_3$	~29,900	---	28,300	160(0.0012)

$^1L_a \leftarrow {}^1A$ TRANSITION

	Absorption (Maximum) Energy(cm^{-1})		Absorption $\epsilon_{max}(f)$	
	3MP	Ethanol	3MP	Ethanol
o-$NH_2\phi COCH_3$	39,530	38,800	5,710(0.098)	5,590(0.072)
m-$NH_2\phi COCH_3$	40,820	39,000	7,710(0.16)	6,580(0.11)
p-$NH_2\phi COCH_3$	35,090	31,500	23,210(0.42)	21,060(0.44)

$S_3 \leftarrow S_o$ TRANSITION

	Absorption (Maximum) Energy(cm^{-1})		Absorption $\epsilon_{max}(f)$	
	3MP	Ethanol	3MP	Ethanol
o-$NH_2\phi COCH_3$	44,400	43,960	30,980(0.62)	17,170(0.25)
m-$NH_2\phi COCH_3$	44,050	43,290	23,030(0.42)	20,920(0.47)
p-$NH_2\phi COCH_3$	44,640	42,920	11,190(0.21)	6,220(0.12)

TABLE 4 (continued)

LIFETIME (τ) and QUANTUM YIELD (ϕ) DATA

MOLECULE	τ_F(ns)	τ_P(s)	Φ_F	Φ_P	Φ_P/Φ_F
o-$NH_2\phi COCH_3$	11.7	0.056	0.58	0.079	0.14
m-$NH_2\phi COCH_3$	32.0	0.23	0.82	0.11	0.13
p-$NH_2\phi COCH_3$	~53	0.72	0.11	0.14	1.3

[a]Absorption measurements were made at 298°K; emission studies were made at 77°K. The experimental error is 50 cm^{-1}, ϵ is the molar decadic absorption coefficient and f is the oscillator strength. The subscripts P and F refer to phosphorescence and fluorescence, respectively.

tionship to fluorescence does exist in both cases. The intrinsic radiative lifetimes, from fluorescence data, are 20 and 38ns for o and m, respectively. The same lifetimes obtained from absorption data for the lowest-energy absorption band are 24 and 38ns, respectively. We conclude that the fluorescences of o and m are $^1L_b \rightarrow {}^1A$.

---Again, however, the situation is different for p (See Figure 11). The fluorescence is not a mirror image of the entire lowest-energy band of the 300°K absorption spectrum. It can, however, be viewed as the inverse of the low-energy "tail" of the lowest-energy absorption process. The intrinsic emissive lifetime, from the fluorescence data, is ~480ns. That calculated from absorption data, assuming that the fluorescence is the inverse of the entire lowest-energy band, is ~4ns. The same lifetime, calculated by assuming the fluorescence to be the inverse of the low-energy "tail" is ~1080ns. While this last value is deviant by a factor of two, we think this unimportant because of the indeterminacy involved in separating the "tail" region from the main portion of the lowest-energy band. One may conclude[38] that the lowest-energy absorption band consists of two electronic transitions, that only a small part of its oscillator strength is due to the $^1L_b \leftarrow {}^1A$ excitation, and that the majority of its oscillator strength is conferred by the $^1L_a \leftarrow {}^1A$ transition.

---Yamaguchi *et al.*[39], have reported the absorption spectrum of p in ethanol at 77°K. They find that there exists a good mirror image relationship between the entire lowest-energy absorption band and the fluorescence spectrum. The lowest-energy absorption band undergoes a red-shift upon decreasing the temperature to 77°K, and the low-energy "tail" is no longer observed. In non-polar solvents, fluorescence

Figure 11.

The fluorescence and absorption spectra of p-amino-acetophenone. The fluorescence refers to an ethanol glass at 77°K. The absorption refers to a 3-methyl-pentane solution at room temperature. The mirror plane position is indicated by a vertical line.

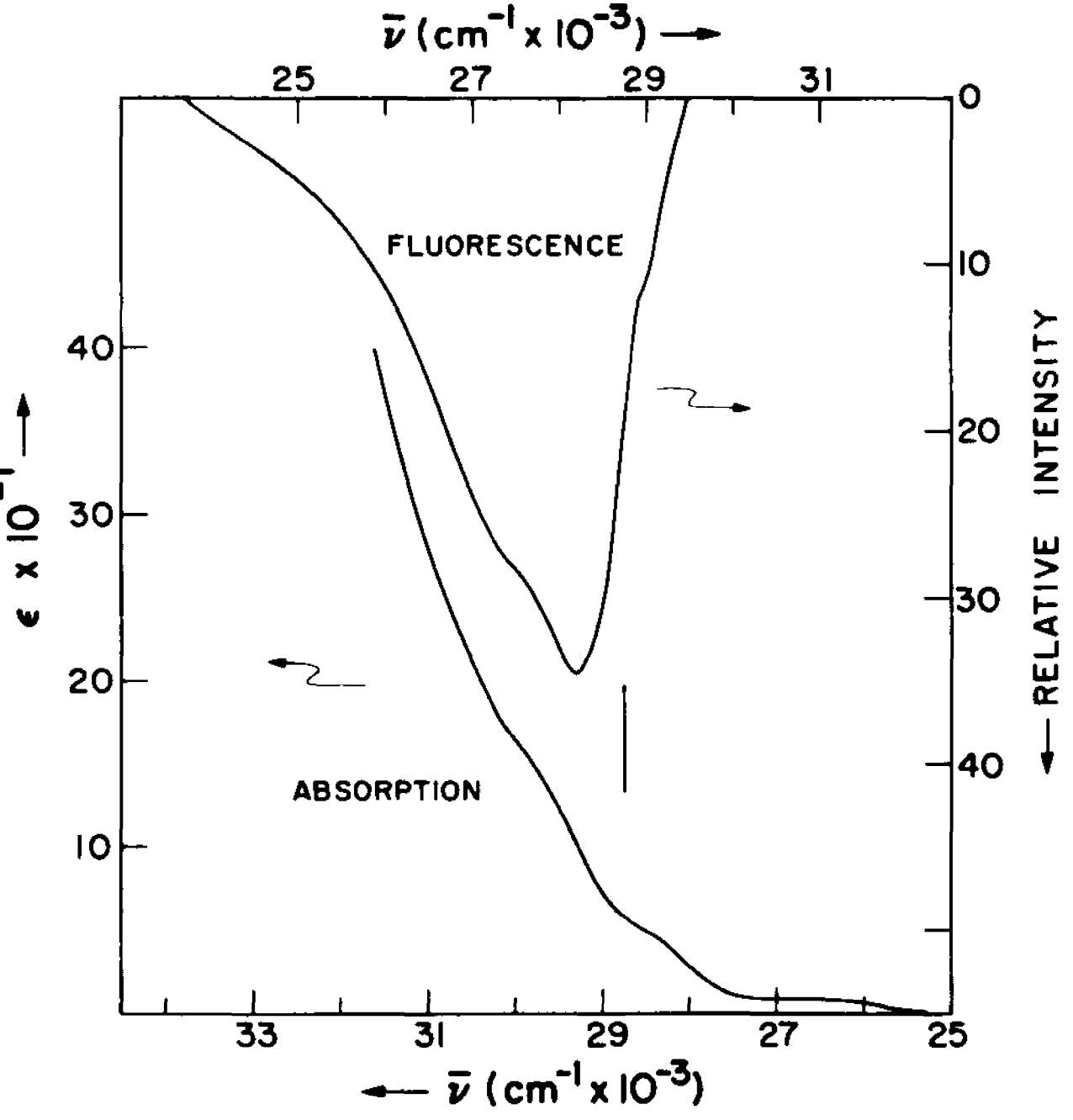
$\bar{\nu}$ (cm^{-1} x 10^{-3}) →
25
27
29
31
0
10
20
30
40
FLUORESCENCE
ABSORPTION
ε x 10^{-1} →
← RELATIVE INTENSITY
33
31
29
27
25
← $\bar{\nu}$ (cm^{-1} x 10^{-3})

was found to be weak and to be observable only when the exciting wavelength was that of the low-energy absorption "tail". While phosphorescence is observed at 77°K, both in polar and in non-polar solvents, the excitation spectra for fluorescence and phosphorescence are not identical in either the polar or non-polar media. They also found that the phosphorescence excitation spectrum in non-polar solvent corresponds to the low-temperature absorption spectrum in non-polar solvent, while the fluorescence excitation spectrum in polar solvent bears some similarity to the low-temperature absorption spectrum in polar solvents. These authors assign the low-energy absorption "tail" as an $n \rightarrow \pi^*$ transition and the lowest-energy absorption band as $\pi \rightarrow \pi^*$. Their results are both surprizing and confusing. We will return to them later.

---A summary of emissive lifetimes and quantum yields is given in Table 4. The Φ_P/Φ_F ratio for p is ~10 times that of either o or m. The primary cause of this effect is that k_F for P is smaller than that for either o or m. The comparatively high-energy of the T_1 state of o and its low radiative lifetime is attributed to a sterically-induced non-planarity between the ring and the substituent systems. For further details, see Lui and McGlynn[38].

5. NITROANILINES: The nitroanilines are highly-polar. Their spectra are shown in Figures 12 and 13. The following general observations may be made:

---The absorption spectra of o and m are similar but differ greatly from that of p.

---The lowest-energy band is distinct in all three isomers while the higher-energy bands exhibit considerable overlapping.

Figure 12.

The absorption spectra of the nitroanilines: (a) in methylcyclohexane at room temperature and (b) in an EPA glass at 77°K.

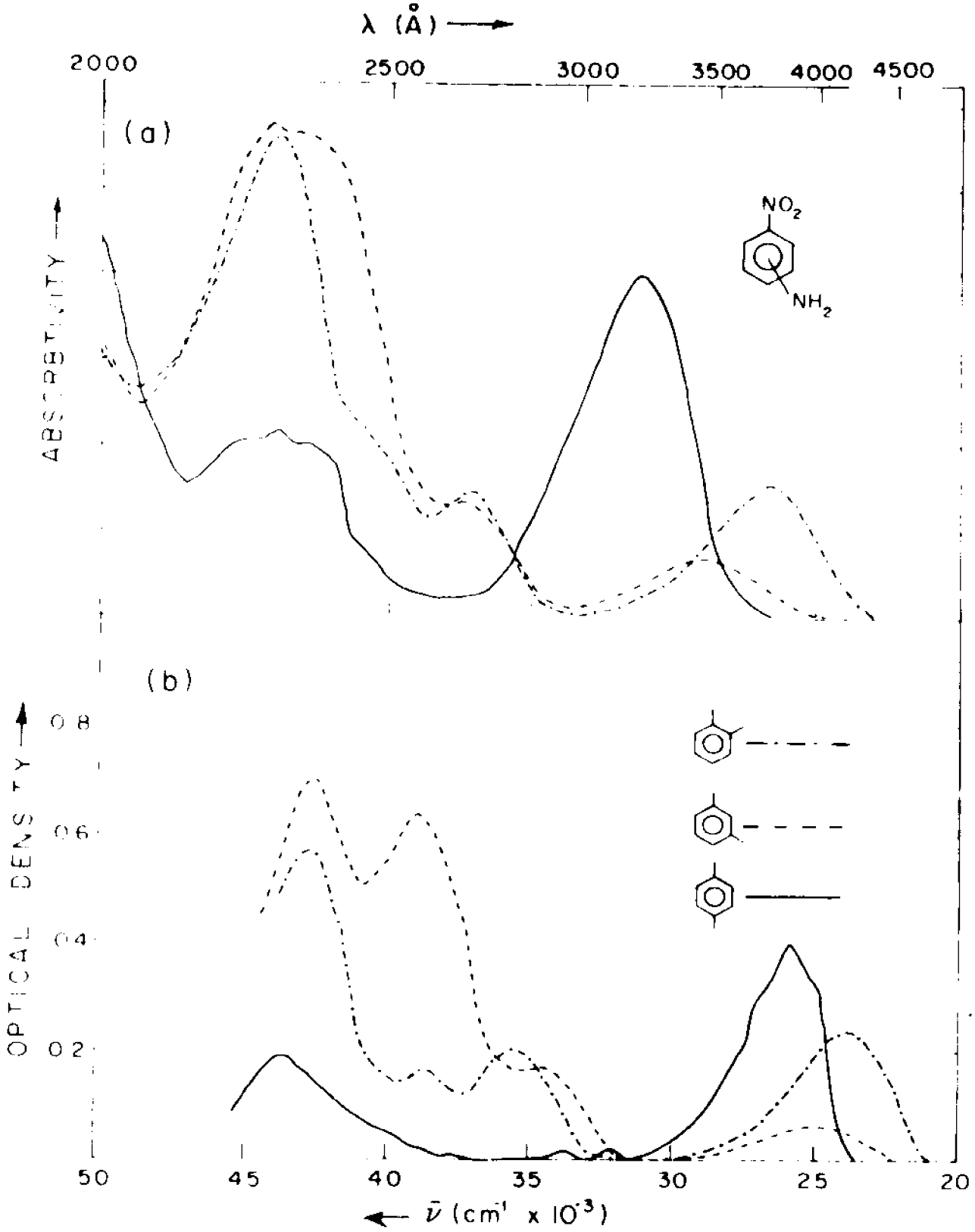
λ (Å) ⟶
2000
2500
3000
3500
4000
4500
(a)
ABSORBANCY ⟶
NO2
NH2
(b)
OPTICAL DENSITY ⟶
0.8
0.6
0.4
0.2
50
45
40
35
30
25
20
ν̄ (cm⁻¹ x 10⁻³) ⟵

Figure 13.

The corrected emission spectra of o-, m-, and p-nitroanilines in EPA glass at 77^{0}K. The total emission of the p-isomer (dashed line) consists solely of phosphorescence, that of the o- (solid line) and m- (dotted line) derivitives consist solely of fluorescence.

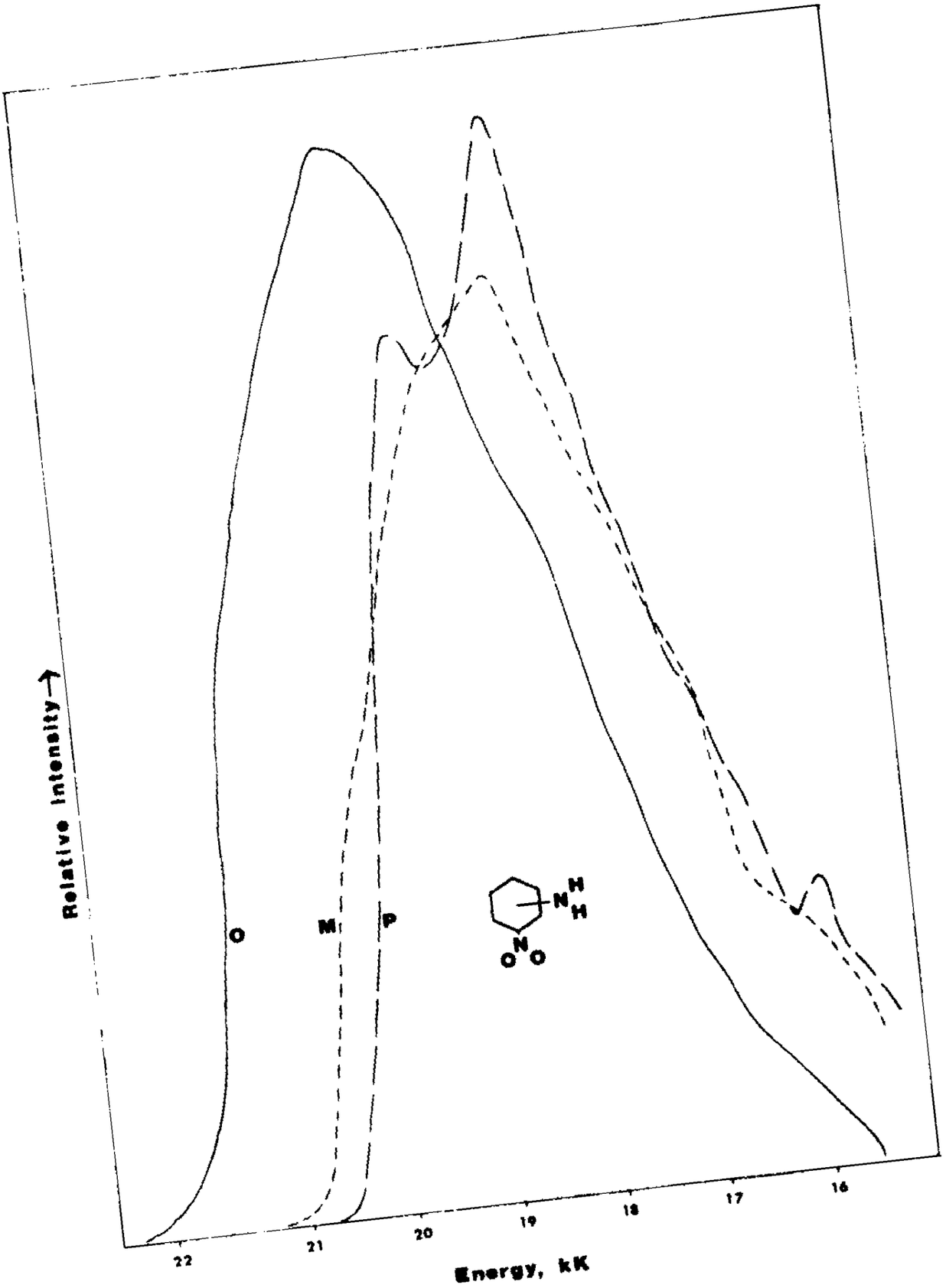
Relative Intensity
O
M
P
22
21
20
19
18
17
16
Energy, kK

---There is a general increase in structure, accompanied by significant band shifts, on going from a non-polar solvent at 300°K to a polar, glassy medium at 77°K. The lowest-energy absorption band undergoes the largest decrease in energy on going to a polar medium: o ($2700cm^{-1}$), m($3700cm^{-1}$) and p($5200cm^{-1}$). Data are collected in Table 5.

---The large solvent-induced red-shift of the lowest-energy absorption band of p uncovers a structured region with apparent origin at $33,000cm^{-1}$. This region is relatively insensitive to solvent polarity or to the degree of N-methylation. A shoulder at $33,000cm^{-1}$ has been detected previously by Tanaka[40,41] in the crystal spectrum of p and assigned as $^1\Gamma_{n\pi^*} \leftarrow {}^1\Gamma_1$. However, the intensity ($\epsilon \approx 1500\,\ell\,mole^{-1}cm^{-1}$) of this transition, coupled with the absence of solvent effects, tends to discredit this assignment. It has been suggested by El-Aassar[42] that this transition is $^1L_b \leftarrow {}^1A$ in nature, and we tend to agree with this assignment (vide infra). However, since no polarization data exist, no rigorous discrimination between $^1\Gamma_{n\pi^*} \leftarrow {}^1\Gamma_1$ or $^1\Gamma_{\pi\pi^*} \leftarrow {}^1\Gamma_1$ assignments is feasible.

---Electrodichroic[43] and solvatochromic[44] studies indicate that the $31,000cm^{-1}$ absorption band (non-polar solvent) of p consists of two electronic transitions; one of these is intense and long-axis polarized, while the other is weaker and short-axis polarized. A similar situation has been found[43] in the corresponding $28,000cm^{-1}$ band of N,N-dimethyl-p-nitroaniline(NNDMPNA).

---The luminescence of the nitroanilines may be summarized as follows:

(i) o and m fluoresce but do not phosphoresce.

TABLE 5

NITROANILINES[a]

ABSORPTION DATA

	Band Maximum(cm^{-1})		ϵ_{max}(f)
	MCH	EPA	MCH
o-Nitroaniline	26,500	23,800	4,800(0.11)
	37,000	35,500	4,600(0.1)
	40,500	38,700	7,000
	43,800	42,700	17,750
m-Nitroaniline	28,700	25,000	2,200(0.04)
	37,200	43,500	4,200(0.08)
	42,000	38,700	17,250
	44,000	42,600	18,200
p-Nitroaniline	31,000	25,970	12,600(0.32)
	33,000-36,000	32,520	1,500
	41,000	40,000	2,500
	45,500	43,700	6,500

[a]The extinction coefficient is denoted ϵ and is cited in units of ℓ $mole^{-1}cm^{-1}$; the oscillator strengths are denoted f; EPA spectra were run at 77°K; methylcyclohexane spectra were run at 300°K.

(ii) p phosphoresces but does not fluoresce in non-polar media.

(iii) A fluorescence of p is induced in polar media, and its intensity in enhanced by an increase of the solvent polarity.

(iv) The quantum yield ratio, Φ_P/Φ_F, of p depends, in certain polar media, on the excitation energy.

For further details, see Khalil et al.[7]

6. A SUMMARY OF SERIES A DATA: Certain trends are evident in the behavior of the five triad of Sections II.A.1-5. We now list these trends:

(i) As molecular dipolarity increases, the $^1L_a \leftarrow {}^1A$ absorption band of p decreases drastically in energy and increases in intensity. The $^1L_b \leftarrow {}^1A$ absorption band of p also decreases in energy, but less dramatically; and it also loses intensity. As a result, the ^1L_a-^1L_b band gap of p, which may be as large as 12kK in a weakly-polar species, can even become negative (i.e., $E(^1L_a) < E(^1L_b)$) in a highly-polar species. Thus, $\Delta E(^1L_a - {}^1L_b)$ decreases and $f(^1L_a \leftarrow {}^1A)/f(^1L_b \leftarrow {}^1A)$ increases with increasing molecular dipolarity.

(ii) In o and m, the $^1L_a \leftarrow {}^1A$ and $^1L_b \leftarrow {}^1A$ absorption bands are less sensitive to molecular dipolarity. In o, the $^1L_a \leftarrow {}^1A$ energy decreases by ~6000cm^{-1} on proceeding from a weakly- to a highly-polar molecule. However, the $^1L_b \leftarrow {}^1A$ energy appears to be a more sensitive function of the molecular dipolarity, with the result that $\Delta E(^1L_a - {}^1L_b)$, which usually lies in the range 8-12kK, tends to increase slightly with increasing molecular dipolarity. $f(^1L_a \leftarrow {}^1A)$ is erratic but does tend to increase; $f(^1L_b \leftarrow {}^1A)$ exhibits a definite increase, with the result that $f(^1L_a \leftarrow {}^1A)/f(^1L_b \leftarrow {}^1A)$, which usually lies in the range 1-10, tends to decrease as the molecular dipolarity increases.

(iii) The behavior of m is very similar to o. Both the $^1L_a \leftarrow {}^1A$ and $^1L_b \leftarrow {}^1A$ energies decrease with increasing molecular dipolarity, the latter being the more sensitive. As a result, $\Delta E(^1L_a - {}^1L_b)$, which usually lies in the range 9-10kK and whose behavior is somewhat erratic, tends to increase with increasing polarity. $f(^1L_a \leftarrow {}^1A)$ either remains constant or decreases slightly; $f(^1L_b \leftarrow {}^1A)$ exhibits a decided increase, with the result that $f(^1L_a \leftarrow {}^1A)/f(^1L_b \leftarrow {}^1A)$---which, where measureable, lies in the 2.5-8 range --- tends to decrease with increasing dipolarity.

(iv) Solvent effects are much greater in the more polar molecules and, within a given triad, for the p-isomer.

(v) In weakly-polar p, the $^1L_b \rightarrow {}^1A$ fluorescence process is more probable than the $^3L_a \rightarrow {}^1A$ phosphorescence. The inverse is true in highly-polar molecules. When the molecular polarity is so high that $\Delta E(^1L_a - {}^1L_b) < 0$, a second reversal occurs and the luminescence is dominantly fluorescence (i.e., $^1L_a \rightarrow {}^1A$).

(vi) The behavior of Φ_P/Φ_F in o and m is erratic but it does exhibit a clear-cut tendency to decrease as the molecular polarity increases. The fluorescence and phosphorescence events can be described, in all instances, as $^1L_b \rightarrow {}^1A$ and $^3L_a \rightarrow {}^1A$, respectively.

These conclusions, while based on a good data set, suffer from the fact that this data set is small. We now attempt to verify these conclusions using a much larger but more qualitative data set.

B. SERIES B AND C.

1. p-ISOMERS: The data set consists of Tables 1-5 as amplified by the more voluminous but less accurate data of Tables 6 and 7.

The p-amino series exemplifies a type B series: The amino group is held constant while the acceptor is varied. The absorption and emission energies for five such molecules are plotted in Figure 14, the molecules being arranged from left to right in order of increasing molecular polarity. It is obvious that the energetic characteristics of the ^1L_a and ^1L_b states agree with point (i) of our summary, Section III.A.6.

When the molecular polarity reaches that of p-aminobenzoic acid, the $^1L_a \leftarrow {}^1A$ and $^1L_b \leftarrow {}^1A$ bands have merged. At this point we assign the lowest-energy absorption band as $^1L_a \leftarrow {}^1A$ since this transition surely constitutes the dominant intensity component of the band. One must bear in mind, however, that the lowest-energy excited singlet state could still be the very weak $^1L_b \leftarrow {}^1A$ transition. Finally, when the polarity has increased to that of p-nitroaniline, fluorescence disappears entirely and phosphorescence dominates the luminescence spectrum.

The p-cyano series exemplifies a Type C series. Data for this series are diagrammed in Figure 15. The ^1L_a state declines in energy more rapidly than does the ^1L_b state; and the two bands merge when molecular polarity has reached that of the p-cyanophenoxide anion. The dominance of phosphorescence over fluorescence is not observed for this series, presumably because these molecules are not as polar as those of the p-amino series.

2. THE ^1L_a RANKING CRITERION: The decline in energy of the $^1L_a \leftarrow {}^1A$ absorption band is assumed to arrange the p set of D-ϕ-A molecules according to increasing polarity. This ranking device is consistent with all the available data and it provides a simple, experimentally-

TABLE 6

POLAR D-ϕ-A MOLECULES

ABSORPTION DATA (kK) IN VARIOUS SOLVENT MEDIA[a]

MOLECULE	ISOMER	$^1L_b \leftarrow {}^1A$			$^1L_a \leftarrow {}^1A$		
		Ethanol	MCH	3MP	Ethanol	MCH	3MP
Methylbenzoic Acid	o	35.97(m)	---	34.03(o)	---	---	42.37(m)
	m	37.17(m)	---	---	45.45(m)	---	---
	p	35.46(o)	---	---	42.37(m)	---	41.49(m)
Fluorobenzonitrile	o	35.59(o)	---	---	43.57(o)	---	---
	m	35.52(o)	---	---	43.67(o)	---	---
	p	36.54(o)	---	---	44.30(m)	---	---
Toluamide	p	35.71(sh)	---	35.71(o)	42.64(m)	---	43.29(m)
Chlorobenzonitrile	m	34.78(o)	---	---	42.92(o)	---	---
	p	35.56(o)	---	35.56(o)	42.46(m)	---	42.37(m)
Bromobenzonitrile	p	35.50(o)	---	35.50(o)	41.04(m)	---	41.07(m)
Methoxybenzoic Acid	m	33.90(m)	---	---	42.92(m)	---	---
	p	39.68(m)	---	36.04(o)	39.06(m)	---	39.53(m)

MOLECULE	ISOMER	$^1L_b \leftarrow {}^1A$			$^1L_a \leftarrow {}^1A$		
		Ethanol	MCH	3MP	Ethanol	MCH	3MP
Cyanoanisole	o	33.90(m)	33.56(o)	---	42.02(o)	42.20(m)	---
	m	33.60(o)	33.70(o)	---	43.48(m)	42.02(o)	---
	p	35.34(o)	35.20(o)	---	40.15(m)	40.80(m)	---
Cyanophenol	o	33.67(m)	33.46(o)	---	42.37(o)	42.55(o)	---
	m	33.90(m)	33.83(o)	---	43.05(m)	42.79(o)	---
	p	35.34(o)	35.30(o)	35.40(o)	42.01(m)	41.67(m)	42.07(m)
Cyanoaniline	o	30.75(m)	31.86(m)	~30.44(o)	40.30(m)	41.06(m)	41.20(m)
	m	31.20(m)	32.26(m)	30.90(o)	39.70(m)	41.24(m)	41.20(m)
	p	---	33.06(o)	33.00(o)	36.20(m)	???	38.20(m)
Cyanophenoxide	p	---	---	---	36.50(m)	---	---
N,N-Dimethylcyanoaniline	p	---	---	---	34.60(m)	---	---
Methyl Aminobenzoate	o	29.51(m)	---	---	---	---	---
	m	31.35(m)	---	---	---	---	---
	p	33.61(sh)	33.61(sh)	33.67(sh)	34.36(m)	---	37.04(m)
Aminobenzoic Acid	p	---	---	---	34.48(m)	---	---

MOLECULE	ISOMER	$^1L_b \leftarrow {}^1A$			$^1L_a \leftarrow {}^1A$		
		Ethanol	MCH	3MP	Ethanol	MCH	3MP
N-Methylaminobenzoic Acid	p	---	---	---	33.28(m)	34.01(m)	---
N,N-Dimethylaminobenzoic Acid	-	---	---	---	32.47(m)	32.51(m)	32.89(m)
Aminoacetophenone	o	27.40(m)	---	28.41(m)	38.80(m)	---	39.53(m)
	m	29.50(m)	---	30.77(m)	39.00(m)	---	40.82(m)
	p	---	---	~29.90(m)	---	---	---
Nitrophenol	p	---	---	---	31.95(m)	---	---
Nitroaniline	o	---	26.50(m)	---	---	37.00(m)	---
	m	---	28.70(m)	---	35.41(sh)	37.20(m)	---
	p	---	---	---	26.90(m)	31.00(m)	31.55(m)
N,N-Dimethylnitroaniline	p	---	---	---	25.80(m)	---	28.49(m)

[a]All energies refer to room temperature. (o) designates a band origin, (m) designates a band maxima, (sh) designates a shoulder. Compounds were purified by standard methods (distillation, crystallization, gas chromatography, volatilization and/or zone refining.

TABLE 7

EMISSION DATA FOR POLAR D-ϕ-A MOLECULES[a,b,c]

MOLECULE	ISOMER	SOLVENT	FLUORESCENCE	PHOSPHORESCENCE		Φ_P/ϕ_F
			ENERGY (cm^{-1})	ENERGY (cm^{-1})	LIFETIME (s)	
Methylbenzoic Acid	o	EPA	---	27,780	1.2	>100
	m	EPA	---	29,710	2.7	>100
	p	EPA	---	30,300	1.7	>100
Fluorobenzonitrile	o	Ethanol	35,000	26,800	2.43	0.18
	m	Ethanol	34,900	26,600	2.60	0.15
	p	Ethanol	35,750	27,100	2.05	0.96
Toluamide	o	EPA	35,590	27,690	0.65	5.3
	m	EPA	34,360	26,870	2.55	6.6
	p	EPA	35,080	27,010	1.25	>100
Chlorobenzonitrile	o	EPA	34,250	25,970	0.38	10.6
	m	EPA	34,480	26,320	0.47	18.7
	p	EPA	34,250	25,840	0.15	16.8
Bromobenzonitrile	o	EPA	34,840(m)	25,970	1.25×10^{-2}	
	m	EPA	34,970(m)	26,320	1.05×10^{-2}	
	p	EPA	34,720(m)	25,770	4.9×10^{-3}	

MOLECULE	ISOMER	SOLVENT	FLUORESCENCE	PHOSPHORESCENCE		Φ_P/Φ_F
			ENERGY (cm^{-1})	ENERGY (cm^{-1})	LIFETIME (s)	
Methoxybenzoic Acid	o	EPA	31,250	25,640	0.96	3.9
	m	EPA	31,250	26,320	2.68	1.7
	p	EPA	33,900	26,460	2.03	6.2
Cyanoanisole	o	Ethanol	33,200	26,000	1.4	0.42
	m	Ethanol	33,000	25,000	1.82	0.45
	p	Ethanol	~35,000-33,900(m)	26,320	1.59	1.01
Cyanophenol	o	EPA	32,050	26,320	2.48	1.31
	m	EPA	32,260	25,320	3.21	0.79
	p	EPA	33,900	26,320	2.63	1.51
Sulfanilamide	m	EPA	28,290(m)	22,320(m)	1.92	1.04
	p	EPA	31,500	25,640	1.22	5.16
Cyanoaniline	o	Ethanol	27,600(m)	24,300(m)	3.65	0.31
	m	Ethanol	27,500(m)	21,510(m)	2.65	0.054
	p	Ethanol	30,000(m)	24,500	2.45	0.73
N,N-Dimethylcyanoaniline	p	EPA	30,770	24,100	2.13	1.2
N,N-Diethylcyanoaniline	p	EPA	30,488	24,100	2	5.3

MOLECULE	ISOMER	SOLVENT	FLUORESCENCE	PHOSPHORESCENCE		Φ_P/Φ_F
			ENERGY (cm^{-1})	ENERGY (cm^{-1})	LIFETIME (s)	
Methyl Aminobenzoate	o	EPA	27,000(m)	22,570(m)	2.45	<0.01
	m	EPA	25,500(m)	23,980(m)	2.4	0.15
	p	EPA	30,303(m)	24,380	1.8	0.20
Aminobenzoic Acid	p	EPA	31,060	24,040	2.1	0.15
N-Methylaminobenzoic Acid	p	EPA	29,630(m)	23,530	2.3	0.13
N,N-Dimethylaminobenzoic Acid	p	EPA	29,590(m)	23,810(m)	1.84	0.18
Aminoacetophenone	o	Ethanol	23,260(m)	22,000(m)	5.55×10^{-2}	0.14
	m	Ethanol	22,600(m)	20,000(m)	0.23	0.13
	p	Ethanol	28,300(m)	22,520(m)	0.72	1.3
Nitroaniline	o	EPA	20,000(m)	---	---	<0.01
	m	EPA	18,000(m)	---	---	<0.01
	p	EPA	---	18,100(m)	0.24	>100
N-Methylnitroaniline	p	EPA	23,260	19,610	0.23	19.3
N,N_Dimethylnitroaniline	p	EPA	22,730	19,230	0.22	2.8

FOOTNOTES TO TABLE 7

[a]All energies refer to 77°K. Quoted energies are for 0,0 bands except where marked by "(m)" which connotes a band maximum. The experimental error is approximately 50 cm^{-1}. The ratio of phosphorescence to fluorescence intensities is denoted by Φ_P/Φ_F and has been corrected for instrument parameters. The absence of any symbolism in a given data slot incidates our inability ro measure the quantity in question.

[b]Compounds were purified by standard methods (distillation, crystallization, gas chromatography, volatilization and/or zone refining) until a constancy of luminescence parameters was achieved. All solvents were fluorometric grade and were non-emissive at the level of sensitivity needed in this work. Measurement procedures have been described elsewhere.[3]

[c]Mesomeric, inductive and steric effects are undoubtedly operative to some extent in all of these systems. It seems reasonable that the relative importance of these effects in the different isomers varies as follows:

o : steric; inductive ≥ mesomeric
m : indictive only
p : mesomeric ≥ inductive

The energies of S_1 and T_1 states will depend on that particular mix of these effects which operates in the given of a given molecule. For example, in the chloro- and bromobenzonitriles, m is of highest T_1 and S_1 energy, presumably because only the indictuve effects operates in this isomer. In a "stronger" DA system, where p possesses the highest T_1 and S_1 energies, we must, it seems, associate this happenstance with a dominant importance of the mesomeric effect in these cases.

Figure 14.

The absorption and emission data for p-amino substituted benzenes. The absorption data refer to non-polar media (3-methylpentane or methylcyclohexane) at room temperature; the emission data refer to glassy ethanol or EPA solutions at 77°K. The circles refer to band origins, the squares refer to band maxima. The molecules are arranged in order of increasing molecular polarity as determined by decreasing $^1L_a \leftarrow {}^1A$ energy. The numbers are the experimental oscillator strengths of the transitions.

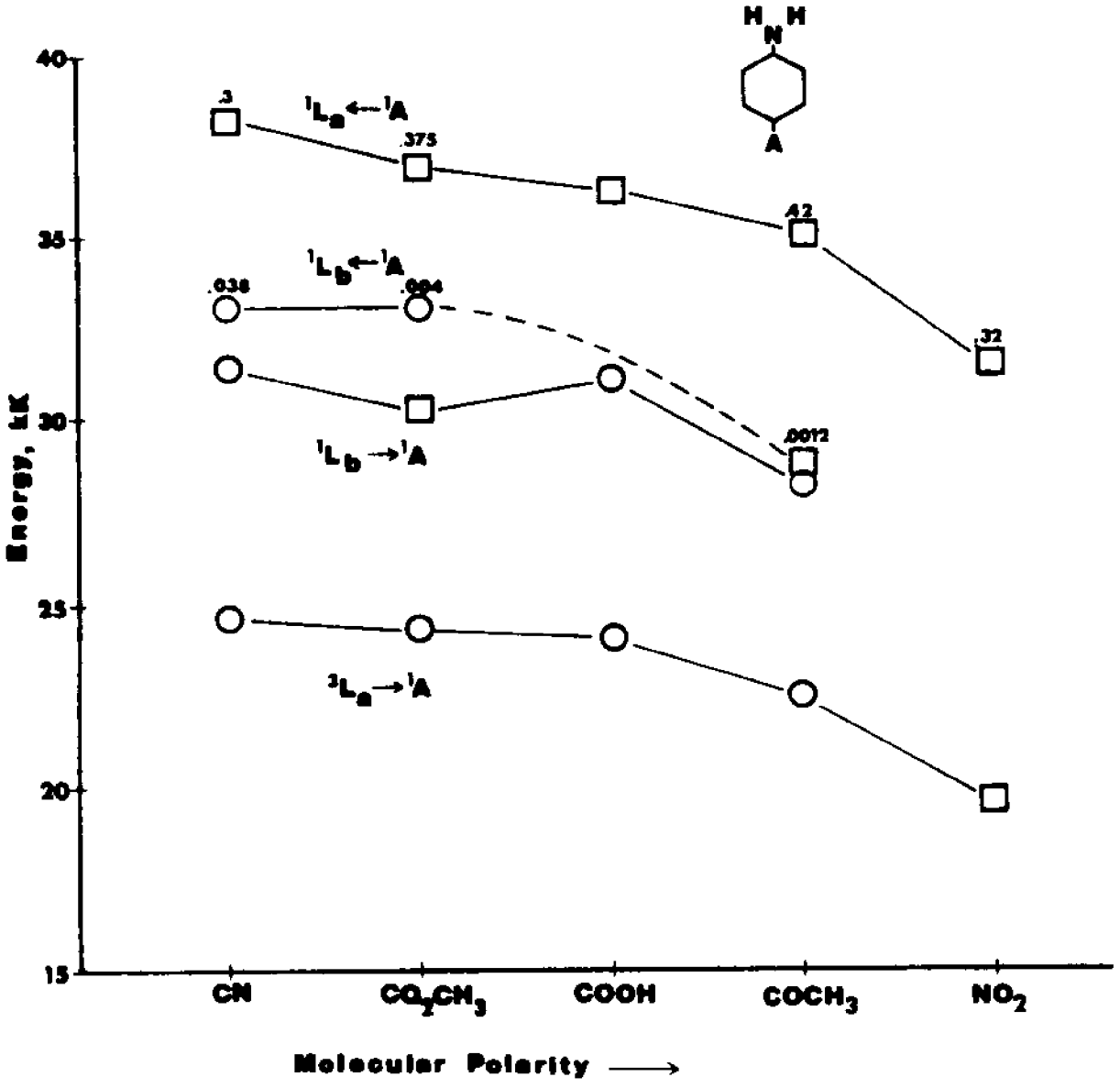
H N H
A
40
35
30
25
20
15
Energy, kK
.3
$^1L_a \leftarrow {}^1A$
.375
.42
.32
$^1L_b \leftarrow {}^1A$
.038
.004
$^1L_b \rightarrow {}^1A$
.0012
$^3L_a \rightarrow {}^1A$
CN
CO_2CH_3
COOH
$COCH_3$
NO_2
Molecular Polarity ⟶

Figure 15.

The absorption and emission data for p-cyano substituted benzenes. The absorption data refer to non-polar media (methylcyclohexane or 3-methylpentane) at room temperature; the emission data refer to glassy ethanol or EPA solutions at 77^{O}K. The squares refer to band maxima, the circles refer to band origins. The molecules are arranged in order of increasing molecular polarity as determined by decreasing $^{1}L_{a} \leftarrow {}^{1}A$ energy. The numbers are the experimental oscillator strengths of the transitions.

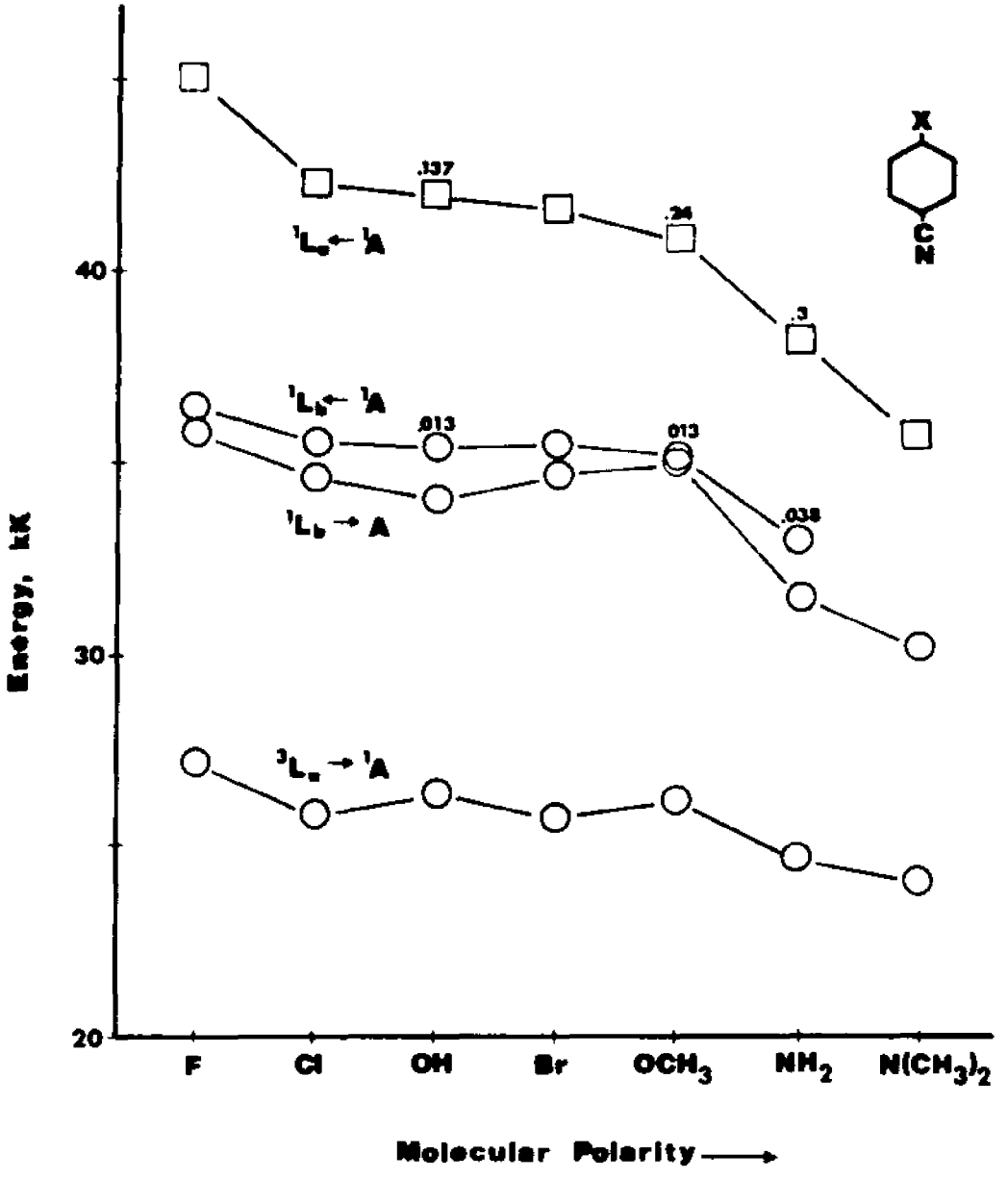
Energy, kK
40
30
20
F
Cl
OH
Br
OCH3
NH2
N(CH3)2
Molecular Polarity
.337
.26
.3
.013
.013
.038
X
C
N

direct method of comparing molecules with completely different substituents.

This ranking parameter also serves to arrange the o and m series according to polarity. In this latter case, however, it is less sensitive simply because the effect of molecular polarity on the $^1L_a \leftarrow {}^1A$ energies is not as large as in the p case.

This ranking device also possesses certain disadvantages. These are:

---The $^1L_a \leftarrow {}^1A$ origin is not usually observed. Therefore, the $^1L_a \leftarrow {}^1A$ band maximum is used. This maximum is usually broad (i.e., not sharp). Furthermore, the energy of this maximum changes markedly with solvent, temperature, and pressure---which may be both bothersome and advantageous.

---The $^1L_a \leftarrow {}^1A$ band envelope may contain more than one transition (e.g., nitroaniline and the N-methyl substituted nitroanilines). One may assume that the $^1L_a \leftarrow {}^1A$ transition dominates, but one cannot always be sure of this.

---Ideally, vapor-phase spectra should be used to obtain accurate $^1L_a \leftarrow {}^1A$ origins which are free of solvatochromic[13] effects. Unfortunately, most highly-polar D-ϕ-A molecules have very low vapor pressures. Therefore, in order to reduce the error that may be caused by large solvatochromic effects, we use the $^1L_a \leftarrow {}^1A$ absorption data for nonpolar solvents.

The absorption and emission data for 20 p-D-ϕ-A molecules arranged according to decreasing $^1L_a \leftarrow {}^1A$ energy are presented in Figure 16. The following trends may be discerned:

---The $^1L_a \leftarrow {}^1A$ band declines in energy faster than does the

Figure 16.

The absorption and emission data for p-disubstituted banzenes, arranged according to increasing molecular polarity as determined by decreasing $^1L_a \leftarrow {}^1A$ energy. The absorption data refers to non-polar media (methylcyclohexane or 3-methylpentane) at room temperature; the emission data refers to glassy ethanol or EPA media at $77^{O}K$. The squares refer to band maxima, the circles to band origins. The molecules are numbered as follows: 1, p-fluorobenzonitrile; 2, p-toluamide; 3, p-chlorobenzonitrile; 4, p-cyanophenol; 5, p-bromobenzonitrile; 6, p-cyanoanisole; 7, p-methoxybenzoic acid; 8, p-cyanoaniline; 9, methyl p-aminobenzoate; 10, p-aminobenzoic acid; 11, N,N-dimethyl-p-aminobenzonitrile; 12, p-nitrophenol; 13, p-aminoacetophenone; 14, N-methyl-p-aminobenzoic acid; 15, N,N-dimethyl-p-aminobenzoic acid; 16, p-nitroaniline; 17, N-methyl-p-nitroaniline; and 18, N,N-dimethyl-p-nitroaniline.

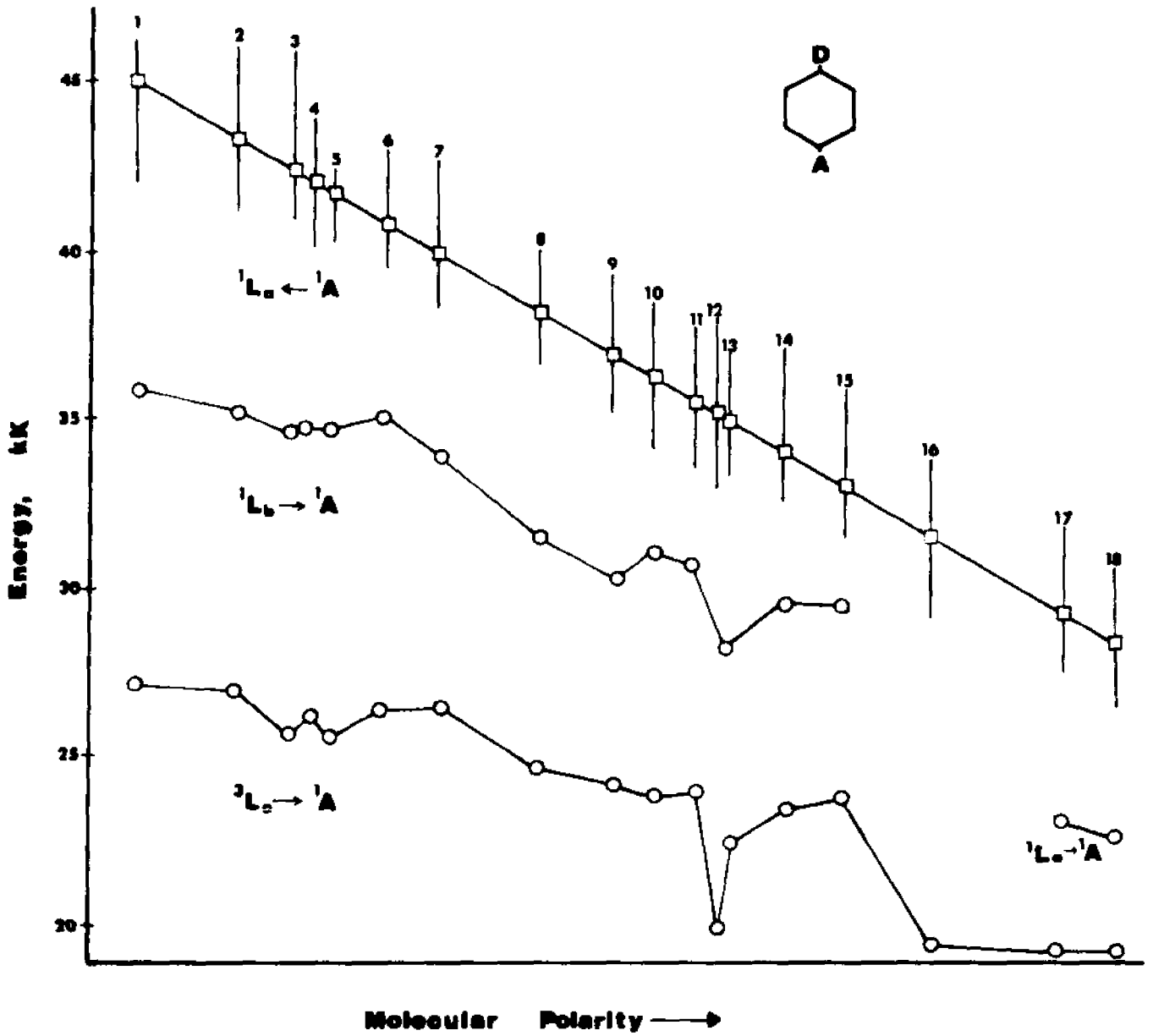
Energy, kK
45
40
35
30
25
20
1
2
3
4
5
6
7
8
9
10
11
12
13
14
15
16
17
18
D
A
$^1L_a \leftarrow {}^1A$
$^1L_b \rightarrow {}^1A$
$^3L_a \rightarrow {}^1A$
$^1L_a \rightarrow {}^1A$
Molecular Polarity ⟶

$^1L_b \leftarrow {}^1A$ band.

---When the energy of the $^1L_a \leftarrow {}^1A$ band has decreased to that of N,N-dimethyl-p-cyanoaniline, the $^1L_b \leftarrow {}^1A$ band is not observed (Figure 15).

---Fluorescence occurs from the ^1L_b state in the less-polar molecules. As the ^1L_a and ^1L_b energy levels converge towards coincidence, however, fluorescence disappears. This is undoubtedly due to the decrease of the $^1L_b \leftarrow {}^1A$ transition dipole moment---which is observed experimentally and expected theoretically[45]---and to the expected increase of molecule-solvent non-radiative depletion routes which compete with the weak $^1L_b \rightarrow {}^1A$ fluorescence pathway.

---Fluorescence re-emerges and becomes the dominant energy-depletion route when the ^1L_a state drops energetically below the ^1L_b state--$^3L_a \rightarrow {}^1A$ phosphorescence remains viable as the $^1L_b \rightarrow {}^1A$ fluorescence efficiency decreases. However, when the $^1L_a \rightarrow {}^1A$ fluorescence pathway becomes feasible, the $^3L_a \rightarrow {}^1A$ phosphorescence tends to disappear.

We are now in a position to interpret the anomalous luminescence of p-aminoacetophenone (*vide supra*). We expect that the low-energy "tail" on the lowest-energy absorption band of p-aminoacetophenone in non-polar media is the $^1L_b \leftarrow {}^1A$ transition. The weak fluorescence reported by Yamaguchi *et al.*[39] in non-polar media is then assigned as $^1L_b \rightarrow {}^1A$. In polar media, however, the ^1L_a level shifts to a lower energy than the ^1L_b level and the fluorescence becomes $^1L_a \rightarrow {}^1A$ in nature. The result is that the fluorescence and absorbance in polar media at 77°K are mirror images of one another whereas, in non-polar media, they are not. The fact that the fluorescence and phosphorescence excitation spectra are different can be explained[39] by invoking

coupling between the two excited singlet states. We agree on this, but disagree in that we assign the "tail" region as $^1\Gamma_{\pi\pi^*} \leftarrow {}^1\Gamma_1$ rather than $^1\Gamma_{n\pi^*} \leftarrow {}^1\Gamma_1$ as they do.

3. SOLVENT EFFECTS: In light of the above, we find it informative to view a polar D-ϕ-A molecule and its solvent cage as one distinct absorbing and emitting entity: A particular molecule embedded in two different solvent cages becomes, in effect, two different "molecules". Because the ^1L_a state is more solvatochromic than is ^1L_b, we can adjust the relative energies of these two states by a judicious choice of solvent. Hydrogen bonding effects[46], of course, are inherently included.

If the energy of the $^1L_a \leftarrow {}^1A$ band is used to arrange a series of these "molecule-solvent species", certain generalizations about fluorescence and phosphorescence may be noted. Such a series is presented in Figure 17. As the polarity of the system increases, fluorescence decreases and phosphorescence dominates. At the point where the ^1L_a and ^1L_b states are approximately isoenergetic, fluorescence disappears entirely. As polarity increases further, however, and as the ^1L_a and ^1L_b states invert, a fluorescence reappears. Finally, when the ^1L_a state has decreased to that of NNDMPNA in polyvinyl alcohol (PVA), phosphorescence disappears and the $^1L_a \rightarrow {}^1A$ fluorescence dominates the emission spectrum.

4. o-ISOMERS: Since long- and short-axes cannot be defined for o and m, the (L_a, L_b)-notation is no longer rigorous. However, all of these isomers possess two low energy $^1\Gamma_{\pi\pi^*}$ states and these can be correlated (vide infra) with the ^1L_b and the ^1L_a states of benzene. In view of this, we designate the lowest-energy $^1\Gamma_{\pi\pi^*}$ state of the o- and p-isomers as "^1L_b" and the second lowest-energy $^1\Gamma_{\pi\pi^*}$

Figure 17.

The absorption and emission of a series of "molecule-solvent species," arranged according to decreasing $^1L_a \leftarrow {}^1A$ energy. The absorption and emission data were recorded in transparent media at 77°K.

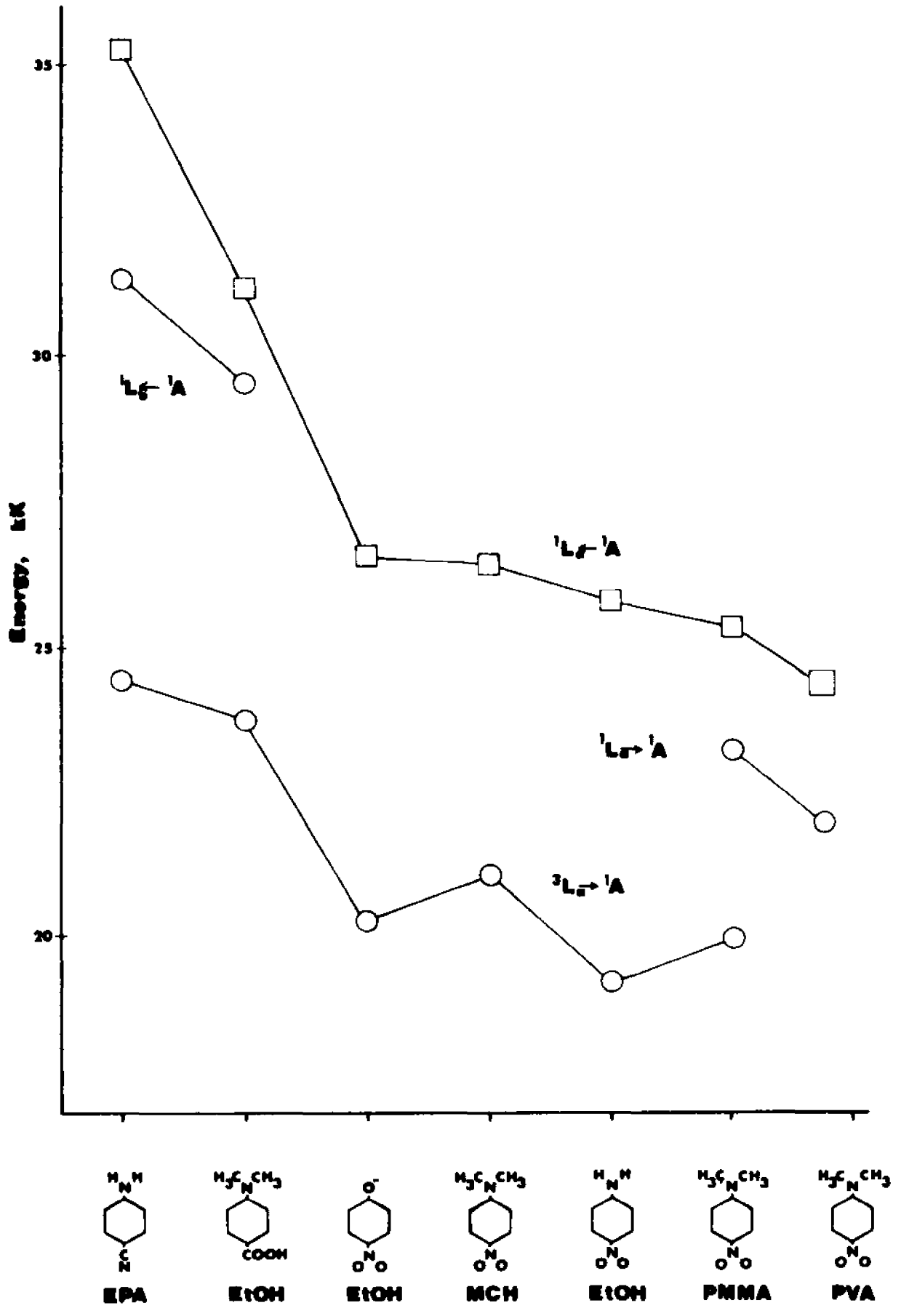
35
30
25
20
Energy, kK
$^1L_b \leftarrow {}^1A$
$^1L_a \leftarrow {}^1A$
$^1L_a \rightarrow {}^1A$
$^3L_a \rightarrow {}^1A$
EPA
EtOH
EtOH
MCH
EtOH
PMMA
PVA

state as "^1L_a". Our use of this notation, then, should cause no confusion.

Data for the o-amino and o-cyano series are presented in Figures 18 and 19, respectively. The molecules are arranged from left to right according to increasing polarity. As is the case for the p-isomers, we see a general decrease in the energy of the $^1L_a \leftarrow {}^1A$ and $^1L_b \leftarrow {}^1A$ absorption bands as the molecular polarity increases. In addition, there is an overall increase in the oscillator strength of the $^1L_b \leftarrow {}^1A$ band across the series, whereas that of the $^1L_a \leftarrow {}^1A$ band tends to decrease. Fluorescence occurs from the ^1L_b state in every case, while phosphorescence presumably always occurs from the ^3L_a state. This latter assignment is substantiated to some extent by the fact that the ^1L_a-^3L_a energy gap remains fairly constant across the series. Phosphorescence tends to decrease as the molecular polarity increases and, finally, in o-nitroaniline, where the intersystem crossing cannot compete with the efficient $^1L_b \rightarrow {}^1A$ fluorescence pathway, it disappears altogether.

Because of the steady decrease of energy of the $^1L_a \leftarrow {}^1A$ band with the molecular polarity, we re-adopt the ranking criterion of Figure 16 and 17. The result is shown in Figure 20, where the molecules are ordered from left to right according to decreasing energy of the $^1L_a \leftarrow {}^1A$ band. The $^1L_b \leftarrow {}^1A$ band does not converge on and meld into the $^1L_a \leftarrow {}^1A$ band as in the p series. In fact, the $^1L_b \leftarrow {}^1A$ band intensifies, becomes more distinct with increasing polarity and, if anything, diverges from the $^1L_a \leftarrow {}^1A$ band. In addition, solvent effects on the $^1L_a \leftarrow {}^1A$ and $^1L_b \leftarrow {}^1A$ bands are quite small. We take these observations to mean that the dipolarity of o is less than that

Figure 18.

Absorption and emission data for o-substituted anilines, arranged according to molecular polarity as determined by the decrease in $^1L_a \leftarrow {}^1A$ energy. The absorption data refers to non-polar media (3-methylbentane or methylcyclohexane) at room temperature; the emission data refers to glassy ethanol or EPA media at 77^{O}K. The circles refer to band origins, the squares refer to band maxima.

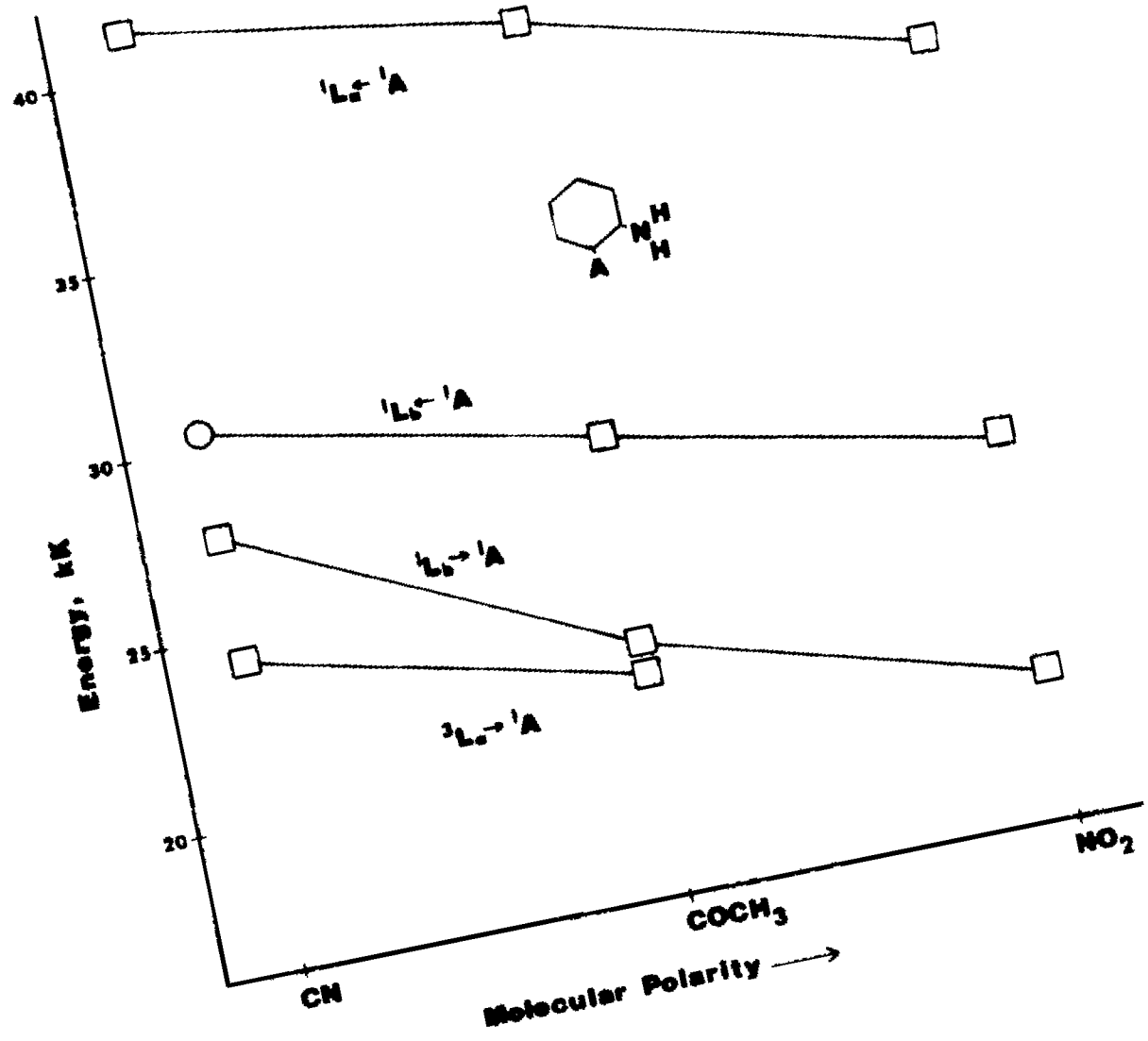
40
35
30
25
20
Energy, kK
$^1L_a \leftarrow {}^1A$
$^1L_b \leftarrow {}^1A$
$^1L_b \rightarrow {}^1A$
$^3L_a \rightarrow {}^1A$
NH
H
A
CN
$COCH_3$
NO_2
Molecular Polarity ⟶

Figure 19.

Absorption and emission data for o-substituted benzonitriles, arranged according to increasing molecular polarity as determined by the decrease in the $^1L_a \leftarrow {}^1A$ energy. The absorption data refers to non-polar media (3-methylpentane or methylcyclohexane) at room temperature; the emission data refers to glassy ethanol or EPA media at $77^{O}K$. The circles refer to band origins, the squares refer to band maxima.

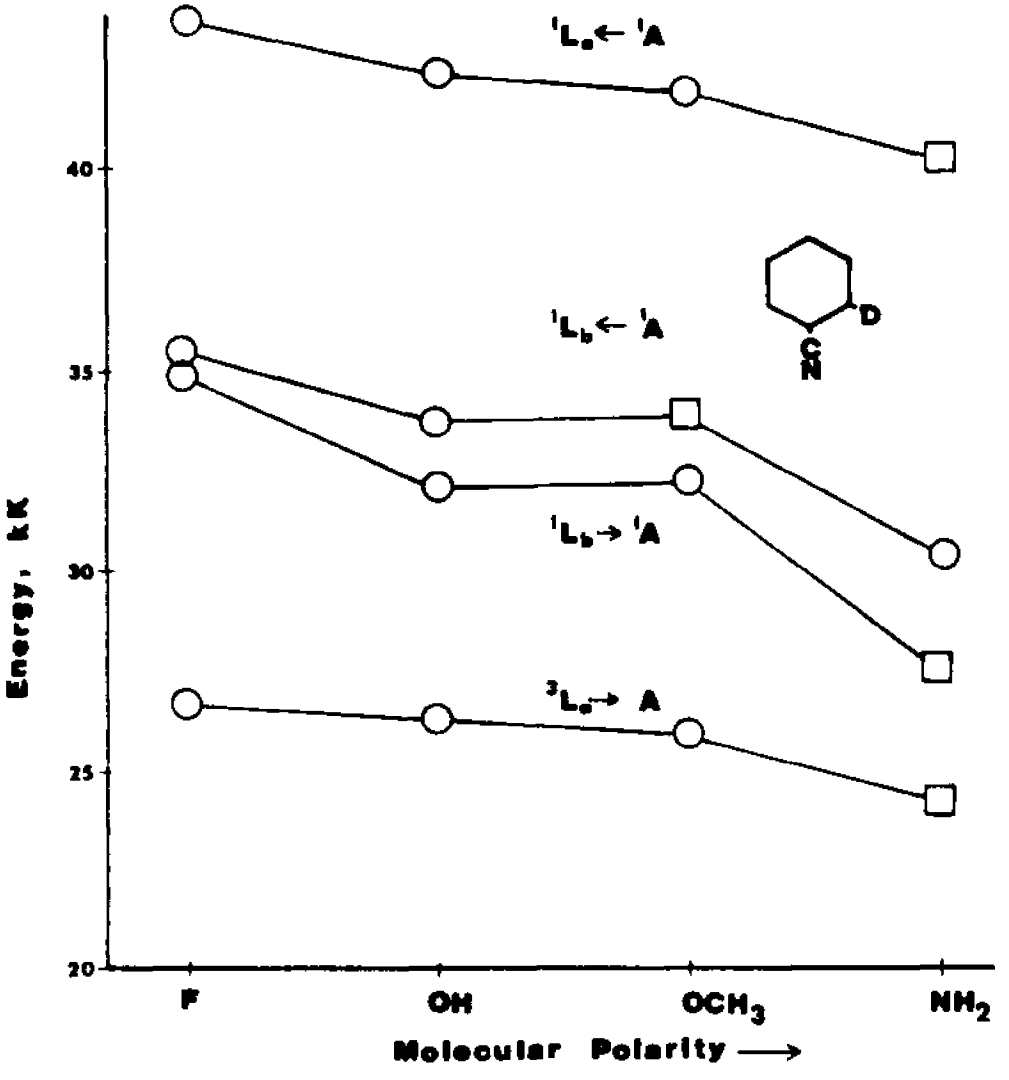
$^1L_a \leftarrow {}^1A$
$^1L_b \leftarrow {}^1A$
$^1L_b \rightarrow {}^1A$
$^3L_a \rightarrow A$
D
C
N
Energy, kK
40
35
30
25
20
F
OH
OCH_3
NH_2
Molecular Polarity ⟶

Figure 20.

The absorption and emission of o-disubstituted benzenes, arranged according to increasing molecular polarity as determined by decreasing $^1L_a \leftarrow {}^1A$ energy. The absorption data refers to non-polar media (methylcyclohexane or 3-methylpentane) at room temperature; the emission data refers to glassy ethanol or EPA media at 77^0K. The circles refer to band origins, the squares refer to band maxima. The numbers are experimental oscillator strengths of the absorptive transitions.

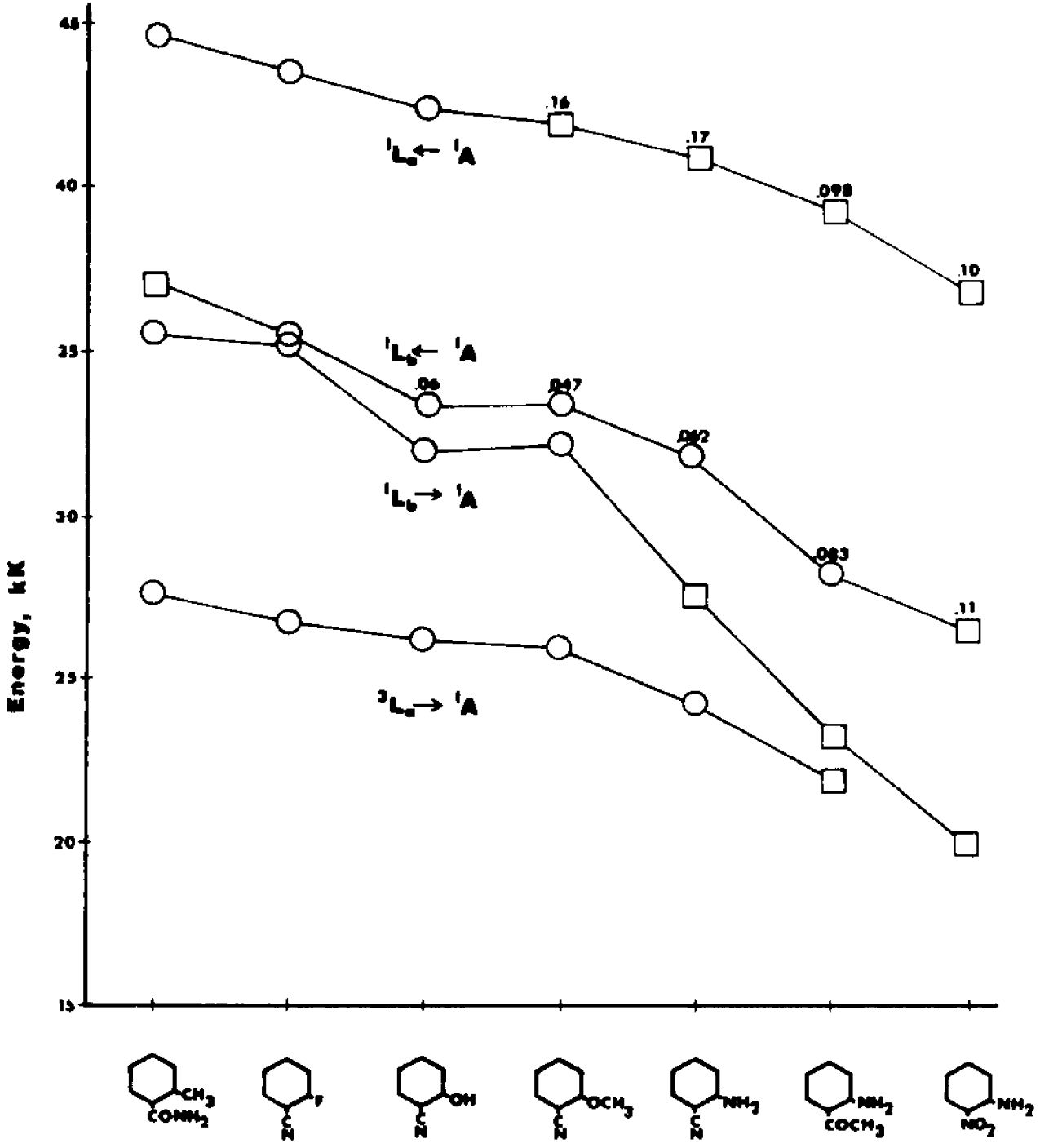
Energy, kK
45
40
35
30
25
20
15
$^1L_a \leftarrow {}^1A$
$^1L_b \leftarrow {}^1A$
$^1L_b \rightarrow {}^1A$
$^3L_a \rightarrow {}^1A$
.16
.17
.098
.10
.06
.047
.062
.083
.11
CONH2
CH3
F
CN
OH
OCH3
NH2
COCH3
NO2

of P---which it should be by a factor of ~2. We also conclude, because of the lack of differential solvent shifts on the two bands, that the charge-transfer character of both the ^1L_a and ^1L_b states is essentially identical and, possibly, is even larger in the ^1L_b state.

5. m-ISOMERS: The m-amino and m-cyano series are presented in Figures 21 and 22, respectively. The same general trends are exhibited as those found for the analogous series of the o-isomers. Figure 23 is generated by using the energy of the $^1L_a \leftarrow {}^1A$ band as the ranking device. From this correlation, we find that fluorescence always occurs from the ^1L_b state, while phosphorescence is always presumed to arise from the ^3L_a state.

C. OTHER EXPERIMENTAL OBSERVATIONS.

1. EMISSION POLARIZATION OF N,N-DIMETHYL-p-NITROANILINE(NNDMPNA):

The $^1L_a \rightarrow {}^1A$ and $^1L_b \rightarrow {}^1A$ transition moments of NNDMPNA are in-plane and mutually perpendicular, the former being directed along the long-axis and the latter along the short axis. The $^3L_a \rightarrow {}^1A$ transition moment, on the other hand, is expected[47] to be directed out-of-plane. Thus, fluorescence, whether $^1L_a \rightarrow {}^1A$ or $^1L_b \rightarrow {}^1A$, should possess a polarization direction which is perpendicular to that of phosphorescence[32]. This, as shown in Figure 24, is clearly the case.

Now, the majority of the intensity of the first absorption band is certainly $^1L_a \leftarrow {}^1A$. Thus, if the fluorescence is $^1L_b \rightarrow {}^1A$, it is expected that the fluorescence excitation spectrum will exhibit either total or nearly total negative polarization. It is obvious from Figure 24 that this is not so. The interpretation of the fluorescence excitation data requires that the fluorescence be $^1L_a \rightarrow {}^1A$ and that no significant part of the absorption intensity be either $^1L_b \leftarrow {}^1A$

Figure 21.

Absorption and emission data for m-substituted anilines, arranged according to molecular polarity as determined by the decrease in ^1L_a - ^1A energy. The absorption data refers to non-polar media (3-methylpentane or methylcyclohexane) at room temperature; the emission data refers to glassy ethanol or EPA media at 77°K. The circles refer to band origins; the squares refer to band maxima.

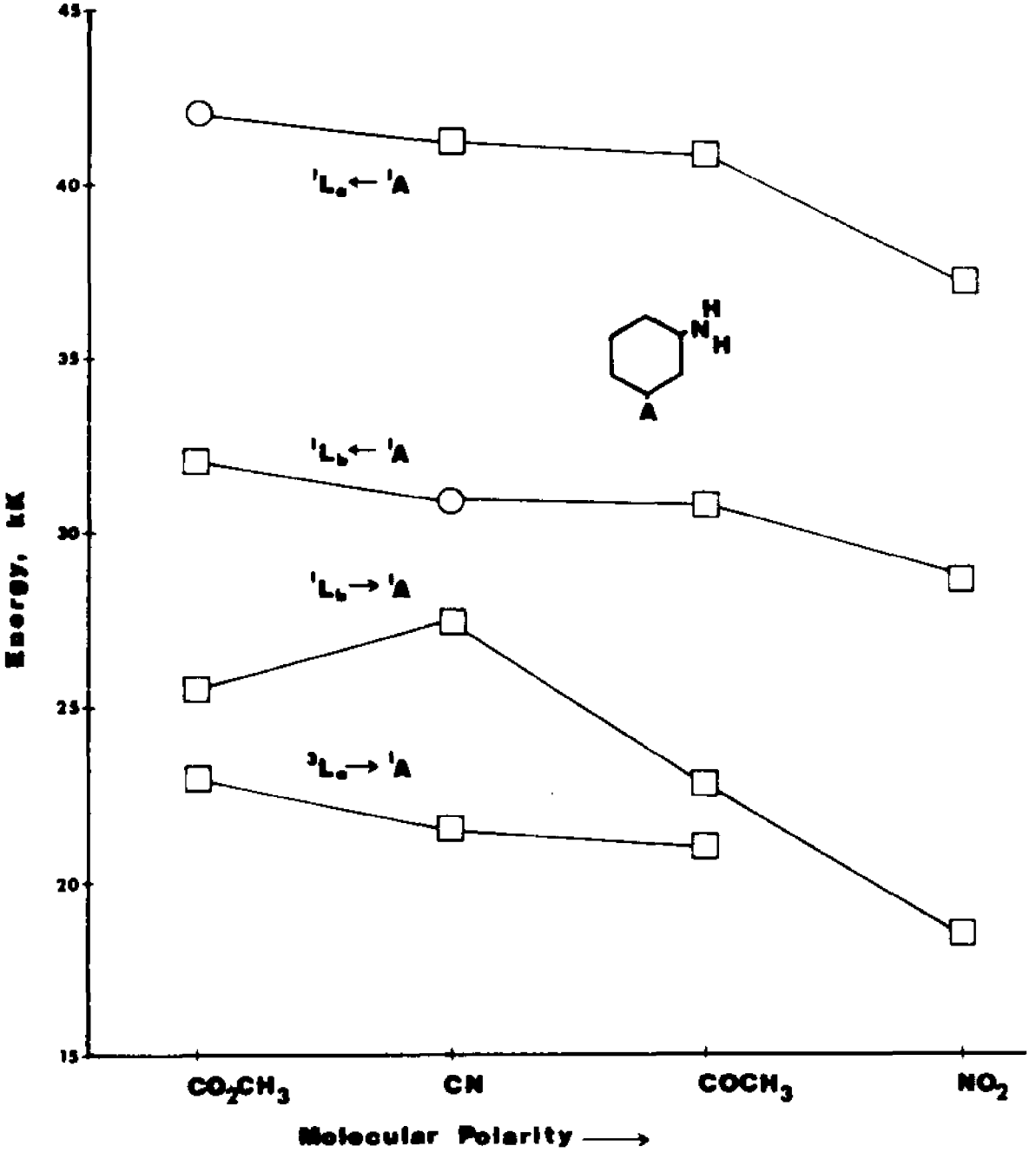
45
40
35
30
25
20
15
Energy, kK
$^1L_a \leftarrow {}^1A$
$^1L_b \leftarrow {}^1A$
$^1L_b \rightarrow {}^1A$
$^3L_a \rightarrow {}^1A$
H
N
H
A
CO_2CH_3
CN
$COCH_3$
NO_2
Molecular Polarity ⟶

Figure 22.

Absorption and emission data for m-substituted benzonitriles, arranged according to molecular polarity as determined by the decrease in $^1L_a \leftarrow ^1A$ energy. The absorption data refers to non-polar media (methylcyclohexane or 3-methylpentane) at room temperature; the emission data refers to glassy ethanol or EPA media at 77°K. The circles refer to band origins; the squares refer to band maxima.

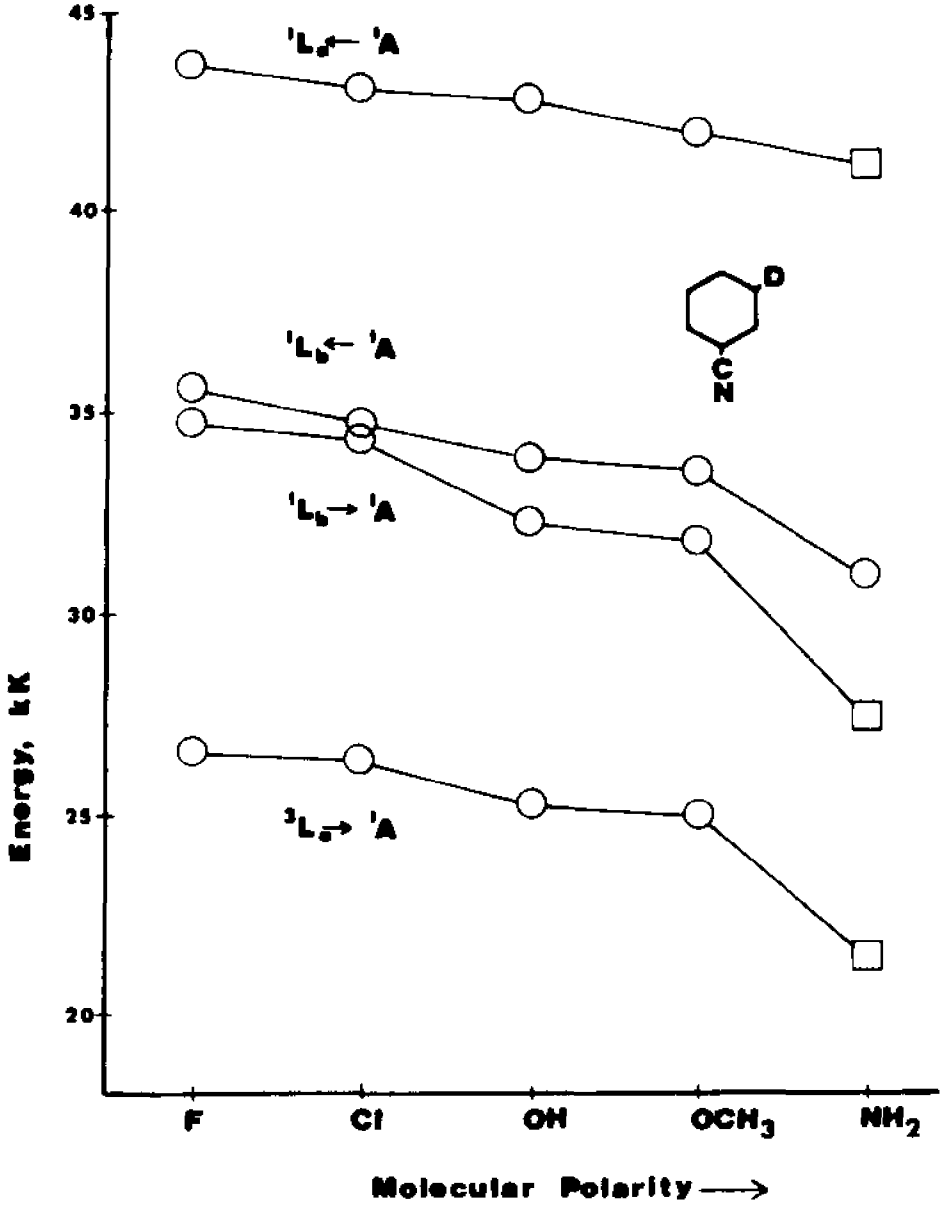
45
40
35
30
25
20
Energy, kK
$^1L_a \leftarrow {}^1A$
$^1L_b \leftarrow {}^1A$
$^1L_b \rightarrow {}^1A$
$^3L_a \rightarrow {}^1A$
D
C
N
F
Cl
OH
OCH_3
NH_2
Molecular Polarity ⟶

Figure 23.

Absorption and emission data for m-disubstituted benzenes, arranged according to increasing molecular polarity as determined by decreasing ^1L_a - ^1A energy. The absorption data refers to non-polar media (methylcyclohexane or 3-methylpentane) at room temperature; the emission data refers to glassy ethanol or EPA media at 77°K. The circles refer to band origins; the squares refer to band maxima. The numbers above the data points are the experimentally determined oscillator strengths.

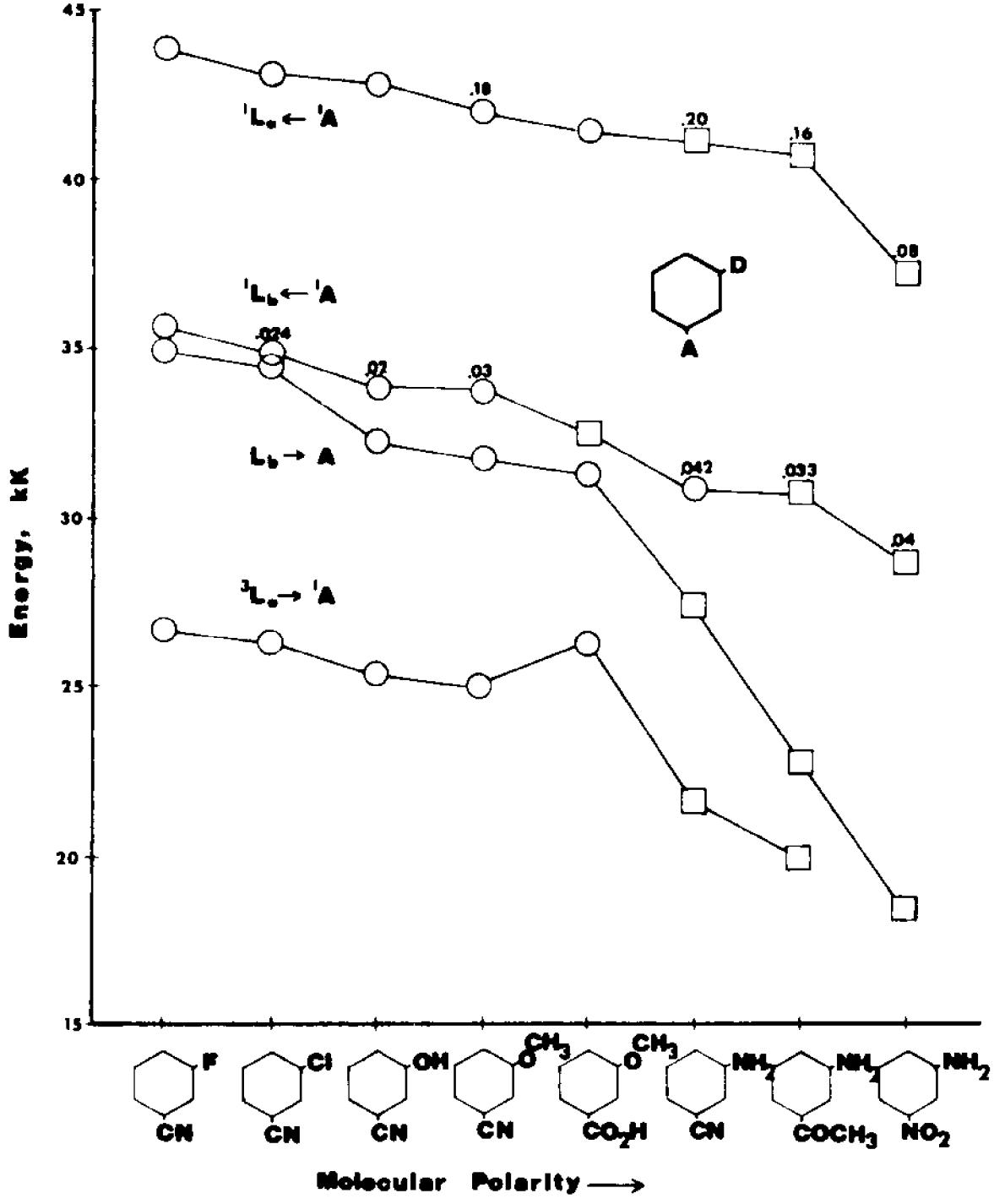
45
40
35
30
25
20
15
Energy, kK
$^1L_a \leftarrow {}^1A$
$^1L_b \leftarrow {}^1A$
$L_b \rightarrow A$
$^3L_a \rightarrow {}^1A$
.18
.20
.16
.08
.024
.02
.03
.042
.033
.04
D
A
F
Cl
OH
O
CH_3
O
CH_3
NH_2
NH_2
NH_2
CN
CN
CN
CN
CO_2H
CN
$COCH_3$
NO_2
Molecular Polarity ⟶

Figure 24.

The emission, emission polarization, excitation, and excitation polarization spectra of N,N-dimethyl-p-nitroaniline in EPA at 77°K, ~ 10^{-5}M. P is the phosphorescence, F is the fluorescence, and TEP is the total emission polarization (λ_{excit} = 380 nm). FE is the fluorescence excitation, and FEP is the fluorescence excitation polarization (λ_{emit} = 490 nm). PE is the phosphorescence excitation and PEP is the phosphorescence excitation polarization (λ_{emit} = 540 nm). A is the absorption spectrum taken in EPA at 77°K. The emission spectrum is not corrected.

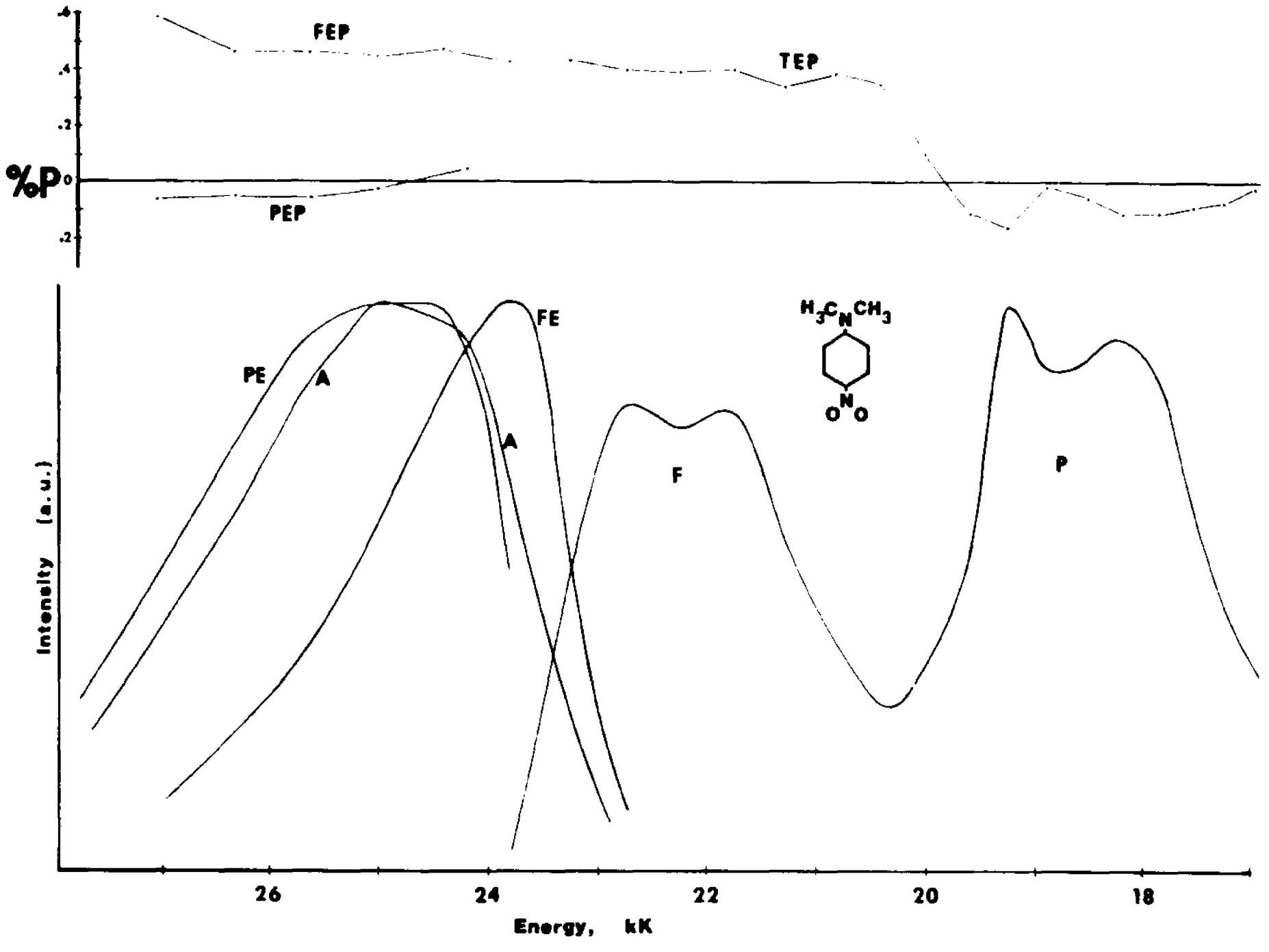
FEP
TEP
PEP
%P
.4
.2
0
.2
PE
A
FE
A
F
P
$H_3C_N{}^{CH_3}$
$O^N O$
Intensity (a.u.)
26
24
22
20
18
Energy, kK

or $^1\Gamma_{n\pi^*} \leftarrow {}^1\Gamma_1$.

If any significant part of the absorption intensity is $^1\Gamma_{n\pi^*} \leftarrow {}^1\Gamma_1$, it is expected that the phosphorescence excitation spectrum will exhibit positive polarization. It is obvious from Figure 24 that this is not the case. Nonetheless, it is a fact that the phosphorescence excitation spectrum is least negative at larger λ and that the fluorescence and phosphorescence excitation spectra are not identical. Thus, somewhere in the vicinity of 410mμ, the vibrational deactivation cross-section within the singlet manifold becomes less than the cross-section for intersystem crossing to the triplet manifold. The most facile interpretation of this datum suggests the intrusion of $^{1,3}\Gamma_{n\pi^*}$ states in the 410mμ region with the consequent enhancement of intersystem crossing via the processes $^1\Gamma_{n\pi^*} \rightsquigarrow {}^3\Gamma_{\pi\pi^*}$ and $^1\Gamma_{\pi\pi^*} \rightsquigarrow {}^3\Gamma_{n\pi^*} \rightsquigarrow {}^3\Gamma_{\pi\pi^*}$. The intrusion of such states in the 410mμ region may also provide a rationale --- weak because of intensity considerations --- for the lesser negativity of phosphorescence polarization in the 410mμ region.

Consequently, we may conclude the following:

---Phosphorescence is either $^3L_a \rightarrow {}^1A$ or $^3L_b \rightarrow {}^1A$. It is not $^3\Gamma_{n\pi^*} \rightarrow {}^1\Gamma_1$.

---Fluorescence is $^1L_a \rightarrow {}^1A$.

---The majority intensity of the lowest-energy absorption band is $^1L_a \leftarrow {}^1A$.

---$^{1,3}\Gamma_{n\pi^*}$ states may well intrude in the 410mμ region. It is well to note that a different interpretation of the disparity between phophorescence and fluorescence excitation spectra --- one which does not invoke the intrusion of $^{1,3}\Gamma_{n\pi^*}$ states and which does not take account of the polarization data --- is available in the literature[7].

2. THE CHARGE-TRANSFER BAND: The concept of a charge-transfer (CT) band in D-ϕ-A molecules has been promoted theoretically[48-52]. The evolution of this concept gave rise to the supposition that a new transition of the type D-ϕ-A $\xrightarrow{h\nu}$ D^+-ϕ-A^-(or D^+-ϕ^--A, or even D-ϕ^+-A^-) should appear in the absorption spectrum[48,53,54]. This charge transfer(CT) transition was expected to be long-axis polarized and quite intense[48], to exhibit large solvent effects[55-60], and to produce a large static excited-state dipole moment directed along the substituent (long-) axis[57,61]. Correlations with Hammett σ-constants[62-68] with charge-transfer intensities, and with the steric effects of substituents[49,69,70] have been investigated.

The interpretation of the electronic absorption spectroscopy of the D-ϕ-A molecules investigated here does not, in our opinion, require the proposition of a separate CT transition. The regular decrease of the ^1L_a energy of the p set of D-ϕ-A molecules, which occurs as the molecular polarity increases, indicated an increasing perturbation of the ^1L_a state by the substituents. This perturbation is consistent with the supposition that the $^1L_a \leftarrow {}^1A$ transition of the p set acquires an increasing degree of charge-transfer nature. It is this charge-transfer component which accounts for the observed trends in solvent shifts, excited state dipole moments, etc.

Thus, while we do not expect a CT transition to intrude at lower energies, the ^1L_a and ^1L_b states of o and m will also acquire increasing CT nature as the D-o-A polarity increases.

We will discuss this point in considerable detail in the computational section.

3. THE TRIPLET STATE: The emissive triplet state is consistently

assigned as ^3L_a (p-isomer) and as ^3L_a-related (o- and m-isomers). The phosphorescence lifetimes are always of the order of 1 second, indicating surely a $^1\Gamma_{\pi\pi^*} \rightarrow {}^1\Gamma_1$ transition. The evidence for the ^3L_a assignment is based 1), on a correlation of the spectral characteristics of the T_1 state of these molecules with the T_1 state (^3L_a)[70] of benzene and 2), on CNDO/s calculations (vide infra).

The singlet-triplet interval ($E_{^1L_a} - E_{^3L_a}$) of the p-isomers are shown in Table 8. They decrease regularly as the molecules become more polar. There are two primary reasons for this decrease: Firstly, since the more polar substituents tend to be bulkier, the molecular size tends to increase with increasing polarity. Consequently, the pertinent exchange integrals grow smaller and the S_1-T_1 interval decreases[47]. Secondly, the extent of charge transfer increases with increasing polarity and this, as is well known[47], leads to a drastic reduction in the magnitude of the relevant exchange integrals. In fact, if the ^3L_a state were 100% CT, the ^1L_a and ^3L_a states would be approximately degenerate.

The ^1L_a state of D-ϕ-A molecules is quite polar (e.g., in NNDMPNA, $\mu(^1L_a) = 15D$[71]). The ^3L_a state is less polar than the ^1L_a state: Considerable structure is usually observed in the phosphorescence spectra but not in the fluorescence spectra of these molecules. It is known that $\mu(^1L_a)$ is long-axis oriented[57-61], as is $\mu(S_o)$. If one assumes that $\mu(T_1)$ is similarly aligned, then the T_1 state will also be solvent-stabilized by the ground state solvent cage. In support of this, it is observed that the T_1 state experiences little geometry change relative to the ground state; the phosphorescence origin is always prominent and is often the most intense peak, indicating a

TABLE 8

SINGLET-TRIPLET INTERVALS, ^1L_a - ^3L_a (kK), OF SOME p-D-ϕ-A MOLECULES[a]

MOLECULE	^1L_a Absorption Maximum	^3L_a Phosphorescence Origin	^1L_a-^3L_a
p-Cyanophenol	40.31	26.37	13.94
p-Cyanoaniline	35.71[b]	24.67	11.04
N,N-dimethyl-p-aminobenzoic acid	31.25	23.81[b]	7.44
p-Nitrophenoxide	26.60	20.26	6.34
p-Nitroaniline	25.84	19.58	6.26

[a]All measurements were made in ethanol at 77°K.

[b]The measurements refer to an DPA glass at 77°K.

favorable Franck-Condon geometric match with the ground state.

The above discussion assumed the existence of a rigid matrix in which no solvent-solute reorganization could occur. It is of note that Yamaguchi et al.[6], have shown that the phosphorescence of p-aminoacetophenone in a rigid matrix (ethanol glass, 77°K) exhibits a prominent (0,0) band which, when warmed to 150°K to allow solvent reorganization to occur, experiences a red-shift (1700cm^{-1}) but remains equally prominent. This shift reflects the increased solvent sensitivity of the T_1 state and suggests that $\mu(T_1) > \mu(S_o)$.

4. DIPOLE MOMENTS AND SOLVENT EFFECTS: As discussed previously, $\mu(^1L_a)$ of the p D-ϕ-A sub-set is parallel to, but larger than $\mu(^1A_1)$. Since neither the solvent nor the solute may rearrange during the course of an electronic transition[71], solvent stabilization should be larger[72] for ^1L_a than for $^1A_1$. Thus, a red-shift of the $^1L_a \leftarrow {}^1A$ band (i.e., a solvatochromism) is expected in polar solvents[44], and the degree of solvatochromism is expected to be proportional to the static dipole moment change which occurs upon excitation (i.e., to $|\mu(^1L_a) - \mu(^1A_1)|$)[66,61]. This latter quantity has been adopted by Saidov et al.[66,67] as a criterion for CT transitions.

In view of prior discussions, we conclude that a correlation between the ^1L_a energy and the degree of solvatochromism is expected. The extent to which such a relationship exists is shown in Figure 25 and is not impressive. Nonetheless, if factors which inhibit the expected relationship are taken into account, most of the deviations may be rationalized. These factors are:

---Solvatochromism is less for alkyl-amino substituted aromatics than for amino substituted aromatics even though the former substi-

Figure 25.

Comparison of solvent shifts and ground state experimental dipole moments of p-disubstituted benzenes. The solvent shifts are calculated from the formula ($\tilde{\nu}$[3mp] - $\tilde{\nu}$[EtOH]) for the $^1L_a \leftarrow {}^1A$ band maximum at room temperature, except for p-tolunitrobenzene. For the latter molecule, the solvents are ethanol and hexane (taken from reference 60). The dipole moments are from reference 74.

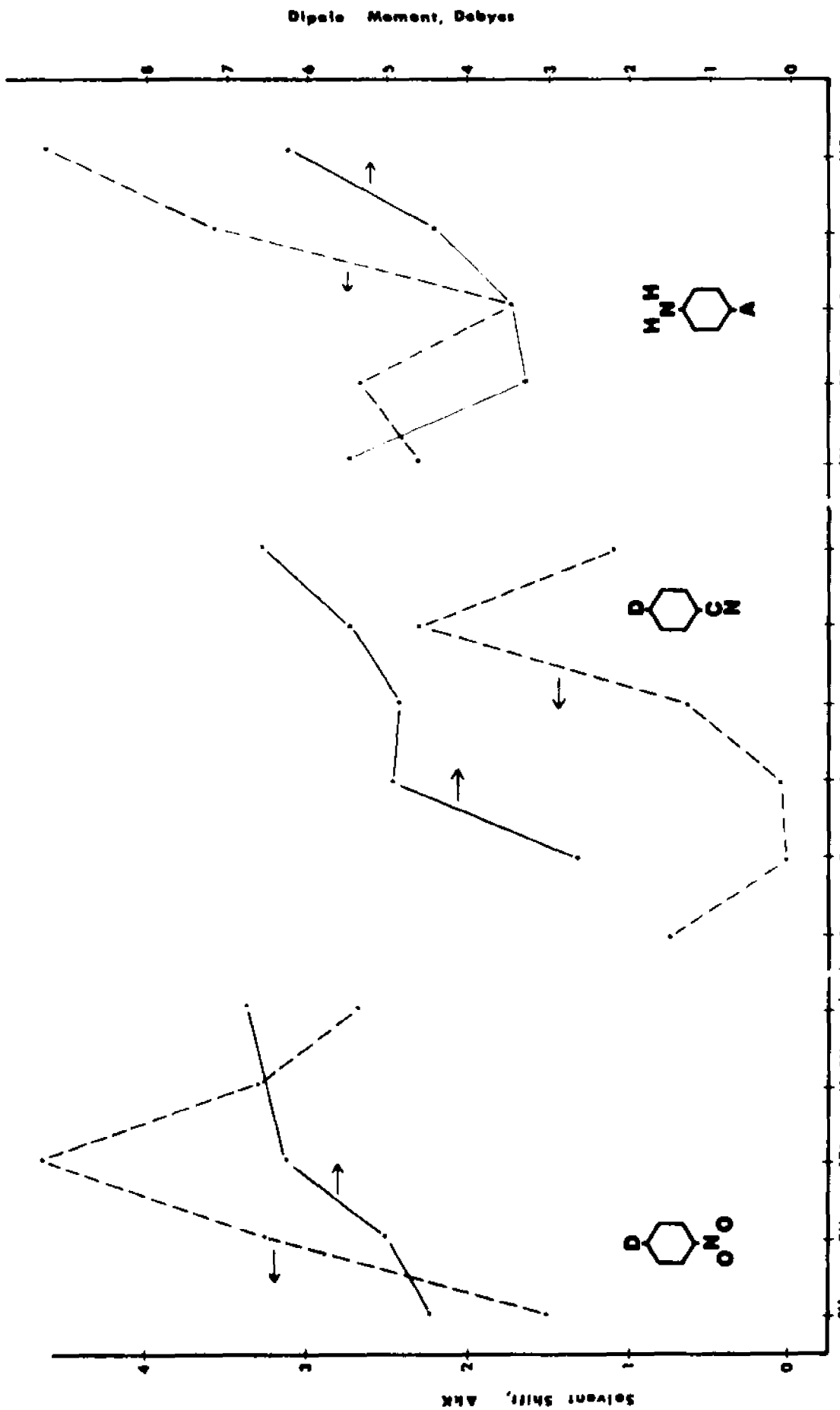
Dipole Moment, Debyes
0
1
2
3
4
5
6
7
8
Solvent Shift, Δkk
CH3
OH
NH2
NHCH3
N(CH3)2
F
Br
OH
OCH3
NH2
N(CH3)2
CN
CO2CH3
CO2H
COCH3
NO2

tuents are known to have the greater electron donating capacity. This deviation may be ascribed to hydrogen bonding[46], to methyl-amino group rotations, and to molecular size[55,61].

A reduction of temperature ($300^{o} \rightarrow 77^{o}K$) causes a red-shift of the $^{1}L_{a} \leftarrow {}^{1}A$ band that is similar to the shift caused by changing from non-polar to polar solvent (e.g., for NNDMPNA, the two shifts are $2500cm^{-1}$ and $2000cm^{-1}$, respectively). This shift is probably due to the reduction of the Onsager radius as the density increases[45]. In general, solvatochromism in both absorption and emission at $77^{o}K$ is less than at $300^{o}K$ (See Table 9). Since neither the $^{1}L_{b}$ nor the $^{3}L_{a}$ states are likely to be as polar as the $^{1}L_{a}$ state[4], they exhibit smaller solvatochromic effects.

5. TEMPERATURE DEPENDENCE: Highly-polar molecules in non-polar solvents are known to dimerize in the ground state, affecting both absorption and emission[37,73]. For example, the absorption spectra of p-cyanoaniline at various temperatures are presented in Figure 26. The lowest-energy absorption band is assumed to be due to the self-complex. Molecules in non-polar solvents at very low concentrations ($<10^{-5}M$) do not ordinarily exhibit dimerization phenomena in the absorption spectra but such effects do appear in the emission spectroscopy.

6. EXCITATION PHENOMENA: In many D-ϕ-A molecules, excitation into the extreme red edge of the lowest-energy absorption band results in a red-shift ($\sim 100cm^{-1}$) of the phosphorescence spectrum. Apparently, the molecules being excited are those whose triplet states are more efficiently solvated and, hence, are lower in energy[45].

Figure 26.

Temperature effects on the absorption spectrum of p-cyanoaniline. The spectra were obtained in a 4.66×10^{-5} M solution in 3-methylpentane. A refers to the room temperature spectrum, B refers to the $77^{\circ}K$ spectrum, and C refers to the spectrum of an intermediate temperature.

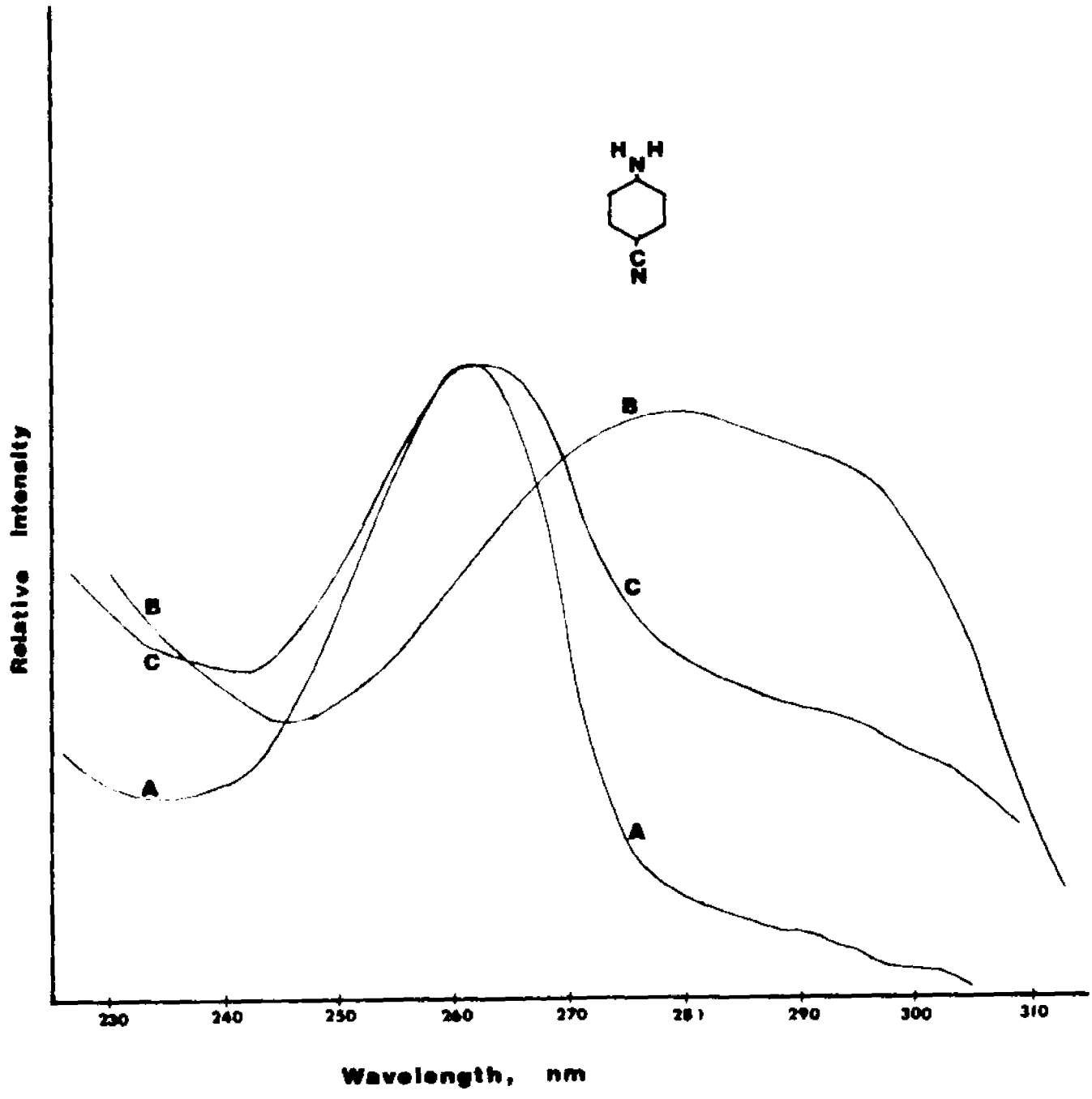
H
N
H
C
N
B
C
A
B
C
A
Relative Intensity
230
240
250
260
270
280
290
300
310
Wavelength, nm

TABLE 9

EFFECT OF SOLVENT ON EMISSION ENERGIES[a]

MOLECULE	$\Delta\bar{\nu}$, FLUORESCENCE, kK		
	o	m	p
Fluorobenzonitrile	1.42	-0.72	-0.24
Cyanophenol	0.21	0.20	---
Cyanoanisole	1.72	1.32	-0.46
Cyanoaniline	-0.75	---	-0.09

MOLECULE	$\Delta\bar{\nu}$, PHOSPHORESCENCE, kK		
	o	m	p
Fluorobenzonitrile	-0.14	-0.11	-0.20
Cyanophenol	-0.0	-0.03	---
Cyanoanisole	-0.01	-1.13	---
Cyanoaniline	0.23	---	-0.05

[a] $\Delta\bar{\nu}$ is the energy difference $\bar{\nu}_{0,0}$(MCH) - $\bar{\nu}_{0,0}$(Ethanol) as measured in glassy solutions at 77°K.

7. LUMINESCENCE OF PARA D-ϕ-NO_2 COMPOUNDS: The luminescence properties of the nitroaromatics have long been a puzzle and the subject of considerable discussion [60, 75-80]. Hence, it may be well to summarize that which is definitely known about these compounds:

---They possess a low-energy $^1\Gamma_{n\pi^*}$ state. This state, for example, is the S_1 state of nitrobenzene [60,77] and 1-nitronaphthalene [78]. As the strength of the donor substituent in D-ϕ-NO_2 is increased, the $^1\Gamma_{n\pi^*}$ energy will either increase slightly or remain constant.

---The T_1 state of 1-nitronaphthalene[82,83], possibly that of nitrobenzene[79], and all D-ϕ-NO_2 species where D is at least as strong as -OH is $^3\Gamma_{\pi\pi^*}$. This conclusion is fully justified by the observed phosphorescence lifetimes of Table 10. The intermediacy of D-ϕ-NO_2 phosphorescence lifetimes between that of a typical $^3\Gamma_{\pi\pi^*}$ state (benzene) and a typical $^3\Gamma_{n\pi^*}$ state (benzaldehyde) vindicates[84] the $^3\Gamma_{\pi\pi^*}$ nature of T_1 states in question and the presence of an adjacent $^1\Gamma_{n\pi^*}$ state (See previous item). The same conclusion follows by comparison with the substituted benzaldehydes of Table 10. As the donor strength of D increases, the energy of this T_1 state (i.e., $^3\Gamma_{\pi\pi^*}$ or L_a) will decrease.

---The lowest $^1\Gamma_{\pi\pi^*}$ state when D is a weak donor is ^1L_b; that, when D is a strong donor, is ^1L_a. Both of these states decrease energetically as the donor strength increases, that of ^1L_a being greatest. It follows, as donor strengths increase, that one may sample the energy sequences: $E(^1\Gamma_{n\pi^*}) < E(^1L_b) < E(^1L_a)$; $E(^1L_b) < E(^1\Gamma_{n\pi^*}) < E(^1L_a)$; $E(^1L_b) \leq E(^1L_a) < E(^1\Gamma_{n\pi^*})$; or $E(^1L_a) < E(^1L_b) < {}^1\Gamma_{n\pi^*}$.

---The lowest-energy absorption band of D-ϕ-NO_2 entities, D being

TABLE 10

PHOSPHORESCENCE LIFETIMES, τ, AS INDICATORS OF THE NATURE OF THE T_1 STATE

MOLECULE	T_1 TYPE	SOLVENT	τ(s)	τ^o(s)	REFERENCE†
Benzene	$^3\Gamma_{\pi\pi^*}$	MCH	8	33	a
ϕCHO	$^3\Gamma_{n\pi^*}$	EPA	0.004	0.005	b
p-$CH_3\phi$CHO	$^3\Gamma_{\pi\pi^*}$	EPA	0.084	0.14	b
p-HOϕCHO	"	"	0.26	0.47	c
p-CH_3OϕCHO	"	"	0.10	0.31	c
p-$H_2N\phi NO_2$	"	3MP	0.20	---	d
p-$H_2N\phi NO_2$	"	EPA	0.24	---	d
p-$H_2N\phi NO_2$	"	Ethanol	0.09	---	e
p-$(CH_3)_2N\phi NO_2$	"	MCH	0.20	---	d
p-$(CH_3)_2N\phi NO_2$	"	EPA	0.22	---	d
p-HOϕNO_2	"	Ethanol	0.08	---	e

†Table references are:

a. C. A. Parker, "Photoluminescence of Solutions," Elsevier, The Netherlands, 1968 p. 281.
b. N. C. Yang et al., J. Amer. Chem. Soc., 89, 5466 (1967).
c. R. Lui and E. C. Lim, J. Chem. Phys. 57, 605 (1972).
d. O. Khalil, C. J. Seliskar and S. P. McGlynn, J. Chem. Phys., 58, 1607 (1973).
e. P. P. Dikun, A. A. Petrov and B. Ya. Sveshnikov, Zhur. Eksptl. Theoret. Fiz. 21, 150 (1951). (c.a. 45:8357i).

a relatively good donor, encompasses all four transitions: $^1L_a \leftarrow {}^1A$, $^1L_b \leftarrow {}^1A$, $^1\Gamma_{n\pi^*} \leftarrow {}^1\Gamma_1$, and $^3\Gamma_{n\pi^*} \leftarrow {}^1\Gamma_1$. It is this proximity of nearly degenerate states which is responsible for the differences in fluorescence and phosphorescence excitation spectra (See Section C.1), and for the gross effects of solvent polarity and seemingly-innocuous chemical subsition (i.e., N-methylation) on the luminescence characteristics.

---The non-radiative intersystem crossing cross-sections $^1\Gamma_{n\pi^*} \rightsquigarrow {}^3\Gamma_{\pi\pi^*}$ or $^1\Gamma_{\pi\pi^*} \rightsquigarrow {}^3\Gamma_{n\pi^*}$ are much more efficient[80] than the routes $^1\Gamma_{\pi\pi^*} \rightsquigarrow {}^3\Gamma_{\pi\pi^*}$ or $^1\Gamma_{n\pi^*} \rightsquigarrow {}^3\Gamma_{n\pi^*}$. It is this fact which underlies the expectations of the previous item.

---The radiative cross-sections, as estimated from typical oscillator strength data, are $\sigma(^1\Gamma_{n\pi^*} \rightarrow {}^1\Gamma_1) \simeq 10^2(^1L_b \rightarrow {}^1A) \simeq 10(^1L_a \rightarrow {}^1A)$.

We are now in a position to rationalize the gamut of observed luminescence behavior. Such a rationalization is schematized in Figure 27 and systems exemplifying the expected behavior are specified.

8. LUMINESCENCE OF ORTHO AND META D-ϕ-NO_2 COMPOUNDS: The luminescence of these compounds, D being a strong donor, consists solely of fluorescence. The reasons for this are three-fold: Firstly, the $^1L_b \leftarrow {}^1A$ band is intense in these systems, with the result that the $^1L_b \rightarrow {}^1A$ cross-section is large. Secondly, the $^1\Gamma_{n\pi^*} \leftarrow {}^1\Gamma_1$ transition is expected to lie at higher energies as one progresses through a given series $\underline{p} \rightarrow \underline{m} \rightarrow \underline{o}$. Thirdly, the $^1L_b \leftarrow {}^1A$ transition is expected to lie at lower energies in $\underline{o}$ and $\underline{m}$ than in $\underline{p}$. Consequently, it is expected that $^{1,3}\Gamma_{n\pi^*}$ states lie at higher energy than ^1L_b. Hence,

Figure 27.

The excited states of p-substituted nitrobenzenes. The molecular polarity increases from left to right. In each of the four systems, the states on the left are singlet states and the states on the right are triplet states. The a refers to L_a, the b refers to L_b, and the n refers to the n,π^* state. Unsubstituted nitrobenzene or nitrobenzene with weakly polar substituents exhibits weak or no emission. More polar nitrobenzenes such as p-nitrophenol phosphoresce but have weak or absent fluorescence. Highly-polar nitrobenzenes such as p-nitroaniline and its methylated derivitives both phosphoresce and fluoresce. The intensities of phosphorescence and fluorescence are substituent and solvent dependent: in the very polar solvent polyvinylalcohol (PVA), only fluorescence is observed.

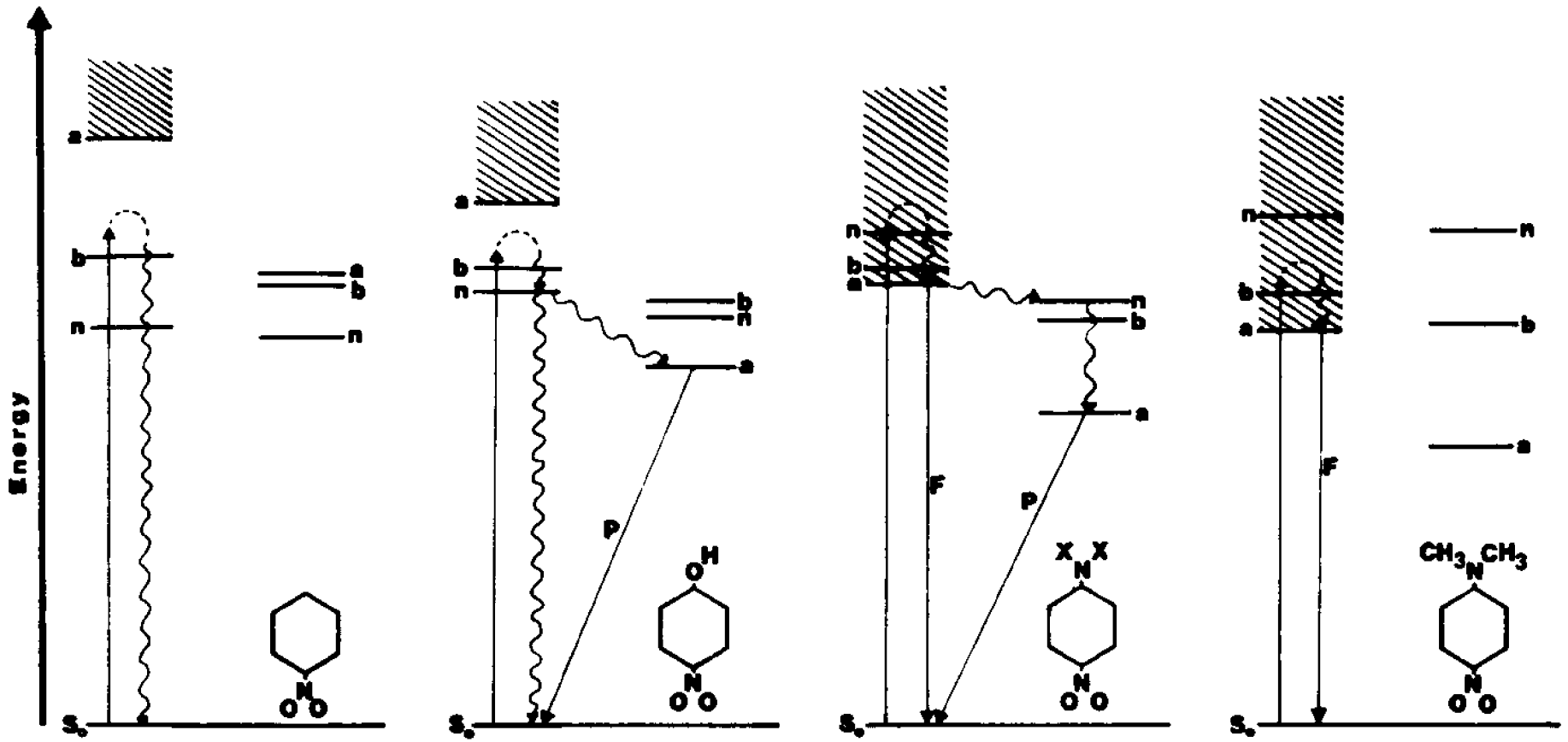
Energy
a
b
n
S₀
P
F
X = H, CH₃
in EPA
Any Solvent
PVA

we expect little intersystem crossing (i.e., weak or no phosphorescence) and an efficient $^1L_b \rightarrow {}^1A$ emissive path (i.e., fluorescence).

IV. QUANTUM CHEMICAL COMPUTATIONAL METHODS

All valence-electron, CNDO/s-CI computations, DelBene-Jaffé formalism[85,86], were performed on an IBM 360/65 computer using QCPE program CNDO 174. The Mataga-Nishimoto approximation[87] for two-center repulsion integrals was used. Convergence criteria and iteration procedures were those of King and Van Putten[88]. Convergence occurred after eleven iterations in all cases except p-fluorobenzonitrile and p-aminobenzoic acid, which needed fifteen and twenty-five, respectively. The parametrizations for C, H, N and O proposed by Del Bene and Jaffé[85] and that proposed for F by Kuehnlenz and Jaffé[89] were used. Only the first thrity mono-excited configurations were included in the CI procedure.

Benzene was considered to be the parent molecule. The xz-plane is the molecular plane, the z-axis bisects ∢ CCC, the y-axis bisects C-C bonds, and the coordinate origin lies on the inversion center. Standard bond lengths and bond angles were used[90].

The coordinate systems, point groups and structural references for all other molecules are presented in Figure 28 and Table 11. A C_s representation was considered adequate for molecules #9 and #10.

Any charge-transfer nature of an electronic transition is assumed to cause a movement of electron density from the vicinity of the donor substituent to the vicinity of the acceptor substituent. The amount of electron density lost by the donor in the transition 2 ← 1 may be expressed, in the absence of CI as

Figure 28.

Geometries and axes for D-ϕ-A molecules. Point groups, index numbering and structural references are compiled in Table 11.

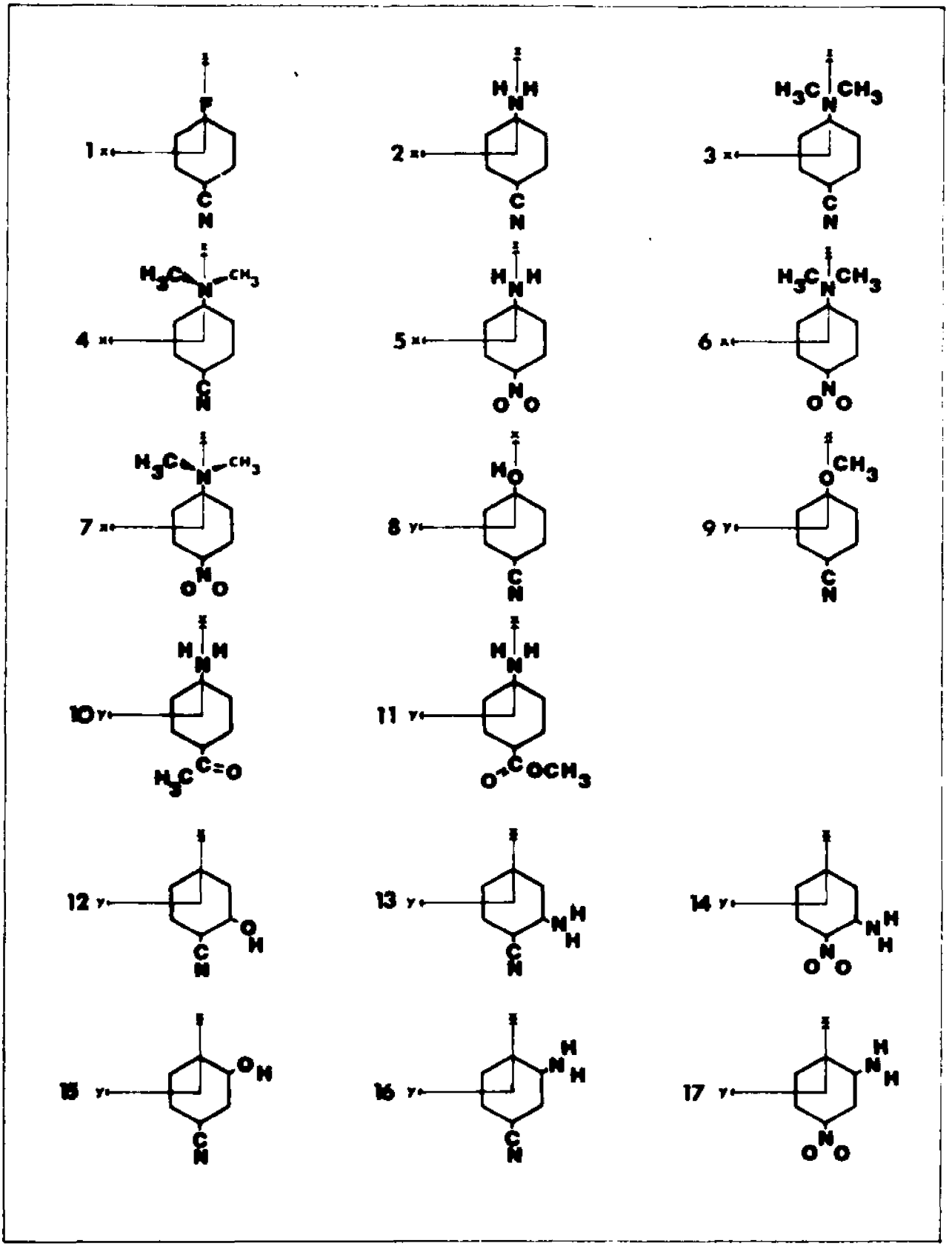
1
2
3
4
5
6
7
8
9
10
11
12
13
14
15
16
17

TABLE 11

NUMBER INDICES, POINT GROUPS AND STRUCTURAL REFERENCES FOR THE MOLECULES OF FIGURE 28

	Molecule	Point Group	Reference
1.	p-flourobenzonitrile	C_{2v}	91
2.	p-cyanoanile	C_{2v}	92
3.	N,N-dimethyl-p-cyanoaniline, planar a)	C_{2v}	92
4.	N,N-dimethyl-p-cyanoaniline, perpendicular a)	C_{2v}	92
5.	p-nitroaniline	C_{2v}	93
6.	N,N-dimethyl-p-nitroaniline, planar a)	C_{2v}	94
7.	N,N-dimethyl-p-nitroaniline, perpendicular a)	C_{2v}	94
8.	p-cyanophenol	C_s	92
9.	p-cyanoanisole	C_s	95
10.	p-aminoacetophenone	C_s	97
11.	p-aminobenzoic acid	C_s	100
12.	o-cyanophenol	C_s	92
13.	o-cyanoaniline	C_s	92
14.	o-nitroaniline	C_s	101
15.	m-cyanophenol	C_s	92
16.	m-cyanoaniline	C_s	92
17.	m-nitroaniline	C_s	101

a) Perpendicular: The (N,C,C)-plane of the dimethylamino group is to the benzenoid plane.
Parallel: The (N,C,C)-plane of the dimethylamino group is coplanar with that of the benzene group.

$$F_D = \left(\sum_i c_i^2\right)_{D,1} - \left(\sum_i c_i^2\right)_{D,2}$$

$$= X_{D_1} - X_{D_2}$$

where $(c_i)_{D,1}$ is the LCAO coefficient of the ith AO of one of the donor atoms in MO #1, and the sum is effected over all AO's of all centers of the donor group in MO #1. Hence, we can define X_{D_1} and X_{D_2} as electron density of the donor in states 1 and 2, respectively. The concept is readily extensible to the CI situation where states 1 and 2 are multi-configurational in nature.

The electron density gained by the acceptor substituent in the transition $2 \leftarrow 1$ is expressed as

$$F_A = \left(\sum_i c_i^2\right)_{A,2} - \left(\sum_i c_i^2\right)_{A,1}$$

$$= X_{A_2} - X_{A_1}$$

Consequently, the quantity $(F_A + F_D)$ constitutes a measure of the charge transfer character of the transition $2 \leftarrow 1$. The quantity $F_A + F_D$, as defined, is always positive -- at least to the extent that A and D behave as <u>bona fide</u> electron acceptors and donors, respectively.

The ground state dipole moments, μ_O, were obtained using the Point-Charge Model[102,103]:

$$\mu_O = 4.8033 \sum_A Q_A \vec{r}_A \text{ (Debyes)}$$

where Q_A is the ground state charge density on center A and $\vec{r}_A$ is the radius vector from the coordinate origin to center A.

V. COMPUTATIONAL RESULTS

A. p-ISOMERS

1. SINGLET STATES: The energies, oscillator strengths and transition moment vectors (i.e., polarizations) of the lower-energy singlet electronic states of the p subset are presented in Table 12. The following observations may be made:

---In all cases, except planar NNDMPNA, the lowest-energy $^1\Gamma_{\pi\pi^*}$ state is ^1L_b, while the second lowest-energy $^1\Gamma_{\pi\pi^*}$ state is ^1L_a. In the case of NNDMPNA, these two states are inverted.

---In molecules containing a cyano group, there are two states which normally lie energetically between the ^1L_b and ^1L_a states. These corresponding transitions are denoted $\pi(CN) \rightarrow \pi^*$ and $\pi \rightarrow \pi^*(CN)$. We define a $\pi(CN)$ orbital as an MO with > 50% of its electron density localized on the CN group in an in-plane π-bonding configuration (e.g., in p-fluorobenzonitrile, the $\pi(CN)$ orbital has 25% of its electron density on the cyano carbon p_x AO and 48% on the nitrogen p_x AO). The two geometric isomers of N,N-dimethyl-p-cyanoaniline (NNDMPCA) exhibit additional $^1\Gamma_{\pi(CN)\pi^*}$ states which lie energetically above the manifold of $^1\Gamma_{\pi\pi^*}$ states.

---The third and fourth $^1\Gamma_{\pi\pi^*}$ states in molecules of low polarity (e.g., p-fluorobenzonitrile) are related to the ^1B states of benzene. However, as molecular polarity increases, a number of higher lying $^1\Gamma_{\pi\pi^*}$ states are pushed into the energy range of the ^1L_b, ^1L_a, ^1B_b and ^1B_a states.

---In p-aminobenzoic acid, the lowest-energy states is $^1\Gamma_{n\pi^*}$, the non-bonding electron density being localized on the carbonyl oxygen. In p-nitroaniline and the two NNDMPNA isomers, the lowest-

TABLE 12

Computed (CNDO/S-CJ) Singlet Electronic States of p-disubstituted molecules.

a) only states whose energies are $\leq$ 7.0 ev are reported.
b) Perpendicular: The (N,C,C)-plane of the dimethylamino group is $\perp$ to the benzenoid plane. Parallel: The (N,C,C)-plane of the dimethylamino group is coplanar with that of the benzene group.
c) The electron density on the methyl hydrogens is not zero in either the initial or final orbital of this state. Hence, a small oscillator strength is computed.

Orbital Promotion	C_6H_6					P-FC_6H_4CN				
				Polarization					Polarization	
	$\Gamma_{C_{2v}}$	E(ev)	f	x	z	$\Gamma_{C_{2v}}$	E(ev)	f	x	z
$\pi \rightarrow \pi^*$	B_1	4.711	0.000	-------	-------	B_1	4.451	8.61×10^{-4}	-------	-------
	A_1	6.005	0.000	-------	-------	A_1	5.364	0.238	0.0002	-1.0000
	B_1	6.830	0.582	-0.9953	0.0967	B_1	6.369	0.459	0.9999	-0.0027
	A_1	6.830	0.582	0.0967	0.9953	A_1	6.471	0.544	0.0003	-1.0000
(CN)$\pi \rightarrow \pi^*$						A_2	4.628	---------		
$\pi \rightarrow \pi^*$(CN)						A_2	4.966	---------		
$n \rightarrow \pi^*$										
$\sigma \rightarrow \pi^*$	A_2	6.725	---------			A_2	6.335	---------		
	B_2	6.739	---------			B_2	6.505	---------		
	A_2	6.739	---------			B_2	6.702	---------		
	B_2	6.753	---------							

TABLE 12--Continued

Orbital Promotion	P-HOC_6H_4CN					P-$H_2NC_6H_4CN$				
				Polarization					Polarization	
	Γ_{C_s}	E(ev)	f	x	y	$\Gamma_{C_{2v}}$	E(ev)	f	x	z
$\pi \rightarrow \pi^*$	A'	4.393	7.78×10^{-3}	-0.0636	-0.9980	B_1	4.311	1.47×10^{-2}	-1.0000	-0.0026
	A'	5.205	0.258	1.0000	-0.0054	A_1	5.018	0.272	0.0006	-1.0000
	A'	6.347	0.454	-0.0104	-0.9999	B_1	6.260	0.401	1.0000	0.0014
	A'	6.486	0.526	1.0000	-0.0074	A_1	6.516	0.508	0.0010	-1.0000
	A'	6.953	7.63×10^{-3}	0.9956	-0.0932	A_1	6.866	4.41×10^{-4}	------	------
$(CN)\pi \rightarrow \pi^*$	A"	4.727	---------			A_2	4.809	---------		
$\pi \rightarrow \pi^*(CN)$	A"	5.081	---------			A_2	5.374	---------		
$n \rightarrow \pi^*$										
$\sigma \rightarrow \pi^*$	A"	6.437	---------			B_2	6.566	---------		
	A"	6.527	---------			A_2	6.606	---------		
	A"	6.810	---------							

TABLE 12--Continued

Orbital Promotion	$P\text{-}H_3COC_6H_4CN$					$P\text{-}(CH_3)_2NC_6H_4CN$ Perpendicular[b]				
				Polarization					Polarization	
	$\Gamma_{C_{2v}}$	E(ev)	f	x	y	$\Gamma_{C_{2v}}$	E(ev)	f	x	z
$\pi \rightarrow \pi^*$	A'	4.442	1.06×10^{-2}	0.2831	0.9591	B_1	4.485	1.35×10^{-3}	-1.0000	0.0007
	A'	5.052	0.320	-0.9996	-0.0286	A_1	5.375	0.242	-0.0002	1.0000
	A'	6.330	0.409	-0.1256	0.9921	B_1	6.408	0.461	1.0000	0.0002
	A'	6.660	0.438	0.9964	0.0847	A_1	6.478	0.537	0.0000	1.0000
	A'	6.872	5.71×10^{-2}	-0.9912	0.1327					
$(CN)\pi \rightarrow \pi^*$	A"	4.879	---------			A_2	4.864	---------		
	A"	6.323	---------			A_2	6.757	---------		
						B_2	6.884	---------		
$\pi \rightarrow \pi^*(CN)$	A"	5.327	---------			A_2	4.976	---------		
$n \rightarrow \pi^*$						A_2	4.718	---------		
						B_2	5.366	---------		
$\sigma \rightarrow \pi^*$	A"	6.114	---------			B_2	6.636	1.44×10^{-4}[c]		
	A"	6.709	---------			A_2	6.961	---------		

TABLE 12--Continued

Orbital Promotion	P-$(CH_3)_2NC_6H_4CN$ Planar[b]				
				Polarization	
	$\Gamma_{C_{2v}}$	E(ev)	f	x	z
$\pi \rightarrow \pi^*$	B_1	4.285	1.01×10^{-2}	-1.0000	-0.0020
	A_1	4.877	0.292	0.0002	-1.0000
	B_1	6.066	0.283	-1.0000	-0.0004
	A_1	6.421	0.164	-0.0004	-1.0000
	A_1	6.533	0.314	0.0009	-1.0000
$(CN)\pi \rightarrow \pi^*$	A_2	5.006	---------		
	B_2	6.561	---------		
$\pi \rightarrow \pi^*(CN)$	A_2	4.823	---------		
$n \rightarrow \pi^*$					
$\sigma \rightarrow \pi^*$	A_2	6.577	---------		
	B_2	6.743	---------		

TABLE 12--Continued

Computed (CNDO/S-CI) Singlet Electronic States of <u>para</u>-Disubstituted Molecules[a]

a) only states whose energies are 7.0 ev are reported

Orbital Promotion	$P\text{-}H_2NC_6H_4COCH_3$					$P\text{-}H_2NC_6H_4CO_2H$				
				Polarization					Polarization	
	Γ_{C_s}	E(ev)	f	x	y	Γ_{C_s}	E(ev)	f	x	y
$\pi \rightarrow \pi^*$	A'	4.483	6.08×10^{-3}	-0.0618	-0.9981	A'	4.437	3.21×10^{-3}	-0.1799	0.9837
	A'	5.138	0.241	-0.9999	-0.0147	A'	5.179	0.211	0.9947	-0.1026
	A'	6.293	0.362	-0.0271	-0.9996	A'	6.184	0.264	0.2200	0.9755
	A'	6.558	0.336	-0.9813	-0.1926	A'	6.404	0.471	-0.9300	0.3676
	A'	6.732	0.150	-0.9900	0.1414	A'	6.719	6.87×10^{-2}	0.8420	0.5395
$\ell \rightarrow \pi^*$										
$n \rightarrow \pi^*$						A"	3.584	---------		
						A"	6.356	---------		
						A"	6.382	---------		
$\sigma \rightarrow \pi^*$	A"	3.002	---------			A"	6.574	---------		
	A"	5.758	---------			A"	6.627	---------		
	A"	5.918	---------							
	A"	6.395	---------							
	A"	6.527	---------							

TABLE 12--Continued

Orbital Promotion	$P\text{-}H_2NC_6H_4NO_2$					$P\text{-}(CH_2)_2NC_6H_4NO_2$ Perpendicular				
				Polarization					Polarization	
	$\Gamma_{C_{2v}}$	E(ev)	f	x	z	$\Gamma_{C_{2v}}$	E(ev)	f	x	z
$\pi \rightarrow \pi^*$	B_1	4.476	1.46×10^{-3}	-1.0000	0.0017	B_1	4.448	0.000	-------	-------
	A_1	4.846	0.221	-0.0001	1.0000	A_1	4.711	0.249	-0.0008	1.0000
	B_1	5.898	0.187	-1.0000	-0.0005	B_1	5.903	0.129	-1.0000	-0.0031
	A_1	5.954	4.00×10^{-3}	0.0011	1.0000	A_1	6.023	9.00×10^{-4}	-------	-------
	A_1	6.591	0.451	0.0004	-1.0000	B_1	6.820	0.600	-1.0000	0.0002
	B_1	6.746	0.501	1.0000	-0.0001	A_1	6.834	0.462	-0.0002	1.0000
$\ell \rightarrow \pi^*$	B_1	5.581	5.14×10^{-3}	-1.0000	0.0012	B_1	5.406	2.33×10^{-2}	-1.0000	0.0053
	A_1	6.257	9.75×10^{-3}	-0.0021	1.0000	A_1	6.359	7.88×10^{-3}	-0.0108	-0.9999
	B_1	6.550	4.48×10^{-2}	-1.0000	-0.0003	B_1	6.494	0.112	-1.0000	-0.0001
$n \rightarrow \pi^*$	A_2	2.798	---------			A_2	2.813	---------		
	B_2	2.954	---------			B_2	2.853	---------		
	A_2	6.968	---------			A_2	4.121	---------		
						B_2	5.352	---------		
$\sigma \rightarrow \pi^*$	A_2	6.179	---------			A_2	6.572	---------		
	B_2	6.354	---------							

TABLE II--Continued

Orbital Promotion	P-$(CH_2)_2NC_6H_4NO_2$ Planar				
				Polarization	
	$\Gamma_{C_{2v}}$	E(ev)	f	x	z
$\pi \rightarrow \pi^*$	A_1	4.230	0.312	0.0001	-1.0000
	B_1	4.303	5.89×10^{-3}	1.0000	0.0003
	A_1	5.488	1.12×10^{-2}	-0.0040	1.0000
	B_1	5.788	0.220	1.0000	0.0012
	A_1	6.566	0.215	0.0009	-1.0000
	B_1	6.675	0.214	-1.0000	-0.0013
$\ell \rightarrow \pi^*$	B_1	5.425	1.32×10^{-3}	-0.9999	0.01650
	A_1	6.293	1.98×10^{-2}	-0.0003	-1.0000
	B_1	6.531	0.180	-1.0000	0.0011
$n \rightarrow \pi^*$	B_2	2.867	---------		
	B_2	2.902	---------		
	B_2	6.968	---------		
$\sigma \rightarrow \pi^*$	A_2	6.155	---------		
	B_2	6.684	---------		

energy excited states are $^1\Gamma_{n\pi^*}$, the non-bonding electron density now being localized on the oxygens of the NO_2 group. Two low-energy $^1\Gamma_{n\pi^*}$ states -- the n MO being largely a $2p_x$ AO localized on the amino nitrogen -- occur also in NNDMPCA but, in this case, they are not computed to be the lowest-energy excited states.

---In all molecules containing a nitro group, states whose orbital promotions initiate in MO's localized on out-of-plane (p_y) oxygen AO's and terminate in π^* MO's are computed to be of low energy. These promotions are denoted $\ell \rightarrow \pi^*$ (ℓ = lone pair) and are of the same symmetry as certain $^1\Gamma_{\pi\pi^*}$ states.

---The highest-energy states in all p-isomers listed result from $\sigma \rightarrow \pi^*$ promotions.

---Similar calculations have been performed on several molecules of Table 17 (p-cyanophenol, p-cyanoaniline and the two geometric isomers of NNDMPCA) by Khalil et al.[11] All states other than $^1\Gamma_{\pi\pi^*}$ states were mistakenly assigned by these authors as $\sigma \rightarrow \pi^*$ promotions.

2. TRIPLET STATES: The energies of the computed triplet states of the p sub-set are presented in Table 13. The following observations are pertinent.

---In every case, except benzene and p-nitroaniline, the lowest-energy $^3\Gamma_{\pi\pi^*}$ state is ^3L_a while the second-lowest energy $^3\Gamma_{\pi\pi^*}$ state is ^3L_b. This result holds even for planar NNDMPNA in which the ^1L_b and ^1L_a states have been inverted. In benzene, the first and the third $^3\Gamma_{\pi\pi^*}$ states derive from L_a and L_b configurations, respectively, whereas the second $^3\Gamma_{\pi\pi^*}$ state (a degenerate state) derives from an E_{1u} configuration (B_a, B_b). The third $^3\Gamma_{\pi\pi^*}$ state of p-nitroaniline is ^3L_b whereas both the first and second $^3\Gamma_{\pi\pi^*}$ states contain a consid-

TABLE 13

Computed (CNDO/S-CI) Triplet Electronic States of para-Disubstituted Molecules[a]

a) only states whose energies are $\leq$ 5.4 ev are reported

Orbital Promotion	C_6H_6		P-FC_6H_4CN		P-HOC_6H_4CN		P-$H_2NC_6H_4CN$		P-$H_3COC_6H_4CN$	
	$\Gamma_{C_{2v}}$	E(ev)	$\Gamma_{C_{2v}}$	E(ev)	Γ_{C_s}	E(ev)	$\Gamma_{C_{2v}}$	E(ev)	Γ_{C_s}	E(ev)
$\pi \rightarrow \pi^*$	A_1	2.909	A_1	2.780	A'	2.831	A_1	2.815	A'	2.845
	B_1	3.810	B_1	3.602	A'	3.511	B_1	3.410	A'	3.622
	$^+A_1$	3.810	A_1	3.653	A'	3.619	A_1	3.580	A'	3.769
	B_1	4.711	B_1	4.444	A'	4.433	B_1	4.453	A'	4.515
	A_1	5.344	A_1	5.114	A'	5.097	A_1	5.020	A'	5.111
	$^+B_1$	5.344								
$(CN)\pi \rightarrow \pi^*$			A_2	4.628	A"	4.727	A_2	4.809	A"	4.879
$\pi \rightarrow (CN)\pi^*$			A_2	4.966	A"	5.081	A_2	5.374	A"	5.327
$n \rightarrow \pi^*$										

TABLE 13--Continued

Computed (CNDO/S-CI) Triplet Electronic States of para-Disubstituted Molecules[a]

a) only states whose energies are $\leq$ 5.4 ev are reported.
b) The electron density on the methyl hydrogens is not zero in either the initial or final orbital of this state. Hence, the triplet energy is 0.0008 ev less than the corresponding singlet energy.

Orbital Promotion	$P\text{-}H_2NC_6H_4COCH_3$		$P\text{-}H_2NC_6H_4CO_2H$		$P\text{-}H_2NC_6H_4NO_2$		$P\text{-}(CH_3)_2NC_6H_4NO_2$			
							Perpendicular		Planar	
	Γ_{C_s}	E(ev)	Γ_{C_s}	E(ev)	$\Gamma_{C_{2v}}$	E(ev)	$\Gamma_{C_{2v}}$	E(ev)	$\Gamma_{C_{2v}}$	E(ev)
$\pi \rightarrow \pi^*$	A'	2.828	A'	2.785	A_1	2.916	A_1	2.650	A_1	2.554
	A'	3.632	A'	3.593	A_1	3.601	B_1	3.677	B_1	3.505
	A'	3.727	A'	3.627	B_1	3.690	A_1	3.687	A_1	3.578
	A'	4.451	A'	4.325	B_1	4.196	B_1	4.252	B_1	4.134
	A'	5.235	A'	4.369	A_1	5.056	A_1	4.753	A_1	4.576
$\ell \rightarrow \pi^*$					B_1	1.558	B_1	1.546	B_1	1.616
							B_1	2.813	A_1	5.218
$n \rightarrow \pi^*$			A"	3.584	A_2	2.798	B_2	2.853	B_2	2.867
					B_2	2.954	A_2	4.121	B_2	2.902
							B_2	5.352		
$\sigma \rightarrow \pi^*$	A"	3.001[b]								

TABLE 13--Continued

Orbital Promotion	P-$(CH_3)_2NC_6H_4CN$			
	Perpendicular		Planar	
	$\Gamma_{C_{2v}}$	E(ev)	$\Gamma_{C_{2v}}$	E(ev)
$\pi \rightarrow \pi^*$	A_1	2.849	A_1	2.719
	B_1	3.638	B_1	3.405
	A_1	3.673	A_1	3.577
	B_1	4.440	B_1	4.365
	A_1	5.188	A_1	4.947
$(CN)\pi \rightarrow \pi^*$	A_2	4.864	A_2	5.006
$\pi \rightarrow (CN)\pi^*$	A_2	4.976	A_2	4.823
$n \rightarrow \pi^*$	A_2	4.718		
	B_2	5.366		

erable L_a configurational component.

---The lowest-energy triplet state of molecules which contain an NO_2 group is of $^3\Gamma_{\ell\pi^*}$ nature. Indeed, all molecules which have $^1\Gamma_{n\pi^*}$ states at energies $\leq$ 5.4eV have energetically-identical $^3\Gamma_{n\pi^*}$ states which, perforce, are included in Table 13. This singlet-triplet degeneracy also holds for $^{1,3}\Gamma_{\pi(CN)\pi^*}$, $^{1,3}\Gamma_{\pi\pi^*(CN)}$ and $^{1,3}\Gamma_{\sigma\pi^*}$ states and is a consequence of the approximations inherent in the CNDO formalism[104].

3. DIPOLE MOMENTS: The computed values of the ground state dipole moment, μ_o, are collected in Table 14 and compared with the experimental values.

The $^1\Gamma_{\pi\pi^*}$ states of the p sub-set, arranged from left to right in order of increasing $|\mu_o|$, are correlated in Figure 29. From reference to Figure 29 and, following the order in which molecular polarity increases, one concludes that:

---The ^1L_a - ^1L_b energy gap decreases.

---The $^1L_a \leftarrow {}^1A$ absorption band decreases in energy to a greater extent than does the $^1L_b \leftarrow {}^1A$ absorption band.

---There is an overall intensity increase in the $^1L_a \leftarrow {}^1A$ absorption band.

---The ^1B_a - ^1B_b energy gap increases.

---When the molecular polarity is very large (e.g., planar NNDMPNA), the ^1L_a and ^1L_b states invert order.

---The ^1L_a - ^3L_a interval decreases. This observation, of course, is not intrinsic to Figure 29 but is validated by the data of Table 15.

In order to test the experimental supposition that a decreasing

TABLE 14

CALCULATED[a] AND EXPERIMENTAL[b] GROUND STATE DIPOLE MOMENTS (DEBYES)

Molecule[c]	μ_o (Calc.)			μ_o	
	X-Dipole	Y-Dipole	Z-Dipole	Calculated	Experimental[d]
Benzene	0.0	0.0	0.0	0.0	0.0
1	0.0	0.0	0.8642	0.8642	---
2	0.0	0.0	3.9689	3.9689	5.96
3	0.0	0.0	4.0152	4.0152	5.94
4	0.0	0.0	3.3249	3.3249	---
5	0.0	0.0	6.4355	6.4355	6.31
6	0.0	0.0	7.6339	7.6339	6.92
7	0.0	0.0	6.4330	6.4330	---
8	2.8919	-0.5407	0.0	2.9420	4.95
9	3.3740	-0.8789	0.0	3.4866	4.90
10	2.5893	2.0530	0.0	3.3044	4.48
11	-2.3639	-2.3922	0.0	3.3632	3.10
12	2.2498	0.1554	0.0	2.2552	---
13	2.2996	-0.9933	0.0	2.5049	---
14	5.0099	-0.2781	0.0	5.0176	4.06
15	2.2114	-0.3298	0.0	2.2358	---
16	3.1863	-0.9037	0.0	3.3120	---
17	5.7456	-0.2113	0.0	5.7495	4.89

a) μ_o is calculated by the point-charge approximation using charge densities taken from CNDO/S computations.

b) All experimental values are from Reference 74. In every case the dipole moment values are from measurement of the dielectric constant (benzene solvent, 25°C).

c) The numbering of molecules refers to Table 11.

d) The percentage of electronic polarization used for atomic polarization in the calculation of dipole moment from dielectric constant data is zero for benzene and molecules 8, 14; five for molecules 2, 5, 9 (average of two values), 10, 11, 17; and fifteen for molecule 3. A "dash" in this column indicates that the value was not reported. No values are listed for molecules 4 and 7, since they are the perpendicular isomers of 3 and 6.

Figure 29.

Correlation of $^1\Gamma_{\pi\pi^*}$ (CNDO/s-C.I.) states of p-disubstituted molecules with the $^1\Gamma_{\pi\pi^*}$ state of benzene. The molecules are arranged from left to right in order of increasing computed ground state dipole moment, $|\mu_0|$. The molecules are denoted as follows: A, benzene; B, p-fluorobenzonitrile; C, p-cyanophenol; D, p-aminoacetophenone; E, N,N-dimethyl-p-cyanoaniline (nonplanar); F, p-aminobenzoic acid; G, p-cyanoanisole; H, p-cyanoaniline; I, N,N-dimetnyl-p-cyanoaniline; J, N,N-dimethyl-p-nitroaniline (non-planar); K, p-nitroaniline; and L, N,N-dimethyl-p-nitroaniline.

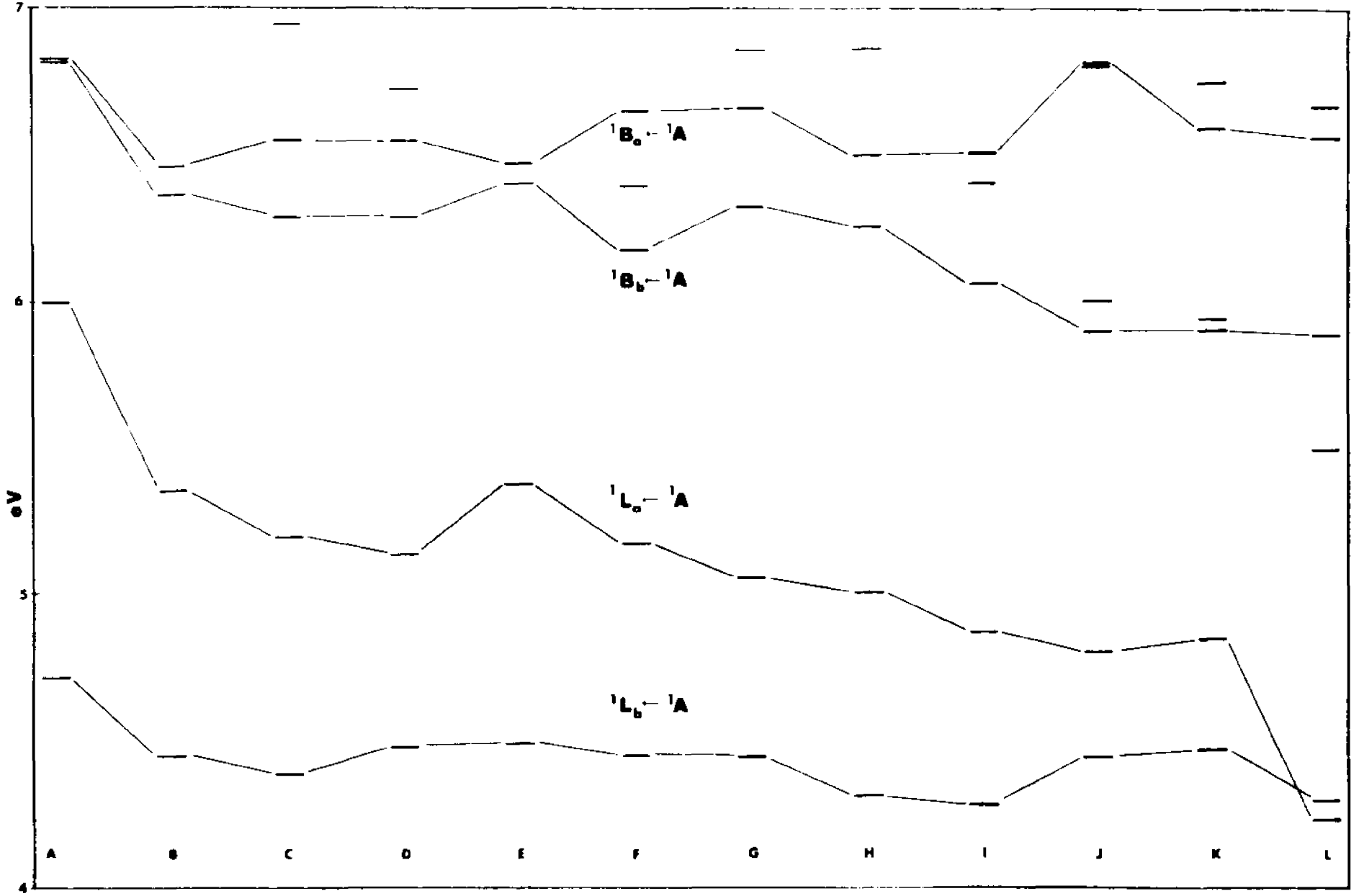
7
6
5
4
eV
$^1B_a \leftarrow {}^1A$
$^1B_b \leftarrow {}^1A$
$^1L_a \leftarrow {}^1A$
$^1L_b \leftarrow {}^1A$
A
B
C
D
E
F
G
H
I
J
K
L

TABLE 15

COMPUTED (CNDO/s-CI) ^1L_a-^3L_a ENERGY SPLIT

Molecule	$E(^1L_a-^3L_a)$ ev
Benzene	3.096
p-fluorobenzonitrile	2.584
p-hydroxybenzonitrile	2.374
p-aminoacetophenone	2.310
p-aminobenzonitrile	2.203
p-cyanoanisole	2.207
p-dimethylaminobenzonitrile, planar a)	2.158
p-dimethylaminobenzonitrile, perpendicular a)	2.526
p-aminobenzoic acid	2.394
p-nitroaniline	1.930
N_1N-dimethyl-p-nitroaniline, planar a)	1.676
N_1N-dimethyl-p-nitroaniline, perpendicular a)	2.061
o-hydroxybenzonitrile	2.531
o-aminobenzonitrile	2.378
o-nitroaniline	2.139
m-hydroxybenzonitrile	2.600
m-aminobenzonitrile	2.469
m-nitroaniline	2.421

energy of the $^1L_a \leftarrow {}^1A$ absorption band implies an increasing molecular polarity, we have re-ranked the molecules of Figure 29 --- the perpendicular geometric isomers of both NNDMPCA and NNDMPNA being omitted --- according to decreasing experimental energy of the $^1L_a \leftarrow {}^1A$ band. The resulting correlation is presented in Figure 30. Even though three molecules in the medium polarity range (i.e., p-cyanophenol, p-cyanoaniline and p-aminoacetophenone) are shifted relative to their ranking in Figure 29, the overall experimental trends of Section III, and the trends evidenced in Figure 29 are reproduced.

4. CHARGE TRANSFER: The charge transfer nature of the ^1L_a state is analyzed in terms of the quantity $F_A + F_D$ in Figure 31. The quantity $F_A + F_D$, for both the ^1L_a and ^1L_b states, is plotted versus the computed ^1L_a energy. The six molecules considered cover the range from relatively non-polar to highly-polar. It is clear that, as molecular polarity increases, the CT nature of both states increases, that of the ^1L_a state being by far the more sensitive. Over the same polarity range, the ^1L_b state exhibits an increase in CT character that is less than half that exhibited by the ^1L_a state.

In specific, it may be said that the ^1L_a state of NNDMPNA is 68% charge transfer in nature, and that the ^1L_a states of PNA is 50% CT. In this sense, it is not illogical to rename the ^1L_a state of NNDMPNA the "CT State". But it is presumptuous to extend this terminology to the ^1L_a states of NNDMPCA, PCA, PCP, or, indeed, to any molecule which lies leftward of PNA in Figure 31. By the same token, it may well be equally presumptuous of us to use the name ^1L_a for that excited state of NNDMPNA which is mostly (i.e., 68%) CT.

The truth of the matter is that the choice of name is irrelevant

Figure 30.

Correlation of $^1\Gamma_{\pi\pi^*}$ (CNDO/s-C.I.) states of p-disubstituted molecules with the $^1\Gamma_{\pi\pi^*}$ states of benzene. The molecules are are arranged from left to right in order of decreasing experimental $^1L_a \leftarrow {}^1A$ energy. The molecules are denoted by the following: A, benzene; B, p-fluorobenzonitrile; C, p-cyanophenol; D, p-cyanoanisole; E, p-cyanoaniline; F, p-aminobenzoic acid; G, N,N-dimethyl-p-cyanoaniline; H, p-aminoacetophenone; I, p-nitroaniline; and J, N,N-dimethyl-p-nitroaniline.

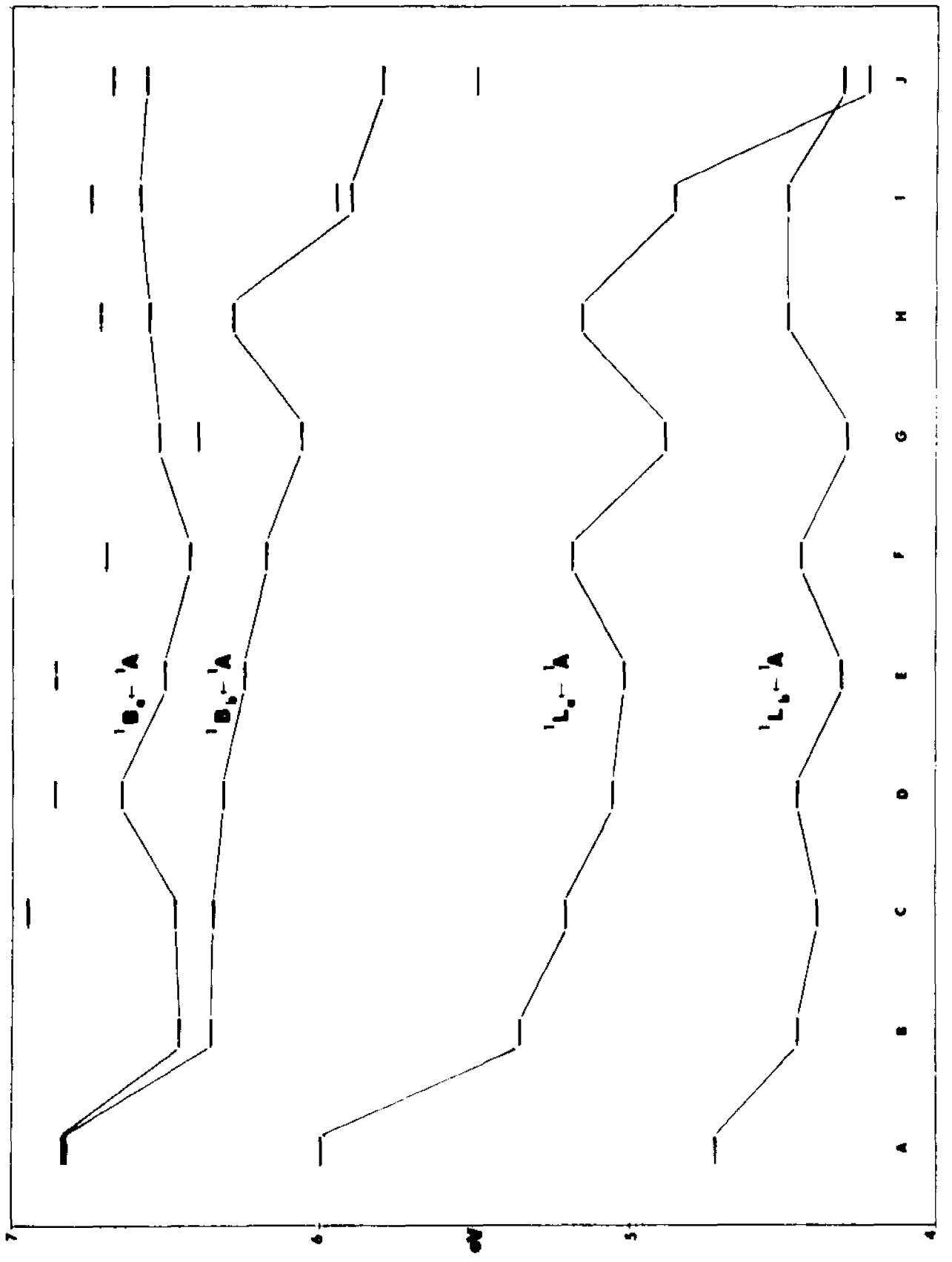
$^1B_a \leftarrow {}^1A$
$^1B_b \leftarrow {}^1A$
$^1L_a \leftarrow {}^1A$
$^1L_b \leftarrow {}^1A$
A
B
C
D
E
F
G
H
I
J
7
6
5
4

Figure 31.

Total charge transferred, as measured by the quantity $F_a + F_b$, in the $^1L_a \leftarrow {}^1A$ transition (open circles) and the $^1L_b \leftarrow {}^1A$ transition (closed circles) of p-disubstituted benzenes. The molecules are denoted as follows: A refers to p-fluorobenzonitrile; B, p-cyanophenol; C, p-cyanoaniline; D, N,N-dimethyl-p-cyanoaniline; E, p-nitroaniline; and F, N,N-dimethyl-p-nitroaniline.

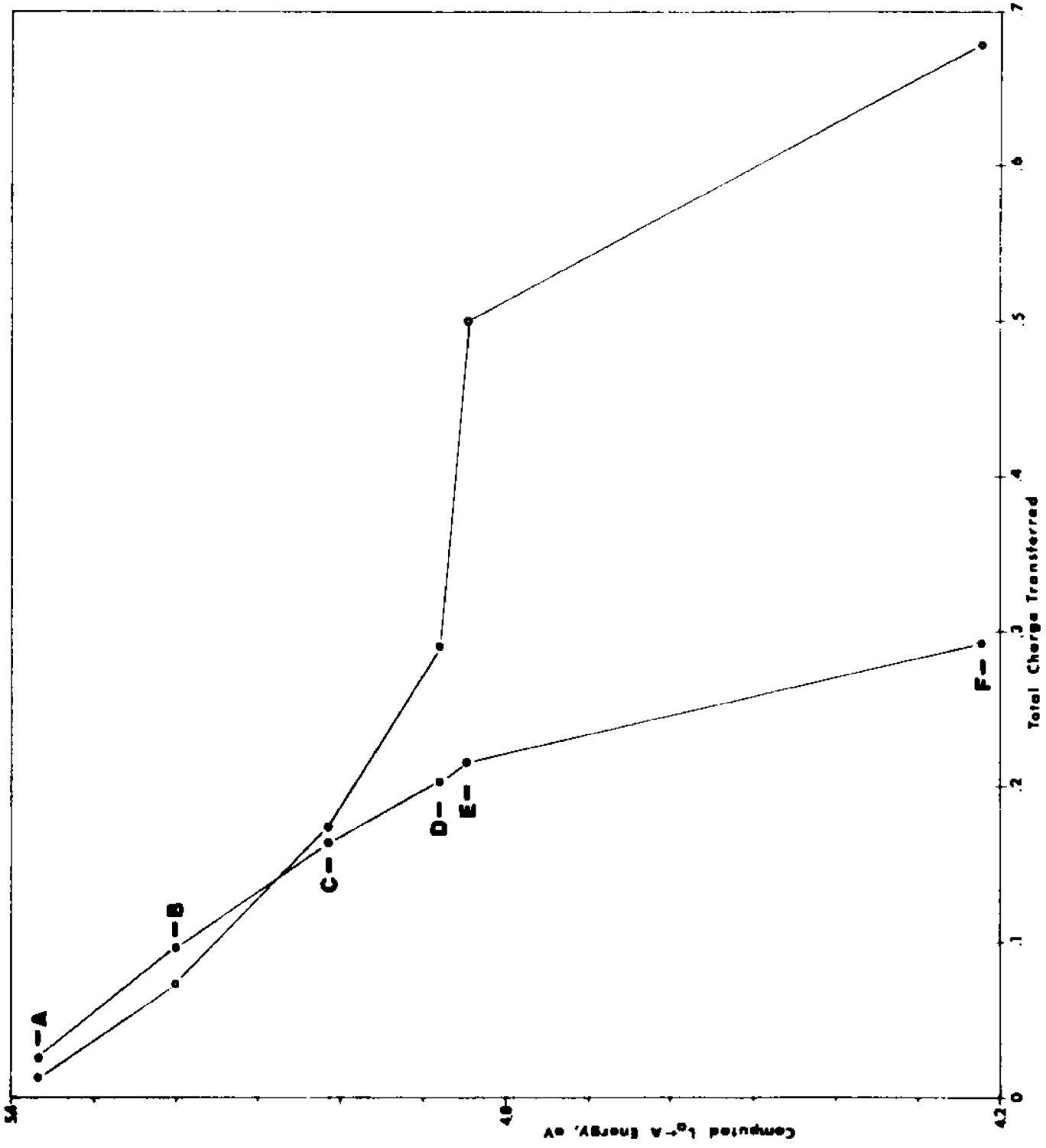
A
B
C
D
E
F
Total Charge Transferred
0
.1
.2
.3
.4
.5
.6
.7
4.2
4.0
3.8
Computed t_{2g}-A Energy, eV

as long as one understands what that name means. The name "CT" refers the state to a zeroth-order description where one obtains total charge separation (i.e., D^{+}-ϕ-A^{-} or 100% electron transfer). It may well be the description of choice for the individual whose interests reside mostly in solvent effects. We prefer the name $^{1}L_{a}$ simply because this state correlates back in a smooth way to benzene, no abrupt change or behavioral alteration being noticeable at any point. The difficulty resides in the subtle differences that different names imply for different people. Thus, should the attribution CT imply the presence of a $^{1}L_{a}$ state somewhere nearby? We think not. Yet, this is precisely the implication extracted by certain authors.

Thus, for precision, we emphasize: The name $^{1}L_{a}$ is preferable since it does not preclude a specifiable, large or small, CT character; since it refers to a readily accessible zeroth-order state, say that of p-F-ϕ-CN or even benzene; and since the progression from the zeroth-order point to the molecule of interest is readily traversed empirically, using any of the experimental trends noted in this work.

5. TRANSITION INTENSITIES: In the p sub-set, a hypothetical intramolecular CT transition which causes a migration of charge from the donor to the acceptor will be long-axis polarized. It is also expected to be intense. The $^{1}L_{a} \leftarrow {}^{1}A$ transition is also long-axis polarized and may obtain intensity by configuration mixing with the CT state. The $^{1}L_{b} \leftarrow {}^{1}A$ transition is short-axis polarized and may not obtain intensity in this fashion. Hence, presuming that the hypothetical CT transition is, in fact, intense and that there is considerable $^{1}L_{a}/{}^{1}CT$ mixing, we expect the nominal $^{1}L_{a} \leftarrow {}^{1}A$ transition to increase in intensity as molecular polarity increases. This is also the case

experimentally. However, it is not the case theoretically. The computed values remain rather constant at $0.2 \leq f \leq 0.35$ and, while larger than $f(^1L_b \leftarrow {}^1A)$ by a factor ranging from 10 to 10^2, they exhibit no discernible trend.

B. o-Isomers

The computed energies, oscillator strengths and transition dipole moment vectors of the singlet electronic states of the ortho-disubstituted molecules are given in Table 16. Since long- and short-axes cannot be uniquely defined for these molecules, the (L_a, L_b)-notation is meaningless. As in the case of the experimental data, however, we have found that certain $^1\Gamma_{\pi\pi^*}$ states may be designated "^1L_b-related" or "^1L_a-related" on the strength of the following computational criteria:

1. The energetic relationship of the computed $^1\Gamma_{\pi\pi^*}$ states of the molecule of interest to the computed ^1L_a or ^1L_b states of benzene; and

2. The configurational relatedness of the lowest and second lowest-energy $^3\Gamma_{\pi\pi^*}$ states to particular $^1\Gamma_{\pi\pi^*}$ states.

Criterion 1 is illustrated in Figure 32 where the $^1\Gamma_{\pi\pi^*}$ states of the o sub-set are correlated with the $^1\Gamma_{\pi\pi^*}$ states of benzene. The molecules are arranged from left to right in order of increasing $|\mu_0|$. The lowest energy $^1\Gamma_{\pi\pi^*}$ state, the "^1L_b-related" state, shows a moderate decrease in energy accompanied by a slight increase in oscillator strength. The second-lowest energy $^1\Gamma_{\pi\pi^*}$ state, the "L_a-related" state, exhibits a decrease in oscillator strength along with a moderate decrease in energy. These results reproduce the experimental findings rather well. In further support of the L_a/L_b labeling,

TABLE 16

Computed (CNDO/S-CI) Singlet Electronic States of ortho-Disubstituted Molecules[a]

a) only states whose energies are ≤ 7.0 ev are reported

Orbital Promotion	o-HOC_6H_4CN					o-$H_2NC_6H_4CN$				
				Polarization					Polarization	
	Γ_{C_s}	E(ev)	f	x	y	Γ_{C_s}	E(ev)	f	x	y
$\pi \rightarrow \pi^*$	A'	4.331	2.49×10^{-2}	0.8190	-0.5737	A'	4.180	4.44×10^{-2}	0.8186	-0.5743
	A'	5.339	8.23×10^{-2}	0.7511	-0.6602	A'	5.121	7.85×10^{-2}	0.2112	-0.9774
	A'	6.103	0.674	0.9094	0.4159	A'	5.972	0.666	0.9448	0.3276
	A'	6.320	0.394	0.4537	-0.8912	A'	6.210	0.291	0.2959	-0.9552
						A'	6.775	6.37×10^{-2}	0.0367	-0.9993
(CN) $\rightarrow \pi^*$	A''	4.889	---------			A''	4.917	---------		
$\pi \rightarrow$ (CN)π^*	A''	5.069	---------			A''	4.645	---------		
$\ell \rightarrow \pi^*$										
$n \rightarrow \pi^*$										
$\sigma \rightarrow \pi^*$	A''	6.348	---------			A''	6.448	---------		
	A''	6.622	---------			A''	6.621	---------		
	A''	6.767	---------			A''	6.820	---------		

TABLE 16--Continued

Orbital Promotion	o-$H_2NC_6H_4NO_2$				
				Polarization	
	Γ_{C_s}	E(ev)	f	x	y
$\pi \rightarrow \pi^*$	A'	4.154	5.65×10^{-2}	0.6530	-0.7573
	A'	5.020	2.86×10^{-2}	0.8392	-0.5438
	A'	5.556	6.74×10^{-2}	0.9715	0.2369
	A'	5.842	0.321	-0.7708	-0.6371
	A'	6.438	7.05×10^{-2}	0.7619	-0.6476
	A'	6.773	0.383	0.3462	-0.9382
	A'	6.894	0.348	0.4700	0.8826
$(CN)\pi \rightarrow \pi^*$					
$\pi \rightarrow (CN)\pi^*$					
$\ell \rightarrow \pi^*$	A'	5.634	6.68×10^{-2}	-0.9722	0.2343
	A'	6.576	1.48×10^{-2}	0.3556	-0.9347
$n \rightarrow \pi^*$	A''	2.595	---------		
	A''	2.962	---------		
	A''	5.995	---------		
	A''	6.348			
$\sigma \rightarrow \pi^*$	A''	6.244	---------		
	A''	6.841	---------		

Figure 4.

Correlation of $^1L_{\pi\pi^*}$ (CNDO/s-C.I.) states of o-disubstituted benzenes with the $^1L_{\pi\pi^*}$ states of benzene. The molecules are arranged from left to right in order of increasing computed ground state dipole moment, $|\mu_g|$.

Energy, eV
4
5
6
7
$|\mu^2|$
$^1L_b \leftarrow {}^1A$
$^1L_a \leftarrow {}^1A$
OH
CN
NH
NH
CN
NH
NH
O
O

our utilization of criterion 2 shows that the lowest-energy $^3\Gamma_{\pi\pi^*}$ state is configurationally akin to the "^1L_a-related" state, while the second lowest-energy $^3\Gamma_{\pi\pi^*}$ state is configurationally akin to the "^1L_b-related" state. This is precisely the same result as found for the p sub-set. Therefore, we use the simple $^{1,3}L_a$ and $^{1,3}L_b$ terminology henceforth. The energies of the triplet electronic states are presented in Table 17.

The o sub-set exhibits trends which are both similar and dissimilar to those of the p sub-set. It is observed, as $|\mu_o|$ increases, that

---The ^1L_a-^1L_b energy gap decreases slightly. This gap is found to be 1.008eV in o-cyanophenol; 0.941eV in o-cyanoaniline; and 0.866eV in o-nitroaniline.

The experimental data suggest the opposite trend, namely that the ^1L_a-^1L_b gap increases slightly with increasing $|\mu_o|$.

---The energy of the ^1L_a state decreases at more or less the same rate as does that of the ^1L_b state. In going from o-cyanophenol to o-cyanoaniline, for example, the ^1L_a decrement is 0.218eV, while the ^1L_b decrement is 0.151eV.

---The third and fourth $^1\Gamma_{\pi\pi^*}$ states are undoubtedly related to the ^1B states of benzene. This conclusion is based on the energetic relationship of these two states to the ^1B state of benzene and their relative energy separations: 0.217eV in o-cyanophenol; 0.283eV in o-cyanoaniline; and 0.286eV in o-nitroaniline. The increase is moderate, but the trend is the same as that exhibited by the P sub-set.

---In the case of o-cyanophenol and o-cyanoaniline, the $^1\Gamma_{\pi(CN)\pi^*}$ and $^1\Gamma_{\pi\pi^*(CN)}$ states lie energetically between the ^1L_b and ^1L_a states,

TABLE 17

Computed (CNDO/S-CI) Triplet Electronic States of ortho-disubstituted molecules[a]

a) only states whose energies are $\leq$ 5.4 ev are reported

Orbital Promotion	o-HOC_6H_4CN		o-$H_2NC_6H_4CN$		o-$H_2NC_6H_4NO_2$	
	Γ_{C_s}	E(ev)	Γ_{C_s}	E(ev)	Γ_{C_s}	E(ev)
$\pi \rightarrow \pi^*$	A'	2.808	A'	2.743	A'	2.881
	A'	3.395	A'	3.208	A'	3.186
	A'	3.604	A'	3.536	A'	3.691
	A'	4.570	A'	4.620	A'	4.730
			A'	5.100	A'	5.022
			A'	5.356	A'	5.382
$(CN)\pi \rightarrow \pi^*$	A"	4.889	A"	4.645		
$\pi \rightarrow (CN)\pi^*$	A"	5.069	A'	4.917		
$\ell \rightarrow \pi^*$					A'	1.849
$n \rightarrow \pi^*$					A"	2.595
					A"	2.962

as also occurs in the p sub-set.

---The two lowest-energy states of o-nitroaniline are $^1\Gamma_{n\pi^*}$ states. Two additional $^1\Gamma_{\ell\pi^*}$ states also lie at low energies.

---The highest-energy states below 7.0eV are of $^1\Gamma_{\sigma\pi^*}$ type in every case.

---The ^1L_a-^3L_a energy gap decreases regularly.

---The $^1L_a \leftarrow {}^1A$ and $^1L_b \leftarrow {}^1A$ transitions are of comparable intensity and $f(^1L_a \leftarrow {}^1A)/f(^1L_b \leftarrow {}^1A)$ decreases slowly but regularly. The $f(^1L_b \leftarrow {}^1A)$ intensities are less for p than for o whereas the opposite is true for $f(^1L_a \leftarrow {}^1A)$. A selected data set supportive of these assertions is shown in Table 18.

---Intramolecular CT increases but is best described as substituent ↔ ring. It is comparable in both ^1L_a and ^1L_b states.

C.

The computed energies, oscillator strengths and transition dipole moment vectors of the singlet electronic states of the m sub-set are presented in Table 19. Following the analysis of the o sub-set, a correlation of the $^1\Gamma_{\pi\pi^*}$ states of the m sub-set with the $^1\Gamma_{\pi\pi^*}$ states of benzene is presented in Figure 33. The following observations may be made:

---It is found that the lowest-energy $^3\Gamma_{\pi\pi^*}$ state is configurationally related to the ^1L_a state and that the second lowest-energy $^3\Gamma_{\pi\pi^*}$ state is related to the ^1L_b state. The energies of the triplet electronic states are collected in Table 20.

---As $|\mu_0|$ increases, one finds an over-all increase in the oscillator strength of the $^1L_b \leftarrow {}^1A$ transition and an over-all decrease in the oscillator strength of the $^1L_a \leftarrow {}^1A$ transition. o-Cyanoaniline

TABLE 18

COMPUTED (CNDO/s-CI) OSCILLATOR STRENGTHS

Molecule	(^1L_a)	(^1L_b)	$(^1L_a + (^1L_b)$
o-hydroxybenzonitrile	8.23×10^{-2}	2.49×10^{-2}	0.107
o-aminobenzonitrile	7.85×10^{-2}	4.44×10^{-2}	0.123
o-nitroaniline	2.86×10^{-2}	5.65×10^{-2}	0.085
m-hydrozybenzonitrile	7.44×10^{-2}	1.92×10^{-2}	0.094
m-aminobenzonitrile	8.11×10^{-2}	3.19×10^{-2}	0.113
m-nitroaniline	4.24×10^{-2}	3.01×10^{-2}	0.073
p-hydroxybenzonitrile	0.258	7.78×10^{-3}	0.266
p-aminobenzonitrile	0.272	1.47×10^{-2}	0.287
p-nitroaniline	0.221	1.46×10^{-3}	0.221

TABLE 19

Computed (CNDO/S-CI) Singlet Electronic States of meta-Disubstituted Molecules[a]

a) only states whose energies are $\leq$ 7.0 ev are reported

Orbital Promotion	m-HOC_6H_4CN			Polarization		m-$H_2NC_6H_4CN$			Polarization	
	Γ_{C_s}	E(ev)	f	x	y	Γ_{C_s}	E(ev)	f	x	y
$\pi \rightarrow \pi^*$	A'	4.384	1.92×10^{-2}	-0.8601	-0.5101	A'	4.210	3.19×10^{-2}	-0.8297	-0.5583
	A'	5.397	7.44×10^{-2}	-0.7639	-0.6453	A'	5.210	8.11×10^{-2}	-0.0875	-0.9962
	A'	6.064	0.688	-0.8982	0.4396	A'	5.891	0.622	-0.9191	0.3941
	A'	6.364	0.425	-0.4739	-0.8806	A'	6.277	0.348	-0.4405	-0.8977
						A'	6.800	2.53×10^{-2}	0.9716	0.2364
$(CN)\pi \rightarrow \pi^*$	A"	4.724	---------			A"	4.779	---------		
	A"	6.792	---------							
$\pi \rightarrow (CN)\pi^*$	A"	5.269	---------			A"	5.639	---------		
$\ell \rightarrow \pi^*$										
$n \rightarrow \pi^*$										
$\sigma \rightarrow \pi^*$	A"	6.342	---------			A"	6.409	---------		
	A"	6.687	---------			A"	6.680	---------		
						A"	6.844	---------		

TABLE 19--Continued

Orbital Promotion	m-$H_2NC_6H_4NO_2$				
				Polarization	
	Γ_{Cs}	E(ev)	f	x	y
$\pi \rightarrow \pi^*$	A'	4.226	3.01×10^{-2}	0.6826	0.7308
	A'	5.193	4.24×10^{-2}	0.6898	0.7240
	A'	5.731	9.32×10^{-3}	0.9642	-0.2652
	A'	5.765	0.408	-0.8508	0.5255
	A'	6.751	0.554	0.2861	0.9582
	A'	6.912	0.198	0.5419	-0.8404
$(CN)\pi \rightarrow \pi^*$					
$\pi \rightarrow (CN)\pi^*$					
$\ell \rightarrow \pi^*$	A'	5.480	4.95×10^{-2}	-0.7494	-0.6621
	A'	6.482	4.28×10^{-2}	0.9999	0.0107
	A'	6.502	4.15×10^{-2}	0.6211	0.7838
$n \rightarrow \pi^*$	A"	2.797	---------		
	A"	3.021	---------		
	A"	6.976	---------		
$\sigma \rightarrow \pi^*$	A"	6.247	---------		
	A"	6.595	---------		
	A"	6.789	---------		

TABLE 20

Computed (CNDO/S-CI) Triplet Electronic States of meta-disubstituted molecules[a]

a) only states whose energies are $\lesssim$ 5.4 ev are reported

Orbital Promotion	m-HOC_6H_4CN		m-$H_2NC_6H_4CN$		m-$H_2NC_6H_4NO_2$	
	Γ_{C_s}	E(ev)	Γ_{C_s}	E(ev)	Γ_{C_s}	E(ev)
$\pi \rightarrow \pi^*$	A'	2.797	A'	2.741	A'	2.772
	A'	3.357	A'	3.169	A'	3.183
	A'	3.596	A'	3.546	A'	3.625
	A'	4.525	A'	4.553	A'	4.659
	A'	5.118	A'	4.95,	A'	5.156
$(CN)\pi \rightarrow \pi^*$	A"	4.724	A"	4.779		
$\pi \rightarrow (CN)\pi^*$	A"	5.269				
$\ell \rightarrow \pi^*$					A'	1.678
$n \rightarrow \pi^*$					A"	2.797
					A"	3.021

Figure 53.

Correlation of $^1\Gamma_{\pi\pi^*}$ (CNDO/s-C.I.) states of m-disubstituted benzenes with the $^1\Gamma_{\pi\pi^*}$ states of benzene. The molecules are arranged from left to right in order of increasing computed ground state dipole moment, $|\mu_0|$.

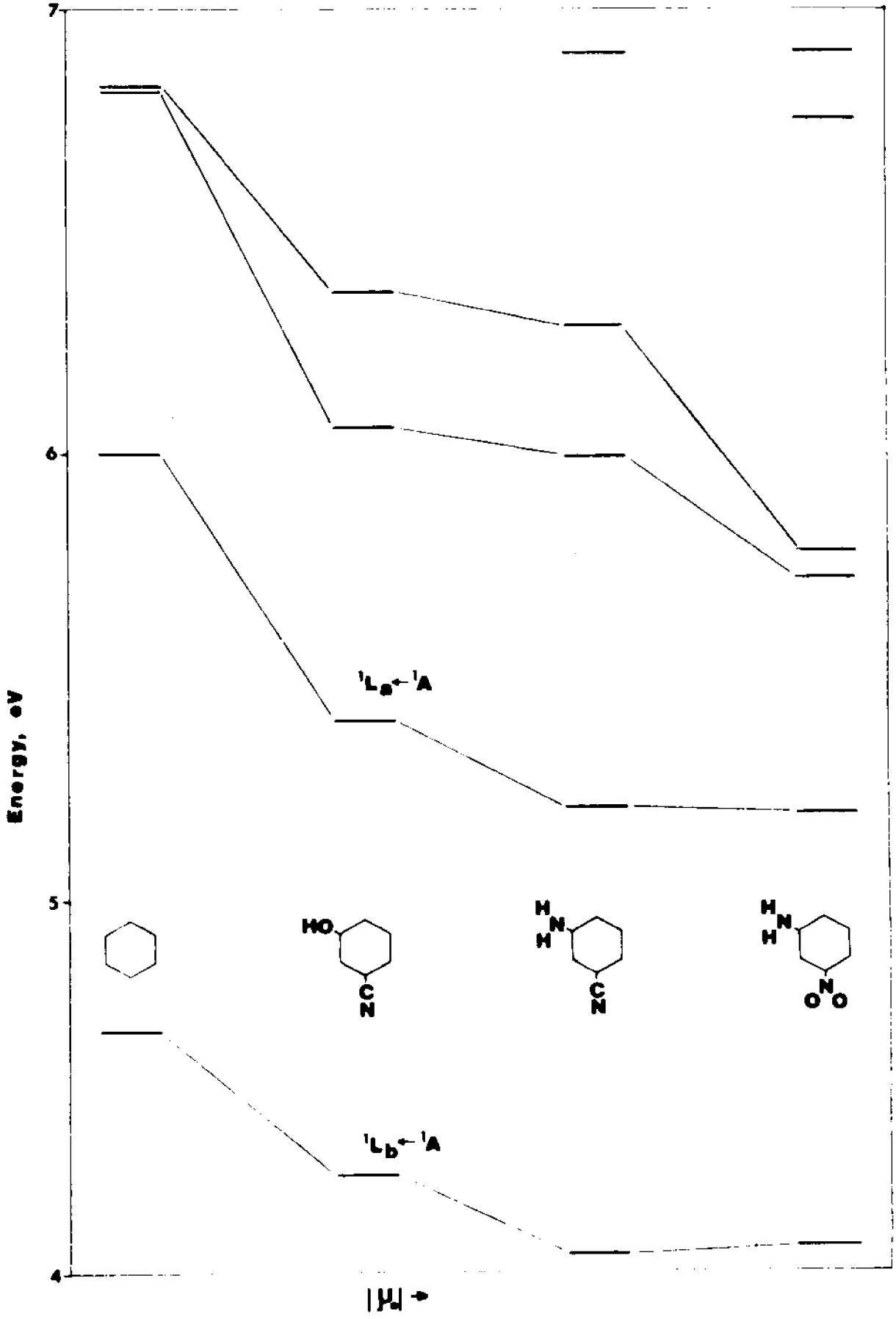
7
6
5
4
Energy, eV
$^1L_a \leftarrow {}^1A$
$^1L_b \leftarrow {}^1A$
HO
C
N
H
N
H
C
N
H
N
H
O
N
O
$|\mu_g| \rightarrow$

is somewhat aberrant in both instances.

---Both the ^1L_a and ^1L_b states exhibit a moderate decrease in energy as the ground state dipolarity increases. The over-all energetic trends of the ^1L_a and ^1L_b states are similar to those found for the p and o sub-set. The ^1L_a-^1L_b energy gap appears to decrease slightly as $|\mu_o|$ increases. This gap is 1.013eV in m-cyanophenol; 1.000eV in m-cyanoaniline; and 0.967 in m-nitroaniline. Experiment indicates that this gap is either constant or slightly increasing.

---The ^1L_a state decreases in energy more rapidly than does the ^1L_b state. Comparing m-cyanophenol to m-cyanoaniline, the ^1L_a decrement is 0.187eV, while the ^1L_b decrement is 0.174eV. In going from m-cyanoaniline to m-nitroaniline, ^1L_a decreases in energy by 0.017eV while ^1L_b increases in energy by 0.016eV.

---The third and fourth $^1\Gamma_{\pi\pi^*}$ states are thought to relate to the ^1B states of benzene. This conclusion is based solely on the energetic correlation of these states to the ^1B state of benzene.

---Two $^1\Gamma_{\pi(CN)\pi^*}$ and $^1\Gamma_{\pi\pi^*(CN)}$ states lie energetically between the ^1L_a and ^1L_b states of m-cyanophenol. The $^1\Gamma_{\pi\pi^*(CN)}$ state lies above the ^1L_a state of m-cyanoaniline. A second $^1\Gamma_{\pi(CN)\pi^*}$ state is the highest-energy state listed below 7.0eV for m-cyanophenol.

---The two lowest-energy states of m-nitroaniline are of $^1\Gamma_{n\pi^*}$ type. Three $^1\Gamma_{\ell\pi^*}$ states also occur at rather low energies. The highest-energy states found below 7.0eV in the case of m-cyanoaniline and m-nitroaniline are $^1\Gamma_{\sigma\pi}$ states.

---The ^1L_a-^3L_a gap decreases as $|\mu_o|$ increases.

REFERENCES

1. L. Doub and J. M. Vandenbelt, J. Amer. Chem. Soc., 69, 2714(1947).
2. L. Doub and J. M. Vandenbelt, J. Amer. Chem. Soc., 71, 2414(1949).
3. W. F. Forbes, W. A. Mueller, A. S. Ralph and J. F. Templeton, Can. J. Chem., 36, 1371(1958).
4. W. F. Forbes and J. R. Leckie, Can. J. Chem., 36, 1371(1958).
5. L. Goodman and H. Shull, J. Chem. Phys., 27, 1388 (1957).
6. P. Suppan, J. Chem. Soc., 1968A, 3125.
7. O. S. Khalil and S. P. McGlynn, J. Luminescence, 11, 185 (1975-6).
8. D. M. Wepster, Rec. trav. Chim., 71, 1159(1952).
9. D. M. Wepster, Rec. trav. Chim., 72, 661(1953).
10. K. Rotkiewicz, K. H. Grellman and Z. R. Grabowski, Chem. Phys. Letters, 39, 457(1976).
11. O. S. Khalil, J. L. Meeks and S. P. McGlynn, Chem. Phys. Letters, 39, 457(1976).
12. M. Godfrey and J. N. Murrell, Proc. Roy. Soc., A278, 71(1964).
13. K. R. Popov, Opt. Spectrosc., 25, 471(1968).
14. S. Nagakura and J. Tanaka, J. Chem. Phys., 22, 236(1954).
15. S. Nagakura, J. Chem. Phys., 23, 1441(1955); Pure and Applied Chem., 7, 79(1963).
16. K. Kimura and S. Nagakura, Theoret. Chim. Acta(Berl.), 3, 164(1965).
17. A. E. Lutskii, J. Gen. Chem., 33, 1562(1963).
18. P. Suppan, J. Mol. Spectrosc., 30, 17(1969).
19. W. Liptay, in "Excited States," Vol. I, E. C. Lim, Ed., Academic Press, New York, 1974; p. 177.
20. W. Liptay and J. Czekalla, Z. Naturforsch A., 15, 1072(1960).

21. W. Liptay and J. Czekalla, Z. Elektrochem., 65, 721(1961).

22. H. Labhart, Helv. Chim. Acta, 44, 445(1961).

23. H. Labhart, Chimia, 15, 20(1961).

24. H. Labhart, Tetrahedron Suppl., 2, 223(1963).

25. H. Labhart and G. Wagniere, Helv. Chim. Acta, 46, 131(1963).

26. H. Labhart, Adv. Chem. Phys., 13, 179(1967).

27. J. Czekalla and G. Wick, Ber. Bunsenges. Phys. Chem., 65, 727 (1961).

28. G. Weber, Biochem. J., 51, 155(1952).

29. G. M. Edelman and W. O. McClure, Acct. Chem. Res., 1, 65(1968).

30. L. Stryer, Science, 162, 526(1968).

31. B. Chance and G. K. Radda, "Probes of Structure and Function of Macromolecules and Membranes," Academic Press, New York, N.Y., I, 11, 1971.

32. T. Azumi and S. P. McGlynn, J. Chem. Phys., 37, 2413 (1962).

33. R. T. Morrison and R. N. Boyd, "Organic Chemistry," 3rd Ed., Allyn and Bacon, Boston, 1973, p. 342.

34. S. J. Strickler and R. A. Berg, J. Chem. Phys., 37, 814(1962).

35. Y. H. Lui and S. P. McGlynn, J. Luminescence, 9, 449(1975).

36. Y. H. Lui and S. P. McGlynn, J. Mol. Spectrosc., 55, 163(1975).

37. Y. H. Lui and S. P. McGlynn, J. Luminescence, 10, 113(1975).

38. Y. H. Lui, Ph.D. Dissertation, Louisiana State University, 1974.

39. G. Yamaguchi, Y. Kakinoki and H. Tsubomura, Bull. Chem. Soc. Japan, 40, 526(1967).

40. J. Tanaka and S. Nagakura, J. Chem. Phys., 24, 1274(1956).

41. J. Tanaka, Bull. Chem. Soc. Japan, 36, 833(1963).

42. M. S. El-Aassar, M.Sc. Thesis, Alexandria University, Egypt, 1964.

43. G. H. Wagniere, in: "The Chemistry of the Nitro and Nitroso Groups," Ed. H. Feuer, Wiley, New York, 1969; Chapter 1.

44. W. Liptay, Angew. Chem. Internat. Edit., 8, 177(1969).

45. P. E. Stevenson, J. Chem. Ed., 41, 234(1964); J. Mol. Spectrosc., 15, 220(1965).

46. P. Suppan, Spectrochim. Acta, 304, 1939(1974).

47. S. P. McGlynn, T. Azumi and M. Kinoshita, "Molecular Spectroscopy of The Triplet State," Prentice-Hall, Englewood Cliffs, N.J., 1969.

48. M. Godfrey and J. N. Murrell, Proc. Roy. Soc., A278, 57, 64(1964).

49. N. Mataga, Bull. Chem. Soc. Japan, 36, 1607(1963).

50. S. Nagakura and J. Tanaka, J. Chem. Phys., 22, 236(1954).

51. S. Nagakura, J. Chem. Phys., 23, 1411(1955).

52. A. E. Lutskii and A. I. Gorokhova, Teor. Eksp. Khim., 6, 490 (1970).

53. S. Nagakura, Pure and Applied Chem., 7, 79(1963).

54. A. E. Lutskii, Zh. Obscl. Khim., 33, 1601(1963); Zh. Obscl. Khim., 33, 1609(1963).

55. N. G. Bakhshiev, M. I. Knyazhanskii, V. I. Minkin, O. A. Osipov, and G. V. Saidov, Russ. Chem. Rev., 38, 740 (1969).

56. K. Semba, Bull. Chem. Soc. Japan, 34, 722 (1961).

57. T. Abe, Bull. Chem. Soc. Japan, 40, 1571 (1967).

58 W. M. Schubert, J. M. Craven, and H. Steadly, J. Am. Chem. Soc., 81, 2695 (1969).

59 B. Vidal and J. N. Murrell, Chem. Phys. Lett., 31, 46 (1975).

60 A. I. Kiss and G. Horvath, Acta Chim. Hung., 42, 15 (1964).

61 M. B. Ledger and P. Suppan, Spectrochim. Acta, 23A, 641 (1967).

62. A. V. Finkelshtein, E. Y. Belyaev, and Z. M. Kuzmina, Russ. J. Phys. Chem., 41, 1044 (1967).

63. P. Tomasik and T. M. Krygowski, Bull. Acad. Pol. Sci. Ser. Sci. Chim., 22, 443, 887 (1974); P. Tomasik, T. M. Krygowski, and T. Chellathurai, Bull. Acad. Pol. Sci. Ser. Sci. Chim., 22, 1065 (1974).

64. R. T. C. Brownlee and R. D. Topsom, Spectrochim. Acta, 29A, 385 (1973).

65. G. P. Schiemenz, Spectrochim. Acta, 24A, 465 (1968); 24A 1735 (1968); 25A, 439 (1969).

66. G. V. Saidov, O. V. Sverdlova, and N. G. Bakhshiev, Dokl. Akad. Nauk. S. S. S. R., 81, 638 (1968).

67. G. V. Saidov and N. G. Bakhshiev, Dokl. Akad, Nauk. S. S. S. R., 175, 1090 (1067).

68. P. P. Shorygin, M. D. Geiderikh, and T. I. Ambrush, Russ. J. Phys. Chem., 34, 157 (1960).

69. D. J. Cowley and L. H. Sutcliffe, Spectrochim. Acta, 25A, 989 (1969).

70. R. B. Cundall and S. M. Ogilvie, in "Organic Molecular Photophysics," Vol. 2, J. B. Birks, Ed., Wiley-Interscience, London, 1975, p. 35.

71. N. S. Bayliss and E. G. McRae, J. Chem. Phys., 58, 1002 (1954).

72. W. M. Schubert, H. Steadly, and J. M. Craven, J. Am. Chem. Soc., 82, 1353 (1960).

73. O. Khalil, R. H. Hofeldt, and S. P. McGlynn, J. Luminescence, 6, 229 (1973).

74. A. L. McClelland, "Tables of Experimental Dipole Moments," W. H. Freeman, San Francisco, 1963.

75. R. Foster, D. L. Hammick, G. M. Hood, and A. C. E. Sanders, J. Chem. Soc., 4865 (1956).

76. M. Kasha, Rad. Res. Suppl., 2, 243 (1960).

77. J. M. Corkill and I. J. Graham-Bryce, J. Chem. Soc., 3893 (1961).

78. O. S. Khalil, H. G. Bach, and S. P. McGlynn, J. Mol. Spectrosc., 35, 455 (1970).

79. R. Hurley and A. C. Testa, J. Am. Chem. Soc., 90, 1949 (1968).

80. V. G. Plotnikov and V. M. Komarov, Spect. Lett., 9, 265 (1976).

81. J. S. Brinen and B. Singh, J. Am. Chem. Soc., 93, 6623 (1971).

82. R. Rusakowicz and A. C. Testa, Spectrochim. Acta, 27A, 787 (1971).

83. E. C. Lim and J. Stanislaus, Chem. Phys. Lett., 6, 195 (1970).

84. L. Vanquickenborne and S. P. McGlynn, J. Chem. Phys., 45, 4755 (1966).

85. J. Del Bene and H. H. Jaffe, J. Chem. Phys., 48, 1808 (1968); J. Chem. Phys., 48, 4050 (1968).

86. J. Del Bene and H. H. Jaffe, J. Chem. Phys., 49, 1221 (1968); J. Chem. Phys., 50, 1126 (1969).

87. N. Mataga and K. Nishimoto, Z. Physik. Chem., 13, 140 (1957).

88. G. W. King and A. A. G. Van Putten, J. Mol. Spectrosc., 42, 514 (1972).

89. G. Kuehnlenz and H. H. Jaffe, J. Chem. Phys., 58, 2238 (1973).

90. J. A. Pople and D. L. Beveridge, "Approximate Molecular Orbital Theory," McGraw-Hill, New York, 1970, p. 111-112.

91. R. T. C. Brownlee and R. W. Taft, J. Am. Chem. Soc., 92, 7007 (1970).

92. Standard bond lengths and bond angles are taken from Reference 90.

93. K. Trueblood, E. Goldish, and J. Donohue, Acta Cryst., 14, 1009 (1961). Bond lengths and bond angles were averaged to give C_{2v} symmetry.

94. T. C. W. Mak and J. Trotter, Acta Cryst., 18, 68 (1965). The N-methyl hydrogen bond lengths and bond angles were taken from the $(CH_3)_3N$ values found in "C. R. C. Handbook of Chemistry and Physics," R. C. West, Ed., 53rd Edition, The Chemical Rubber Company Press, Cleveland, 1972, p. F-182.

95. The structure of the upper half of this molecule was taken from 1,4-dimethoxybenzene (Reference 96, p. 146), while that of the lower half was taken from p-iodobenzonitrile (Reference 96, p. 97), except for the CN group (standard bond lengths from Reference 90).

96. R. W. G. Wyckoff, "Crystal Structures," Vol. 6, part 1, 2nd Edition, Interscience, New York, 1969.

97. The structure of the upper half of this molecule was taken from p-aminobenzoic acid (Reference 98), while that of the lower half was taken from acetophenone (Reference 99).

98. T. F. Lai and R. E. Marsh, Acta Cryst., 22, 885 (1967).

99. Y. Tanimoto, H. Kobayashi, S. Nagakura, and Y. Saito, Acta Cryst., B29, 1882 (1973).

100. M. Alleaume, G. Salas-Ciminago, and J. Decap, Comptes Rendes C262, 416 (1966).

101. A. C. Shapski and J. L. Stevenson, J. Chem. Soc. Perkins II, 1197 (1973). Amino hydrogen and aromatic hydrogen bond lengths and bond angles are from Reference 93.

102. S. P. McGlynn, L. G. Vanquickenborne, M. Kinoshita, and D. G. Carroll, "Introduction to Applied Quantum Chemistry," Holt, Rinehart, and Winston, New York, 1972, p. 324-325.

103. J. A. Pople and G. A. Segal, J. Chem. Phys., 43, S136 (1965).

104. R. L. Ellis, G. Kuehnlenz, and H. H. Jaffe, Theoret. Chim. Acta (Berl.), 26, 131 (1972).

CHAPTER TWO.

SPECTROSCOPIC STUDIES OF SOME SIMPLE INORGANIC ANIONS.

Abstract

Two mechanisms which rationalize the non-additivity of certain absorption bands in the spectra of cation - anion complexes are described: charge-transfer transitions and enhanced singlet-triplet transitions. The latter effect is more likely to dominate if the cation is a heavy-metal ion.

The electronic spectra of the chlorite and sulfate ion have been investigated. In the spectrum of the chlorite ion, a transition is observed which is interpreted as a singlet-triplet transition. An examination of the electronic spectrum of the sulfate ion reveals a previously unreported transition which is identified as a singlet-triplet transition.

The tungstate and molybdate ions are known to emit in the solid phase. In the solution spectra of salts of these anions, a previously unreported transition is observed which resembles the emission excitation band. This transition is examined and interpreted as a singlet-triplet transition of the anion.

I. INTRODUCTION

The colors of ionic compounds or complexes can usually be attributed to the combined absorption of the component ions. This effect has been termed the 'Principle of additivity of ionic colors.'[1] It should be noted that the absorptions are subtracted from, not added to, the incident white light.[2]

Deviations from this rule are common and a partial list of these is given in Table 1 and 2. Efforts to understand the origins of the unusual colors have resulted in the elucidation of different mechanisms of color production.

II. THE CHARGE-TRANSFER MECHANISM

In 1941, Pitzer and Hildebrand published a study of the colors of various iodides.[3] The heats of formation, solubilities, and bond distances of these compounds suggested that they were partially covalent. Since essentially ionic compounds can undergo an anion → cation electronic charge-transfer transition, the color of the iodides were thought to be due to such a transition. The transition was red-shifted by an amount thought to be proportional to the deviation from pure ionic bonding. This has become known as the 'Pitzer-Hildebrand Rule.'

Jorgensen has developed a method of describing charge-transfer transitions in MX_n^{-m} complexes, where X is a ligand and M is a transition metal.[4] The regularities exhibited by the ligand → metal charge-transfer transition energies of such complexes can be

TABLE 1

SOME DEVIATIONS FROM THE COLOR ADDITIVITY RULE[1]

COMPOUND	COLOR
Bromates	
Ce^{+++}	reddish
Sr^{++}	yellowish
Carbonates	
Y^{+++}	lt. red
Ag^{+}	yellow
Hg^{++}	yellow
Chromates	
Ag^{+}	dark red
Tl^{+}	yellow-green
Hg^{++}	red
Nitrates	
Be^{+++}	lt. yellow
Y^{+++}	lt. red
Cs^{+}	yellow
Hg^{++}	lt. red
Molybdates	
Y^{+++}	yellow
Ag^{+}	yellow
Pb^{++}	yellow
Bi^{+++}	yellow
Nitrites	
NH_4^{+}	yellow
Na^{+} (solution)	yellow
K^{+}	lt. yellow
Ca^{+++}	yellow
Ag^{+}	yellow
Cd^{++}	lt. yellow
Hg^{++}	yellow
Tl^{+}	orange-yellow
Pb^{++}	orange-yellow
Phosphates	
Ag^{+}	yellow
Ce^{+++}	yellow
Tungstates	
Cd^{++}	yellow
Ng^{++}	yellow
Chlorites[2]	
Ag^{+}	green-yellow
Tl^{+} (solution)	yellow
Pb^{++}	orange-yellow
MX_6^{-6} Salts	
$AgOsF_6$	pale orange[4]
$AgIrF_6$	deep orange[4]
$AgRuF_6$	orange[5]
$TlRuF_6$	orange[5]
$AgPF_6$	yellow-brown[6]
$AgTaF_6$	pale yellow[7]
$AgVF_6$	orange-red[8]
Tl_2IrCl_6	dark blue-green[9]
Ag_2IrCl_6	dark blue[9]
$AgReCl_6$	orange[10]
$AgOsCl_6$	brown[10]
$TlOsCl_6$	olive green[10]
$TlOsBr_6$	dark green[10]
$TlIrCl_6$	dark green[10]
Miscellaneous	
$AgReO_4$	yellow-white[11]
Ag_4SiO_4	red[3]

TABLE 1

(Continued)

Unless otherwise referenced, colors are taken from

1. R. C. Weast, Ed., Handbook of Chemistry and Physics, Chemical Rubber Corp., Cleveland, Ohio, 48th Edition (1967)
2. S. P. McGlynn, Iz. Akad. Nauk SSR, Ser. Fiz. 37, 546 (1973)
3. E. Thilo and F. Wodtcke, Z. Anorg. Allgem. Chem. 295, 247 (1958)
4. M. A. Hepworth, P. L. Robinson, and G. J. Westland, J. Chem. Soc. 4269 (1954)
5. M. A. Hepworth, R. D. Peacock, and P. L. Robinson, J. Chem. Soc. 1197 (1954)
6. A. A. Woolf and H. J. Emeleus, J. Chem. Soc. 2865 (1949); 1050 (1950)
7. V. Gutman and H. J. Emeleus, J. Chem. Soc. 1046 (1950)
8. H. J. Emeleus and V. Gutman, J. Chem. Soc. 2979 (1949)
9. M. Delepine, Ann. Chim. 7, 227 (1917)
10. C. K. Jorgensen, Oxidation Numbers and Oxidation States, Springer-Verlag, New York, 1969, p. 196
11. F. Buschendorf, Z. Phys. Chem. B20, 237 (1933)

TABLE 2

SILVER-OXYGEN DISTANCES IN SOME SILVER SALTS

COMPOUND	COLOR	SHORTEST Ag-O DISTANCE, A	REFERENCE
$AgNO_3$	none	2.51	1
$AgClO_3$	none	2.51	2
Ag_2SO_4	none	2.50	3
Ag_2MoO_4	yellow	2.42	4
$KAgCO_3$	none	2.42	5
$AgNO_2$	yellow	2.42	6
$AgClO_2$	yellow	2.4	7
Ag_2CrO_4	dark red	2.35	8
Ag_3PO_4	yellow	2.34	9
Ag_3AsO_4	red-black	2.34	3
$AgMnO_4$	black	2.32	10
Ag_2CO_3	yellow	2.30	5
Ag_2SO_3	none	2.234	11
Ag_2O	brown-black	2.06	3

1. P. F. Lindley and P. Woodward, J. Chem. Soc., A 123 (1966)
2. I. Naray-Szabo and J. Pocza, Z. Krist., 104, 28 (1942)
3. L. Helmholz and R. Levine, J. Am. Chem. Soc., 64, 354 (1942)
4. J. Donohue and W. Shand, J. Am. Chem. Soc., 69, 222 (1947)
5. J. Donohue and L. Helmholz, J. Am. Chem. Soc., 66, 295 (1944)
6. R. E. Long and R. E. Marsh, Acta Cryst., 15, 448 (1962)
7. J. Cooper and R. E. Marsh, Acta Cryst., 14, 202 (1961)
8. M. L. Hackert and R. A. Jocopson, J. Sol. St. Chem., 3, 364 (1971)
9. L. Helmholz, J. Chem. Phys., 4, 316 (1936)
10. E. G. Boonstra, Acta Cryst., B24, 1053 (1968)
11. O. Larsson, Acta Chem. Scand., 23, 2261 (1969)

processed to yield values of 'optical electronegativities' for both the ligand and the metal. Charge-transfer transition energies for different complexes of the same stoichiometry can be calculated, if the optical electronegativities of the metal and ligand were known. By such a procedure, Jorgensen has assigned the transitions causing the intense colors of $AgMnO_4$ and Ag_2CrO_4 to silver 4d → anion transitions.[5] A more complete description of the method, and a table of optical electronegativities may be found in reference 4.

Inter-molecular charge-transfer transitions in inorganic systems have been studied in solution by several workers.[6-10]. Generally, these transitions are fairly intense.[8] The energies of metal ion → anion charge-transfer transitions are related to the nature of the metal: if the transition is metal → anion, the energy of the transition should be proportional to the M^n/M^{n+1} redox potential; if the transition is anion → metal, the energy should be proportional to the M^n/M^{n-1} redox potential.[7]

In summary, charge-transfer transitions are known to cause non-additive color in many instances, in both solution and the solid phase. The ease of optical oxidation and reduction of the components of the complex determines the energy of the transition. If the transition is of optical frequency, the color will be intense.

III. ENHANCEMENT OF THE SINGLET-TRIPLET TRANSITION

Investigations of a number of colored metal-anion complexes in this laboratory have demonstrated that the transition responsible for the color is the anion $T_1 \leftarrow S_o$ transition, enhanced by the presence of the metal ion via spin-orbit coupling.[11] In the colorless nitrite ion, for example, the lowest triplet state has an origin at 18959 cm^{-1} (527.45 nm).[12] A heavy metal ion such as silver is capable of increasing the probability of the $T_1 \leftarrow S_o$ transition to an extent which causes the low color of silver nitrite crystals.[13]

A singlet-triplet transition differs considerably from a charge-transfer transition. The oscillator strength of the former is usually much less than that of the latter. The significant metal attribute in the former is atomic number; in the latter, it is the ease of photo-oxidation or reduction. The singlet-triplet transition must lie at lower energy than the associated singlet-singlet transition whereas the charge-transfer transition has no such restriction. For emissive molecules, the inverse of the singlet-triplet absorption, which is known as phosphorescence, lies at lower energies and has a longer lifetime than the inverse of the charge-transfer absorption (which is known as fluorescence). Other important experimental methods of differentiation exist. The various methods have been outlined in Table 3.

Among the metal ions which induce color in metal-anion complexes are those of the post-transition metals (i.e. Ag^+, Tl^+, HG^{++}, etc.). Having filled d shells, these ions do not undergo d-d

TABLE 3

EXPERIMENTAL METHODS OF DIFFERENTIATING

CHARGE-TRANSFER AND SINGLET-TRIPLET TRANSITIONS

Characteristic	Triplet Mechanism	Charge-Transfer Mechanism
Wavelength	Not affected by use of different metal cations.	Related to the redox potentials of different metal cations.
Intensity	Roughly related to Z^4, where Z is the atomic number of the metal cation.	No obvious relationship to atomic number of the metal cation.
Position	Lies to the red of the $S_1 \rightarrow S_0$ transition.	Does not necessarily lie to the red of the $S_1 \rightarrow S_0$ transition.
Polarization	Determined by the polarization of the $S_n \rightarrow S_0$ transition from which the $T_1 \rightarrow T_0$ transition gains intensity.	Polarized along the direction of charge transfer.
Emission	Long (10^{-1} sec.) lifetime. Mirror image relationship with the $T_1 \rightarrow S_0$ transition.	Short (10^{-8} sec.) lifetime. Mirror-image relationship with the charge-transfer transition.
Electron Spin Resonance	Has an E. S. R. spectrum.	No E. S. R. spectrum is expected.

transitions which might obscure the anion $T_1 \leftarrow S_o$ transition. Post-transition metals are capable of covalent bonding through donation of electron density from a filled d orbital to the anion, or through the acceptance of electron density from the anion into an empty s or p orbital.[14] In addition, these metal ions are capable of charge-transfer transitions, either d $\leftrightarrow$ anion or anion $\leftrightarrow$ s (or p).

There are a number of post transition metal-anion complexes where no non-additive color is observed. However, an additional transition, either quite weak or lying outside the visible region of the spectrum, may be detected. It is likely that this new transition is either a charge-transfer transition or an enhanced singlet-triplet transition. The remainder of this chapter will be devoted to the discussion of several metal-anion complexes where this new transition has been observed.

IV. EXPERIMENTAL METHODS

A. Preparation of Chlorites

Sodium chlorite, analytic grade (Matheson, Coleman, and Bell) was recrystallized from water solution to which a trace of sodium hydroxide had been added in order to stabilize the chlorite ion. Silver chlorite was precipitated from sodium chlorite in water solution by the addition of reagent grade silver nitrate (Mallinckrodt). Silver perchlorate monohydrate (Matheson, Coleman, and Bell) was used as received. Reagent grade silver sulfate was used as obtained.

B. PREPARATION OF SULFATES

Lithium potassium sulfate was prepared from stoichiometric quantities of reagent grade lithium sulfate (Mallinkrodt) and reagent grade potassium sulfate (Faker).

C. MOLYBDATE AND TUNGSTATE CRYSTALS

Silver molybdate was precipitated from a solution of reagent grade sodium molybdate (Merck) by the addition of silver nitrate. The silver molybdate crystal was grown from a solution made by dissolving the filtered precipitate in ammonium hydroxide solution. The thallium tungstate crystal was grown from a water solution containing reagent grade sodium tungstate (Matheson, Coleman, and Bell) and purified thallium nitrate (Fisher Scientific Company).

D. TUNGSTATE SALTS

Cadmium tungstate solution was prepared from a washed precipitate formed by the addition of reagent grade cadmium chloride (Baker) to sodium tungstate in water. Sodium tungstate solution was prepared from reagent grade sodium tungstate, recrystallized from water. Cesium tungstate solution was prepared from 99.9% cesium tungstate from Roc Ric Research. Lead tungstate solution was prepared from a washed precipitate formed by the addition of lead chloride (Apache, 99.999%) solution in water to sodium tungstate solution. Thallium tungstate solution was prepared by dissolving the thallium tungstate crystals described previously.

E. MOLYBDATE SOLUTIONS

Lead molybdate solution was prepared from a washed precipitate formed by the addition of lead chloride solution to a sodium molybdate solution in water. Cadmium molybdate solution was prepared from a precipitate formed by the addition of cadmium chloride solution to a sodium molybdate solution in water. Sodium molybdate solution was prepared from recrystallized sodium molybdate. Ethanol was refluxed over calcium oxide and distilled from magnesium turnings.

F. TUNGSTATE SALTS

The silver tungstate was prepared by the method described above for silver molybdate crystals. The cesium tungstate was used as obtained from Roc Ric Research. Sodium tungstate was recrystallized from water solution and annealed for one hour at 500°C.

G. MOLYBDATE SALTS

Silver molybdate was prepared as described previously. Lead molybdate was prepared by annealing a finely powdered mixture of lead acetate and molybdenum trioxide for 3-4 hours at 900°C. The molybdenum trioxide was prepared by standard methods.[15] Barium molybdate was prepared by annealing a finely powdered mixture of molybdenum trioxide and Baker reagent grade barium carbonate for 3-4 hours at 900°C. Calcium molybdate was prepared by annealing a finely powdered mixture of calcium carbonate and molybdenum trioxide for 2-3 hours at 800°C. Strontium molybdate was precipitated from sodium molybdate solution by the addition

of reagent grade strontium nitrate (Mallinckrodt), and washed with water. Cadmium molybdate was prepared by annealing a finely powdered mixture of molybdenum trioxide and cadmium carbonate for 2-3 hours at 800°C. Bismuth molybdate was precipitated from a solution of sodium molybdate by the addition of bismuth nitrate, then annealed for 6 hours at 400°C and again at 600°C for 5 hours. Zinc molybdate was prepared by annealing a finely powdered mixture of Fisher Scientific Company reagent grade zinc acetate and molybdenum trioxide at 600°C for 5 hours. Sodium molybdate was recrystallized from water.

All absorption spectra were obtained on a Cary model 14 or 15 spectrophotometer in conjunction with a liquid nitrogen contact dewar. Emission spectra were recorded on a Jarrel-Ash Mark V 1/2-meter scanning monochromator with a Princeton Applied Research phase-sensitive detection system and a 500W xenon arc excitation source. All emission spectra were recorded with the sample cooled to 77°K with a liquid nitrogen immersion dewar, and are uncorrected for instrument response. Lifetime measurements were made with a Xenon Corporati-n Model 437 or EGG Model 550/551 flashlamp with a Tektronix 556 dual beam oscilloscope.

V. THE CHLORITE ION

The chlorite ion, ClO_2^-, is a unique twenty-electron anion. The ultraviolet spectrum of sodium chlorite is characterized by two weak transitions, a maximum at 264 nm and a shoulder at 310 nm, in ethanol (Figure 1). The corresponding values in water solution are 260 nm and 290 nm. These transitions have been assigned by Friedman[16] (after Mulliken[17]) as $B_2 \leftarrow A_1$ and $B_1 \leftarrow A_1$, respectively. Calculations on the chlorite ion performed by the author[18] lead to assignments of $B_1 \leftarrow A_1$ and $A_2 \leftarrow A_1$, respectively, for these two transitions.

A third, very weak transition, 360 nm in Figure 1, is of particular interest. The transition is more apparent in the spectrum of silver chlorite doped into a silver perchlorate lattice (Figure 2). The entire spectrum is red-shifted in Figure 2 as compared to Figure 1, but the relative positions of the three bands are unchanged.

The intensity of the 360 nm transition, assuming it is intrinsic to the chlorite ion, is ~ 7 ℓ/mole cm in Figure 2. Charge-transfer transitions are much more intense.[8] Also, a charge-transfer transition is likely to undergo a more significant shift in energy when the metal cation is changed from Na^+ to Ag^+ than is seen in Figures 1 and 2. The singlet-triplet interval in Figure 1, assuming the 360 nm transition is the triplet and the 310 nm transition is the associated singlet, is ~ 0.5 eV, similar to that of sodium nitrite.[12]

The intensity of the 360 nm transition, and its position

relative to the two stronger transitions, lead to the assignment of the 360 nm transition as the $T_1 \cdot S_o$ transition.

Figure 1.

Absorption spectra of $NaClO_2$ in Ethanol at room temperature

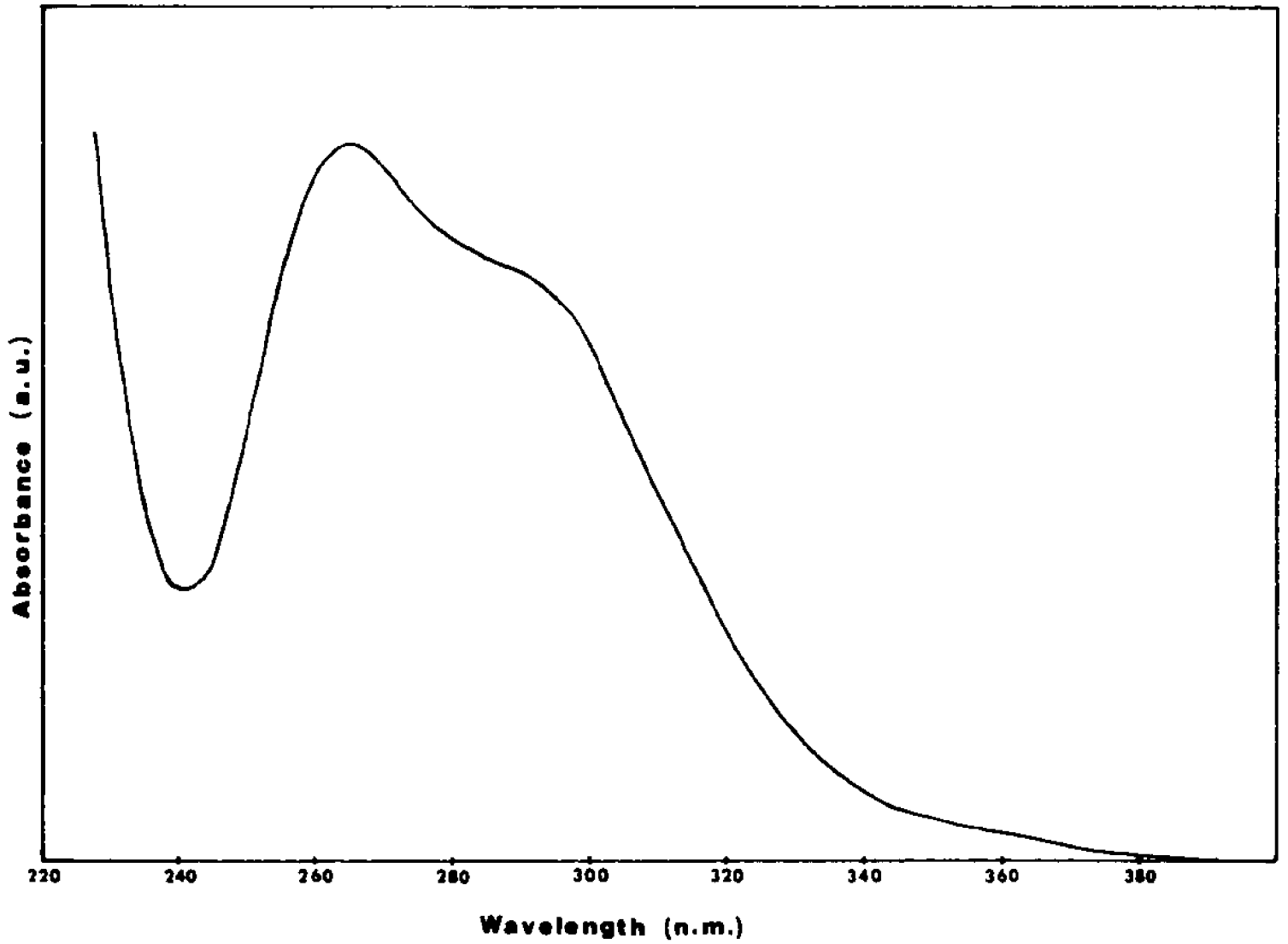
Absorbance (a.u.)
220
240
260
280
300
320
340
360
380
Wavelength (n.m.)

Figure 2.

Absorption spectra of silver chlorite doped into silver perchlorate crystals, taken at room temperature.

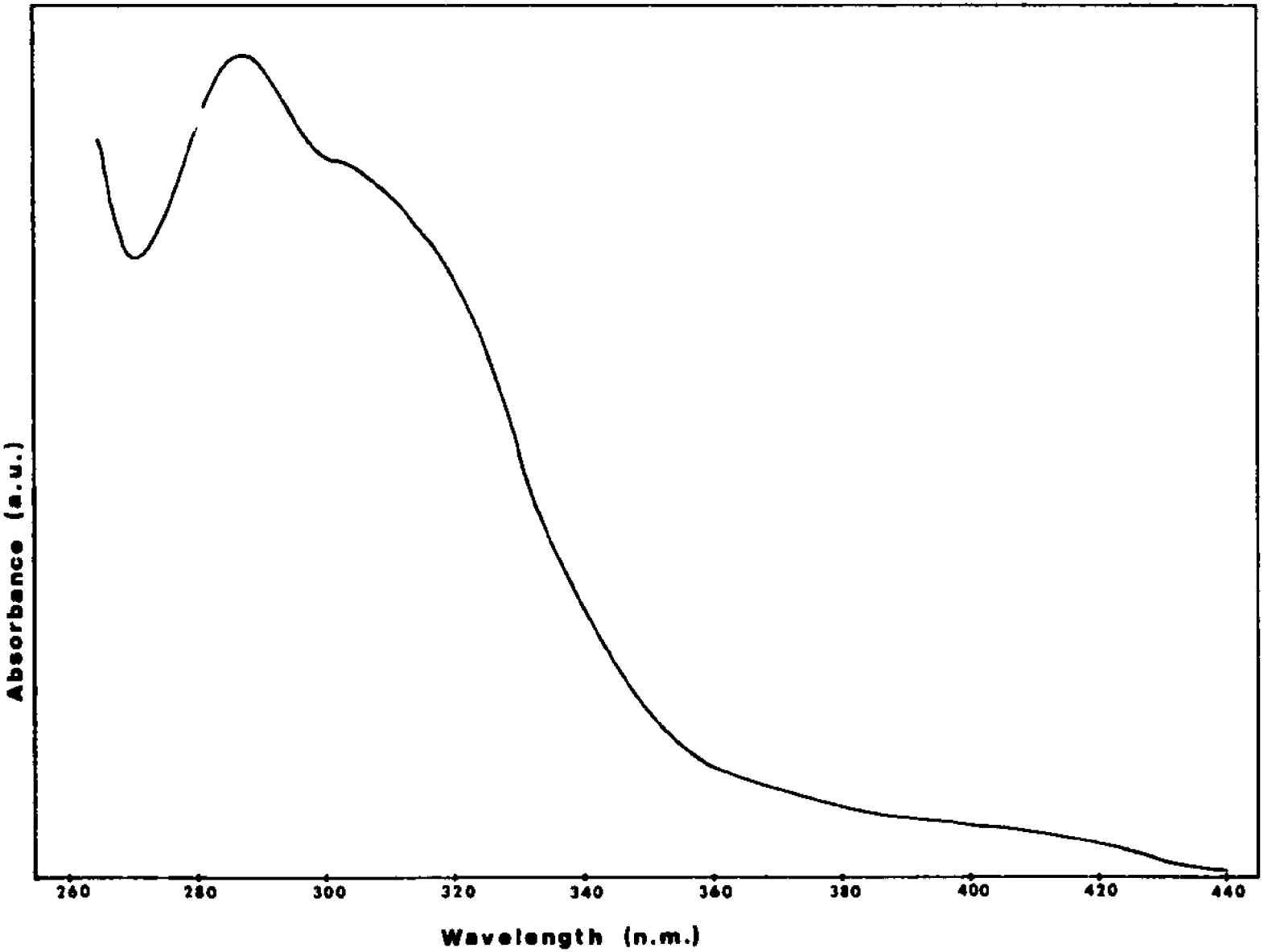
Absorbance (a.u.)
240
280
300
320
340
360
380
400
420
440
Wavelength (n.m.)

VI. THE SULFATE ION:

Previously published absorption spectra of the sulfate ion, $SO_4^=$, indicate the onset of an absorption abnd at 200 nm.[6,19] Our investigations have revealed an additional transition observed at 270 nm in room temperature solutions of silver sulfate (Figure 3). The transition is also observed in thallium sulfate solutions at the same wavelength, though at much lower intensity. The transition is difficult to observe, as it is easily obscured by the nearby, more intense (~600 ℓ/mole·cm) Ag^+ transition at 225 nm. Concentration changes or the addition of Ag^+ or $SO_4^=$ ions cause changes of intensity and energy in the transition (Figure 4). One may conclude that the degree of cation-anion association has a large effect on the transition characteristics.

The transition may also be observed in Ag^+ doped $LiKSO_4$ crystals (Figure 5). Upon cooling from room temperature to 77°K, the band intensity increases but without an increase in resolution.

The intensity of the band may be roughly calculated by assuming that the transition is due to the isolated sulfate ion. Based on the intensity of the Ag^+ transition at 210 nm ($\varepsilon \sim 1000$ ℓ/mole·cm),[6] the 270 nm band has an extinction coefficient of ~600 ℓ/mole·cm. This is an acceptable value for the extinction coefficient of a charge-transfer transition, but is somewhat high for a $T_1 \leftarrow S_0$ transition. The $T_1 \leftarrow S_0$ transition in metal nitrite solutions are less intense.[20] However, the related $S_1 \leftarrow S_0$ transition in the nitrite ion is considerably less intense ($\varepsilon \simeq 30$ ℓ/mole·cm)[21] than that of the sulfate ion.[6]

The 270 nm transition is not observed in solutions of sodium

Figure 3.

Absorption spectra of ~ 2.5×10^{-3} molar Ag_2SO_4 in water. The transition at 225 nm is due to the Ag^+ ion.

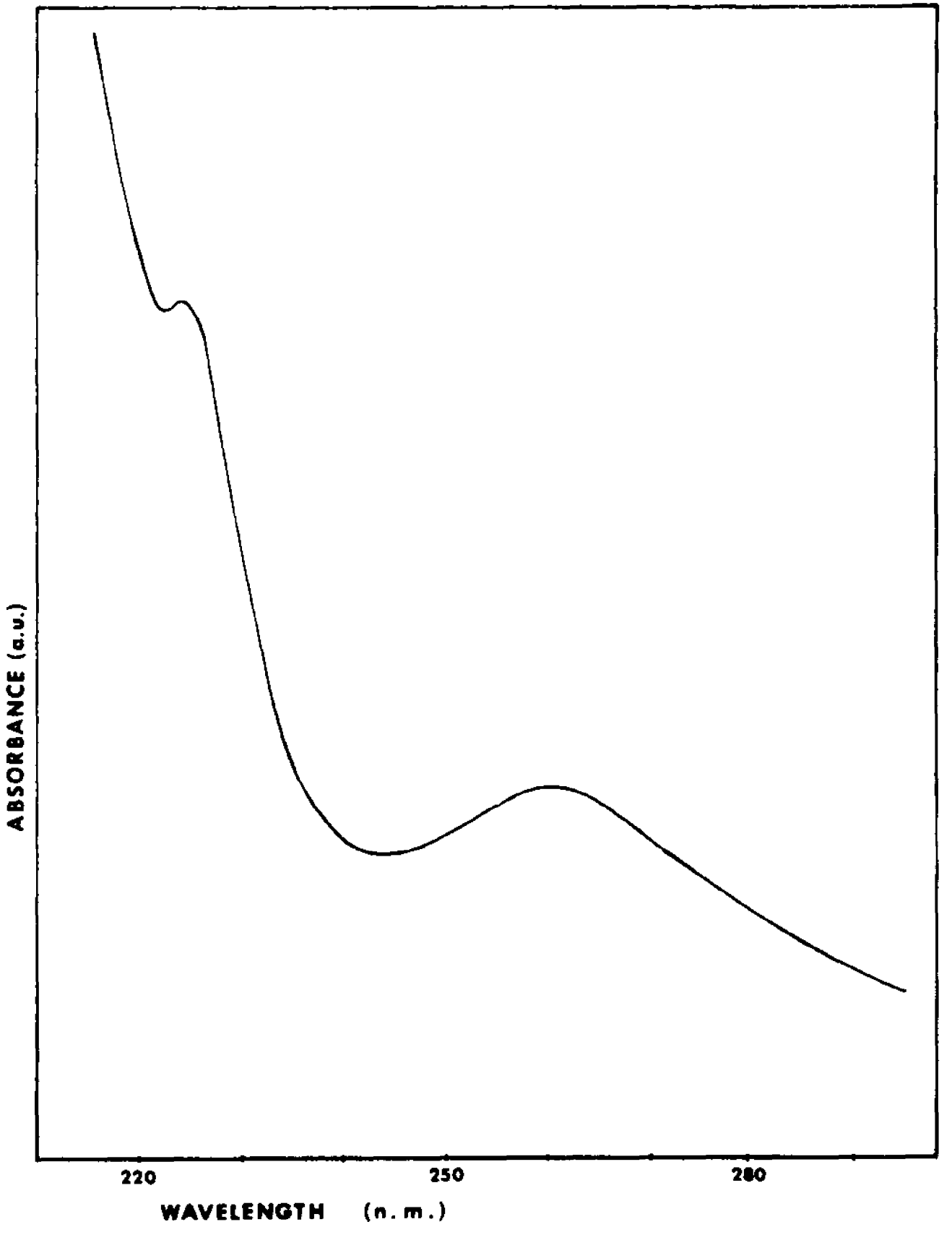
ABSORBANCE (a.u.)
220
250
280
WAVELENGTH (n.m.)

Figure 4.

The absorption spectra of some Ag_2SO_4 solutions in water. —— indicates pure Ag_2SO_4, — — — indicates Ag_2SO_4 with added Na_2SO_4, —— —— indicates Ag_2SO_4 with added $AgNO_2$. The NO_3^- ion has an absorption band at 300 nm.

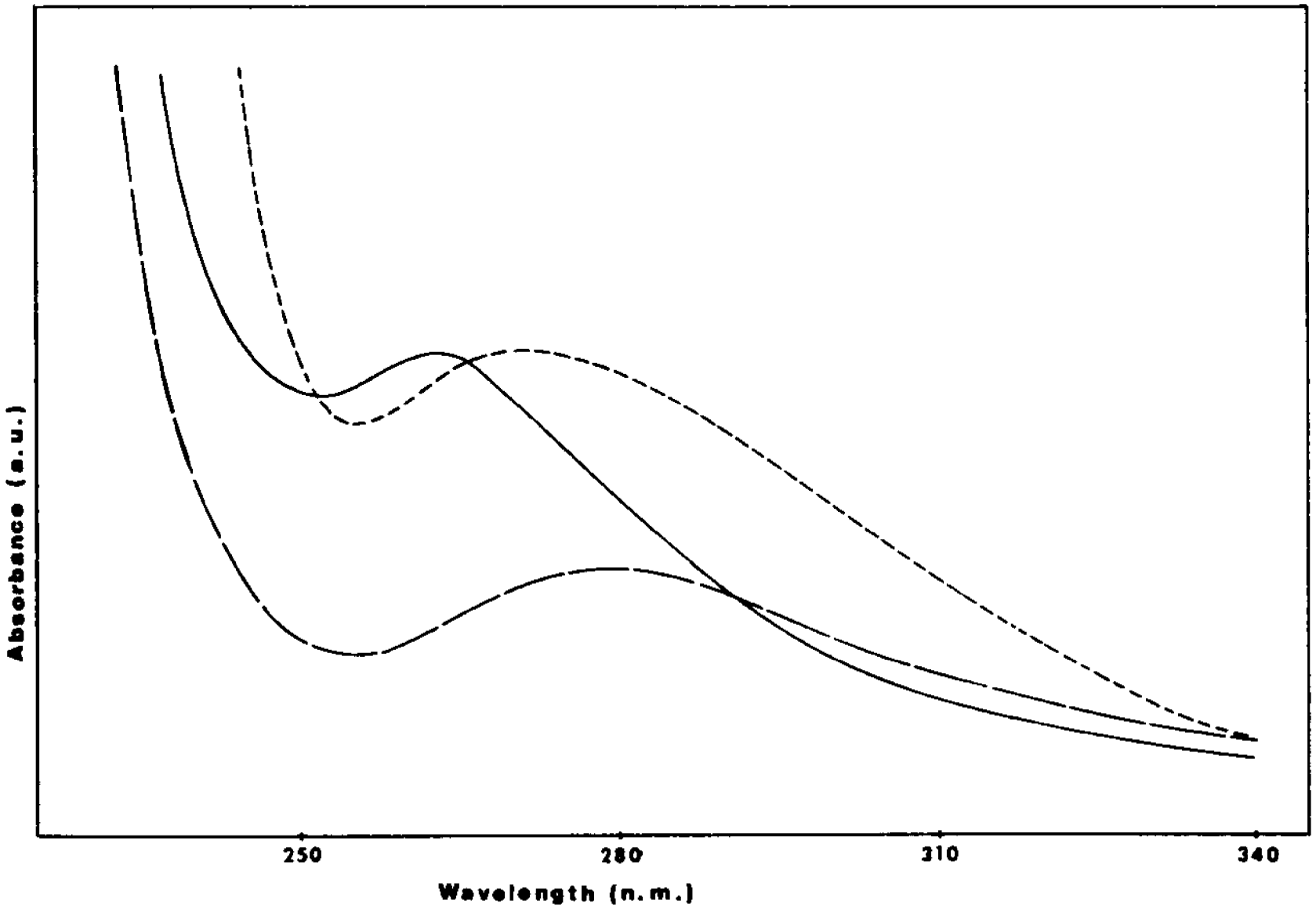
Absorbance (a.u.)
250
280
310
340
Wavelength (n.m.)

Figure 5.

The absorption spectrum of an Ag:$LiKSO_4$ single crystal. ——— indicates the absorption at room temperature, — — — indicates the absorption at 77°K. The transition at 225 nm is due to Ag^+.

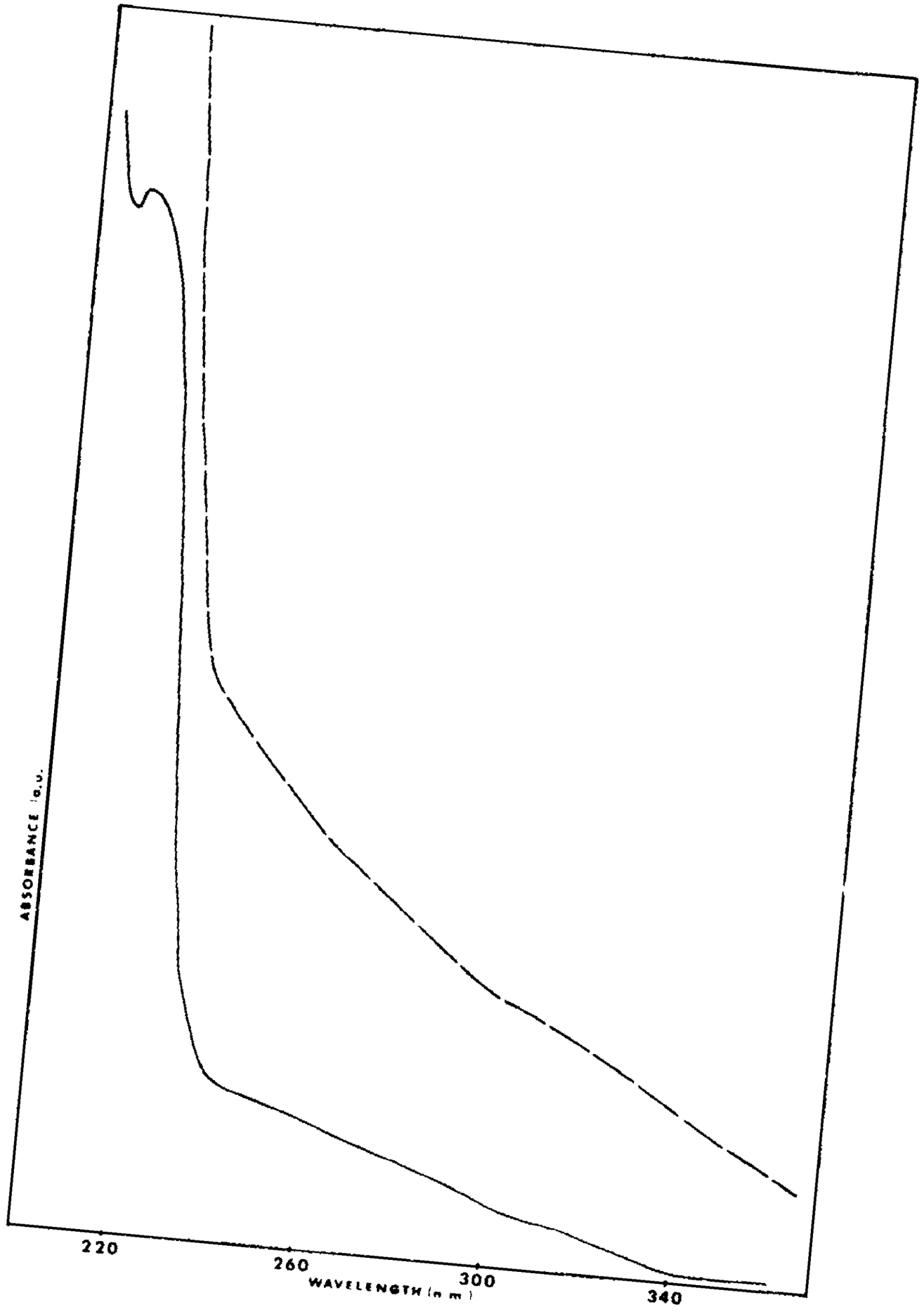
ABSORBANCE (a.u.)
220
260
300
340
WAVELENGTH (n m)

sulfate in water.[19] This fact indicates that the solution is not a sulfate ion charge-transfer-to-solvent transition. The fact that the transition appears at the same wavelength in the thallium and silver salt solution spectra, but does not appear in the spectrum of the sodium salt solution is consistent with the characteristics of a singlet-triplet transition.

The 270 nm transition is energetically distant from the sulfate $S_1 \leftarrow S_0$ transition. Assuming that the 270 nm transition is the $T_1 \leftarrow S_0$ transition and the associated singlet transition is at 180 nm,[c] the singlet-triplet interval would be 2.3 eV. Although this is a large interval, it is not unprecedented. The tetrahedral ions discussed in the next section have singlet-triplet intervals of 1.6 eV.

Sulfate ions have no intrinsic luminescence in solution, so that a triplet state cannot be located by this means.

With the above experimental considerations in view, we propose to assign the 270 nm transition shown in Figures 3-5 as the sulfate ion $T_1 \leftarrow S_0$ transition.

VII. TUNGSTATES AND MOLYBDATES:

The tungstate, molybdate, and vanadate ions are d^0, tetrahedral ions which luminesce in the solid phase.[22-28] They also act as efficient sensitizers for rare-earth emission[22,29-30] The observed emission is not defect, impurity, or band emission, but is a self activated molecular emission from the oxyanion. The related oxyanions permanganate, pertechnetate, and chromate do not emit. None of the anions, for reasons that are not clear, emit in the liquid phase.

The absorption and emission spectra of a number of tungstate and molybdate salts have been investigated. The absorption spectra of the salts in water solution are shown in Figures 6 and 7, and summarized in Table 4. The absorption edges seen at higher energies are the onsets of an intense singlet-singlet transition due to the anion. For the molybdate ion, the band maximum of this transition is ~227 nm; for the tungstate ion, the maximum is ~200 nm. For a given ion, the position of the absorption edge changes because of the different concentrations required to observe the weaker transition to the red of the edge. It is this weaker transition that is of interest.

The energies of the weak bands do not correlate with metal redox potentials. Na_2WO_4 has the lowest energy weak band, yet Na^+ is one of the most difficult ions to reduce ($Na^+ + e = Na$, $E = -2.714$ V[31]). The weak bands, which show some variation in band maxima, would show less if the absorption due to the underlying singlet-singlet transition could be accurately subtracted out. More variation

Figure 6.

The absorption spectra of some tungstate salts in water at room temperature.

——————— refers to Tl_2WO_4

—— —— refers to Na_2WO_4

—— – —— refers to Cs_2WO_4

—— – – —— refers to $PbWO_4$

– – – – – – refers to $CdWO_4$

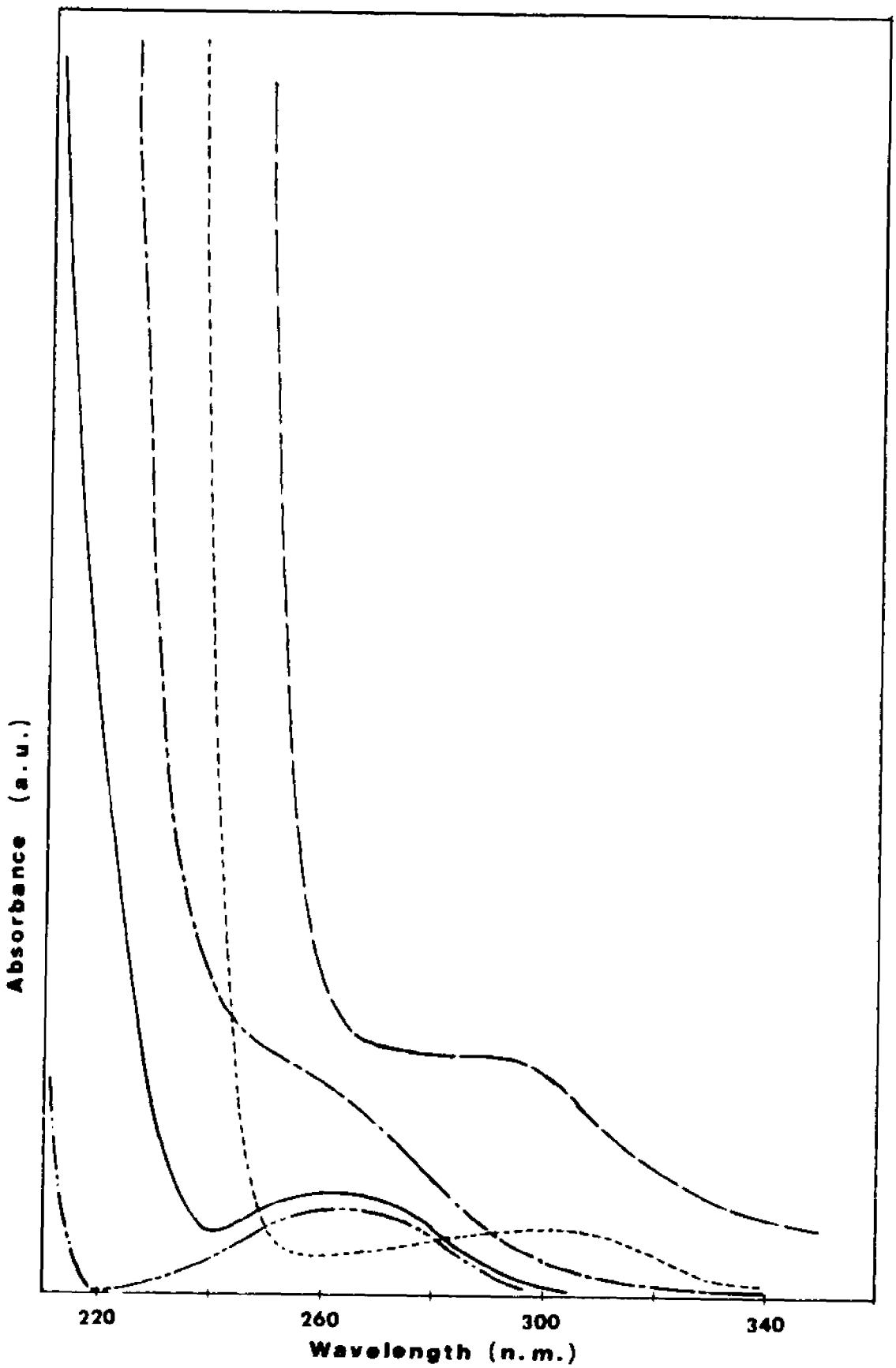
Absorbance (a.u.)
220
260
300
340
Wavelength (n.m.)

Figure 7.

The absorption spectra of some molybdate salts in water at room temperature.

———————— refers to Na_2MoO_4

—— —— —— refers to $PbMoO_4$

—— - - - —— refers to $CdMoO_4$

- - - - - - - refers to Tl_2MoO_4

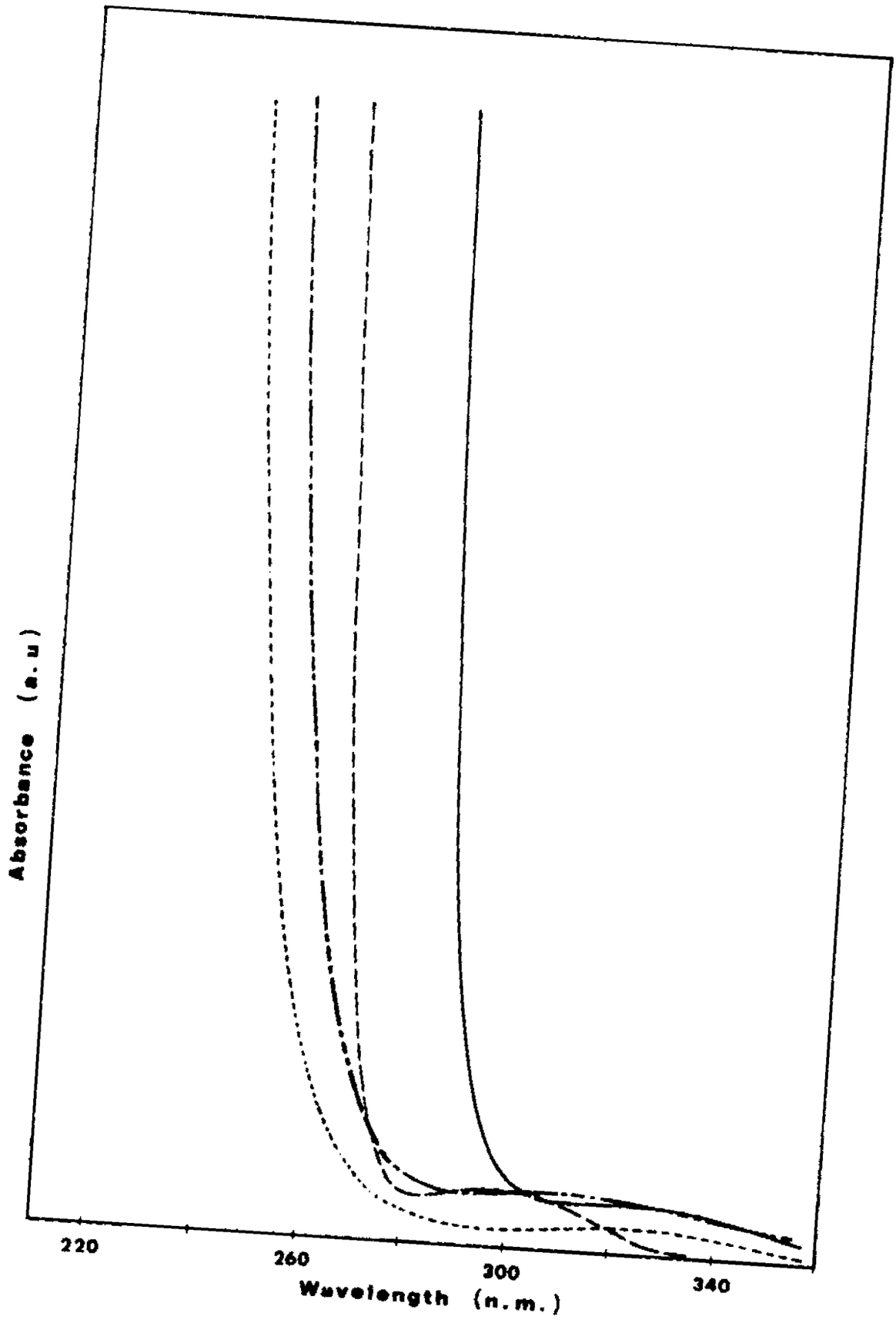
Absorbance (a.u)
220
260
300
340
Wavelength (n.m.)

TABLE 4

Characteristics of the Weak Absorption Band in Tungstate and Molybdate Solutions

Molecule	λ max (nm)	Extinction Coefficient (ℓ/mole cm)
Na_2MoO_4	330	1.5
$CdMoO_4$	315	14.
$PbMoO_4$	305	7.
Na_2WO_4	285	0.4
Cs_2WO_4	262	50.
$CdWO_4$	300	71
Tl_2WO_4	263	40.5
$PbWO_4$	265	200.

in band maxima would be expected if the transition were a ligand → metal charge-transfer transition. In general, the metal ions used are not those expected to be easily reduced photochemically.

The possibility that the bands are due to metal solvent transitions was investigated by recording the spectra of the metal chlorides in neutral water solutions. Thallium chloride solution has an absorption band at 212 nm, lead chloride absorbs at 208 nm. The other metal ions had no absorptions which resemble those in Figures 6 and 7, in agreement with the literature.[32-34]

Are the transitions singlet → triplet? Examining intensitics first, a difficulty arises because the extinction coefficients are quite difficult to measure. The values listed in Table 4 were computed assuming that the isolated anion was the absorbing species. With that assumption, it is evident from Table 4 that the transition probability generally increases with increase of cation atomic weight. This is a characteristic effect of heavy atoms on singlet-triplet transitions.[35] It may be added that the transitions are also quite weak.

The singlet-triplet intervals are similar for both anions (1.6 eV), assuming the singlet and triplet energies respectively are 227 and 320 nm ($MoO_4^=$), and 200 and 279 nm ($WO_4^=$). This is an acceptable value: for $Cd(NCO)_2$ the interval is 1.5 eV,[36] for $Zn(SCN)_2$ the interval is 2.0 eV.[37]

Additional evidence of the triplet nature of the weak transition is provided by the emission characteristics of molybdate and

tungstate salts. Representative emission spectra obtained at 77°K are shown in Figures 8 and 9. The emission bands are nearly gaussian.[37] No correlation with cation reduction potentials exists, indicating that the transition is not charge-transfer.

The wavelengths of maximum excitation and emission, and the lifetimes of the emission of several molybdate and tungstate salts are given in Tables 5 and 6. The few salts for which temperature dependencies of emission have been reported[25,27,38] show a plateau at or near 77°K, below which the lifetimes increase. The lifetimes listed in Tables 5 and 6 were obtained at 77-82°K.

The following conclusions from the emissive lifetimes can be drawn. First, the lifetimes are quite short for $T_1 \rightarrow S_0$ emission, but not unprecedented.[39] They reflect the strong spin-orbit coupling perturbation of the heavy nuclei involved. Second, the lifetime of a molybdate salt is almost always greater than that of the tungstate salt of the same cation. Third, the heavier the cation, the shorter is the lifetime. The clarity of this observation is obscured somewhat by the effects of trapping levels, methods of preparation, impurities, and temperature effects.[25,27,36]. If the conclusions are genuine, they are consistent with the effects of external heavy atoms on a $T_1 \rightarrow S_0$ transition.[35]

Normally, the excitation spectrum of an emitting molecule closely resembles its absorption spectrum.[40] The excitation maxima listed in Tables 5 and 6 lie far to the red of the strong singlet-singlet transitions of the molybdate ion (227 nm) and the tungstate

Figure 8.

The uncorrected emission spectra of some tungstate salts at 77°K. Spectrum 1 is $CaWO_4$, spectrum 2 is Cs_2WO_4, and spectrum 3 is Na_2WO_4.

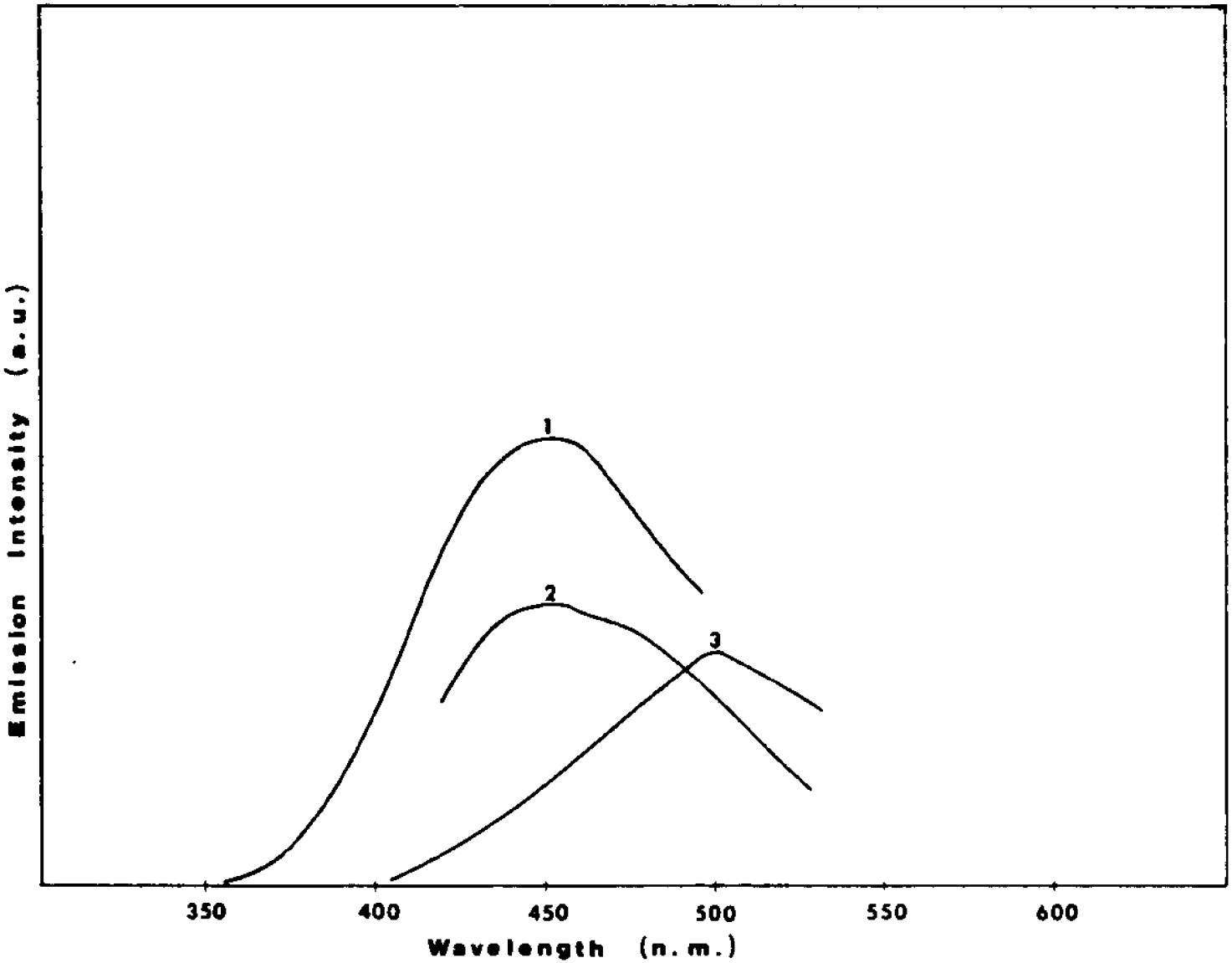
Emission Intensity (a.u.)
1
2
3
350
400
450
500
550
600
Wavelength (n.m.)

Figure 9.

The uncorrected emission spectra of some molybdate salts at 77°K. Spectrum 1 is Ag_2MoO_4, spectrum 2 is $PbMoO_4$, spectrum 3 is $BaMoO_4$, spectrum 4 is $CaMoO_4$, spectrum 5 is $SrMoO_4$, spectrum 6 is $CdMoO_4$, spectrum 7 is $Bi_2(MoO_4)_3$, spectrum 8 is $ZnMoO_4$, and spectrum 9 is Na_2MoO_4.

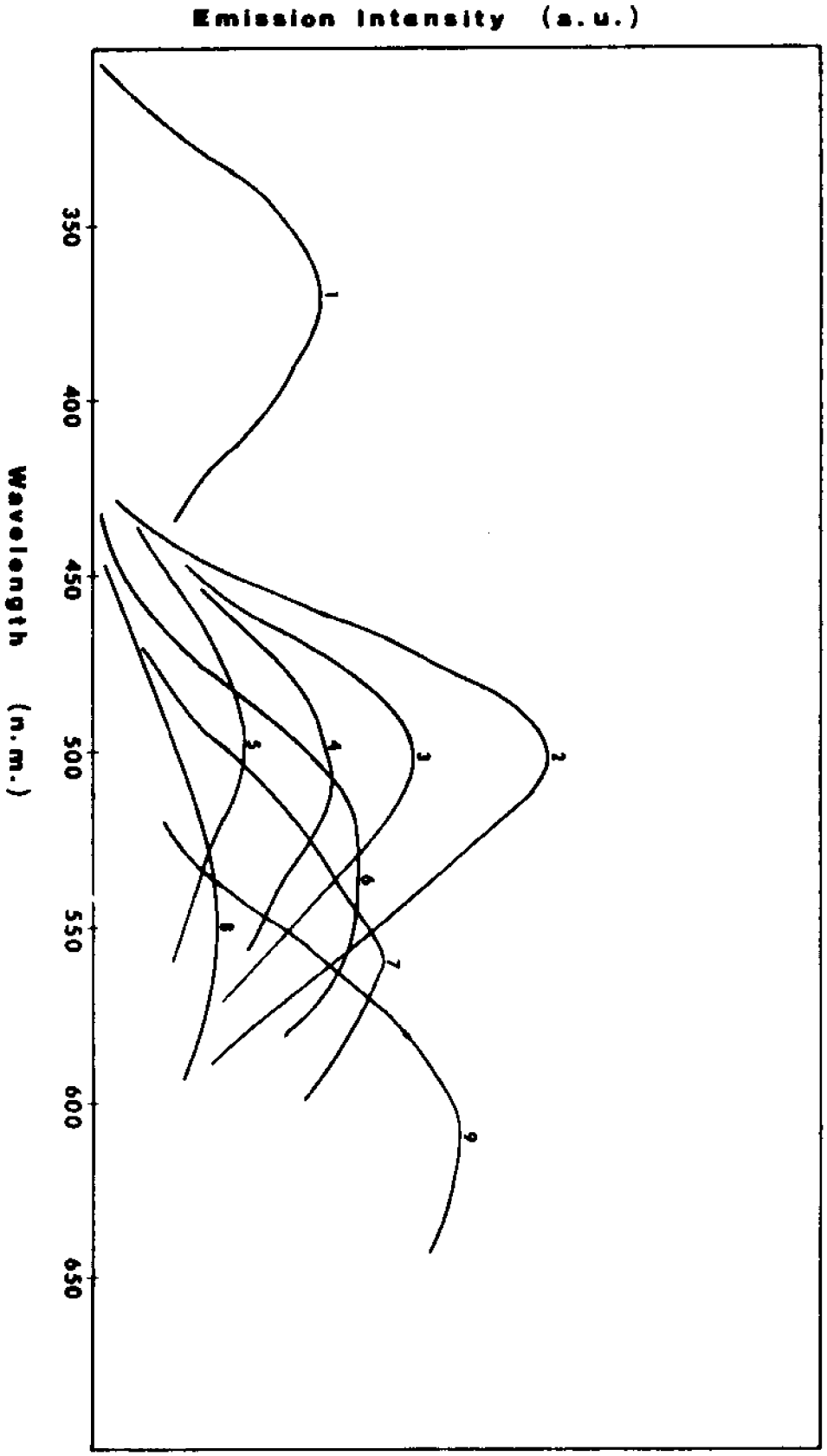
Emission Intensity (a.u.)
Wavelength (n.m.)
350
400
450
500
550
600
650
1
2
3
4
5
6
7
8
9

TABLE 5

Characteristics of Tungstate Salt Emission[1]

Salt	Excitation Maximum (nm)	Emission Maximum (nm)	Lifetime (μsec)
Li_2WO_4			46
Na_2WO_4	285	505	186
$MgWO_4$	280[2]		48[2], 55[3]
$CaWO_4$	264[4], 269[5]	435[6]	7[3],43[5], 8
$ZnWO_4$			30[2], 36[3], 44
$SrWO_4$			193
$CdWO_4$			16[2], 23[3], 24
$CsWO_4$	412	450	
$PbWO_4$			8

[1]Unless otherwise referenced, the data is the authors.

[2]D. Hahn and K. Lertes, Z. Physik. 169, 331 (1962)

[3]V. Schafer, Z. Physik. 166, 429 (1962)

[4]H. Brinkman and C. C. Vlam, Physica 14, 650 (1949)

[5]M. Treadaway and R. Powell, J. Chem. Phys. 61, 4003 (1974)

[6]R. Kalyanasundaram, R. Lakshminarayanan, N. Rajaram, M. I. A. Siddiqui, and C. V. Suryanarayana, Indian J. Pure Appl. Phys. 9, 14 (1971)

TABLE 6

Characteristics of Molybdate Salt Emission[1]

Salt	Excitation Maximum (nm)	Emission Maximum (nm)	Lifetime (μsec)
Li_2MoO_4	328	610	10
Na_2MoO_4	325	611	880
$CaMoO_4$	305	508	220[2]
$ZnMoO_4$	294	550	
$SrMoO_4$	245	500	156
Ag_2MoO_4	290	570	
$CdMoO_4$	337	535	230, 200[2]
Cs_2MoO_4	370	395	
$BaMoO_4$	348	508	
$PbMoO_4$	359	503	10^3
$Bi_2(MoO_4)_3$	318	560	

[1] Unless otherwise referenced, data is from the author.

[2] D. Hahn and K. Lertes, Z. Physik. 169, 331 (1962)

[3] B. I. Maksakov, A. M. Morozov, and N. G. Romanova, Opt. Spectrosc. 14, 111 (1963)

ion (200 nm) in solution. In most cases, the excitation maxima correlate with the weak transitions listed in Table 4.

The single crystal specular reflection spectra of silver molybdate and thallium tungstate have been obtained,[41] and are shown in Figure 10. Specular reflection bands correspond roughly to absorption bands, except that the reflection band maxima are shifted to the red.[42] Silver molybdate has a reflection band at 300 nm which corresponds closely with its emission excitation maximum at 295 nm. The 250 nm band is probably a transition in Ag^+ (225 nm in solution). The solution absorption spectrum of silver molybdate does not unequivocally show a transition near 300 nm, partially because of Tyndall scattering by silver molybdate particles.

The specular reflection spectrum of thallium molybdate shows a band at 293 nm and several shoulders to the blue of that band which may correspond with the weak solution band at 263 nm.

In summary, both specular reflection spectra show bands other than those related to the anion and cation solution spectra. Further, the bands observed show a correspondence with the weak transitions seen in the solution spectrum (thallium tungstate) and with the emission spectrum (silver molybdate).

The most rational explanation for the above observation is the assignment of the weak transition observed in solution, and the intrinsic molecular emission of molybdate and tungstate ions as due to the $T_1 \leftrightarrow S_0$ transition.

Figure 10.

The specular reflection spectrum of Ag_2MoO_4 (———) and Tl_2WO_4 (—— —— ——) at room temperature.

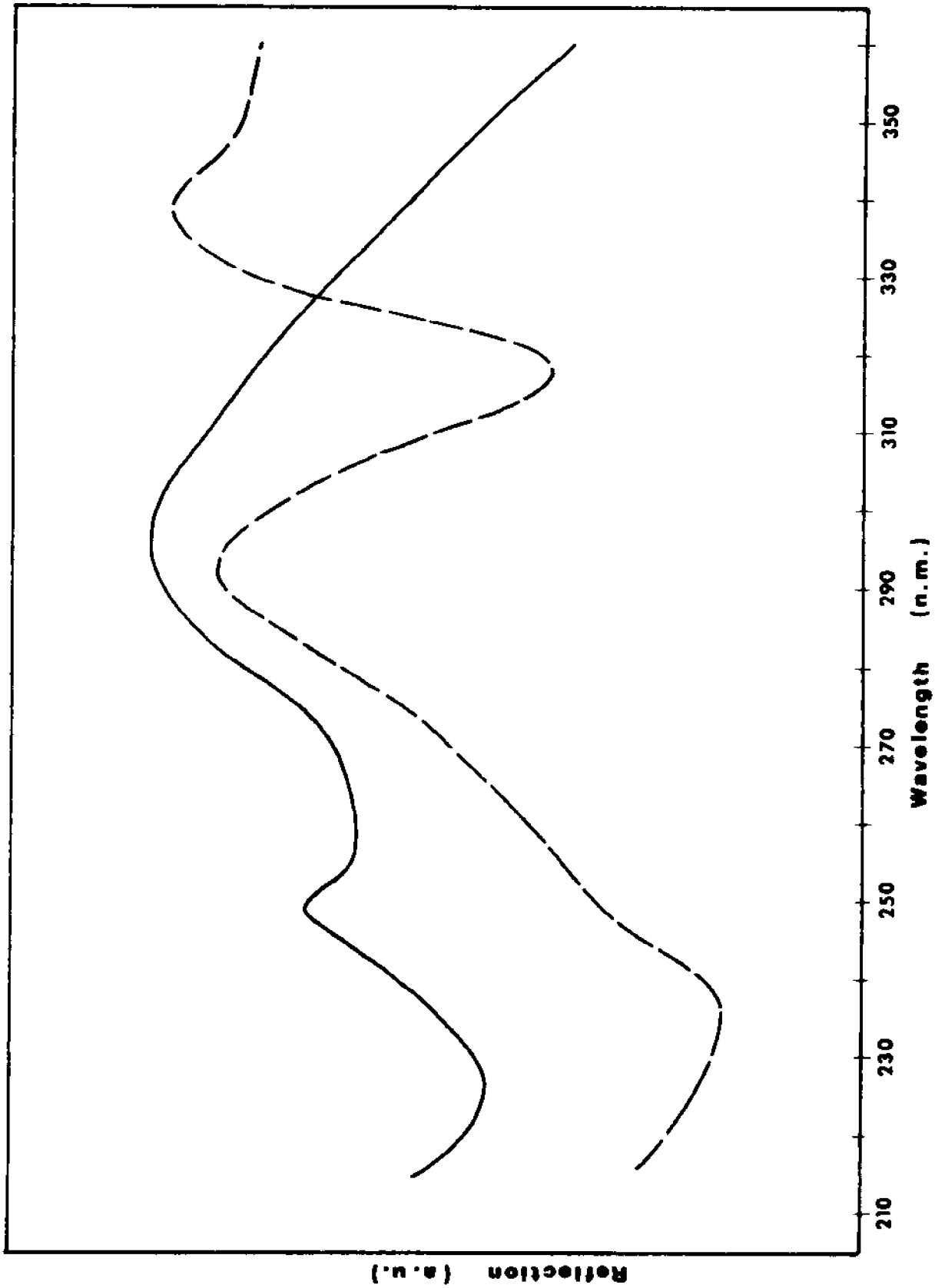
Reflection (a.u.)
210
230
250
270
290
310
330
350
Wavelength (n.m.)

REFERENCES

1 C. K. Jorgensen, Mol. Phys., 4, 235 (1961).

2 "Light and Color", General Electric Energy Company, Cleveland, Ohio, p. 14.

3 K. Pitzer and J. H. Hildebrand, J. Am. Chem. Soc., 63, 2472 (1941)

4 C. K. Jorgensen, "Oxidation Numbers and Oxidation States," Springer Verlag, New York, 1969, p. 141.

5 C. K. Jorgensen, Acta Chem. Scand., 17, 1034 (1963).

6 E. Rabinowitch, Rev. Mod. Phys., 14, 112 (1942).

7 F. S. Dainton, J. Chem. Soc., 1533 (1952).

8 L. E. Orgel, Quart. Rev., 8, 422 (1954).

9 S. P. McGlynn, Chem. Rev., 58, 1113 (1958).

10 G. Stein and A. Treinin, Trans. Far. Soc., 55, 1086, 1091 (1959).

11 S. P. McGlynn, in "Luminescence of Crystals, Molecules, and Solutions," F. Williams, Ed., Plenum, New York, 19 , p. 339.

12 W. C. Allen and R. N. Dixon, Trans. Far. Soc., 65, 1168 (1969).

13 S. P. McGlynn, Izv. Akad. Nauk SSSR, Ser. Fiz., 37, 546 (1973).

14 R. S. Mulliken and W. B. Person, "Molecular Complexes," Wiley-Interscience, New York, 1969, p. 271.

15 M. L. Freedman, J. Am. Chem. Soc., 81, 3834, (1959).

16 H. L. Friedman, J. Chem. Phys., 21, 319 (1953).

17 R. S. Mulliken, Rev. Mod. Phys., 14, 204 (1942).

18 CNDO/2, CNDO/S-C.I., and Gaussian-70 calculations by the author.

19 J. L. Weeks, G. M. A. C. Meaburn, and S. Gordon, Rad. Res., 19, 559 (1963).

20 H. J. Maria, A. Wahlborg, and S. P. McGlynn, J. Chem. Phys., 49, 4295 (1968).

21 S. J. Strickler and M. Kasha, J. Am. Chem. Soc., 85, 2899 (1963).

22 F. A. Kroger, "Some Aspects of the Luminescence of Solids," sevier, Ner York, 1948.

23 C. C. Vlam, Physica, 15, 609 (1949).

24 C. B. Beard, W. H. Kelly, and M. L. Mallory, J. Appl. Phys., 33, 144 (1962).

25 D. Hahn and K. Lertes, Z. Physik, 169, 331 (1962).

26 B. I. Maksakov, A. M. Morozov, and N. G. Romanova, Opt. Spectrosc., 14, 166 (1963).

27 M. Treadaway and R. C. Powell, J. Chem. Phys., 61, 4003 (1974).

28 W. V. Loo, Phys. Stat. Sol., A28, 227(1975).

29 A. K. Levine and F. C. Patilla, Appl. Phys. Lett., 5, 118 (1964).

30 M. Aia, J. Electrochem. Soc., 114, 367 (1967).

31 H. A. Laitinen, "Chemical Analysis," McGraw-Hill, New York, 1960, p. 280.

32 F. Getman, J. Phys. Chem., 29, 865 (1925).

33 S. Kato, Sci. Pap. Inst. Physic. Chem. Res. Tokio, 12, 230 (1930).

34 C. Merritt, H. M. Henderson, and L. B. Rogers, Anal. Chem., 25 572 (1953).

35 S. P. McGlynn, T. Azumi, and M. Kinoshita, "Molecular Spectroscopy of the Triplet State," Prentice Hall, New Jersey, 1969, p. 315.

36 J. W. Rabalais, J. R. McDonald, and S. P. McGlynn, J. Chem. Phys., 51, 5095 (1969).

37 J. R. McDonald, V. M. Scherr, and S. P. McGlynn, J. Chem. Phys., 51, 1723 (1969).

38 V. Schafer, Z. Physik, 116, 429 (1962).

39 H. J. Maria, A. T. Armstrong, and S. P. McGlynn, J. Chem. Phys., 48, 4694 (1968).

40 C. A. Parker, "Photoluminescence of Solutions," Elsevier, Amsterdam, 1968, p. 21.

41 With the assistance of Dr. B. G. Anex of the University of New Orleans.

42 B. G. Anex, Mol. Cryst., 1, 1 (1966).

CHAPTER THREE.

SPIN-ORBIT COUPLING IN THE SILVER NITRITE MOLECULE.

Abstract

A model which describes the interaction between a metal cation and an inorganic anion is developed using first-order perturbation theory. The model does not invoke vibronic spin-orbit coupling. All one-electron excitations of the highest-occupied and lowest-occupied metal and anion orbitals are investigated. Expressions which describe all sources of $S_o \rightarrow T_1$ intensity are derived and given. These expressions are computed for the silver nitrite molecule and are compared with experiment. The results indicate the critical role of charge-transfer transitions in the mechanism of the enhancement of $T_1 \leftrightarrow S_o$ probabilities.

I. INTRODUCTION:

The nitrite ion, a nonlinear eighteen electron molecule, is characterized by three singlet transitions below 200 nm:[1] an intense $\pi\pi^*(B_1 \leftarrow A_1)$ transition at 210 nm and two $n\pi^*$ transitions, one at 350 nm ($B_1 \leftarrow A_1$) and the other at 290 nm ($A_2 \leftarrow A_1$), in solution. The lowest triplet state has been identified as a $^3B_1$.[2,3,4] In sodium nitrite, the $^3B_1 \leftarrow {}^1A_1$ transition is polarized almost entirely in plane, perpendicular to the two-fold axis (y-polarization). Zeeman studies[2,4] indicate that the zero-field spin state is T_z (A_2). The phosphorescence spectrum exhibits quite weak non-totally symmetric vibrations, thus disallowing a vibronic spin-orbit coupling mechanism. The transitions $^1B_2 \leftarrow {}^1A_1$ and the $^1B_1 \leftarrow {}^1A_2$ have been suggested as primarily candidates for the $^3B_2 \leftarrow {}^1A_1$ transition intensity.[2,4,5]

An enhancement of the $T_1 \leftarrow S_0$ absorption is known to occur with heavy metal salts or solutions of nitrite.[6] For example, silver is observed to increase the oscillator strength of that transition by two orders of magnitude in the crystal,[7] thallium by three.[8] In contrast to the case of sodium nitrite, in silver sodium nitrite ($AgNa(NO_2)_2$) the polarization of the $T_1 \leftarrow S_0$ absorption is totally along the two-fold (z)axis.[7] In silver nitrite, evidence exists that the emitting triplet is the $^3A_2$.[9] In this salt, a charge-transfer transition previously predicted[5] is observed at 390 nm.[9]

The silver nitrite molecule has thus been well described experimentally. In addition, the enhanced $T_1 \leftarrow S_0$ transition mech-

anism is known to operate in this molecule.[5,6] For those reasons, a more thorough quantum mechanical description of silver nitrite has been developed. It is hoped that general conclusions which are helpful in the understanding of other metal-anion systems will be generated.

II. THE MODEL:

The model describes the enhancement of the anion $T_1 \leftarrow S_o$ transition via spin-orbit coupling. It is assumed that the electronic structure of the isolated anion and metal cation are known. All interactions are restricted to the highest-occupied and lowest-unoccupied spinorbitals of the anion and the metal. We denote the highest-occupied and lowest-unoccupied spinorbitals of the anion as a and a*, respectively. Similarly, for the metal, we use m and m*, respectively. In the case of the nitrite ion, for example, a may represent any one of the a_2, b_2, or a_1 spinorbitals, all of which are occupied in the ground state (vide supra).

At large metal-anion distances, the spinorbitals, as written above, remain orthogonal. The possible electronic configurations derived from these four spinorbitals (assuming no interaction between the metal and the anion) are given by the wave functions of Table 1. These wave functions will be denoted the zero-order wave functions. Only single-electron excitations have been included in Table 1. These wave functions are neither orthogonal nor normalized. The five con-

TABLE 1

CONFIGURATION	CONFIGURATIONAL WAVE FUNCTIONS (Slater Determinental Form)		
	Singlets	Triplets	M_S
Ψ_O	$\lvert a\bar{a}m\bar{m}\rvert$		
$\Psi_{A'}$	$\frac{1}{\sqrt{2}}(\lvert a\bar{a}^*m\bar{m}\rvert + \lvert a^*\bar{a}m\bar{m}\rvert)$	$\lvert aa^*m\bar{m}\rvert$	1
		$\lvert\bar{a}^*\bar{a}m\bar{m}\rvert$	-1
		$\frac{1}{\sqrt{2}}(\lvert a\bar{a}^*m\bar{m}\rvert - \lvert a^*\bar{a}m\bar{m}\rvert)$	0
$\Psi_{M'}$	$\frac{1}{\sqrt{2}}(\lvert a\bar{a}m\bar{m}^*\rvert + \lvert a\bar{a}m^*\bar{m}\rvert)$	$\lvert a\bar{a}mm^*\rvert$	1
		$\lvert a\bar{a}\bar{m}^*\bar{m}\rvert$	-1
		$\frac{1}{\sqrt{2}}(\lvert a\bar{a}m\bar{m}^*\rvert + \lvert a\bar{a}m^*\bar{m}\rvert)$	0
Ψ_{CT}	$\frac{1}{\sqrt{2}}(\lvert a\bar{m}^*m\bar{m}\rvert + \lvert m^*\bar{a}m\bar{m}\rvert)$	$\lvert am^*m\bar{m}\rvert$	1
		$\lvert\bar{a}\bar{m}^*m\bar{m}\rvert$	-1
		$\frac{1}{\sqrt{2}}(\lvert a\bar{m}^*m\bar{m}\rvert - \lvert m^*\bar{a}m\bar{m}\rvert)$	0
Ψ_{RCT}	$\frac{1}{\sqrt{2}}(\lvert a\bar{a}m\bar{a}^*\rvert + \lvert a\bar{a}a^*\bar{m}\rvert)$	$\lvert a\bar{a}a^*m\rvert$	1
		$\lvert a\bar{a}\bar{a}^*\bar{m}\rvert$	-1
		$\frac{1}{\sqrt{2}}(\lvert a\bar{a}m\bar{a}^*\rvert - \lvert a\bar{a}a^*\bar{m}\rvert)$	0

figurations shown have immediate spectrochemical interpretations, which are illustrated in Figure 1.

The spinorbitals a and a* are eigenfunctions of the total hamiltonian of the anion,

$$H_a = \sum_{i=1}^{N_a} \left(-\tfrac{1}{2}\nabla_i^2 + \sum_{j<i} \tfrac{1}{r_{ij}} - \sum_x \frac{Z_x}{r_{ix}} \quad \sum \xi \vec{l}_i \cdot \vec{s}_i \right) \tag{1}$$

and m and m* are eigenfunctions of the total hamiltonion of the metal,

$$H_m = \sum_{p=1}^{N_m} \left(-\tfrac{1}{2}\nabla_p^2 + \sum_{q<p} \tfrac{1}{r_{pq}} - \frac{Z_m}{r_{pm}} + \xi \vec{l}_{mp} \cdot \vec{s}_p \right) \tag{2}$$

where i, j, p, and q are electron indices, N_a is the total number of electrons in the anion, N_m is the total number of electrons in the metal, x is the atomic center index, and ξ is the spin-orbit coupling coefficient.

At wide separation, where there is no overlap between the metal and the anion, the total hamiltonian of the metal + anion complex is just $H_a + H_m$. We will follow a first-order perturbative description. As the ions are brought closer and allowed to interact, there is an additional term H' in the total hamiltonian H_t:

$$H_t = H_a + H_m + H' \tag{3}$$

where

$$H' = \left(\sum_i^{N_a} \sum_p^{N_m} \tfrac{1}{r_{ip}} \right) - \left(\sum_q \sum_{x \subset a} \frac{Z_x}{r_{qx}} + \sum_i^{N_a} \frac{Z_m}{r_{im}} \right) + \left(\sum_{x \subset a} \frac{Z_x Z_m}{r_{xm}} \right) + \left(\sum_i \sum_x \xi \vec{l}_{ix} \cdot \vec{s}_i \right) \tag{4}$$

The right side of equation (4) has been grouped into four

FIGURE 1

ILLUSTRATION AND INTERPRETATION OF THE FIVE CONFIGURATIONAL WAVE FUNCTIONS

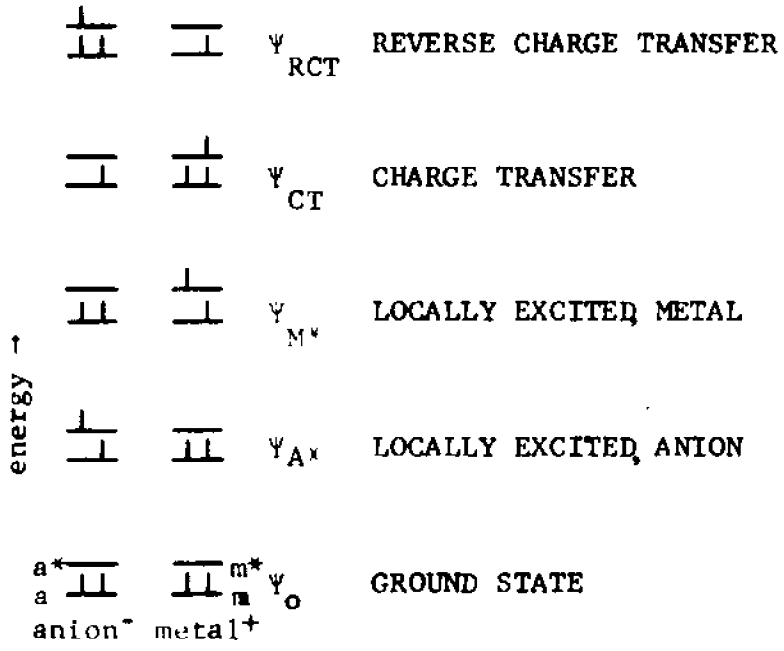

terms. The first term describes the repulsion of electrons on the metal by the electrons on the anion (and vice versa); the second describes the attraction of the metal nucleus for the electrons of the anion (and vice versa); the third describes the metal nucleus - anion nuclei repulsions; and the fourth describes the spin-orbit coupling. We make the assumption that only the fourth term will influence the probability of the $T_1 \leftarrow S_o$ transition of the anion. Hereafter, H' will denote the spin-orbit coupling term.

The effect of the perturbation H' on the configurational zero-order wave functions of Table 1 will be to mix singlet wave functions with triplet wave functions. This mixing permits the singlet triplet transition to exhibit a non-zero intensity, as is discussed in the next section.

III. SINGLET-TRIPLET TRANSITION DIPOLE MOMENTS:

The intensity of an electric dipole transition $\Psi_1 \rightarrow \Psi_2$ is proportional to the square of the transition dipole moment $\vec{M}$, given by

$$\vec{M} = \langle \Psi_2 | \sum_i e\vec{r}_i | \Psi_1 \rangle \qquad (5)$$

where $\vec{r}_i$ is the coordinate of the i^{th} electron, e is the electron charge, and the wave functions Ψ_1 and Ψ_2 are the total wave functions for the molecule in the initial and final states, respectively.

Assuming an LCAO (Linear Combination of Atomic Orbitals) description of the electronic states Ψ_1 and Ψ_2, if Ψ_1 is a singlet

and Ψ_2 is a triplet state, $\vec{M}$ becomes, for a 2n-electron molecule,

$$\begin{aligned}\vec{M} &= \langle {}^3\Psi_2 \left| \sum_i e\vec{r}_i \right| {}^1\Psi_1 \rangle \\ &= \langle |\varphi_1\alpha\cdot\varphi_1\beta\cdots\varphi_n\beta\cdot\varphi_{n+1}\beta \left| \sum_i e\vec{r}_i \right| \varphi_1\alpha\cdot\varphi_1\beta\cdots\varphi_n\alpha\cdot\varphi_n\cdot\beta| \rangle \\ &= \langle \varphi_{n+1} |e\vec{r}| \varphi_n \rangle \langle \beta | \alpha \rangle \\ &= 0,\end{aligned}$$

where φ_n is the space, and α (β) is the spin function of the spinorbital. The $M_s = -1$ spin component of the triplet state ${}^3\Psi_2$ was used above, but similar expressions for the other two spin components also have a zero transition dipole moment.

The above equations demonstrate that a pure singlet ↔ triplet transition has a zero transition dipole moment. How, then, is this transition ever observed? The answer lies in the mixing of singlet and triplet wave functions by spin-orbit coupling.[10]

Using the wavefunctions of Table 1, the (singlet) ground state is ${}^1\Psi_O$ and the triplet state is ${}^3\Psi_{A^*}$, for the anion singlet ↔ triplet transition. Spin-orbit coupling will allow the mixing in of an excited singlet state, for example ${}^1\Psi_{CT}$, into ${}^3\Psi_{A^*}$. The resulting wave function is designated ${}^3\Psi_{A^*}'$, given by

$${}^3\Psi_{A^*}' = {}^3\Psi_{A^*} + e''' {}^1\Psi_{CT}. \qquad (6)$$

The coefficient e''' is expressed, using first-order perturbation theory, by

$$e''' = \frac{\langle {}^1\Psi_{CT} | H' | {}^3\Psi_{A^*} \rangle}{{}^3E^O_{A^*} - {}^1E^O_{CT}} \qquad (7)$$

where ${}^3E^O_{A^*}$ and ${}^1E^O_{CT}$ are the energies of the metal-anion complex in the electronic states ${}^3\Psi_{A^*}$ and ${}^1\Psi_{CT}$ without spin-orbit coupling, re-

spectively. The transition dipole moment $\bar{M}$ for the transition ${}^3\Psi_{A*}' \cdot \Psi_O$ becomes

$$\begin{aligned}
\vec{M} &= \langle {}^3\Psi_{A*}' \,|\Sigma e\vec{r}\,|\Psi_O\rangle \\
&= \langle ({}^3\Psi_{A*} + e''' {}^1\Psi_{CT}) \,|\textstyle\sum_I e\vec{r}_I|\Psi_O\rangle \\
&= \langle {}^3\Psi_{A*} \,|\Sigma e\vec{r}\,|\Psi_O\rangle \;+\; e''' \langle {}^1\Psi_{CT} \,|\textstyle\sum_I e\vec{r}_I|\Psi_O\rangle \\
&= 0 + \frac{\langle {}^1\Psi_{CT} \,|H'\,|{}^3\Psi_{A*}\rangle}{{}^3E^O_{A*} - {}^1E^O_{CT}} \langle {}^1\Psi_{CT} \,|\textstyle\sum_I e\vec{r}_I|\Psi_O\rangle \qquad (8) \\
&\neq 0.
\end{aligned}$$

Each of the five excited singlet states may be able to mix with the anion triplet state ${}^3\Psi_{A*}$. Thus the full expression for ${}^3\Psi_{A*}'$ would be

$${}^3\Psi_{A*}' = {}^3\Psi_{A*} + b''' {}^1\Psi_O + c''' {}^1\Psi_{A*} + d''' {}^1\Psi_{M*} + e''' {}^1\Psi_{CT} + f''' {}^1\Psi_{RCT},$$

where the coefficients are expressed in a manner similar to equation 7. However, if we insert the full expression into equation 8, the result is too unwieldy and not instructive. Instead we will consider separately each of the following spin-orbit coupling corrected configurational wave functions:

$$\begin{aligned}
{}^3\Psi_{A*}' &= {}^3\Psi_{A*} + b''' {}^1\Psi_O \\
" &= " + c''' {}^1\Psi_{A*} \\
" &= " + d''' {}^1\Psi_{M*} \\
" &= " + e''' {}^1\Psi_{CT} \\
" &= " + f''' {}^1\Psi_{RCT}.
\end{aligned}$$

Spin-orbit coupling may also mix triplet states into the ground state, this process also leads to non-zero transition dipole

moments for the singlet → triplet transition. The spin-orbit coupling corrected grand state configurational wave functions are, by analogy to the above

$$\Psi_O' = \Psi_O + b'' \, {}^3\Psi_{A*}$$
$$" = " + c'' \, {}^3\Psi_{M*}$$
$$" = " + d'' \, {}^3\Psi_{CT}$$
$$" = " + e'' \, {}^3\Psi_{RCT}$$

The expressions for $\bar{M}$ using each of the nine spin-orbit coupling corrected configurational wave functions listed above are easily worked out. In addition, it is possible to expand the configurational wave functions, using Table 1, into linear combinations of one-electron orbitals. The result will be a large number of expressions for $\bar{M}$, using one-electron orbitals instead of configurations. Since the H' and $\sum_i er_i$ operators are one-electron operators, many of these expressions will be zero. The expressions which are non-zero are given in Table 2. The Table lists only the expressions for the H_z component of H',[11] the analogous expressions for H_x and H_y are similar except for numerical coefficients. The spin operator matrix elements were evaluated using Table 3.

The following conclusions may be drawn from Table 2.

1) No intensity is conferred upon the singlet ↔ triplet transition from the mixing of excited metal triplet states into the ground state. This is because the triplet - triplet transition ${}^3\Psi_{M*} \rightarrow {}^3\Psi_{A*}$ is a two-electron transition and is therefore forbidden.

TABLE 2

TRANSITION DIPOLE MOMENT EXPRESSIONS*

(Without Overlap)

a)	$\Psi_O + b'' {}^3\Psi_{A^*}$	$-\frac{2\langle a^* \lvert H' \rvert a\rangle(\mu_{A^*})}{E_O - {}^3E_{A^*}}$
b)	$\Psi_O + c'' {}^3\Psi_{M^*}$	0
c)	$\Psi_O + d'' {}^3\Psi_{CT}$	$-\frac{2\langle m^* \lvert H' \rvert a\rangle\langle m^* \lvert \vec{r} \rvert a^*\rangle}{E_O - {}^3E_{CT}}$
d)	$\Psi_O + d'' {}^3\Psi_{RCT}$	$-\frac{2\langle a^* \lvert H' \rvert m\rangle\langle a \lvert \vec{r} \rvert m\rangle}{E_O - {}^3E_{RCT}}$
e)	${}^3\Psi_{A^*} + b''' \Psi_O$	$-\frac{2\langle a \lvert H' \rvert a^*\rangle(\mu_O)}{{}^3E_{A^*} - E_O}$
f)	${}^3\Psi_{A^*} + c''' {}^1\Psi_{A^*}$	$\frac{2(\langle a \lvert H' \rvert a\rangle - \langle a^* \lvert H' \rvert a^*\rangle)\langle a \lvert \vec{r} \rvert a\rangle}{{}^3E_{A^*} - {}^1E_{A^*}}$
g)	${}^3\Psi_{A^*} + d''' {}^1\Psi_{M^*}$	0
h)	${}^3\Psi_{A^*} + e''' {}^1\Psi_{CT}$	$-\frac{2\langle m^* \lvert H' \rvert a\rangle\langle a \lvert \vec{r} \rvert m\rangle}{{}^3E_{A^*} - {}^1E_{CT}}$
i)	${}^3\Psi_{A^*} + f''' {}^1\Psi_{RCT}$	$\frac{2\langle a \lvert H' \rvert m\rangle\langle m \lvert \vec{r} \rvert a^*\rangle}{{}^3E_{A^*} - {}^1E_{RCT}}$

* μ_O is the dipole moment of the ground electronic state, μ_{A^*} is the dipole moment of the molecule in the ${}^3\Psi_{A^*}$ state. H' refers to H'_z. Expressions for H'_x or H'_y differ primarily in the coefficients only.

TABLE 3

SPIN OPERATOR EIGENFUNCTIONS*

	H_x	H_y	H_z
$\langle a \lvert H \rvert b \rangle$	0	0	$\langle a \lvert H_z' \rvert b \rangle$
$\langle a \lvert H \rvert \bar{b} \rangle$	$\langle a \lvert H_x' \rvert \bar{b} \rangle$	$-i\langle a \lvert H_y' \rvert b \rangle$	0
$\langle \bar{a} \lvert H \rvert b \rangle$	$\langle a \lvert H_y' \rvert b \rangle$	$i\langle a \lvert H_y' \rvert b \rangle$	0
$\langle \bar{a} \lvert H \rvert \bar{b} \rangle$	0	0	$-\langle a \lvert Hz' \rvert b \rangle$

* where $H' = \frac{1}{2}\hbar \sum_n \xi_n \ell$. Taken from reference 11, p. 343.
Superscript - above a letter designates a β spin; otherwise, the spin is α.

2) No intensity is derived from the mixing of excited metal singlet states into $^3\Psi_{A*}$. d''' is zero because $^3\Psi_{A*}$ and $^1\Psi_{M*}$ differ by two orbitals, while the operator Hz' is a one-electron operator.

3) It is common to make the assumption that all two-center spin-orbit coupling integrals (e.g., $\langle a^* | Hz' | m \rangle$) are zero.[11] With this assumption, expressions c, d, h, and i are zero.

4) Expression f does not include any contribution from the metal. It therefore cannot describe the enhancement of the singlet - triplet transition due to the presence of the metal.

5) The remaining expressions, a and e, describe transition intensity arising from the dipolar nature of the ion. Such a mechanism for the enhancement of intensity has been observed previously and described.[12,13] However, if this is the only mechanism operating, one would expect the enhancement of the singlet - triplet transition intensity to be independent of the nature of the metal ion, which is contrary to what is observed.

The inability of the expressions in Table 2 to relate to experiment is due to the exclusion of metal-anion overlap. This assumption was made in the expansion of the configurational wave functions by taking the one-electron orbitals a, a*, m, and m* (Table 1) to be orthogonal. A method for the evaluation of matrix elements of a non-orthogonal basis set has been given by Lowdin.[14] According to him,[14] the matrix element of a one-electron operator Ω_1 with respect to two Slater determinants U and V is given by:

$$\int U^* \Omega_1 V dx = \sum_{k\ell} \{k|\Omega_1|\ell\} D_{UV}(k|\ell)$$

where k is an element of U, ℓ is an element of V, and $D_{UV}(k|\ell)$ is the minor of the overlap matrix $\int U^* V dx$, produced by striking out the k^{th} row and the ℓ^{th} column of the matrix.

The inclusion of overlap by the above method is possible for both the spin-orbit coupling integral and the transition moment integral. The resulting expressions for $\bar{M}$ using each of the nine spin-orbit coupling corrected configurational wave functions previously listed are given in Table 4.

A considerable reduction in the complexity of these expressions can be achieved by the use of the following:

1. Two-center spin-orbit coupling integrals (e.g., $\langle a|H'|m\rangle$) will be small because of the strong inverse dependence of the spin-orbit coupling constant ξ on distance, and may be neglected.[11]

2. The spin-orbit coupling operator is not able to mix wave functions which differ in the quantum number ℓ.[15] If the metal under consideration is a post-transition metal, the metal filled orbital m will be a d orbital and the unoccupied orbital m* will be either an s or p orbital. Therefore, spin-orbit coupling integrals of the type $\langle m|H'|m^*\rangle$ will be zero.

3. The expansion of many of the expressions listed will produce terms with overlap in the second power. These terms will be small and may be neglected. This has been done in Table 4.

Because the orbital designations a, a*, m, and m* may each

Table 4

TRANSITION DIPOLE MOMENT EXPRESSIONS*

(With Overlap)

a) $$-\sqrt{2}\,\frac{\langle a^* |H'| a\rangle}{E_O - {}^3E_{A^*}}\Big(\big(\mu_{A^*}\big) - Sam\,\big(\langle a|\vec{r}|m\rangle + \langle m|\vec{r}|a\rangle\big) - Sa^*m\big(\langle a^*|\vec{r}|m\rangle + \langle m|\vec{r}|a^*\rangle\big)\Big)$$

b) $$-\sqrt{2}\,\frac{\langle m^* |H'| m\rangle}{E_O - {}^3E_{M^*}}\Big(-Sam\langle a^*|\vec{r}|m^*\rangle - Sa^*m^*\langle m|\vec{r}|a\rangle\Big)$$

c) $$\sqrt{2}\,\frac{(Sam^*\langle a|H'|a\rangle + Sam\langle m^*|H'|a\rangle)}{E_O - {}^3E_{CT}}\Big(\langle m^*|\vec{r}|a^*\rangle - Sam^*\langle a|\vec{r}|a^*\rangle - 2Sa^*m^*\langle m|\vec{r}|m\rangle + Sa^*m\langle a|\vec{r}|a\rangle - Sa^*m\langle m^*|\vec{r}|m\rangle\Big)$$

d) $$\sqrt{2}\,\frac{(Sa^*m\langle m|H'|m\rangle + Sam\langle a^*|H'|a\rangle)}{E_O - {}^3E_{RCT}}\Big(\langle a|\vec{r}|m\rangle + Sam\big(\langle a|\vec{r}|a\rangle + \langle a^*|\vec{r}|a^*\rangle + \langle m|\vec{r}|m\rangle\big)\Big)$$

e) $$-\sqrt{2}\,\frac{\langle a|H'|a^*\rangle}{{}^3E_{A^*} - E_O}\Big(\big(\mu_O\big) - 2Sam\big(\langle a|\vec{r}|m\rangle + \langle m|\vec{r}|a\rangle\big)\Big)$$

f) $$\sqrt{2}\,\frac{(-\langle a^*|H'|a^*\rangle + \langle a|H'|a\rangle)}{{}^3E_{A^*} - {}^1E_{A^*}}\Big(\langle a|\vec{r}|a^*\rangle - Sa^*m\langle a|\vec{r}|m\rangle - Sam\langle m|\vec{r}|a\rangle\Big)$$

g) $$\sqrt{2}\,\frac{(Sam\langle m^*|H'|a\rangle + Sa^*m^*\langle a|H'|m\rangle)}{{}^3E_{A^*} - {}^1E_{M^*}}\Big(\langle m|\vec{r}|m^*\rangle - Sam^*\langle m|\vec{r}|a\rangle - Sam\langle a|\vec{r}|m\rangle\Big)$$

h) $$\sqrt{2}\,\frac{(Sa^*m\langle m^*|H'|m\rangle + Sa^*m^*\langle a|H'|a\rangle - Sam^*\langle a|H'|a^*\rangle)}{{}^3E_{A^*} - {}^1E_{CT}}\Big(\langle a|\vec{r}|m^*\rangle - Sam\langle m|\vec{r}|m^*\rangle + Sam\langle a|\vec{r}|a\rangle + 2Sam^*\langle m|\vec{r}|m\rangle\Big)$$

i) $$-\sqrt{2}\,\frac{Sam\big(\langle a|H'|a\rangle + \langle m|H'|m\rangle - \langle a^*|H'|a^*\rangle\big)}{{}^3E_{A^*} - {}^1E_{RCT}}\Big(\langle m|\vec{r}|a^*\rangle - Sam\langle a|\vec{r}|a^*\rangle + Sa^*m\big(2\langle a|\vec{r}|a\rangle + \langle m|\vec{r}|m\rangle\big)\Big)$$

*μ_O is the dipole moment of the ground state; μ_{A^*} is the dipole moment of the ${}^3\Psi_{A^*}$ state. H' refers to H_z'. Sam is the overlap between the anion orbital a and the metal orbital m.

represent more than one orbital in a particular molecule (in the original definition), it is important to determine whether this ambiguity exists in the expressions in Table 4. For this determination, most of the expressions were recalculated using six-orbital wave functions: the four listed on Table 1 plus two 'dummy' orbitals. For example, the following wave functions would be appropriate to determine if the two a orbitals in the integral $\langle a|H'|a\rangle$ (expression f, Table 4) must be identical:

$$^1\psi_{A^*} = \frac{1}{\sqrt{2}} \left(|a\bar{a}^*b\bar{b}m\bar{m}| + |a^*\bar{a}b\bar{b}m\bar{m}| \right)$$

$$^3\psi_{A^*} = \frac{1}{\sqrt{2}} \left(|a\bar{a}^*b\bar{b}m\bar{m}| - |a^*\bar{a}b\bar{b}m\bar{m}| \right)$$

It turns out that they must be identical, and since H' cannot be totally symmetric in a number of symmetries (including C_{2v}), the integral is zero in molecules with those symmetries.

The expressions for $\vec{M}$ including the approximations described on the previous page and the identity discussed above are given in Table 5. The molecular symmetry is assumed to be C_{2v}. No other refinements are required prior to the application of the model to a particular molecule.

Table 5

USABLE TRANSITION DIPOLE MOMENT EXPRESSIONS*

a) $$\frac{-\sqrt{2}\langle a^* |H'| a\rangle((\mu_{A^*}) - Sa'm'(\langle a' |\vec{r}| m'\rangle + \langle m' |\vec{r}| a'\rangle) - Sa^*m'(\langle a^* |\vec{r}| m'\rangle + \langle m' |\vec{r}| a^*\rangle))}{E_O - {}^3E_{A^*}}$$

b) $$0$$

c) $$\frac{\sqrt{2}Sa'm^{*\prime}\langle a' |H'| a\rangle\langle m^{*\prime} |\vec{r}| a^*\rangle}{E_O - {}^3E_{CT}}$$

d) $$\frac{\sqrt{2}(Sa^*m'\langle m |H'| m'\rangle + Sa'm'\langle a^{\times} |H'| a'\rangle\langle a |\vec{r}| m'\rangle}{E_O - {}^3E_{RCT}}$$

e) $$\frac{\sqrt{2}\langle a |H'| a^{\times}\rangle((\mu_O) - 2Sa'm'(\langle a' |\vec{r}| m'\rangle + \langle m' |\vec{r}| a'\rangle)}{{}^3E_{A^*} - E_O}$$

f) $$0$$

g) $$0$$

h) $$\frac{-\sqrt{2}Sa'm^{*\prime}\langle a' |H'| a^*\rangle\langle a' |\vec{r}| m^{*\prime}\rangle}{{}^3E_{A^*} - {}^1E_{CT}}$$

i) $$\frac{-\sqrt{2}Sa'm'(\langle m' |H'| m\rangle + \langle a |H'| a'\rangle - \langle a^* |H'| a^*\rangle)\langle m' |\vec{r}| a^*\rangle}{{}^3E_{A^*} - {}^1E_{RCT}}$$

*The primed orbitals have the following meaning: Within a particular expression, all primed orbitals of a single type (e.g., a') must represent the same LCAO wave function. Unprimed orbitals may represent any LCAO wave function of that class (i.e., a may be any of the filled anion orbitals). Other symbols are explained in the footnote to Table 4.

IV. NUMERICAL RESULTS:

It is possible to evaluate numerically all of the expressions in Table 5 for the silver nitrite molecule. This will require reasonably accurate values for the following:

1. Spin-orbit coupling integrals (e.g., $\langle a^* |H'| a \rangle$).

2. The dipole moment of silver nitrite in the ground and $^3\psi_{A^*}$ state.

3. Overlap integrals between nitrite molecular orbitals and silver atomic orbitals.

4. Transition dipole moments for nitrite molecular orbitals and silver atomic orbitals.

5. The energies of the silver nitrite molecule in the various electronic configurations listed on Table 1.

In order to determine these quantities, a number of computer programs were utilized on the L. S. U. IBM 360/65 computer:

1. CNDO/S-C.I. (Quantum Chemistry Program Exchange CNDO 174): This program was used to calculate nitrite anion wavefunctions and eigenvalues. CNDO/S-C.I. is of the type originated by Pople.[16] It uses the Mataga-Nishimoto approximation[17] for two-center integrals and a configuration-interaction subroutine in which the first thirty mono-excited configurations are used.

2. Zipmol: A non-iterative extended Huckel program written by R. Hoffman, which uses single-zeta Slater-type orbitals. It was used for overlap integral evaluations only. Zeta values which were opti-

mized for proper overlaps (i.e., overlap matched atomic orbitals), were taken from L. E. Harris, H. J. Maria, and S. P. McGlynn[5].

3. Zevc: An iterative, double zeta, Slater-type orbital, extended Huckel program was used for dipole moment calculations and for whole molecule ($AgNO_2$) calculations. The coulomb integrals were approximated by negative valence state ionization potentials (-VSIP).[5] The resonance integrals were obtained by Cusach's approximation:[18]

$$H_{ij} = \frac{1}{2}\left(2 - |S_{ij}|\right)(H_{ii}-H_{jj}).$$

4. Soced: This program, written by L. Vanquickenborne, calculates singlet-triplet transition moments and lifetimes from Löwdin orthogonalized molecular orbitals obtained from Zevc. Only one-center spin-orbit coupling integrals are evaluated.[19]

5. CNDO/2 (a modified version of Quantum Chemical Program Exchange Nr. 141), and Gaussian-70 were used for comparison to cndo/s-C.I. nitrite eigenvalues.

It is important to begin with accurate eigenvectors and eigenvalues for the nitrite ion. The MO order of and the MO energies of the nitrite ion are quite dependent on the type of calculation used (Figure 2). Figure 2 also shows the approximate band half-widths from the only available ESCA spectrum of the NO_2^- ion.[20]

In all the calculations except Gaussian-70 and Zevc the three highest-occupied orbitals are of the same symmetry and are separate from the fourth highest-occupied orbital. The latter point is in apparent agreement with the photoelectron spectrum.

Figure 2.

Orbital energies of the nitrite ion. All calculations are from reference 21, using atomic dimensions from crystal structure data,[22] except the ab initio calculation. The latter was taken from reference 23. The orbital exponents used in Zevc were from E. Clementi.[24] The lowest unoccupied orbital is denoted by a box. The lowest unoccupied orbital as calculated by the CNDO/2 program was too high in energy to be included in the diagram.

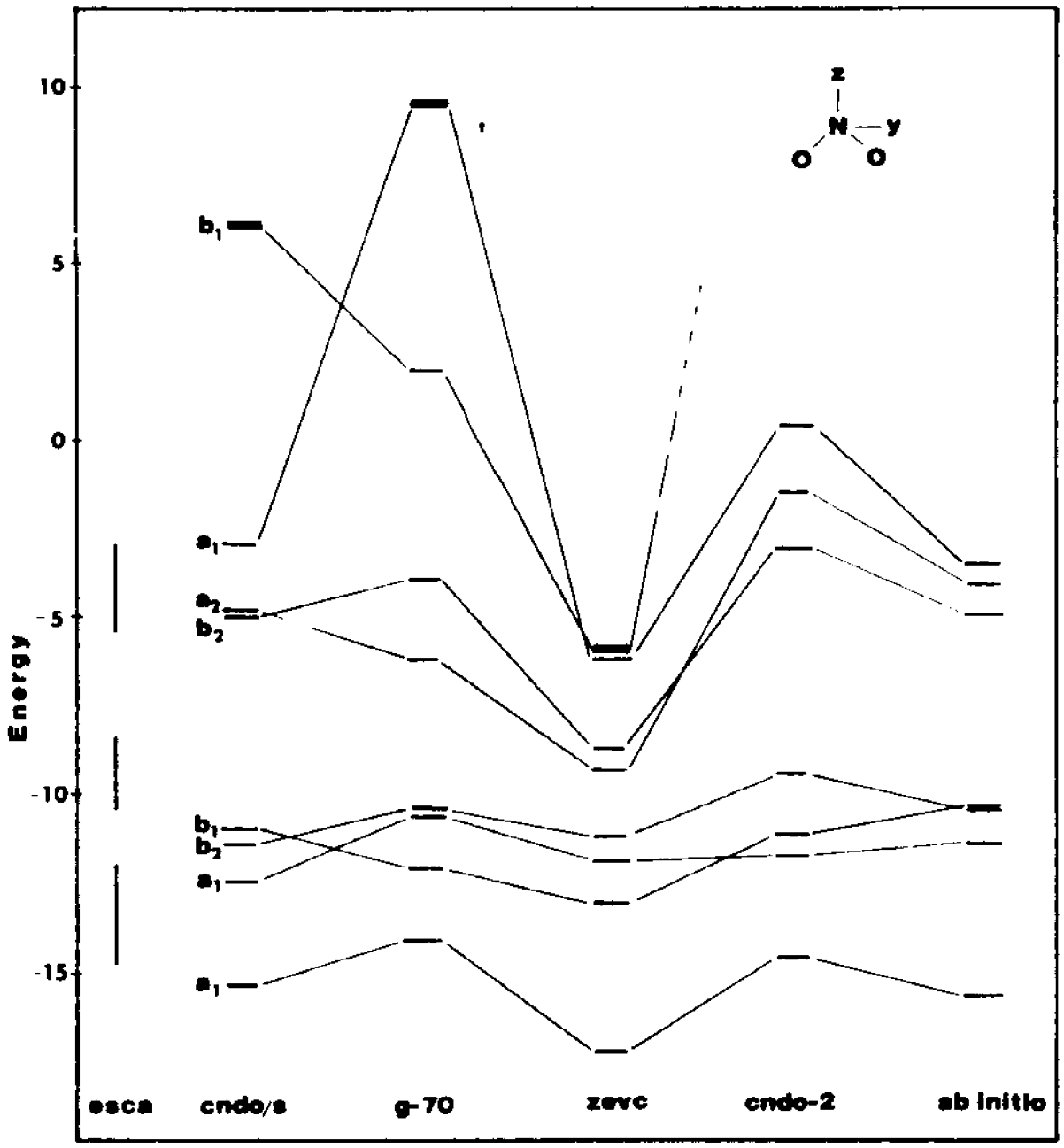
10
5
0
-5
-10
-15
Energy
z
N
y
O
O
b1
a1
a2
b2
b1
b2
a1
a1
esca
cndo/s
g-70
zevc
cndo-2
ab initio

The lowest-unoccupied orbital is energetically separated from the second lowest unoccupied orbital in all calculations used. The symmetry of this orbital is the same (b_1) in all calculations except Gaussian-70. Transitions from the aforementioned three highest occupied orbitals to the b_1 unoccupied orbital are observed in the ultraviolet spectrum of the NO_2^- ion.[1] (The reason for the non-agreement of the Gaussian-70 data is not known.)

It is evident from the above that the lowest-energy electronic transitions involve primarily the highest three occupied orbitals and the lowest unoccupied orbital. These four orbitals are shown in Figure 3, taken from the CNDO/S-C.I. calculation. The anion a orbital (Table 1) is taken to be any of the three highest occupied orbitals, and the a* orbital is taken to be the b_1 unoccupied orbital.

The orbital energies from the CNDO/S-C.I. calculation agree best with the photoelectron spectrum energies (Figure 2). For this reason, eigenvectors (orbital exponents and atomic orbital coefficients) from this calculation were used for the analytic form of the anion a and a* orbitals (Table 6). All atomic orbital contributions of > 10% were included. The coefficients were rounded off to three significant figures.

The molecular geometry of the nitrite ion varies, according to x-ray crystallographic studies of nitrite crystals,[22] with the metal cation. The geometry chosen for all the calculations reported here is from the crystal structure of silver nitrite.[22]

Figure 3.

The orbitals of the nitrite ion. The b_1 orbital is the lowest unoccupied orbital. The molecular z axis is the C_{2v} axis, the y axis is in-plane. The b_1 and a_2 orbitals have a node in the yz plane. The orbitals were drawn using data from a CNDO/s-C.I. calculation.[21]

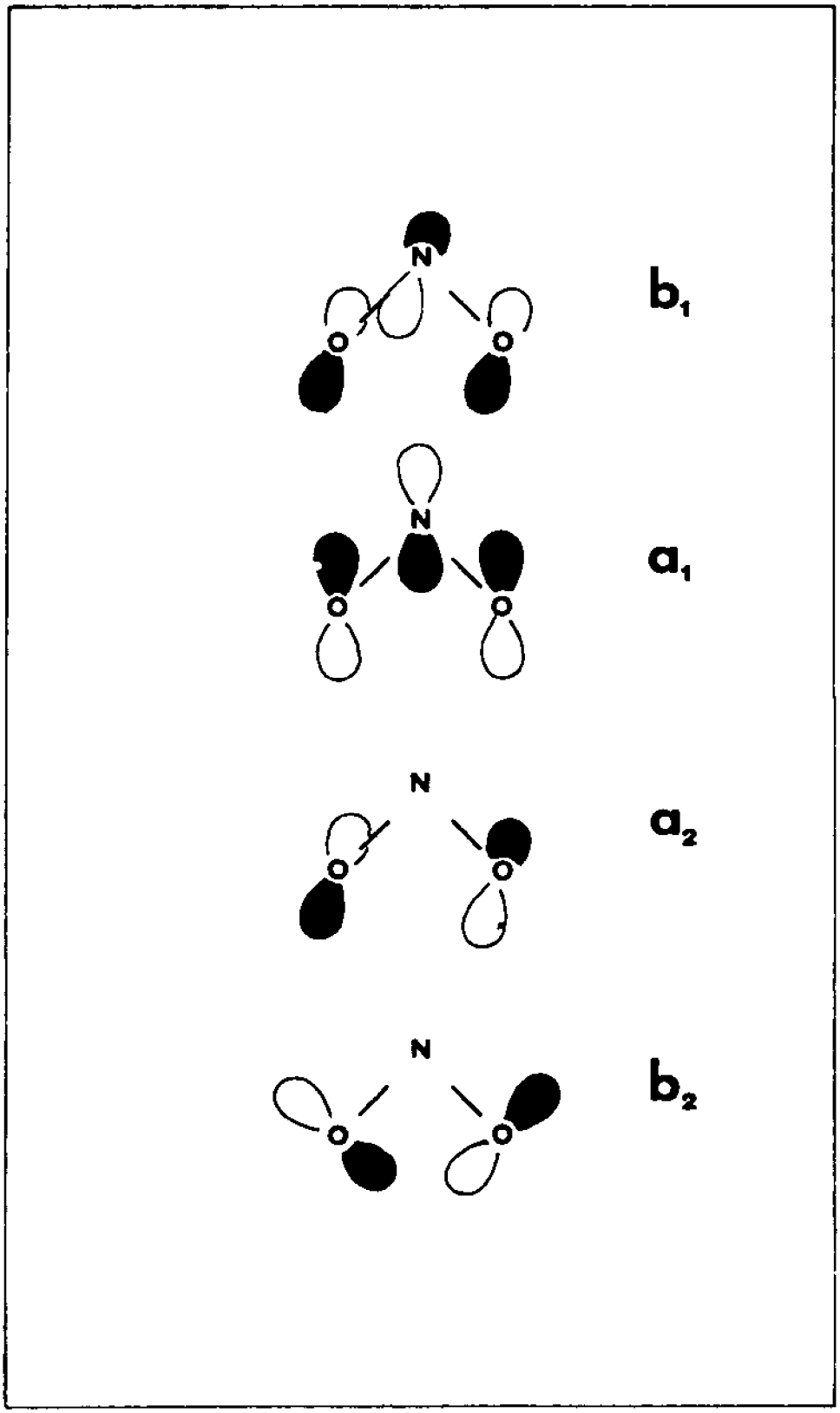
N
O
O
b1
N
O
O
a1
N
O
O
a2
N
O
O
b2

Table 6

NITRITE ION MOLECULAR ORBITALS[1,2]

$b_1 = (0.747)p_x(N) - (0.470)p_x(O_1) - (0.470)p_x(O_2)$

$a_1 = (0.241)s(N) + (0.560)p_z(N) - (0.556)p_z(O_1) - (0.556)p_z(O_2)$

$a_2 = -(0.707)p_x(O_1) + (0.707)p_x(O_2)$

$b_2 = (0.122)p_y(N) - (0.440)p_y(O_1) - (0.546)p_z(O_1) - (0.440)p_y(O_2) + (0.546)p_z(O_2)$

ORBITAL EXPONENTS[1]

Nitrogen	2s	$\zeta = 1.95$
	2p	$\zeta = 1.95$
Oxygen	2s	$\zeta = 2.275$
	2p	$\zeta = 2.275$

---

[1] From CNDO/s-C.I. Analytic form of the orbital is $\Psi = Ar^{n-1}e^{-\zeta r}Y_{\ell m}(\theta,\varphi)$ where A is the normalization factor, n is the principle quantum number, and $Y_{\ell m}(\theta,\varphi)$ is the spherical harmonic.

[2] Nitrite geometry from R. E. Long and R. E. Marsh, Acta Cryst., 15, 448 (1962).

In silver nitrite,[22] a silver atom is located along the C_{2v} axis of the nitrite ion 2.47 Å away from the nitrogen atom in both directions. It is impossible to predict a priori which geometry is important for the interaction which enhances the anion $T_1 \leftarrow S_0$ transition. For this reason, parallel calculations in the two geometries were carried out. The geometry in which the silver atom is located away from the oxygen atoms is denoted 'Structure I,' the geometry in which the silver atom is located nearer the oxygen atoms is denoted 'Structure II.' (Figure 4).

In a previous analysis of the silver nitrite molecule,[5] the silver - nitrogen distance was taken to be 2.5 Å. In addition, only one molecular geometry was used (Structure I). In the calculations presented here, the more accurate silver - nitrogen distance (2.47 Å) and both molecular geometries were used.

The zeta values for the silver 4d, 5s, and 5p wave functions were taken from reference 5. These were used for the calculation of the overlap matrix for the silver nitrite molecule, using Zipmol. The resulting overlap matrix was used for the calculation of transition dipole moments (vida infra), and for use with Zevc.

A. METAL-ANION OVERLAPS:

The evaluation of the expressions in Table 5 require the calculation of a number of metal - anion overlaps, e.g., Sam, Sa*m, etc. The calculation is straightforward: the appropriate atomic orbital

Figure 4.

The two structures of the silver nitrite molecule used in the present calculations. The upper structure is denoted Structure I, the lower is denoted Structure II. Only the position of the silver atom changes in the two structures, the nitrite atomic coordinates remain unchanged. The data was taken from an X-ray crystallographic study of the silver nitrite crystal (reference 22).

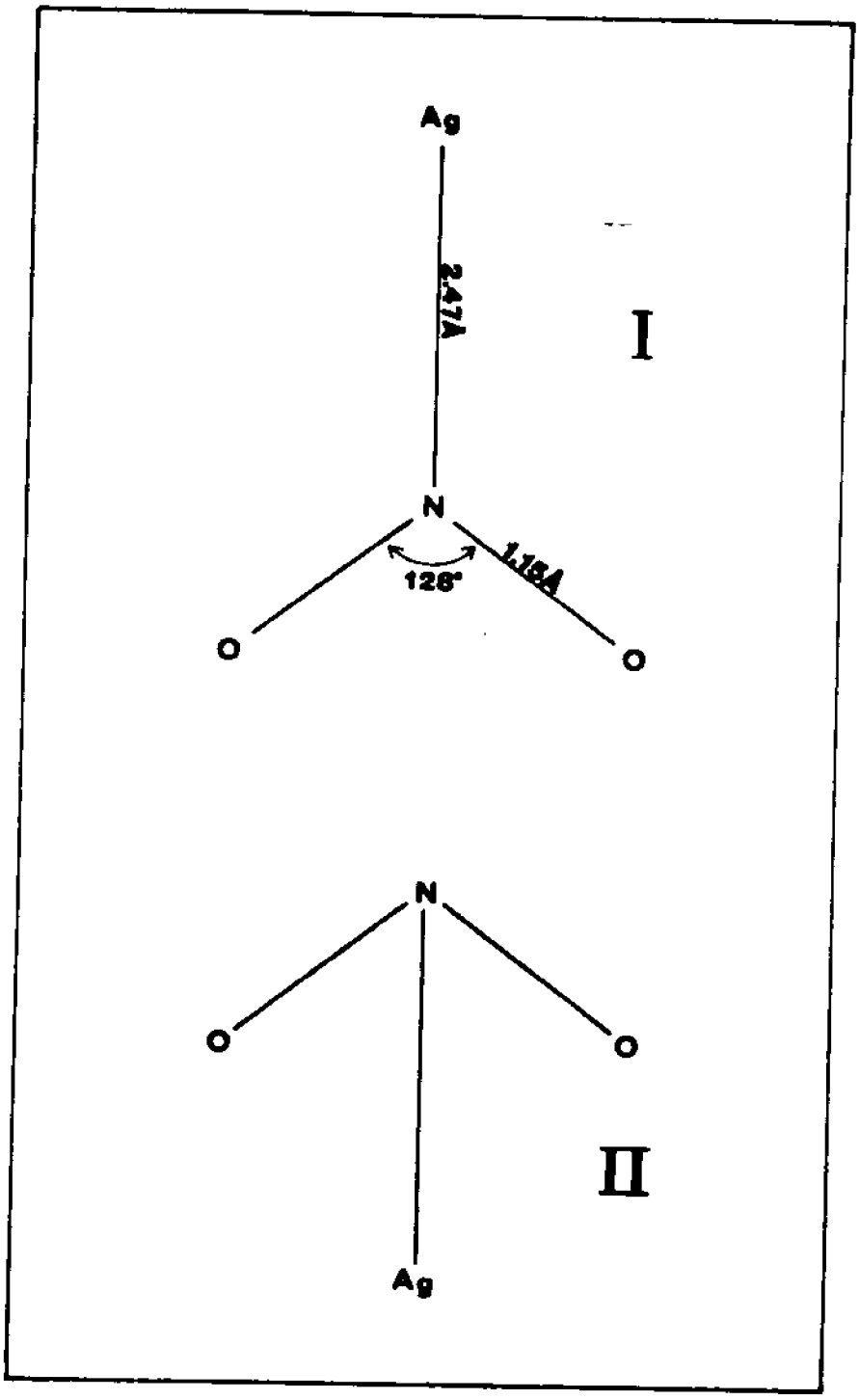
Ag
2.47Å
I
N
128°
1.18Å
O
O
N
O
O
II
Ag

overlaps are taken from a Zipmol output. The results are given in Table 7.

B. SPIN-ORBIT COUPLING INTEGRALS:

The spin-orbit coupling integrals $\langle a|H'|a^*\rangle$, etc., are calculated as follows: In order for the integral to be non-zero, it is required that

$$\Gamma_a \times \Gamma_{H'} \times \Gamma_{a^*} \supset \Gamma_{A_1}.$$

If a is Ψ_{a_1} and a^* is Ψ_{b_1}, then H' must transform as $B_1(R_y)$, a rotation about the y axis. Expansion into atomic orbitals yields

$$\langle \Psi_{a_1}|H'_y|\Psi_{b_1}\rangle = \langle \sum_i C_i^{a_1}\varphi_i \left| \frac{1}{2}\sum_k \xi_k \hat{\ell}_k^y \cdot \vec{s}_k \right| \sum_j C_j^{b_1}\varphi_j \rangle \qquad (9)$$

where φ_i and φ_j are the anion atomic orbitals which comprise the Ψ_{a_1} and Ψ_{b_1} molecular orbital functions (Table 6) respectively; where k denotes an atomic center (nitrogen, oxygen-1, or oxygen-2); where $C_i^{a_1}$ and $C_j^{b_1}$ are the atomic orbital coefficients for the $^1\Psi_{a_1}$ and $^1\Psi_{b_1}$ molecular orbital functions; where ξ_k is the spin-orbit coupling coefficient for atomic center k; and where $\hat{\ell}_k^y$ and $\hat{s}_k$ are the orbital and spin operators for atomic center k, respectively.

Since the coordinates of the spin function are not the same as position coordinates of the electrons, the integration over the spin coordinates can be performed independently. Only certain eigenvalues of the spin operator are non-zero, these have been tabulated in Table 3. The spin operator acts upon the configurational wave functions (Table 1) and has been evaluated in Table 5.

It is advantageous to replace the theoretical spin-orbit coup-

TABLE 7

OVERLAPS FOR SILVER NITRITE

NAME	ANION ORBITAL	METAL ORBITAL	OVERLAP STRUC. I	OVERLAP STRUC. II
Sam	a_1	Dz^2	.0351	.0175
"	a_1	Dx^2-y^2	.0007	.0175
"	b_2	Dyz	.0011	.0681
"	a_2	Dxy	.0004	.0137
Sa*m	b_1	Dxz	.0108	-.0057
Sam*	a_1	S	.0697	.0796
"	a_1	Pz	-.1056	.0910
"	b_2	Py	.0115	.1133
Sa*m*	b_1	Px	.0281	.0153

ling coefficient ξ_k with the empirical parameter ζ_k. Tables of ζ values are available from the literature.[25-27] Introduction of the one-center approximation and the ζ_k parameter into equation (9) yields

$$\langle \Psi_{a_1} | H'_y | \Psi_{b_1} \rangle = -i\Sigma C_i^{a_1} C_j^{b_1} \zeta_k \langle \varphi_i^{a_1} | \hat{\ell}_k^y | \varphi_j^{b_1} \rangle \qquad (10)$$

where $\varphi_i^{a_1}$ and $\varphi_j^{b_1}$ are the angular parts of the atomic orbitals which comprise the Ψ_{a_1} and Ψ_{b_1} molecular orbital functions (the radial parts having been incorporated into the ζ_k). The summation is over one-center terms only.

Operation of the $\hat{\ell}_q$ (q=x,y,z) operator on an atomic orbital results in the rotation of that orbital around one of the cartesian axes. If the new orbital is denoted φ', the integral in the right side of (10) is

$$\langle \varphi_i^{a_1} | \varphi'_j{}^{b_1} \rangle$$

which is an overlap integral.

Tables describing the result of the $\hat{\ell}q$ (q = x, y, and z) operator on s, p, d, and f orbitals are given in reference 11, p. 347 and Appendix H. These tables were used with the nitrite molecular orbitals in Table 6 to calculate the anion spin-orbit coupling integrals. The spin-orbit coupling integrals for silver may be calculated from the tables alone (ζ values from Reference 5). The results are given in Table 8.

C. TRANSITION DIPOLE MOMENTS:

Transition dipole moment integrals in Table 5 (e.g., $\langle a | \vec{r} | m \rangle$), are derived from expressions such as equation (8). In equation (8), the transition moment is

TABLE 8

VALUES OF SPIN-ORBIT COUPLING INTEGRALS FOR SILVER NITRITE[1]
(cm^{-1})

$\langle a \lvert H' \rvert a \rangle$			
$\langle a_2 \lvert H'_y \rvert b_2 \rangle = -i117.35$			
$\langle b_2 \lvert H'_x \rvert a_1 \rangle = -i79.152$			
$\langle a \lvert H' \rvert a^* \rangle$			
$\langle b_2 \lvert H'_z \rvert b_1 \rangle = i69.247$			
$\langle a_1 \lvert H'_y \rvert b_1 \rangle = -i108.724$			
$\langle a^* \lvert H' \rvert a^* \rangle$			
$= 0$			
$\langle m \lvert H' \rvert m \rangle$	Hx	Hy	Hz
	$\langle xy \lvert\lvert xz \rangle = -i913$	$\langle xy \lvert\lvert yz \rangle = 913$	$\langle xy \lvert\lvert x^2-y^2 \rangle = i1826$
	$\langle yz \lvert\lvert x^2-y^2 \rangle = -i913$	$\langle xz \lvert\lvert x^2-y^2 \rangle = -913$	$\langle xz \lvert\lvert yz \rangle = -i913$
	$\langle yz \lvert\lvert z^2 \rangle = -i1581$	$\langle xz \lvert\lvert z^2 \rangle = 1581$	
$\langle M^* \lvert H' \rvert m \rangle$			
$= 0$			

[1]Spin-orbit coupling constants are: Oxygen, ζ_{2p}=152 cm^{-1}; Nitrogen, ζ_{2p}= 70 cm^{-1}; Silver, ζ_{4p}= 613 cm^{-1}, ζ_{4d}= 1826 cm^{-1}.

$$\vec{M} = \langle {}^1\Psi_{CT} | \Sigma e\vec{r}_i | {}^1\Psi_O \rangle. \qquad (11)$$

The integral is evaluated in the following manner: First, the configuration wave functions ${}^1\Psi_{CT}$ and ${}^1\Psi_O$ are expressed as Slater determinants (Table 1). Since the $e\vec{r}$ operator is a one-electron operator, the only non-zero matrix element in the expansion of equation (11) will contain the two molecular orbitals which differ between ${}^1\Psi_{CT}$ and ${}^1\Psi_O$.[29] Thus $\vec{M} = \langle {}^1\Psi_{CT} | \Sigma e\vec{r}_i | {}^1\Psi_O \rangle = \langle \frac{1}{\sqrt{2}}(|a\bar{m}^* m\bar{m}| + |m^* \bar{a} m\bar{m}|) | \Sigma e\vec{r}_i | |a\bar{a}m\bar{m}| \rangle$

$$= \frac{1}{\sqrt{2}}(\langle |a\bar{m}^* m\bar{m}| | \Sigma e\vec{r}_i | |a\bar{a}m\bar{m}| \rangle + \langle |m^* \bar{a} m\bar{m}| | \Sigma e\vec{r}_i | |a\bar{a}m\bar{m}| \rangle)$$

$$= \frac{1}{\sqrt{2}}(\langle \bar{m}^* | e\vec{r} | \bar{a} \rangle + \langle m^* | e\vec{r} | a \rangle)$$

$$= \sqrt{2} \langle m^* | e\vec{r} | a \rangle$$

as found (without the electronic charge e) in Table 5.

Second, the molecular orbitals m* and a are expressed as linear combinations of atomic orbitals, yielding

$$\vec{M} = \sum_i \sum_j C_i^{m^*} C_j^a \langle \varphi_i^{m^*} | e\vec{r} | \varphi_j^a \rangle. \qquad (12)$$

The analytic forms for the resultant functions $\langle \varphi | \vec{r}$, where $\vec{r}$ = x, y, or z and φ is a Slater-type ns, np, or nd (n = 3) orbital, are available from reference 11, Appendix F. The integral in equation (12) evolves into an overlap integral. In order to facilitate computation, the coordinate $\vec{r}$ was always assumed to act upon the anion atomic orbital. Care was taken to preserve the sign of the overlap. The overlaps were taken from the output of a Zipmol calculation. For the sake of thoroughness, all symmetry allowed anion $\rightarrow$ metal transitions were calculated (Table 9).

TABLE 9

TRANSITION DIPOLE MOMENTS FOR SILVER NITRITE

TRANSITION	POLARIZATION	STRUCTURE I	STRUCTURE II
b_1 - Pz	x	-.0745	-.0260
" Dz^2	x	.0080	.0126
" S	x	.0503	-.0492
" Dxy	x	.0000	.0000
" Px	z	.0255	.0408
" Dxz	z	.0495	.0165
" Dx^2-y^2	z		-.0042
a_1 - Dxz	x	.0234	.0170
" Px	x	.0651	.0352
" Py	y	.0201	.1603
" Dyz	y	-.0180	.0611
" Pz	z	.0652	-.1840
" S	z	-.1173	-.1712
" Dz^2	z	.0643	-.0146
" Dx^2-y^2	z		.0437
b_2 - Dxy	x	-.0003	.0229
" Pz	y	.0011	.0161
" Dz^2	y	.0171	.0190
" S	y	.0118	.0744
" Py	z	.0110	.1110
" Dzy	z	-.0059	.0682

TABLE 9
(Continued)

a_2 - Py	x	-.0065	-.0643
" Dyz	x	.0003	.0200
" Dxz	x	.0000	-.0022
" Px	x	-.0040	.0369
" Dxy	z	-.0011	.0320

D. MOLECULAR DIPOLE MOMENTS:

Static molecular dipole moments are needed for the calculation of expression 'e' listed in Table 5. The dipole moments were computed in the collapsed-core, point charge approximation using the output of the Zevc program:

$$D = \sum_i \vec{R}_i q_i$$

where $\vec{R}_i$ is the coordinate of the i^{th} atomic center, and q_i is the net atomic charge of that center. The values of q_i and the resulting dipole moments for silver nitrite in Structures I and II (for the ground electronic state) are given in Table 10.

The dipole moment of the silver nitrite molecule in the excited state ($^3\psi_{A*}$) is needed for expression 'a' of Table 5. This quantity is difficult to obtain, either experimentally or by calculation. For this reason, this dipole moment was assumed to be the same as that of the ground electronic state.

E. ENERGY DENOMINATORS:

A number of configuration energies are required for the perturbation coefficients in the expressions on Table 5. Considerable care must be taken to ensure that reasonable values be obtained for these energies.

The only whole-molecule silver nitrite calculations available are the extended Huckel programs Zipmol and Zevc. Several problems occur in these calculations: First, the program outputs refer to

TABLE 10

NET ATOMIC CHARGES AND STATIC DIPOLE MOMENTS OF THE SILVER NITRITE MOLECULE

	Net Atomic Charge	Dipole Moment
Structure I		
Nitrogen	+0.223	
Oxygen	-0.168	
Silver	+0.113	0.450 eÅ = 2.160 Debye
Structure II		
Nitrogen	+0.122	
Oxygen	-0.076	
Silver	+0.023	0.133 eÅ = 0.642 Debye

orbitals which are linear combinations of nitrite atom and silver atomic orbitals, while the perturbation equations have been developed for a formalism using distinct nitrite and silver orbitals. Second, they do not evaluate any exchange integrals and thus assume a degeneracy of singlet and triplet states. Thirdly, extended Huckel calculations are not noted for their accuracy in the calculation of excited state energies. Consequently, these calculations are not particularly suited to our needs.

The CNDO/S-C.I. program is not parameterized for silver, nor does it calculate exchange intervals for excitations of $n\pi^*$ type. It is, however, capable of calculating rather closely the transition energies of the nitrite ion $S_n \leftarrow S_0$ $(n \leq 3)$ and $T_1 \leftarrow S_0$ transitions (Table 11).

We have chosen to remain as empirical as possible. All energies not available from experiment were judiciously interpolated from the computational data. For purposes of expediency, we have also assumed that orbital energies are approximately equal to electronic transition energies.

The term $^1E_{A^*}$ in Table 5 may refer to the energy of the excited state produced by excitation out of any of the three highest occupied nitrite orbitals (a_1, a_2, or b_2). These states will be designated $\Psi_{A^*}(b_1 \leftarrow a_1)$, $\Psi_{A^*}(b_1 \leftarrow a_2)$, and $\Psi_{A^*}(b_1 \leftarrow b_2)$, respectively. Experimental energies for the $b_1 \leftarrow a_1$, $b_1 \leftarrow a_2$, and $b_1 \leftarrow b_2$ electronic transitions were taken from reference 1 and assigned as the energies of the $^1E_{A^*}$-

TABLE 11

ELECTRONIC TRANSITIONS IN THE NITRITE MOLECULE

(kK)

Transition	CNDO/s-C.I. GEOMETRY 1[1]	CNDO/s-C.I. GEOMETRY 2[2]	CNDO/s-C.I. GEOMETRY 3[3]	Experimental Value[4]
$^1B_1 \leftarrow {}^1A_1$	21.31	16.41	21.49	28.0
$^1A_2 \leftarrow {}^1A_1$	29.31	40.65	28.50	35.0
$^1B_2 \leftarrow {}^1A_1$	51.06	60.65	50.32	48.0
$^3B_1 \leftarrow {}^1A_1$	21.31	16.41	21.49	22.7

[1]M. I. Kay and B. C. Frazer, Acta Cryst., 14, 56 (1961). N-O=1.24Å, ONO=114.9°

[2]R. E Long and R. E. Marsh, Acta Cryst., 15, 448 (1962). N-O=1.15Å, ONO=128°

[3]M. R. Truter, Acta Cryst., 7, 73 (1954). N-O=1.247Å, ONO=114.2°

[4]Singlet-singlet transition energies from S. J. Strickler and M. Kasha, J. Am. Chem. Soc., 85, 2899 (1963), singlet-triplet transition energy from H. J. Maria, A. Wahlborg, and S. P. McGlynn, J. Chem. Phys., 49, 4925 (1968).

($b_1 \leftarrow a_1$), $^1E_{A*}(b_1 \leftarrow a_2)$, and $^1E_{A*}(b_1 \leftarrow b_1)$ configurations, respectively. Note that the nomenclature has been extended.

In a similar manner, the $^3E_{A*}(b_1 \leftarrow a_1)$ energy was taken from the nitrite ion $T_1 \leftarrow S_0$ transition energy maximum in water solution;[28] the energy of the $p \leftarrow d$ transition of Ag^+ in water[30] was taken for $^1E_{M*}(p \leftarrow d)$; and, the energy of the transition assigned as charge-transfer in $AgNO_2$[8] was taken for $^1E_{CT}(s,p \leftarrow a_1)$. The silver 5s and 5p orbitals are assumed to have the same energy.

The values of $^1E_{CT}(s,p \leftarrow a_2)$ and $^1E_{CT}(s,p \leftarrow b_2)$ were generated by assuming that these energies increase relative to the $^1E_{CT}(s,p \leftarrow a_1)$ energy by exactly the same amount as the corresponding nitrite transitions which terminate on the b_1 orbital. For example, $^1E_{A*}(b_1 \leftarrow a_2)$ is 2.48 eV higher than $^1E_{A*}(b_1 \leftarrow a_1)$. This amount is added to the energy of $^1E_{CT}(s,p \leftarrow a_1)$ to give the value of $^1E_{CT}(s,p \leftarrow a_2)$.

The value for $^1E_{RCT}(b_1 \leftarrow d)$ was obtained by algebraic manipulation of the other energies. $^1E_{A*}$-$^3E_{A*}$ intervals were all taken to be 5,000 cm^{-1} (the experimentally observed value for the $b_1 \leftarrow a_1$ transition). The singlet-triplet intervals for E_{CT} and E_{RCT} should be much less; however no experimental data is available. Both are assumed to be 1,000 cm^{-1}. The resulting energies are given in Table 12.

TABLE 12

STATE ENERGIES FOR SILVER NITRITE
(cm^{-1})

STATE	SINGLETS	TRIPLETS
Ψ_G	0	
$\Psi_{A^*}(b_1 \leftarrow a_1)$	28,000	22,700
" $(b_1 \leftarrow a_2)$	48,000	43,000
" $(b_1 \leftarrow b_2)$	36,000	31,000
$\Psi_{M^*}(s,p \leftarrow d)$	37,000	(not used)
$\Psi_{CT}(s,p \leftarrow a_1)$	25,600	24,600
" $(s,p \leftarrow a_2)$	45,600	44,600
" $(s,p \leftarrow b_2)$	33,600	32,600
$\Psi_{RCT}b_1 \leftarrow d)$	40,000	39,000

V. RESULTS AND DISCUSSION:

The numerical evaluation of all expressions derived from Table 5 are listed on Table 13, and summarized on Table 14. The following observations can be made.

A few suspected intensity-enhancing mechanisms do not contribute to the ${}^3\Psi_{A^*} \leftarrow \Psi_O$ transition intensity. The metal excited states Ψ_{M^*} cannot spin-orbit couple with the anion (in relation to the above singlet-triplet transition) except via two-center spin-orbit coupling integrals, which we take to be zero. Similarly, the mechanism ${}^3\Psi_{A^*} + c'''{}^1\Psi_{A^*}$ is ineffective because of symmetry restrictions on c''' (which contains $\langle a|H'|a\rangle$ and $\langle a^*|H'|a^*\rangle$ integrals, but $\Gamma_{\text{spin-orbit coupling}}$ does not contain Γ_{A_1} in C_{2v}).

The largest transition moments derive from expressions containing static dipole moments. (These transition moments are designated by a # in Table 14.) The expressions involved are a) and e) in Tables 2 and 5. The energy denominators in these expressions are of opposite signs. Consequently, the transition moments derived from them tend to cancel (assuming the ground state and ${}^3\Psi_{A^*}$ state dipole moments are equal). If the actual dipole moment of the ${}^3\Psi_{A^*}$ state were used in the calculation, then the sum of the # transition moments would relate to the change of the dipole moment upon excitation.

The mixing of singlet charge-transfer states into ${}^3\Psi_{A^*}$ accounts for the next largest set of transition dipole moments. This results both from the small energy difference between the ${}^3\Psi_{A^*}$ state

TABLE 13

EVALUATION OF TRANSITION DIPOLE MOMENT EXPRESSIONS FOR SILVER NITRITE

Structure I

	$\frac{\text{Structure I}}{(\text{cm}^{-1})}$
$\Psi_0 + b'' {}^3\Psi_{A^*}$	$\frac{-i\langle b_1 \lvert H'_y \rvert a_1\rangle(\mu_{A^*} - 2S a_1,z^2\langle a_1 \lvert \vec{r}_z \rvert b_1\rangle}{E_0 - {}^3E_{A^*}(b_1 \leftarrow a_1)} = \frac{-i(\ i\ 108{,}724)}{0-22{,}700}(\mu_{A^*}-2(.0351)(.0643)) = -2.133 \times 10^{-3}$
"	$\frac{-\sqrt{2}\langle b_1 \lvert H'_z \rvert b_2\rangle(\mu_{A^*})}{E_0 - {}^3E_{A^*}(b_1 \leftarrow b_2)} = \frac{-\sqrt{2}(-169.247)(\mu_{A^*})}{0 - 31{,}000} = -11.4216 \times 10^{-3}$
$\Psi_0 + d'' {}^3\Psi_{CT}$	$\frac{S a_1,z\langle a_1 \lvert H'_x \rvert b_2\rangle\ \langle z \lvert \vec{r}_x \rvert b_1\rangle}{E_0 - {}^3E_{CT}(z \leftarrow a_1)} = \frac{1(-.1056)(i\ 79.152)(-.0745)}{0-24{,}600} = 2.5\text{x}10^{-5}$
"	$\frac{S a_1,s\langle a_1 \lvert H'_x \rvert b_2\rangle\ \langle s \lvert \vec{r}_x \rvert b_1\rangle}{E_0 - {}^3E_{CT}(s \leftarrow a_1)} = \frac{i\ (.0697)(i\ 79.152)(.0503)}{0-24{,}500} = 1.1\text{x}10^{-5}$
$\Psi_0 + e'' {}^3\Psi_{RCT}$	$\frac{S b_1,xz\langle xy \lvert H'_x \rvert xz\rangle\langle a_1 \lvert \vec{r}_x \rvert xz\rangle}{E_0 - {}^3E_{RCT}(b_1 \leftarrow d)} = \frac{(.0108)(-i\ 913.0)(.0234)}{0\ -\ 39{,}000} = i5.9\text{x}10^{-6}$

$^3\Psi_0 + e''{}^3\Psi_{RCT}$: $\dfrac{-iSb_1,xz\langle x^2-y^2|H'_y|xz\rangle\langle a_1|\vec{r}_x|xz\rangle}{E_0 - {}^3E_{RCT}(b_1\leftarrow d)} = \dfrac{-i(.0108)(913.0)(.0234)}{0 - 39{,}000} = i5.9\times10^{-6}$

" : $\dfrac{Sb_1,xz\langle yz|H'_z|xz\rangle\langle a_1|\vec{r}_x|xz\rangle}{E - {}^3E_{RCT}(b_1\leftarrow d)} = \dfrac{\sqrt{2}(.0108)(1913.)(.0234)}{0 - 39{,}000} = -18.4\times10^{-6}$

" : $\dfrac{-iSa_1,z^2\langle b_1|H'_y|a_1\rangle\langle a_1|\vec{r}_z|z^2\rangle}{E_0 - {}^3E_{RCT}(b_1\leftarrow d)} = \dfrac{-i(.0351)(1108.724)(.0643)}{0 - 39{,}000} = -6.3\times10^{-6}$

$^3\Psi_{A*} + b'''\Psi_0$: $\dfrac{-\sqrt{2}\langle b_2|H'_z|b_1\rangle(\mu_0 - 4Sa_1,z^2\langle a_1|\vec{r}_z|z^2\rangle)}{{}^3E_{A*}(b_1\leftarrow b_2) - E_0} = \dfrac{-\sqrt{2}(169.247)(\mu_0 - 4(.0351)(.0643))}{31{,}000 - 0} = 1.393\times10^{-3}$

$\dfrac{i\langle a_1|H'_y|b_1\rangle(\mu_0 - 4Sa_1,z^2\langle a_1|\vec{r}_z|z^2\rangle)}{{}^3E_{A*}(b_1\leftarrow a_1)} = \dfrac{i(-1108.724)(\mu_0 - 4(.0351)(.0643))}{31{,}000 - 0} = 2.112\times10^{-3}$

$^3\Psi_{A*} + e''{}^1\Psi_{CT}$: $\dfrac{i/\sqrt{2}Sa_1,s\langle a_1|H'_y|b_1\rangle\sqrt{2}\langle a_1|\vec{r}_z|s\rangle}{{}^3E_{A*}(b_1\leftarrow a_1)} = \dfrac{i(.0697)(-1108.724)(-.1173)}{22{,}700 - 24{,}600} = 2.68\times10^{-4}$

$^3\Psi_{A^*} + e^{m\,1}\Psi_{CT}$

$$\frac{i/\sqrt{2}\,Sa_1,z\langle a_1|H'_y|b_1\rangle\sqrt{2}\langle a_1|\vec{r}_z|z\rangle}{^3E_{A^*}(b_1\leftarrow a_1) - {}^1E_{CT}(z\leftarrow a_1)} = \frac{i(-.1056)(-1108.724)(.0652)}{22{,}700-24{,}600} = 3.94\times10^{-4}$$

"

$$\frac{-Sb_2,y\langle b_2|H'_z|b_1\rangle\sqrt{2}\langle b_2|\vec{r}_z|y\rangle}{^3E_{A^*}(b_1\leftarrow b_2) - {}^1E_{CT}(y\leftarrow b_2)} = \frac{-\sqrt{2}(.0115)(i\ 69.247)(.0110)}{31{,}000-32{,}600} = -17.7\times10^{-6}$$

$^3\Psi_{A^*} + f^{m\,1}\Psi_{RCT}$

$$\frac{1/\sqrt{2}\,Sa_1,z^2(\langle b_2|H'_x|a_1\rangle + \langle z^2|H'_x|yz\rangle)\sqrt{2}\langle z^2|\vec{r}_x|b_1\rangle}{^3E_{A^*}(b_1\leftarrow a_1) - {}^1E_{RCT}(b_1\leftarrow d)} = \frac{(.0351)[-i\ 79.152-i\ 1581.]\ (.0080)}{22{,}700 - 40{,}000}$$

$$= 12.7\times10^{-5}$$

"

$$\frac{-1/\sqrt{2}\,Sa_1,z^2\ \langle z^2|H'_y|xz\rangle\sqrt{2}\langle z^2|\vec{r}_x|b_1\rangle}{^3E_{A^*}(b_1\leftarrow a_1) - {}^1E_{RCT}(b_1\leftarrow d)} = \frac{-i(.0351)(-1581)(.0080)}{22{,}700 - 40{,}000} = -12.7\times10^{-5}$$

$^3\Psi_{A^*} + f^{m\,1}\Psi_{RCT}$

$$\frac{1/\sqrt{2}\,Sa_1,x^2-y^2\langle x^2-y^2|H'_y|xz\rangle\langle b_1|\vec{r}_x|x^2-y^2\rangle\sqrt{2}}{^3E_{A^*}(b_1\leftarrow a_1) - {}^1E_{RCT}(b_1\leftarrow d)} = \frac{(.0175)(913.)(-.0042)}{22{,}700 - 40{,}000} = 3.9\times10^{-6}$$

"

$$\frac{1/\sqrt{2}\,Sa_1,x^2-y^2\langle x^2-y^2|H'_z|xy\rangle\sqrt{2}\langle b_1|\vec{r}_x|x^2-y^2\rangle}{^3E_{A^*}(b_1\leftarrow a_1) - {}^1E_{RCT}(b_1\leftarrow d)} = \frac{(.0175)(-11826)(-.0042)}{22{,}700 - 40{,}000} = 7.8\times10^{-6}$$

Structure II

$\Psi_O + b''^3\Psi_{A*}$:

$$\frac{-i\langle b_1|H'_y|a_1\rangle(-2Sa_1,z^2\langle a_1|\vec{r}_z|z^2\rangle)}{E_O - {}^3E_{A*}(b_1\leftarrow a_1)} = \frac{-i(108.724)(-2(.0175)(.0146))}{0 - 22{,}700} = 2.4 \times 10^{-6}$$

" :

$$\frac{-i\langle b_1|H'_y|a_1\rangle(-2Sxz,b_1\langle b_1|\vec{r}_z|xz\rangle)}{E_O - {}^3E_{A*}(b_1\leftarrow a_1)} = \frac{-i(108.724)(-2)(.0057)(.0165)}{0 - 22{,}700} = 9.1 \times 10^{-7}$$

" :

$$\frac{-i\langle b_1|H'_y|a_1\rangle(-2Sb_2,yz\langle b_2|\vec{r}_z|yz\rangle)}{E_O - {}^3E_{A*}(b_1\leftarrow a_1)} = \frac{-i(108.724)(-2)(.0681)(.0682)}{0 - 22{,}700} = 4.45 \times 10^{-5}$$

" :

$$\frac{-i\langle b_1|H'_y|a_1\rangle(-2Sa_2,xy\langle a_2|\vec{r}_z|xy\rangle}{E_O - {}^3E_{A*}(b_1\leftarrow a_1)} = \frac{-i(108.724)(-2)(.0137)(.0137)}{0 - 22{,}700} = 1.8 \times 10^{-6}$$

" :

$$\frac{-i\langle b_1|H'_y|a_1\rangle(\mu_{A*})}{E_O - {}^3E_{A*}(b_1\leftarrow a_1)} = \frac{-i(108.724)(\mu_{A*})}{0 - 22{,}700} = -6.370 \times 10^{-4}$$

" :

$$\frac{-\sqrt{2}\langle b_1|H'_z|b_2\rangle(\mu_{A*}\text{-}2Sa_1,z^2\langle a_1|\vec{r}_z|z^2\rangle\text{-}2Sa_1,x^2-y^2\langle a_1|r_z|x^2-y^2\rangle)}{E_O - {}^3E_{A*}(b_1\leftarrow b_2)} = \frac{-\sqrt{2}(-169.247)(\mu_{A*}}{0 - 31{,}000}$$

$$-2(.0175)(-.0146)-2(.0175)(.0437)) = 12.948 \times 10^{-4}$$

$\Psi_0 + d''^3\Psi_{CT}$

$$\frac{-S a_1, s \langle a_1 | H'_x | b_2 \rangle \langle b_1 | \vec{r}_x | s \rangle}{E_0 - {}^3E_{CT}(s \leftarrow a_1)} = \frac{-(.0796)(\ i79.152)(.0503)}{0 - 24{,}600} = i1.3 \times 10^{-5}$$

$\Psi_0 + d''\,{}^3\Psi_{CT}$

$$\frac{-S a_1, z \langle a_1 | H'_x | b_2 \rangle \langle b_1 | \vec{r}_x | z \rangle}{E_0 - {}^3E_{CT}(z \leftarrow a_1)} = \frac{-(.0910)(-179.152)(-.0745)}{0 - 24{,}600} = -i2.2 \times 10^{-5}$$

$\Psi_0 + e''\,{}^3\Psi_{RCT}$

$$\frac{-iS a_1, z^2 \langle b_1 | H'_y | a_1 \rangle \langle b_2 | \vec{r}_y | z^2 \rangle}{E - {}^3E_{RCT}(b_1 \leftarrow d)} = \frac{-i(.0175)(-i108.724)(.0190)}{0 - 39{,}000} = -9.3 \times 10^{-7}$$

"

$$\frac{-iS a_1, x^2-y^2 \langle b_1 | H'_y | a_1 \rangle \langle a_1 | \vec{r}_z | x^2-y^2 \rangle}{E_0 - {}^3E_{RCT}(b_1 \leftarrow d)} = \frac{-i(.0175)(-i108.724)(.0437)}{0 - 39{,}000} = -2.1 \times 10^{-6}$$

"

$$\frac{\sqrt{2} S b_1, xz \langle yz | H'_z | xz \rangle \langle a_1 | \vec{r}_x | xz \rangle}{E_0 - {}^3E_{RCT}(b_1 \leftarrow d)} = \frac{\sqrt{2}(-.0057)(i913.0)(.0170)}{0 - 39{,}000} = i3.2 \times 10^{-6}$$

"

$$\frac{S b_1, xz \langle xy | H'_x | xz \rangle \langle a_1 | \vec{r}_x | xz \rangle}{E_0 - {}^3E_{RCT}(b_1 \leftarrow d)} = \frac{(-.0057)(-i913.0)(.0170)}{0 - 39{,}000} = -i2.3 \times 10^{-6}$$

"

$$\frac{-iS b_1, xz \langle z^2 | H'_y | xz \rangle \langle a_1 | \vec{r}_x | xz \rangle}{E_0 - {}^3E_{RCT}(b_1 \leftarrow d)} = \frac{-i(-.0057)(-1581.)(.0170)}{0 - 39{,}000} = i3.9 \times 10^{-6}$$

$\Psi_o + e''^{3}\Psi_{RCT}$ | $\dfrac{\sqrt{2}Sb_2,yz\langle b_1|H'_z|b_2\rangle\langle b_2|\vec{r}_z|yz\rangle}{E_o - {}^3E_{RCT}(b_1\leftarrow d)} = \dfrac{\sqrt{2}(.0681)(169.247)(.0682)}{0 - 39{,}000} = 1.2 \times 10^{-5}$

$^3\Psi_{A*} + b''' \Psi_o$ | $\dfrac{i\langle a_1|H'_y|b_1\rangle(-4Sa_1,z^2\langle a_1|\vec{r}_z|z^2\rangle)}{{}^3E_{A*}(b_1\leftarrow a_1) - E_o} = \dfrac{-i(-i108.724)(.0175)(.0146)4}{22{,}700 - 0} = -4.9 \times 10^{-6}$

" | $\dfrac{i\langle a_1|H'_y|b_1\rangle(-4Sa_1,x^2-y^2\langle a_1|\vec{r}_z|x^2-y^2\rangle)}{{}^3E_{A*}(b_1\leftarrow a_1) - E_o} = \dfrac{-i(-i108.724)(4)(.0175)(.0437)}{22{,}700 - 0} = -1.47 \times 10^{-5}$

" | $\dfrac{i\langle a_1|H'_y|b_1\rangle(-4Sb_2,yz\langle b_2|\vec{r}_z|yz\rangle)}{{}^3E_{A*}(b_1\leftarrow a_1) - E_o} = \dfrac{-i(-i108.824)(4)(.0681)(.0682)}{22{,}700 - 0} = -8.90 \times 10^{-5}$

" | $\dfrac{i\langle a_1|H'_y|b_1\rangle(-4Sa_2,xy\langle a_2|\vec{r}_z|xy\rangle}{{}^3E_{A*}(b_1\leftarrow a_1) - E_o} = \dfrac{-i(-i108.724)(4)(.0137)(.0320)}{22{,}700 - 0} = -8.4 \times 10^{-6}$

" | $\dfrac{i\langle a_1|H'_y|b_1\rangle(\mu_o)}{{}^3E_{A*}(b_1\leftarrow a_1) - E_o} = \dfrac{i(-i108.724)(\mu_o)}{22{,}700 - 0} = 6.37 \times 10^{-4}$

$\dfrac{-\sqrt{2}\langle b_2|H'_z|b_1\rangle(\mu_o)}{{}^3E_{A*}(b_1\leftarrow b_2) - E_o} = \dfrac{-\sqrt{2}(169.247)(\mu_o)}{31{,}000 - 0} = -14.21 \times 10^{-5}$

$^3\Psi_{A^*} + e^{III}\,^1\Psi_{CT}$

$$\frac{\frac{1}{\sqrt{2}}\,Sa_1,s\langle a_1|H'_y|b_1\rangle\sqrt{2}\langle a_1|\vec{r}_z|s\rangle}{^3E_{A^*}(b_1\leftarrow a_1) - {}^1E_{CT}(p\leftarrow a_1)} = \frac{(.0796)(-i108.724)(-.1712)}{22{,}700 - 24{,}600} = -i\,7.80 \times 10^{-4}$$

"

$$\frac{\frac{1}{\sqrt{2}}Sa_1,z\langle a_1|H'_y|b_1\rangle\langle a_1|\vec{r}_z|z\rangle}{^3E_{A^*}(b_1\leftarrow a_1) - {}^1E_{CT}(p\leftarrow a_1)} = \frac{(.0910)(-i108.724)(-.1814)}{22{,}700 - 24{,}600} = -i9.45 \times 10^{-4}$$

"

$$\frac{-Sb_2,y\langle b_2|H'_z|b_1\rangle\sqrt{2}\langle b_2|\vec{r}_z|y\rangle}{^3E_{A^*}(b_1\leftarrow b_2) - {}^1E_{CT}(p\leftarrow b_2)} = \frac{(.1133)(169.247)(.1110)(1.414)}{31{,}000 - 32{,}600} = -17.70 \times 10^{-4}$$

$^3\Psi_{A^*} + f^{III}\,^1\Psi_{RCT}$

$$\frac{\frac{1}{\sqrt{2}}Sa_1,z^2(\langle b_2|H'_x|a_1\rangle + \langle z^2|H'_x|yz\rangle)\sqrt{2}\langle b_1|\vec{r}_x|z^2\rangle}{^3E_{A^*}(b_1\leftarrow a_1) - {}^1E_{RCT}(b_1\leftarrow d)} = \frac{(.0175)(-179.152-i1581)(-.0042)}{22{,}700 - 40{,}000} = -i7.1 \times 10^{-6}$$

"

$$\frac{\frac{1}{\sqrt{2}}\,Sa_1,x^2-y^2(\langle b_2|H'_x|a_1\rangle + \langle x^2-y^2|H'_x|yz\rangle)\sqrt{2}\langle x^2-y^2|\vec{r}_x|b_1\rangle}{^3E_{A^*}(b_1\leftarrow a_1) - {}^1E_{RCT}(b_1\leftarrow d)} = \frac{(.0175)(-179.152+1913.)(-.0042)}{22{,}700 - 40{,}000}$$

$$= i3.5 \times 10^{-6}$$

"

$$\frac{\frac{1}{\sqrt{2}}Sa_1,z^2\langle z^2|H'_y|xz\rangle\sqrt{2}\langle b_1|\vec{r}_x|z^2\rangle}{^3E_{A^*}(b_1\leftarrow a_1) - {}^1E_{RCT}(b_1\leftarrow d)} = \frac{(.0175)(-1581)(-.0042)}{22{,}700 - 40{,}000} = -6.7 \times 10^{-6}$$

TABLE 14

SUMMARY OF TABLE 13

	X POLARIZED	Y POLARIZED	Z POLARIZED
		Structure I	
$\hat{M}$	2.5×10^{-5} 1.1×10^{-5} 15.9×10^{-6} 15.9×10^{-6} -18.4×10^{-6} 12.7×10^{-5} -12.7×10^{-5} 3.9×10^{-6} 7.8×10^{-6}	0	-2.133×10^{-3}# -11.422×10^{-3}# -6.3×10^{-6} 1.393×10^{-3}# 2.112×10^{-3}# 2.68×10^{-4} 3.94×10^{-4} -17.7×10^{-6}
$\lvert\vec{M}_{total}\rvert$	4.78×10^{-5}	0	2.48×10^{-3}
f	5.63×10^{-10}	0	1.516×10^{-6}
		Structure II	
$\hat{M}$	11.3×10^{-5} -12.2×10^{-5} 13.2×10^{-6} -12.3×10^{-6} 13.9×10^{-6} -17.1×10^{-6} 13.5×10^{-6} -6.7×10^{-6}	-9.3×10^{-7}	2.4×10^{-6} 9.1×10^{-7} 4.5×10^{-5} 1.8×10^{-6} -6.37×10^{-4}# 12.948×10^{-4}# 1.2×10^{-5} -4.9×10^{-6} -1.47×10^{-5} -8.9×10^{-5} -8.4×10^{-6} 6.37×10^{-4}# -14.21×10^{-5}# -2.1×10^{-6} -17.8×10^{-4} -19.45×10^{-4} -17.7×10^{-4}
$\lvert\vec{M}_{total}\rvert$	1.03×10^{-5}	9.3×10^{-7}	2.239×10^{-3}
f	2.60×10^{-11}	2.13×10^{-13}	1.235×10^{-6}

designates a static dipole moment contribution.

and the $^1\Psi_{CT}$ state, and the large z-polarized transition moments ($a_1 \rightarrow p_z$ and $a_1 \rightarrow s$) which are mixed in by this perturbation. It is important to note that the large spin-orbit coupling available from the silver atom is not operative here.

The smallest transition moments arise from the mixing of $^1\Psi_{CT}$ states into $^3\Psi_{A*}$ or Ψ_O. The low transition moments are caused both by large energy denominators and by the small transition moments mixed in by this perturbation, notwithstanding the large silver spin-orbit coupling which occurs.

In general, the results for the two structures are about the same. The $^3\Psi_{A*} \leftarrow \Psi_O$ transition is polarized primarily along the z axis, with an oscillator strength of $\sim 1.3 \times 10^{-6}$ and an intrinsic lifetime[31] of 2.2×10^{-3} seconds. Weaker transitions are calculated with x and y polarizations. The singlet $\rightarrow$ triplet transition intensity is derived primarily from $a_1 \rightarrow p_z$ and $a_1 \rightarrow s$ charge-transfer transitions.

The experimental observation of the z polarization of the singlet $\rightarrow$ triplet absorption[7] in $AgNa(NO_2)_2$ has been mentioned. The experimental value of the $T_1 \leftarrow S_O$ absorptive oscillator strength[7] of $\simeq 1.6 \times 10^{-4}$ is higher than the calculated value. Also, the experimentally measured lifetime[32] of 2×10^{-4} is shorter. Both of these disparities may be due to the assumption that $\mu_{A*} = \mu_O$. If $|\mu_O| - |\mu_{A*}| = 1e\mathring{A}$ (4.8 D) for the $^1B_1 \leftarrow {}^1A_1$ transition, the resulting oscillator strength conferred on the $T_1 \leftarrow S_O$ transition would be 5.65×10^{-6}. Also, the wave functions employed for the nitrogen and oxygen atoms (from CNDO/s-C.I.) were not parameterized for a calculation which

included a heavy atom such as silver.

The experimental data for pure silver nitrite[8] is not similar to that of $AgNa(NO_2)_2$.[7] In the former, $T_1 \leftarrow S_0$ absorption occurs along all three axes with relative intensities of $x > y > z$, while in the latter the absorption is confined solely to the z axis. This is not indicated by our calculations. The quality of data is considerably higher, however, in the latter as compared to the former.

The conclusion that the singlet → triplet transition in silver nitrite contains significant contributions from charge-transfer transitions remains. The existence of an intense transition in the spectrum of silver nitrite tentatively assigned as charge-transfer[8] has been mentioned.

According to this model, the mechanism of $T_1 \leftarrow S_0$ intensity enhancement in silver nitrite is quite different than that which is operative in sodium nitrite. In the latter molecule, no significant possibility of spin-orbit coupling or charge-transfer with the cation exists, and the $T_1 \leftarrow S_0$ transition is not intense. ($f \sim 8 \times 10^{-8}$).[4]

REFERENCES

1. S. J. Strickler and M. Kasha, J. Am. Chem. Soc., 85, 2899 (1963).
2. W. C. Allen and R. N. Dixon, Trans. Far. Soc., 65, 1168 (1969).
3. J. Sidman, J. Am. Chem. Soc., 79, 2669 (1957).
4. R. M. Hochstrasser and A. P. Marchetti, J. Chem. Phys., 50, 1727 (1969).
5. L. E. Harris, H. J. Maria, and S. P. McGlynn, Czech. J. Phys., B5, 654 (1970).
6. S. P. McGlynn, Izv. Akad. Nauk. S.S.S.R. Ser. Fiz., 37, 546 (1973).
7. L. E. Reznik and L. M. Rumyantseva, Opt. Spectrosk., 39, 895 (1973).
8. L. E. Reznik, P. R. Garber, and A. E. Fesun, Fiz. Tvert. Tela, 15, 3280 (1973).
9. L. E. Reznik and P. R. Garber, Opt. Spectrosk., 34, 418 (1973).
10. S. P. McGlynn, T. Azumi, and M. Kinoshita, Molecular Spectroscopy of the Triplet State, Prentice-Hall, New Jersey, 1969, p. 200.
11. S. P. McGlynn, L. G. Vanquickenborne, M. Kinoshita, and D. G. Carroll, Introduction to Applied Quantum Chemistry, Holt, Rinehart, and Winston, New York, 1972, p. 342.
12. H. Hameka and L. Goodman, J. Chem. Phys., 42, 2305 (1965).
13. L. L. Lohr, J. Chem. Phys., 45, 1362 (1966).
14. P. Löwdin, Phys. Rev., 97, 1474 (1955).
15. S. P. McGlynn, L. G. Vanquickenborne, M. Kinoshita, and D. G. Carroll, op. cit. p. 346.
16 J. A. Pople, D. P. Santry, and G. A. Segal, J. Chem. Phys., 43, 5129 (1965).
17. N. Mataga and K. Nishimoto, Z. Physik. Chem. 13, 140 (1957).
18. L. C. Cusachs, J. Chem. Phys., 43, 1528 (1965).
19. D. G. Carrol, L. Vanquickenborne, and S. P. McGlynn, J. Chem. Phys., 45, 2777 (1966).
20. M. Barber, J. C. Conner, I. H. Hillier, and V. R. Saunders, in Electron Spectroscopy, D. A. Shirley, Ed., American Elsevier, New York, 1972, p. 379.
21. CNDO/2, CNDO/S-C.I., and Gaussian-70 calculations.
22. R. E. Long and R. E. Marsh, Acta Cryst., 15, 448 (1962).
23. J. F. Wyatt, I. H. Hillier, V. R. Saunders, and J. A. Conner, J.

Chem. Phys., 54, 5311 (1971).

24. E. Clementi, J. Chem. Phys., 40, 1944 (1964).
25. T. M. Dunn, Trans. Far. Soc., 57, 1441 (1961).
26. B. W. N. Lo, K. M. S. Saxena, and S. Fraga, Theor. Chim. Acta (Berl.), 25, 97 (1972).
27. K. Wittel and R. Manne, Theor. Chim. Acta (Berl.), 33, 347 (1974).
28. S. P. McGlynn, L. G. Vanquickenborne, M. Kinowhita, and D. G. Carroll, op. cit. p. 284.
29. H. J. Maria, A. Wahlborg, and S. P. McGlynn, J. Chem. Phys., 49, 4925 (1968).
30. F. Volbert, Z. Phys. Chem., A149, 382 (1930).
31. S. P. McGlynn, T. Azumi, and M. Kinoshita, op. cit., p. 18.
32. H. J. Maria, A. T. Armstrong, and S. P. McGlynn, J. Chem. Phys., 48, 4694 (1968).

VITA

Thomas Preston Carsey was born in Monterrey, Mexico, on January 24, 1946. He was graduated from Hatch Valley High School, Hatch, New Mexico, in 1963. He entered the New Mexico State University in 1963 and graduated from that Institution with a B.Sc. degree in Chemistry in 1969. He attended the graduate school of New Mexico State University from 1970 to 1971.

In September, 1972, he joined the Graduate School at the Louisiana State University. He is presently a candidate for the degree of Doctor of Philosophy.

On December 31, 1970, he married the former Susan Pamela Wier. They have two children.